Generation of functional iPSC-derived astrocytes to model the neurodevelopmental disorder, Rett Syndrome.

Marianne Catherine King

Doctor of Philosophy

Aston University

March 2021

©Marianne Catherine King, 2021.

Marianne Catherine King asserts her moral right to be identified as the author of this thesis.

This copy of the thesis has been supplied on condition that anyone who consults it is understood to recognise that its copyright belongs to its author and that no quotation from the thesis and no information derived from it may be published without appropriate permission or acknowledgement.

Aston University

Generation of functional iPSC-derived astrocytes to model the neurodevelopmental disorder, Rett Syndrome.

Marianne Catherine King

Doctor of Philosophy

March 2021

Thesis Summary

Rett Syndrome (RTT) is one of the leading causes of mental disability in girls. It is a neurodevelopmental disorder caused by mutations in the MeCP2 gene, a ubiquitously expressed transcriptional repressor whose expression is particularly enriched in the central nervous system (CNS). It affects around 1 in 10,000-15,000 girls. It currently has no cure and treatments focus on symptom management; therefore, it is imperative that new methods of modelling RTT are developed that provide translational data. Primary human brain tissue is difficult to obtain, but in order to study neurological disorders it is vital that human brain cells can be studied.

Human induced pluripotent stem cells (iPSCs) could provide a possible solution, as it is possible to generate neural cell types from healthy and patient donors. In this thesis two healthy iPSCs lines and a RTT patient iPSC line were used to generate astrocytes, and one healthy iPSC line was used to generate neurons. Astrocytes were consistently generated as highly enriched populations with minimal neuronal contamination.

iPSC-derived astrocytes demonstrated spontaneous calcium events and could also respond to glutamate and ATP. In addition, they could remove glutamate from their surroundings and release lactate in response. Thus, this thesis has potentially demonstrated the first astrocyte-neuron lactate shuttle in an iPSC-derived system. RTT iPSC-derived astrocytes removed significantly less glutamate from their surroundings compared to astrocytes from a healthy control iPSC line, showing that this model is capable of showing differences in astrocyte function in disease. RTT iPSC-derived astrocytes secreted significantly less lactate in response to glutamate uptake compared to healthy lines. Astrocyte-condition media (ACM) was also generated from the two healthy iPSC and RTT iPSC-derived astrocytes which was used to treat healthy iPSC-derived neurons. It was noted that this had an effect on the neuronal calcium response to glutamate, with healthy ACM potentially increasing this response. RNA sequencing performed on healthy and RTT iPSC-derived astrocytes revealed differentially expressed genes which were mostly enriched in the extracellular matrix organisation pathway.

This thesis has shown that functional, enriched of astrocytes can be generated from healthy and RTT iPSCs. These astrocytes demonstrate functions typical of astrocytes *in vivo* and also reveal differences between healthy and RTT conditions. Therefore, it is feasible that iPSC-derived astrocytes are an ideal tool to model the astrocytic component of RTT.

Key words: Rett Syndrome, astrocyte, neuron, iPSCs.

Acknowledgements

I would like to firstly thank my supervisors Dr Eric Hill and Dr Rhein Parri for giving me the opportunity to do a PhD and for rescuing me from my awful job. Thank you Eric for being such a kind and positive role model in addition to being an inspiringly enthusiastic scientist – I hope we can collaborate on astrocytes together again one day. Also, thank you to Rhein for always making me ask what the question is and for knowing everything about astrocytes. I'd also like to add my thanks to Dr Keeley Brookes for the invaluable guidance and help with my RNA sequencing data and chapter. Thank you also to Dr Richard Elsworthy for the oxidative stress experiments, as the virus-who-will-not-be-named would not allow us to do them together. Lastly, thank you to the MRC for funding this project and for providing me with an extension so that I could finish my research.

To the best lab friends ever, James, Adele and Ally, thank you for making the long, long hours in tissue culture so fun. I will miss working with you in the lab maybe more than anything else. Thank you for keeping me going when my neural inductions failed for the 90th time and for making days/nights out at Gosta so fun. James and Adele, lockdown last year would have been so many times more miserable without your support.

Thank you to my best friend Janine for always being a perfect pal and for still being in Sheffield when I came back again.

To Sylvester, thank you for keeping me company as I wrote my thesis and for making sure I woke up bright and early.

Granny and Grandad, thank you for always encouraging my interest in science from when I was very little and for being such wonderful grandparents – I want to be like you when I grow up. Mama, even though you're not here anymore, you're the reason I wanted to go into neurological disease research; whenever I felt like I couldn't do it anymore, I thought of you.

Without my Mum and Dad, I would have achieved absolutely nothing. Thank you for supporting me in every way possible and for all your encouragement and love. Also thank you for very gently steering me away from considering Fine Art at university – it was the right decision. You're the best parents in the world, especially because you send me regular pictures of Branston and Pickle.

My lovely fiancé Ryan, I don't think I could have finished this PhD without you. Sorry for always moving around the UK costing us lots of money in petrol and train fares. Thank you for visiting me no matter where I am and for never complaining about it. Thank you for picking me up at 10pm at night after a bad lab day and for listening to me cry about cells and other nonsense. Lastly, and most importantly, thank you for the vague grammatical changes you made to my intro, I really appreciate it – I'm the luckiest girl in the world.

Contents

List of Abbreviations

ACM – Astrocyte-conditioned medium

aCSF – Artificial cerebrospinal fluid

Aldh1l1 – 10-formyltetrahydrofolate dehydrogenase

ALS – Amyotrophic lateral sclerosis

AMPA – α-amino-3-hydroxy-5-methyl-4-isoxazolepropionic acid

ANLS – Astrocyte-to-neuron lactate shuttle

AQP4 – Aquaporin 4

Ascl1 – Achaete-Scute Family BHLH Transcription Factor 1

BDNF – Brain derived neurotrophic factor

bHLH – Basic helix-loop-helix

BMP – Bone morphogenetic protein

bp – Base pairs

CaMKII – Calmodulin-dependent protein kinase II

CaMKIIα – Calcium/calmodulin dependent protein kinase II alpha

CDKL5 – Cyclin dependent kinase like 5

ChIP – Chromatin immunoprecipitation

CNS – Central nervous system

CNTF – Ciliary neurotrophic factor

Cx30 – Connexin 30

Cx43 – Connexin 43

DHPG – (S)-3,5-Dihydroxyphenylglycine

DMEM – Dulbecco's modified eagle medium

DMSO – Dimethyl sulphoxide

FGF – Fibroblast growth factor

FoxG1 – Foxhead box G1

FXYD1 – FXYD Domain Containing Ion Transport Regulator 1

Gapdh – Glyceraldehyde 3-phosphate dehydrogenase

GFAP – Glial fibrillary acidic protein

Glast-1 – Glutamate aspartate transporter 1

GCM – Glial-conditioned medium

Glt-1 – Glutamate transporter 1

GPCR – G-protein coupled receptor

GPCRs – G-protein coupled receptors

GSH – Glutathione

Gsx – Genomic screen homeobox

Hapln1 – Hyaluronan and proteoglycan link protein 1

Has3 – Hyaluronan synthase 3

HDAC – Histone deacetylase

Her2 – Erb-B2 Receptor Tyrosine Kinase 2

Hes – Hairy and enhancer of split

ICC – Immunocytochemistry

Id1 – Inhibitor of DNA binding 1

IGF1 – Insulin-like growth factor 1

IL-1α – Interleukin 1α

IL-1β – Interleukin 1β

IL-6 – Interleukin 6

Jak/Stat – Janus kinase/signal transducer and activator of transcription proteins

Kir4.1 – Potassium Inwardly Rectifying Channel Subfamily J Member 10

Kir5.1 – Potassium Inwardly Rectifying Channel Subfamily J Member 16

Klf4 – Kruppel like factor 4

KR – Krebs'-Ringer-HEPES buffer

LDH1 – Lactate dehydrogenase 1

LDH5 – Lactate dehydrogenase 5

LIF – Leukaemia inhibitory factor

LPS – Lipopolysaccharide

LTP – Long-term potentiation

MAP2 – Microtubule associated protein

MAPK – Mitogen-activated protein kinase

MBD – Methyl binding domain

MCT1 – Monocarboxylate transporter 1

MCT2 – Monocarboxylate transporter 2

MeCP2 – Methyl CpG binding protein 2

MEGF10 – Multiple EGF-like-domains 10

MERTK – MER Proto-oncogene, tyrosine kinase

mGluR – Metabotropic glutamate receptor

mIPSCs – Miniature inhibitory postsynaptic currents

MMPs – Matrix metalloproteinases

NCoR – Nuclear receptor co-repressor

NECs – Neuroepithelial cells

NF1A – Nuclear factor 1 A

Nkx2.2 – NK2 Homeobox 1

NMDAR – N-methyl-D-aspartate receptor

NMM – Neural maintenance media

Oct4 – Octamer binding transcription factor 4

Pax6 – Paired box protein Pax-6

PBS – Phosphate buffered saline

PFA – Paraformaldehyde

PLC – Phospholipase C

PSD95 – Postsynaptic density protein 95

qPCR – Real-time polymerase chain reaction

RGCs – Radial glia cells

RTT – Rett Syndrome

Sox2 – Sex determining region Y-box 2

Sox9 – Sex determining region Y-box 9

SOD1 – Superoxide dismutase 1

SOD2 – Superoxide dismutase 2

TBOA – DL-threo-β-Benzyloxyaspartic acid

TGF-β – Transforming growth factor β

TNF-α – Tumour necrosis factor α

TRD – Transcriptional repressor domain

TRPC4 – Transient receptor potential cation channel subfamily C member 4

TSP2 – Thrombospondin 2

TTX – Tetrodotoxin

Tuj – βIII-tubulin

VGLUT1 – Vesicular glutamate transporter 1

Wnt – Wingless-related integration site

WT – Wild type

XCI – X chromosome inactivation

YWHAZ – Tyrosine 3-monooxygenase/tryptophan 5-monooxygenase activation protein zeta

List of Figures

List of Tables

Chapter One – Introduction

1.1 What is Rett Syndrome?

Rett syndrome (RTT) is a neurodevelopmental disorder that almost exclusively affects girls (Hagberg et al., 1983). It was first described in 1966 by Dr Andreas Rett, in Vienna (Haas, 1988). It is caused by mutations in the methyl CpG binding protein 2 (MeCP2) gene (Amir et al., 1999), a ubiquitously expressed gene that is highly expressed in the central nervous system (CNS). Whilst considered a rare disease it is the second leading cause of learning difficulty in girls, affecting between 1:10,000 – 1:15,000 individuals (Laurvick et al., 2006). Patients often live into middle and old age, but many require constant care. Their risk of sudden death is also increased compared to the general population (Acampa and Guideri, 2006). There are currently no cures available for RTT; the syndrome can only be managed.

1.2 Symptoms of RTT

Symptoms of RTT are wide-ranging, affecting many physiological functions and behaviours. Symptoms start to appear when girls reach around eighteen months old, usually following a period of seemingly normal development. The disease then progresses in four stages, plateauing in adolescence or early adulthood (Hagberg et al., 1983).

Girls with RTT demonstrate repetitive hand movements such as hand mouthing and hand wringing (Goldman and Temudo, 2012). Some may struggle to use their hands for manual tasks, such as holding cutlery. Problems with mobility are also common, although some patients can learn to walk but this ability can be lost as the disease progresses; many will end up requiring the use of a wheelchair. The specific mutation within the MeCP2 gene also appears to be important, e.g. patients carrying R294X MeCP2 mutations are more likely to result in complex motor abilities being lost (Foley et al., 2011). Other motor changes can include rigidity.

Communication difficulties are another hallmark of RTT. During the progression of the disease affected individuals can become socially withdrawn; they can avoid eye contact and may disliked being touched. These parameters have meant that RTT has been considered an autism-spectrum disorder in the past. The nature of the repetitive hand movements in RTT can be used to differentiate between these patients and those with an autism spectrum disorder (Goldman and Temudo, 2012).

Hyperventilation and breath holding behaviours are present, with 63-95% of patients demonstrating hypo- and hyperventilation during the day, in addition to other types of disordered breathing. The onset of breathing problems tends to occur during early childhood (Mackay et al., 2017). Breath holding, hyperventilation and abdominal bloating were found to have a significant impact on the individual's quality of life, with aberrant breathing behaviours

being associated with dysregulated cardio-respiratory coupling. Patients with p.Arg294* mutations were most severely affected (Mackay et al., 2017).

Cardiac problems are prevalent in girls with RTT. Patients with RTT can have a prolonged QT interval with delayed ventricular repolarisation. Some patients suffer from tachycardia and bradycardia. These cardiac issues are considered as potential contributors towards the higher rate of sudden death in RTT (Acampa and Guideri, 2006).

60-80% of patients develop seizures at around seven years old. Seizures are found to be more frequent in patients with large deletions or T158M mutations in their MeCP2 gene. Seizures are less common in individuals where the MeCP2 mutation is located in the C-terminal of the gene (Operto et al., 2019).

Patients' growth can be slower and their heads are smaller than those without the disease (Armstrong, 1992). 45% of patients in one study had preserved somatic growth and this had positive associations, including better development and fewer seizures. However, microcephaly was persistent amongst all individuals included in the study. Poor growth in RTT correlates with greater disease severity and is associated with mutations prior to the C-terminal end of MeCP2 and the R270X mutation (Tarquinio et al., 2012).

One study has shown that oropharyngeal dysfunction was present in 100% of individuals with RTT with gastroesophageal dysmotility present in 69%. Dysfunction included difficulty using the tongue and absence of waves throughout the gut and reduced peristalsis (Motil et al., 1999).

RTT progresses in four stages (Hagberg et al., 1983):

Stage 1: Symptoms typically start to be noticed after around 18 months, when babies stop reaching expected developmental milestones.

Stage 2: At around one year old the child enters a regressive period. During this time gained skills involving hand movement and language can be reduced or completely lost. Following stage 2, this regression eventually ceases, and the individual enters stage 3.

Stage 3: Their skills can remain stable and can potentially improve during this time. This is the stage where stereotypical repetitive movements can manifest.

Stage 4: This stage commences usually when the individual is in their teenage years or twenties. The stage is also known as the late motor decline stage, as it is here where the individual may lose the ability the walk, if they had learned.

1.3 Pathophysiology of RTT

Brain weight of patients with RTT is reduced by 12.1–33.8% alongside increased ventricle size, compared to healthy age-matched individuals (Armstrong, 1992). Patients with RTT have a

reduction in cerebral volume compared to healthy age-matched individuals but do not show signs of neurodegeneration (Reiss et al., 1993). Specific areas of reduced volume include the frontal and parietal lobes, with relative preservation of the occipital lobe (Carter et al., 2008).

1.4 Genetics of RTT

Two genetic forms of RTT have been described. Typical RTT is caused by loss of function mutations in the MeCP2 gene (Amir et al., 1999). Due to the almost exclusive appearance of RTT in girls, it was hypothesised to be an X-linked disorder (Hagberg et al., 1983). Indeed, MeCP2 was found to be located on the X chromosome, at Xq28 (Sirianni et al., 1998). Atypical RTT can be caused by mutations in the forkhead box G1 (FoxG1) gene (Ariani et al., 2008) or cyclin dependent kinase like 5 (CDKL5) gene (Kalscheuer et al., 2003). However, mutations in FoxG1 are sometimes described as a separate FoxG1 syndrome (Vegas et al., 2018). CDKL5 mutations result in CDKL5 deficiency disorder (Kadam et al., 2019) and whilst being a distinct disorder from RTT, CDKL5 deficiency disorder has some similar symptoms and pathology to RTT, such as seizures and reduced frontal lobe volume (Liang et al., 2011). The neurodevelopmental disorders that result from mutations in FoxG1 or CDKL5 can affect boys. This thesis will discuss the typical version of RTT caused by mutations in MeCP2.

MeCP2 was first identified in 1992 when its location was found to match that of methyl-CpG sites on chromosomes (Lewis et al., 1992) and is now known to bind to methylated DNA. The MeCP2 protein contains a methyl binding domain (MBD), a transcriptional repressor domain (TRD), an N-terminal domain and a C-terminal domain (Hansen et al., 2011). Through alternative splicing MeCP2 has two main isoforms that differ at the N-terminal: MeCP2-e1 and MeCP2-e2 (Kriaucionis and Bird, 2004). E1 is the predominant isoform and is the isoform that is conserved across vertebrates, whereas the e2 isoform is only found in mammals (Tillotson and Bird, 2019). The e2 isoform interacts with FoxG1, a gene involved in neuronal survival and maturation. Both isoforms have been detected in astrocytes, neurons and oligodendrocytes in mouse hippocampi (Olson et al., 2014), and are thought to be functionally interchangeable (Tillotson and Bird, 2019).

In girls with RTT one of their X chromosomes carries the mutant MeCP2 gene and the other will carry a healthy copy of the gene. Early in development one X chromosome is randomly inactivated throughout the blastula (Gartler et al., 1985). This process is known as X chromosome inactivation (XCI). Progeny from these cells will maintain their inactivation status. This results in a mosaic expression of mutant and healthy MeCP2 throughout the body during development. As males have XY chromosomes there is no compensatory healthy MeCP2 gene on the other X chromosome if it is mutated, sadly resulting in death shortly after birth. In one case however, a boy had Kleinfelter's in addition to RTT. His XXY chromosomes meant that he could survive with the condition (Schwartzman et al., 2001).

1.4.1 Clinical variability in RTT

There are over 200 unique mutations in the MeCP2 gene that cause RTT. 5-10% of cases are caused by mutations within the C-terminal, and 60% of cases are caused by one of eight mutations: R168X, R255X, R270X, R294X, R306C, R106W, R133C and T158M (see Figure 1.1) (Neul et al., 2008, Calfa et al., 2011). R168X is one of the most common MeCP2 mutation that causes RTT, accounting for 11.5% of cases (Bienvenu et al., 2002). Mutations in the exon 1 splice variant of MeCP2 do not affect translation the exon 2 variant. Re-expression of MeCP2-e2 can rescue RTT phenotypes in MeCP2-null mice (Kerr et al., 2012).

The clinical severity of RTT can vary depending on the mutation. Those with the R133C mutation or with mutations within the C-terminal are less severely affected (Neul et al., 2008), as MeCP2 carrying this mutation retains the most DNA binding of all RTT-causing mutations (Brown et al., 2016). These individuals are more likely to be able to walk and use their hands. One study found that, after looking at phenotypes such as hand use, mobility and communication skills, the R270X and R255X mutations were most severe, with R133C and R294X being the least (Bebbington et al., 2008).

Most of the mutations that cause RTT are located within the MBD or the TRD (Heckman et al., 2014). Mutations found within this MBD result in more severe symptoms than mutations in other regions of the gene (Fabio et al., 2014). Full length MeCP2 missing this MBD cannot rescue defects in MeCP2 knockdown mice, including dendrite length, branching, synapse number and calcium oscillations. However, the defects could be partly rescued by MeCP2 containing the T158M within the MBD region. This shows the importance of a functioning MBD in the MeCP2 gene (Zhao et al., 2015).

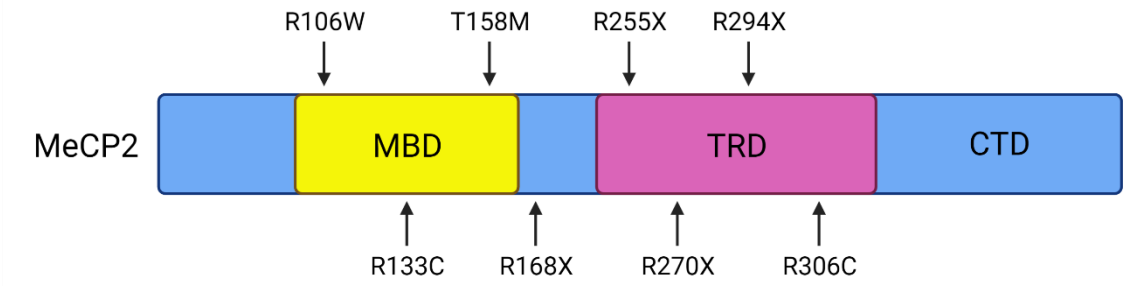

Figure 1.1: Schematic illustrating the MeCP2 gene. Schematic includes the MeCP2 gene with the MBD, TRD and CTD. 8 of the most common RTT-causing mutations are featured. Adapted from (Xu and Pozzo-Miller, 2013).

In addition to particular mutations, around 20% of clinical variability in RTT can be explained by differing levels of cells that express either the mutant or healthy MeCP2 gene, caused by XCI (Neul et al., 2008). This variability can occur amongst individuals with the same mutation.

In individuals with the R168X mutation, their disease severity increased if the number of cells expressing mutant MeCP2 increased. This was also found to be the case with the T158M mutation (Archer et al., 2007).

MeCP2 is central to the development of RTT syndrome. Therefore it is important to consider the cellular function of MeCP2 and how its dysfunction leads to disease.

1.5 The role of MeCP2

MeCP2 was originally thought to be a transcriptional repressor, but further work has indicated its role could be much broader. MeCP2 was found to specifically bind to the promoter of brain derived neurotrophic factor (BDNF), repressing its expression (Chen et al., 2003). DNA methylation is associated with repression and MeCP2 was found to repress methylated genes *in vitro,* in addition to containing a TRD (Nan et al., 1997). This TRD can recruit other corepressors such as Sin3A, histone deacetylase (HDAC) 1 and HDAC2 (Jones et al., 1998) (Nan et al., 1998), further supporting MeCP2's role as a transcriptional repressor (seen in figure 1.2). However, other studies have indicated that the MeCP2 might not be restricted to the repression of specific genes.

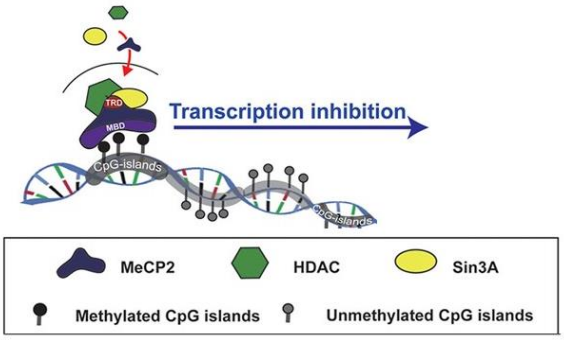

Figure 1.2: MeCP2 binding to methylated DNA. Figure shows MeCP2 binding to methylated DNA and recruiting HDAC and Sin3a, resulting in transcription inhibition (adapted from (Jin et al., 2017).

1.6 Role of MeCP2 in the development and maturation of the CNS

Whilst MeCP2 is expressed in all tissues in humans it reaches the abundance levels of histones in neurons by around 10 years old (Skene et al., 2010) with particular enrichment in the CNS (Balmer et al., 2003). In mice, MeCP2 is expressed first in older structures of the CNS, such as the spinal cord and the brainstem. Its expression then appears in the cortex, with deeper cortical layers expressing it first before the younger more superficial layers (Shahbazian et al., 2002). These data indicate that the appearance of MeCP2 correlates with the development and maturation of the CNS.

MeCP2 is involved in differentiation of cells in the CNS. MeCP2 was found to regulate neural cell differentiation in zebrafish. MeCP2 knockdown in the developing zebrafish brain resulted in a larger amount of Nestin-positive neural progenitor cells, which were also more proliferative when compared to wild type (WT) zebrafish. Following from this their brains had increased expression of glial fibrillary acidic protein (GFAP) and reduced microtubule associated protein 2 (MAP2), indicating an increase in astrocytes and decrease in mature neurons, respectively. MeCP2 usually binds to the inhibitor of DNA binding 1 (id1) promoter in development, inhibiting its expression. However, when MeCP2 is mutated it cannot bind, allowing id1 to be expressed and activate Erb-B2 Receptor Tyrosine Kinase 2 (Her2). This caused an over-proliferation of neural precursor cells (NPCs) (Gao et al., 2015).

Epigenetic regulation of MeCP2 can influence the proliferation and differentiation of adult NPCs taken from mouse hippocampi. When MeCP2 was mutated so that phosphorylation could not occur at S421 the NPCs had a decrease in their proliferation potential but an increase in their differentiation potential, with an increase in cells staining positively for βIII-tubulin (Tuj) and MAP2. Transcriptome analysis showed that this regulation of NPC proliferation and differentiation potential was mediated via the Notch pathway. Decreases in expression of the Notch ligands, receptor and target genes were found, confirmed by chromatin immunoprecipitation (ChIP); the mutated MeCP2 had increased binding at Notch pathway promoters. Overexpressing the Notch intracellular domain (NICD) was able to reverse the decreased proliferation and increased differentiation potential of the NPCs. Interestingly, overexpressing WT MeCP2 did not impact the NPCs, showing that the phosphorylation of MeCP2 is crucial in the regulation of NPC proliferation and differentiation (Li et al., 2014). MeCP2 is also involved in the switch from neurogenesis to astrogenesis (see section 1.11.1).

MeCP2 is integral to the maturation and maintenance of the adult CNS. MeCP2-null mice develop normally until they are 5 weeks old. RTT-like symptoms then commence, and death follows within 6-12 weeks. Their brains are lighter with small neuronal soma, consistent with findings in human RTT brains (Chen et al., 2001a). This highlights the importance of MeCP2 in early development. To assess whether MeCP2 is required during adulthood, a mouse model was created where MeCP2 could be deleted in mature adult mice. Following the deletion, these mice started exhibiting deficits in their behaviour that were similar to that of MeCP-null mice, such as reduced activity, abnormal gait and reduced nest building. Their survival was also reduced compared to WT mice. This shows how MeCP2 is not only required in development but also to the maintenance of the adult brain (McGraw et al., 2011). Further to this, removing MeCP2 from mice at both juvenile and adult stages induces RTT phenotypes. Their hippocampal neurons also showed fewer dendritic branches, with a 50% reduction in levels of synaptic proteins such as N-methyl-D-aspartate receptor (NMDAR) 2A, vesicular glutamate

transporter 1 (VGLUT1) and synapsin 1. Calcium/Calmodulin Dependent Protein Kinase II Alpha (CaMK2α), a protein critical in synaptic plasticity and for stabilising dendritic arbours, had a 50% reduction also (Nguyen et al., 2012).

Mice who had MeCP2 knocked out at 15 weeks old (adulthood) displayed a marked and rapid decline into a severe RTT phenotype, more severe than if MeCP2 was removed at an earlier time point. Their neuronal somas shrank, resulting in an overall shrinkage of the brain. Dendritic arbours shrank by over 50% within a few days, a far more accelerated pace than MeCP2 was removed at 10 weeks (Du et al., 2016). This shows that lack of MeCP2, even when specifically removed at postnatal stages of development, has a detrimental impact on the structure and circuitry of neurons. MeCP2 is therefore vital in maintaining neuronal phenotype in the adult mouse brain. In MeCP2-KO mice MeCP2 is not required for initial generation of neurons in the dentate gyrus of the hippocampus, rather it is involved in the maturation of these neurons (Smrt et al., 2007). Additionally, a number of glial specific genes were found to have elevated expression in post-mortem RTT brains, indicating perhaps that gene repression had been released (Colantuoni et al., 2001).

1.7 Cellular Dysfunction in RTT

At the cellular level, RTT brains do not demonstrate signs of neurodegeneration, atrophy, gliosis, demyelination or neuronal migration defects (Boggio et al., 2010). This raises the question as to what causes the wide range of symptoms experience by RTT patients. The next section will cover some of the cellular dysfunction demonstrated by cells in RTT.

1.7.1 Neuronal Dysfunction in RTT

Neurons in RTT brains have abnormal dendritic branching in certain cortical areas. Pyramidal neurons in layers II and III of the cortex showed reduced dendritic branching (Belichenko et al., 1994). Post-mortem analysis of brain samples from RTT patients show that CA1 neurons of the hippocampus have reduced spine density in RTT, compared to age-matched controls (Chapleau et al., 2009). This finding was also seen in rats that overexpress mutant MeCP2, with further analysis showing that there was a specific reduction in the number of mature spines present but no difference in the number of immature spines. A similar result was noted in rats who overexpressed WT MeCP2 (Chapleau et al., 2009).

Newly generated neurons in the hippocampal dentate gyrus of MeCP2-KO mice display altered density and distribution of dendritic spines (Smrt et al., 2007). This study also identified some of the target genes regulated by MeCP2, including syndecan 2, which is involved in synaptogenesis. It was found to be more highly expressed in MeCP2-KO neurons than in WT (Smrt et al., 2007). This gene, alongside MeCP2, is expressed by mature spines of the neurons in the dentate gyrus and is involved in driving this maturation (Ethell and Yamaguchi, 1999). MeCP2 could negatively regulate this gene in order to control synaptogenesis. Without this

negative regulation syndecan 2 could therefore be more highly expressed and result in more synapses present. Notably, when the WT mice matured between weeks 4-8 the number of synaptic clusters in the molecular layer of the hippocampus decreased. Such an observation was not noted in the MeCP2-KO mice; their synapse cluster number did not change during the same period. VGlut1 immunolabelling has reduced intensity in 2-week-old MeCP2 KO mice (Chao et al., 2007).

In addition to morphological abnormalities there are also functional differences in the synapses in RTT brains. Whole-cell patch-clamp recordings of layer V pyramidal neurons in the S1 cortex of MeCP2-KO mice showed decreased spontaneous EPSCs and action potential firing, with a reduced excitatory drive into layer V. The resultant increased inhibition therefore shows that the excitatory to inhibitory ratio in RTT brains could be awry (Dani et al., 2005).

1.7.2 Microglia Dysfunction in RTT

Microglia in RTT are dysfunctional. Microglia from MeCP2-null mice were cultured and used to generate conditioned media. This media proved detrimental when added to hippocampal neurons; neurons displayed thinner and shorter dendrites with reduced MAP2 intensity. Additionally, synapse number was reduced as demonstrated by a reduction in postsynaptic density protein 95 (PSD95) puncta, though the presynaptic marker synaptophysin was unaffected. The MeCP2-deficient microglia released higher levels of glutamate than WT microglia, which could possibly be the factor behind the toxic effects on the hippocampal neurons. Removing glutamate from the MeCP2-null microglia conditioned media preserved normal dendritic morphology (Maezawa and Jin, 2010).

1.8 Current Treatments

There is currently no cure for RTT and treatments are mainly focussed on symptom management, for example anti-epileptic drugs or laxatives for gastrointestinal problems (Fu et al., 2020). However, insulin-like growth factor 1 (IGF1) is currently being trialled as a potential treatment for RTT. IGF1 is involved in cell proliferation, neurogenesis and neuronal maturation (Brooker et al., 2000), eliciting its effects via activation of the PI3K/mTOR/AKT1 (phosphatidylinositol-3 kinase/mammalian target of rapamycin/serine-threonine-specific protein kinase AKT-PKB), and MAPK/ERK (mitogen-activated protein kinases/extracellular signal-regulated kinases) pathways (Costales and Kolevzon, 2016). Adding IGF1 to RTT neuron and RTT astrocyte co-cultures improved the neuronal neurite length (Williams et al., 2014). It can also cross the blood brain barrier and has shown to improve symptoms and lifespan in MeCP2-null mice, as well as increased synaptic density and EPSC amplitude in these mice (Castro et al., 2014). Recent work has shown that these effects are mediated by downregulation of the Na^+/K^+-ATPase subunit, FXYD Domain Containing Ion Transport Regulator 1 (FXYD1), which is upregulated in MeCP2-mutant mice (Yuan et al., 2020). These

promising results lead to IGF1 being trialled in human RTT patients. Positive results were observed, such as caregivers noting improvement in communication abilities as well as in aberrant breathing behaviours (Pini et al., 2012). However, this trial was not considered a significant success. This indicates that very positive outcomes noted in animal or cell models do not always exactly translate into human trials, necessitating the need for better models of human brain disease.

It is vital that all cell types and their interactions are considered when studying RTT in order to maximise the chance of finding a potential treatment or cure. To achieve this, relevant models must be used so that the most translational data can be generated.

1.9 Models of Human Brain Disease

Animal models, such as mice, are invaluable for studying whole systems, and give us information about disease progression and interventions that could improve symptoms or halt disease. However, the limitations of using animals to model human brain diseases must be recognised; human brains and human brain cells are vastly more complex than those of mice. For example, human astrocytes are much larger than mouse astrocytes and also extend considerably more processes (Oberheim et al., 2009). Chimeric mice that contain human astrocytes demonstrated that human astrocytes propagate calcium waves more quickly than mouse astrocytes and also accentuated excitatory synaptic transmission in the mouse hippocampus. In addition, the human astrocytes affected synaptic plasticity in the brains of these mice, by enhancing long-term potentiation (LTP) in the hippocampi. The chimeric mice also scored better in learning and memory tasks compared to those without human astrocytes (Han et al., 2013). Furthermore, human neocortex contains astrocyte populations that are not present in mice which also adds to the increased complexity of human astrocytes compared to mice (Oberheim et al., 2009). Such results indicate that human astrocytes are significantly different to those from mice, which may limit what mouse astrocytes can tell us about human neurological disease.

Access to human astrocytes also presents a problem as live human brain tissue is in scarce supply as it removed during surgeries for conditions such as epilepsy. Post-mortem tissue only provides information of the very end stages of disease. These limitations mean that mice remain an attractive model for human brain disease.

1.10 The Human Brain

The human brain is responsible for an exceptional myriad of functions that are vital for life. The adult human brain is comprised of 86 million neurons and an equal number of non-neuronal cells, known as glia (Azevedo et al., 2009). This vast number of cells renders the brain hugely complex, especially as our neurons are capable of forming billions of connections (Hawkins

and Ahmad, 2016) in the form of synapses. In addition, there is a complex interplay between the neurons and glial cells, resulting in intricate relationships between multiple cell types that inform brain development, function and disease. Dysfunction within these relationships cause brain disease, at a great societal cost. The cost of brain disorders including dementia, stroke and mental health conditions is thought to cost the UK £112 billion annually, as of 2013 (Fineberg et al., 2013). This does not include the emotional toll these conditions also take on carers and loved ones of those with brain disorders. It is imperative that these conditions are properly funded so that treatments can be found. In order to do this multiple cell types must be considered, with the influence of astrocytes on neurons not being underestimated; re-expression of MeCP2 in astrocytes in a MeCP2-deficient mouse can alleviate many aspects of the RTT phenotype such as improving locomotion, respiratory problems, and prolonging their lifespan. Notably, the re-expression of MeCP2 in these astrocytes also exhibited a beneficial effect on the neurons *in vivo*, increasing the number of dendrite branches by 25% after treatment (Lioy et al., 2011).

In order to understand the nature of these diseases it is imperative that appropriate models are developed to study neurodevelopment and homeostasis in both health and disease in order to understand the role that different cells play.

1.11 Neurodevelopment in Health and Disease

Every tissue in the body arises from one of the three germ layers: endoderm, mesoderm and ectoderm. These layers are formed early during development. At embryonic day 13 (E13) a process called gastrulation commences. At this point the embryo is a two-layered structure, consisting of epiblast cells (the upper layer) and hypoblast cells (the lower layer). A groove appears in the embryo, known as the primitive streak. Epiblast cells start to migrate through this streak, eventually passing underneath the upper layer of cells. The cells that migrated deepest form the endoderm; the shallower cells form the mesoderm. Cells that remained in the upper layer form the ectoderm. The cells of the endoderm form the gut and respiratory system, and the mesoderm forms muscle, bones and heart. The epidermis and cells of the nervous system both arise from the ectoderm. The only exception to this are the microglia, the immune cells of the central nervous system (CNS); these arise from the mesoderm (Stiles and Jernigan, 2010a).

To further differentiate the ectoderm into the epidermal ectoderm and the neuroectoderm, the epiblast cells that migrated to the primitive streak have to pass a signalling centre known as the primitive node (known as Spemann's organiser in amphibians). This node secretes bone morphogenetic protein (BMP) antagonists such as chordin and noggin, forming a gradient (Bond et al., 2012). This causes a series of gene expression changes in the cells that migrate past it. The cells that were exposed to high levels of BMP antagonists migrate beneath the

upper layer they produce a protein that binds to the surface of the upper cells, causing them to differentiate into the neuroectoderm. This area becomes known as the neural plate (Stiles and Jernigan, 2010a).

The neural plate must then form the first defined structure in the development of the human nervous system: the neural tube. Two ridges form either side of the neural plate, which eventually close to form the neural tube. NPCs form a single layer that line the neural tube. The neural tube forms the basis of the entire CNS. A rod called notochord extends beneath the neural tube which secretes Sonic Hedgehog (Shh). This activates Shh release in the ventral portion of the neural tube, whilst the dorsal side secretes BMP. The two morphogen gradients mutually inhibit each other, resulting in varying overlapping domains that trigger gene expression. This creates a pattern than gives rise to the different cells of the neural tube and ultimately the CNS, including neurons, astrocytes and oligodendrocytes (Patten and Placzek, 2000). Further patterning molecules also help generate different areas of the CNS by forming morphogen gradients, such as fibroblast growth factor (FGF) and wingless-related integration site (Wnt) (Paridaen and Huttner, 2014). The rostral end of the neural tube will form the brain, with the hollow centre of the neural tube eventually forming the complex ventricular structure of the brain (Stiles and Jernigan, 2010b).

The human brain contains 86 billion neurons, with the six-layered neocortex being the structure that carries out all higher functions considered unique to humans. The development of this neural structure requires carefully orchestrated timing and differentiation of all cell types. The brain starts with the neural tube. The neural tube wall is initially formed of neuroepithelial cells (NECs) which undergo a switch in identity to form radial glia cells (RGCs). What causes this switch to occur is incompletely understood, but the transient expression of FGF10 by NECs is necessary for this switch, with the knockdown of FGF10 resulting in a delay in NEC to RGC transition (Sahara and O'Leary, 2009). RGCs are bipolar cells whose cell bodies reside in the proliferative ventricular zone and have processes that span to the pial surface (Götz et al., 1998). Consequently, they are capable of dividing and generating daughter cells and can provide scaffolding for migrating neurons (Nadarajah and Parnavelas, 2002). RGCs initially divide symmetrically, but switch to asymmetric division at the onset of neurogenesis (Paridaen and Huttner, 2014), forming another RGC and a differentiated cell such as a neuron.

The patterning of the neural tube results in RGCs that may produce different differentiated cell types during the neurogenesis period. For example, RGCs in the dorsal telencephalon were found to express the basic helix-loop-helix (bHLH) proneural genes neurogenin (Ngn) 1 and 2 and give rise to glutamatergic pyramidal neurons, whereas RGCs in the ventral telencephalon express Genomic Screened Homeo Box (Gsx) 1 and 2, NK2 Homeobox 1 (Nkx2.1) and Achaete-Scute Family BHLH Transcription Factor 1 (Ascl1). Ascl1 helps instruct the formation

of the inhibitory GABAergic interneurons (Paridaen and Huttner, 2014). Interneurons are the only cortical neurons not to form in the ventricular zone, but rather tangentially migrate to the ventricular zone from the ganglion eminences of the ventral or subpallial telencephalon (Marín and Rubenstein, 2001). They then utilise RGCs to migrate into the cortex. Neurogenesis can be regulated by the transcription factor paired box protein pax 6 (Pax6). Pax6 can promote the proliferation of RGCs whilst also promoting neurogenesis via initiating transcription of Ngn 1 and 2 (Sansom et al., 2009). Pax6 can bind directly to other genes that are involved in neurogenesis, such as Ascl1, Hes1 and Neurog2 (Sansom et al., 2009).

The cortex develops in an 'inside-out' manner, with younger neurons forming the lower layers and later stage neurons forming the outer layers. The first neurons to form in the cortex are Cajal-Retzius cells. These cells secrete Reelin, a glycoprotein that helps guide neurons to the correct layer of the cortex. Newer neurons migrate past previous neurons until they reach the area of Reelin signalling where they then stop. Mutations in Reelin prevent the correct organisation of the neocortex. The molecule was called Reelin because mutations caused a distinct 'reeling' phenotype in the Reeler mutant mouse (Falconer, 1951).

1.11.1 Neuron to Astrocyte Switch

Neurons are not the only cell type that is required in the formation of the neocortex. Astrocytes are also vitally important to brain development and their arrival is strictly regulated and timed. Neurons appear before astrocytes during the development of the nervous system (Bayer and Altman, 1991). Later, RGCs themselves directly differentiate into astrocytes (Kanski et al., 2014). In rat, precursors isolated at a time of peak neurogenesis only differentiated into neurons (Ghosh and Greenberg, 1995). However, precursors that were taken later differentiated into astrocytes (Bonni et al., 1997). The timing of this switch is very tightly regulated in order to ensure the correct proportions of each cell type are present in the brain. A number of pathways are involved in ensuring the correct timing of this switch.

The appearance of astrogenic factors is not sufficient to trigger astrogenesis. Leukaemia inhibitory factor (LIF) is an example of this as, despite being an astrogenic factor, early cortical NPCs in mice do not become astrocytic when exposed to it (Fan et al., 2005). Instead, NPCs must gradually acquire the ability to respond to such cues. As mentioned previously, Ngn1 is critical for the development of neurons. It functions as a transcriptional activator, with overexpression of Ngn1 resulting in an increase number of NPCs that become neurons. Ectopic expression of Ngn1 can also prevent astrogenesis from occurring, even in the presence of astrogenesis-inducing cytokines. It does so by sequestering the transcriptional activator complex CBP/p300 and SMAD and preventing it from binding to astrocyte gene promoters (Sun et al., 2001).

During neurogenesis, Ngn1 and another bHLH transcription factor Mash1 inhibit astrogenesis by inhibiting the Janus kinase/signal transducer and activator of transcription proteins (Jak/Stat) pathway. They achieve this by competing for the p300 binding site and by directly inhibiting Stat (Sun et al., 2001). Therefore, the components required for the Jak/Stat pathway remain insufficient to initiate astrocyte-specific genes. However, during development Ngn1 levels decrease, removing the inhibition on the Jak/Stat pathway. The decrease in Ngn1 is thought to be mediated by the Polycomb group of proteins, which accumulate during astrogenesis and may be responsible for inhibiting Ngn1 by remodelling chromatin (Hirabayashi et al., 2009). This is one example of how NPCs may become competent to respond to factors that promote astrogenesis.

Notch/Delta signalling is also instrumental in the timing of neurogenesis to astrocytes. The Notch signalling pathway is crucial for maintaining NPC populations during development and preventing neurogenesis from commencing too early. Notch can be activated by delta, serrate and jagged, which are expressed on neighbouring cells. The causes the Notch intracellular domain (NICD) molecule to be produced. This translocates to the nucleus, binds to RBP-J and activates hairy and enhancer of split (Hes) 1 and 5. Hes1, as mentioned previously, is involved in RGC development. It is a basic helix-loop-helix protein which represses the transcription of genes that promote neurogenesis, such as Mash1 (Ishibashi et al., 1995). Hes1-deficient mice have premature differentiation of neurons due to premature Mash1 expression, preventing precursor formation. This results in neural tube defects (Kageyama and Ohtsuka, 1999). Infecting mice with a constitutively active form of Notch blocks neurogenesis. This can be alleviated by knocking out Hes1 and 5, showing that these genes are essential in the timing of neurogenesis (Ohtsuka et al., 1999).

Activation of Notch signalling also induces the demethylation of the GFAP promoter via activating nuclear factor I-a (NFIA) has also been identified as a crucial regulator of the neurogenesis to astrogenesis switch (Takouda et al., 2017). Transient expression of NFIA in the presence of other astrocytic factors also promotes astrocyte differentiation of stem cells (Tchieu et al., 2019). It is also required for the onset of astrogenesis in the spinal cord (Deneen et al., 2006).

NFIA can also form a complex with Sox9, which appears before NFIA. Ectopic expression of Sox9 is sufficient to initiate the expression of astrocytic markers such as glutamate and aspartate transporter 1 (GLAST) in embryos, but is incapable of doing so in the absence of NFIA (Kang et al., 2012). The same authors found that Sox9 was in fact responsible for the initiation of NFIA expression, rather than Notch. In mouse spinal cord, specific ablation of Sox9 resulted in a lack of astrocytic differentiation and reduced numbers (Stolt et al., 2003). NFIA induction at E11.5 in mice correlates strongly with the commencement of astrogenesis and is

triggered by the transcription factor Sox9. The NFIA/Sox9 complex is vital for the onset of astrogenesis. Specifically removing Sox9 from NPCs in mice resulted in a delay in the appearance of GLAST expression in the ventricular zone of the developing spinal cord, along with a delay in NFIA expression. Additionally, the NFIA/Sox9 complex is also integral in triggering the expression of genes that are necessary for gliogenesis, for example in glia metabolism, proliferation and migration. Fifteen genes were found to contain binding sites for both NFIA and Sox9 of which eight appeared between E11.5 and E12.5, indicating their possible role in astrogenesis. Three of these genes could restore astrogenesis in the absence of NFIA and Sox9: Apcdd1, Mmd2 and Zcchc24 (Kang et al., 2012).

Another switch mechanism is mediated by MeCP2. MeCP2 binds to the methylated CpG sites on the GFAP promotor (Setoguchi et al., 2006). This methylation is critical for preventing premature onset of astrogenesis. MeCP2 recruits HDACs and histone methyltransferases to remodel chromatin into an inactive form, inhibiting the gene. Mouse embryos with a mutation in DNA methyltransferase I (Dnmt1) demonstrated an increase in astrocytic protein levels such as GFAP and S100β in their brain and spinal cord tissues compared to their WT counterparts. In addition, GFAP staining was detected at embryonic day 12 (E12), whereas in WT this staining did not appear until E14. This has also been demonstrated *in vitro* using primary cultures. Premature onset of astrogenesis in these Dnmt1 knockout cells occurred at the expense of neurogenesis. As neurogenesis progresses towards astrogenesis the methylation on CpG sites in astrogenesis genes, such as GFAP, S100b and Stat1, decreases. As MeCP2 is no longer able to bind the chromatin remodelling allows other proteins to bind, initiating the transcription of astrogenesis associated genes (Fan et al., 2005).

Two pathways that are also involved in astrogenesis are the Jak/Stat pathway and the BMP pathway. In the Jak/Stat pathway CNTF (ciliary neurotrophic factor), IL6 (interleukin 6) and LIF act on cell surface membrane receptors that share the gp130 co-receptor. Binding of these cytokines activates tyrosine kinases in the Jak family which go on to phosphorylate and activate Stat1 and 3. These dimerise, translocate to the nucleus and initiate gene transcription of astrocytic genes, including GFAP (Kessaris et al., 2008). The BMP pathway acts through serine-threonine kinase cell-surface receptors. Upon BMP binding the receptors become phosphorylated and activate SMAD proteins. GFAP has binding sites for both Stat3 and SMAD1, showing how these two pathways can interact (Nakashima et al., 1999). Once bound, Stat3 and SMAD1 are bridged by the p300/CBP binding protein. This complex can also bind RNA polymerase II, leading to an increase in transcription. This shows how both pathways could collaborate in astrogenesis (Janknecht et al., 1998).

After astrogenesis, the process of astrocyte maturation is also highly important. BDNF is very involved in astrocytic morphogenesis during maturation, as astrocytes highly express the

BDNF receptor TrkB. Treating rodent primary astrocyte cultures with BDNF for 24 hours resulted in their complexity increasing 2-fold. Removing all BDNF from the media inhibited this increase in complexity. TrkB.T1 receptor KO mice did not display an increase in astrocytic volume between PND 14 and 28, despite being the case in WT mice and with no difference being observed at PND 14. Astrocytes isolated from the KO mice also did not respond to BDNF with an increase in morphological complexity, whereas astrocytes from the WT mice did (Holt et al., 2019).

The presence of neurons is also vital to the maturation of astrocytes, with neuronal activity driving the expression of astrocytic genes. Such genes included those involved in the astrocyte-neuron lactate shuttle. Additionally, the presence of rat neurons drive human primary astrocytes to form the stellate morphology *in vitro*, the morphology mostly found *in vivo*. When astrocytes are removed from these neurons, the astrocytic gene profile is downregulated (Hasel et al., 2017). This shows the importance of the presence of other cell types in the development of others.

Unfortunately, the highly regulated process of neurodevelopment can go wrong, resulting in neurodevelopmental disorders, such as RTT.

1.12 The Role of Neurons

Following neurodevelopment and the generation of the cell types of the brain, it is then important to consider the individual properties of these cells and the role they play in maintaining brain health and function.

Neurons are electrically excitable cells that form billions of connections throughout our bodies and brains. Their functions, morphology and molecular biology are vastly heterogeneous. They can form connections called synapses between each other, a process which can be highly plastic even in the adult brain. Around 80% of our neurons are excitatory and 20% are inhibitory, depending on the brain region.

To communicate with each other, neurons generate action potentials. These are electrical signals that can propagate along axons and trigger neurotransmitter release at the synapse that can then activate the postsynaptic neuron. The understanding of how these are generated came from seminal work from Hodgkin and Huxley on squid giant axons. Using electrodes they measured the first action potential (Hodgkin and Huxley, 1939) but then had to stop their exciting work due to World War Two (Schwiening, 2012). Following the war they returned to their collaboration and used voltage-clamping to measure the ionic currents flowing across the giant axon membrane (Hodgkin et al., 1952). This lead them to develop a mathematical model of the action potential, based on previous work they had performed on currents formed by specific ions and membrane properties (Hodgkin and Huxley, 1952).

In order to generate action potentials neurons must maintain a negative membrane potential of -70mV. This maintenance requires a Na^+/K^+-ATPase to pump out three positively charged sodium ions and pump in two positively charged potassium ions. This ensures that the inside of the neuron is negatively charged relative to the outside. This is known as the resting membrane potential. Maintaining the resting membrane potential requires a huge amount of ATP and helps explain why the human brain uses around 20% of all oxygen and therefore energy produced by the body (Raichle and Gusnard, 2002).

If the neuron is stimulated sufficiently, the membrane potential increases. If it reaches a critical point, around -55mV, an action potential can be fired. This point is known as the threshold potential. Once the threshold potential is reached, voltage-gating sodium channels open. This results in an influx of positively charged sodium ions which further depolarise the neuronal membrane. The depolarising positive charge can propagate down the axon as sodium ions diffuse along it opening voltage-gated sodium channels, depolarising further regions and opening more voltage-gated sodium channels. This process is significantly faster in myelinated neurons as the voltage-gated sodium channels are only located at the nodes of Ranvier so the positive charge can move in a process known as saltatory conduction. The membrane then enters a refractory period where no more action potentials can be generated. This is because voltage-gated sodium channels close and cannot be reactivated for a short period. This prevents the action potential from travelling backwards. As the membrane potential approaches 40mV voltage-gated sodium channels begin to close and voltage-gated potassium channels start to open. Potassium ions then start to flood out of the neuron, repolarising the membrane. After a period of hyperpolarisation the resting membrane potential is reached again.

When an action potential reaches the synaptic knob it can cause neurotransmitter to be released. The depolarisation causes voltage-gated calcium channels to open, causing calcium to enter the cell. This calcium then binds to synaptic vesicles containing neurotransmitter and causes them to fuse with the presynaptic membrane. Neurotransmitter is then released into the synaptic cleft and can then bind to receptors on the postsynaptic neuron. This can then trigger an action potential in the postsynaptic neuron.

Neurons can be highly specialised depending on the area of the brain they are in, depending on the functions they need to carry out. They are hugely heterogeneous and can be categorised based on their morphology, maturity or their predominant neurotransmitter, such as glutamate or GABA, the main excitatory and inhibitory neurotransmitters in the CNS respectively.

1.13 The Role of Astrocytes

Astrocytes have long been overlooked as mere passive players in the CNS. The concept of glia was coined in 1852 as '*Nervenkitt'* or nerve glue. In 1856 Rudolf Virchow described glia as "cement that binds the nervous elements together", this being in line with the theory at the time that the nervous system was a continuous network rather than one made up of individual cells (Bellot-Saez et al., 2017). Later, exquisite drawings by Ramon y Cajal in 1897 showcased the morphological heterogeneity of glia cells, highlighting the fact that glia comprise of different cell types. Traditionally astrocytes were subdivided into either fibrous or protoplasmic astrocytes, present in the white and grey matter respectively (Molofsky et al., 2012). However, it is now realised that there is far larger scale of diversity amongst astrocytes.

Astrocytes have a huge influence on neuronal activity and neuronal health, being in close proximity to sometimes thousands of synapses (Bushong et al., 2002). The relationship between astrocytes and neurons is integral to normal brain function. The functions of astrocytes are immensely wide-ranging, with an overview of some of these functions depicted in figure 1.2. They take up excess potassium and glutamate released from neurons during action potentials (Sofroniew and Vinters, 2010). Additionally they are involved in synaptogenesis, have roles in the immune system (Farina et al., 2007) and are key in brain metabolism. They are also integral to the maintenance of the blood brain barrier (Heithoff et al., 2020). Such was their instrumental role in supporting neurons and synapses, the phrase 'tripartite synapse' was coined in the 1990s, consisting of the pre- and post-synaptic neuron, alongside the astrocyte (Araque et al., 1999). This acknowledged the integral ways astrocytes can modulate the traditional synapse.

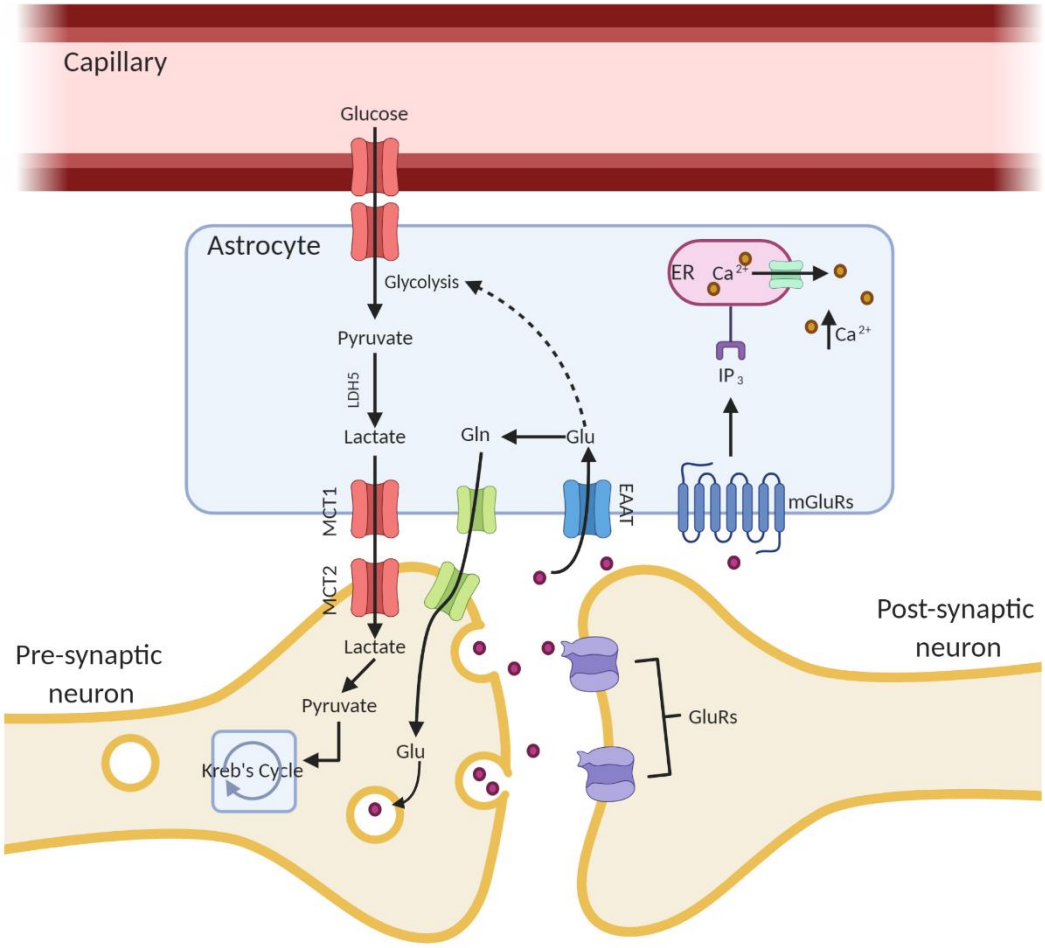

Figure 1.3: Diagram displaying overview of astrocytic functions. Astrocytes remove glutamate (Glu) from the synaptic cleft released by pre-synaptic neurons, taking it up through EAATs. The glutamate can then be converted to glutamine (Gln) which is released back to the pre-synaptic neuron. This is then converted back to glutamate and repackaged into vesicles for release. Glutamate taken up can also trigger glycolysis, generating pyruvate which is converted to lactate via lactate dehydrogenase 5 (LDH5). This is released to the pre-synaptic neuron where it is converted to pyruvate via lactate dehydrogenase 1. This can then enter the Kreb's Cycle to provide ATP for the neuron. Astrocytes can also take up glucose directly from the blood which can also undergo glycolysis to provide lactate for neurons. Glutamate can trigger metabotrophic glutamate receptors (mGluRs) on astrocytes, releasing IP_3 which acts on receptors on the endoplasmic reticulum (ER). This causes calcium (Ca^{2+}) release from the ER, raising intracellular calcium concentration within the astrocyte.

1.13.1 Potassium buffering

Potassium homeostasis is vital to normal brain function. The normal extracellular concentration of potassium in the CNS is maintained between 2.8-3.2mM (Somjen, 1979). This can increase to 12mM during intense neuronal activity, but normal physiological activity results in the extracellular potassium concentration increasing by around 1mM (Larsen et al., 2016a) due to potassium flooding out of repolarising neurons during action potentials. If this potassium remains it can make neuronal membranes hyperexcitable due to the resting membrane potential being shifted closer to the threshold potential. Action potentials could therefore fire more readily in response to inappropriate stimuli, an undesirable event. Astrocytes can take up excess potassium as their membranes are highly permeable to potassium, and so are able to take up excess potassium due to their large number of potassium channels, such as Potassium Inwardly Rectifying Channel Subfamily J Member 10 (Kir4.1) (Chever et al., 2010). Kir4.1 is an inwardly rectifying potassium channel, allowing inward currents of potassium (Ohno, 2018). It can exist on its own or form a heterodimer with Potassium Inwardly Rectifying Channel Subfamily J Member 16 (Kir5.1). Both Kir4.1 and Kir4.1/Kir5.1 are integral to the potassium buffering capabilities of astrocytes. In mice, knocking out the Kir4.1 gene resulted in reduced potassium clearance and seizures (Djukic et al., 2007) showcasing the importance of astrocytes in potassium homeostasis and the impact its dysfunction can have on the brain. Mutations in Kir4.1 also causes EAST (epilepsy, ataxia, sensorineural deafness and tubulopathy) syndrome in humans (Bockenhauer et al., 2009). In addition to Kir4.1, the astrocytic Na^+/K^+-ATPase can also help remove K^+ from the synaptic cleft during times of high activity (Larsen et al., 2016b).

1.13.2 Glutamate uptake

In addition to potassium clearance, astrocytes are able to clear excess glutamate via excitatory amino acid transporters (EAATs), namely glutamate transporter 1 (Glt1) and GLAST, also known as EAAT2 and EAAT3 respectively (Rothstein et al., 1996). These transporters take up glutamate, requiring one molecule of ATP each cycle, rendering the process very energy intensive. The glutamate can be converted within the astrocyte to the biologically inactive molecule glutamine which is transported back to the neuron. The neuron can convert glutamine back to glutamate, showcasing some efficient recycling. Part of the glutamate taken up by astrocytes can also enter their citric acid cycle and be used for energy (Murphy-Royal et al., 2017). NMR studies have shown that 13C-glutamate added to culture media results in more lactate than glutamine incorporating the 13C, something which could only occur via the citric cycle (Sonnewald et al., 1993). It has also shown to be metabolised to α-ketoglutarate (McKenna et al., 2016).

Removing excess glutamate from the synaptic cleft is important as inhibition of glutamate transporters has negative and sometimes irreversible consequences for surrounding neurons,

including increased extracellular glutamate concentration and neuronal death from excitotoxicity due to excess stimulation (Selkirk et al., 2005, Rothstein et al., 1996). Indeed, excitotoxicity plays a role in a number of neurodegenerative diseases such as Alzheimer's Disease and amyotrophic lateral sclerosis (ALS) (Dong et al., 2009). This has been shown to be at least partly caused by glutamate uptake dysfunction in astrocytes (Sheldon and Robinson, 2007). However, extracellular glutamate can also trigger internal calcium release from astrocytes (Cornell-Bell et al., 1990), which in turn causes them to release glutamate which can help coordinate neuronal activity (Mahmoud et al., 2019). Such a process was called 'gliotransmission', discussed in section 1.13.3.

In addition, this glutamate can diffuse outside of the synaptic cleft and cause glutamate spillover that results in synaptic crosstalk (Asztely et al., 1997). Due to the potential of glutamate spillover the positioning of astrocytic processes near synapses can be important. The spillover of glutamate that results in activation of other postsynaptic neurons can remodel dendritic spines and form new synapses. Again, inhibiting glutamate uptake by astrocytes prevented this remodelling from occurring (Verbich et al., 2012). Therefore, the role of astrocytes in glutamate uptake also has implications for synaptic plasticity and remodelling in the brain.

1.13.3 Calcium dynamics and gliotransmission

Astrocytes exhibit spontaneous calcium oscillations *in vitro*, *in situ* and *in vivo* (Fatatis and Russell, 1992, Parri et al., 2001, Hirase et al., 2004). Spontaneous calcium oscillations are intrinsic to the astrocyte and do not rely on neurotransmitter release, as demonstrated by inhibiting exocytosis in brain slices. Instead, the oscillations arise in a calcium-dependent manner that triggers calcium release from internal stores (Parri and Crunelli, 2003). Spontaneous oscillations are dependent on internal stores of calcium and can spread as a wave throughout the astrocyte network, resulting in NMDA-dependent activation of nearby neurons. The number of spontaneously active astrocytes decrease significantly through postnatal day 4 – 14, indicating that these oscillations could play a part in development and the generation of neuronal circuits. The role of NMDA in particular indicates that these oscillations could play a part in synaptic strengthening (Parri et al., 2001).

Astrocytes also express a wide range of G-protein coupled receptors (GPCRs) that can respond to endogenous neurotransmitters. Hippocampal CA1 astrocytes can respond to ligands that activate purinergic, adrenergic, muscarinic, glutamatergic, GABAergic and endocannaboid receptors, all of which cause an increase of calcium (Agulhon et al., 2008). Both forms of calcium increases can affect neuronal activity. There are multiple mechanisms that are responsible for astrocytic increases in calcium. The most studied is the IP_3R-dependent pathway that requires exogenous stimulation from ligands. Astrocytes preferentially

express IP_3R2, and neurons IP_3R1 and 3. The activation of the metabotropic glutamate receptors (mGluRs) on the astrocyte membrane causes activation of phospholipase C (PLC) which hydrolyses phosphatidylinositol 4,5-bisphosphate to generate DAG and IP_3. IP_3 can then activate IP_3R2 and cause calcium release from the endoplasmic reticulum (Agulhon et al., 2008).

Stimulation of astrocytes by neurotransmitters can also impact neuronal function. The stimulation of glutamatergic neurons in rat slices was found to trigger calcium waves in adjacent astrocytes (Dani et al., 1992). Later, it was found that astrocytes could respond to glutamate released from synapses with increases in intracellular calcium (Porter and McCarthy, 1996), with glutamatergic stimulation of one astrocyte also being able to trigger a calcium wave across the astrocyte syncytium, demonstrating their capability for long-range signalling (Cornell-Bell et al., 1990). Exocytosis was blocked in Müller cells (a subset of astrocytes) in the retina, which resulted in inhibition of vesicular glutamate release (Slezak et al., 2012). Astrocytes can release glutamate when their intracellular calcium levels increase, which can then stimulate neighbouring neurons and cause a neuronal rise in calcium (Parpura et al., 1994). This has also been observed with inhibitory neurons in the hippocampus. Direct stimulation of astrocytes resulted in potentiated miniature inhibitory postsynaptic potentials (IPSCs) in the inhibitory neurons. However, this effect was abolished when BAPTA was administered to prevent astrocytic calcium signalling (Kang et al., 1998). Such evidence indicates that astrocytes can perhaps ‘listen’ to synapses and respond in order to modulate synaptic activity. This astrocytic involvement in neuronal activity was what gave rise to the term ‘tripartite synapse’.

However, the astrocytic role of gliotransmission is still disputed (Sloan and Barres, 2014), with a summary of the arguments both for and against gliotransmission summarised in a recent review (Savtchouk and Volterra, 2018). The main criticism against the notion of gliotransmission came from the observation that a mouse model thought to specifically inhibit vesicle release in astrocytes by inhibiting SNARE driven by a GFAP promoter had a large effect on processes such as LTP, previously thought to be only neuronal in nature (Pascual et al., 2005). However, another group noted that this SNARE inhibition was also observed in neurons due to leaky expression of the dominant negative SNARE (Fujita et al., 2014). The group therefore postulated that the results seen from blocking exocytosis in astrocytes could have been due to the exocytotic blockage affecting neurons also, therefore casting doubt on findings in such studies (Pascual et al., 2005). Rodent astrocytes isolated by immunopanning also did not demonstrate glutamate release in response to ATP stimulation (Foo et al., 2011). However, rodent astrocytes stimulated with bradykinin to increase their internal calcium concentration responded with glutamate release (Parpura et al., 1994).

Astrocytes were also found to express very little of other genes associated with exocytosis, such as synaptotagmin, a necessary protein for calcium-mediated exocytosis (Zhang et al., 2014). However, it is important to consider that transcriptome level data does not always reflect the proteome. Other studies have demonstrated that astrocytes do contain exocytotic machinery as well as VGLUTs, required to transport glutamate into vesicles (Zhang et al., 2004, Montana et al., 2004). Pharmacological inhibition of these VGLUTs prevented calcium-mediated glutamate release from astrocytes (Montana et al., 2004).

However, astrocytes in the cerebellum have also been observed to release GABA via non-vesicular means. They released GABA via the Bestrophin 1 anion channel, with blocking of this channel resulting in removal of tonic inhibition in the cerebellum (Lee et al., 2010).

Another criticism levelled at these studies that are in support of gliotransmission are that they are only performed in cultured cells, but such studies are performed in freshly isolated primary rodent cells (Montana et al., 2004). Other work has shown that astrocytes remain mature for a few days after removal from co-culture (Hasel et al., 2017), possibly this would be the case with removal from *in vivo* to *in vitro* also. However, the criticism that monocultures receive, and their lack of physiological relevance only enhances the need to develop more complex models, even though this will add a level of complexity that could present its own problems.

1.13.4 Neurovascular coupling

Neurovascular coupling is the mechanism by which the brain increases blood flow to areas that require more oxygen and glucose. Astrocytes are ideally situated to regulate blood flow throughout the brain, with their endfeet enveloping capillaries, observed by Santiago Ramón y Cajal. Astrocytes are able to release vasoactive substances in order to trigger vasoconstriction and vasodilation, thought to be mediated by astrocytic calcium activity (Filosa et al., 2016). Such substances could be by-products of arachidonic acid such as prostaglandins, produced by astrocytes after activation of their mGluRs by glutamate (Attwell et al., 2010).

1.13.5 Metabolic support

The brain is a very metabolically demanding organ, requiring 20% of all energy the body produces (Erbsloh et al., 1958) despite only comprising 2% of our body weight. In particular, it is neurons that are responsible for this greediness as they require a large amount of ATP for their Na^+/K^+-ATPases to function in order to maintain their resting membrane potential (Deitmer et al., 2019).

Astrocytes are ideally situated in order to provide metabolic support to neurons, as they are in close contact to both neurons and capillaries. Astrocytic endfeet can wrap capillaries (Mathiisen et al., 2010) and also express the glucose transporter, Glut1 (Vannucci et al., 1997), so that glucose can enter astrocytes via facilitated diffusion. This glucose is rapidly phosphorylated inside the astrocyte, ensuring a strong gradient of glucose into the cells. It can

be either stored as glycogen, a large, branched polysaccharide of glucose accumulated around a glycogenin core, or it can be metabolised via the glycolytic pathway. The end product of glycolysis is pyruvate, which can be converted to lactate within the astrocyte by lactate dehydrogenase 5 (LDH5) and exported to neighbouring neurons via monocarboxylate transporter 1 (MCT1). The neuron can then take up the lactate via MCT2 and convert it back to pyruvate with lactate dehydrogenase 1 (LDH1) (Pierre et al., 2000, Bittar et al., 1996). Pyruvate can then enter Kreb's cycle in the neuron. This is the basis of the 'Astrocyte-to-neuron lactate shuttle', or ANLS (Magistretti et al., 1999).

This metabolic support of neurons by astrocytes is disputed (Mangia et al., 2009), citing that the glucose uptake of astrocytes would have to be significantly increased for there to be an ANLS. However, it has been observed that neurons cultured alone do not survive very long, whereas when co-cultured with glia neurons survived longer (Whatley et al., 1981). This beneficial effect is dependent on the presence of glycogen within the astrocytes (Swanson and Choi, 1993). Increasing or decreasing the glycogen content of neighbouring astrocytes impacted the number of action potentials a rodent optic nerve could fire. Incubating astrocytes with glucose prior to the experiment in order to increase glycogen content resulted in a longer time period before action potentials were unable to fire. Inhibiting the breakdown of glycogen using a glycogen phosphorylase inhibitor resulted in a shorter time to action potential firing failure (Brown et al., 2005). This indicates that astrocytic glycogen and metabolism is necessary to sustain neuronal activity.

A further argument for astrocytic metabolic support of neurons is that astrocytes are the main source of glycogen in the brain, and contain the enzymes required to synthesise and metabolise glycogen, glycogen synthase and glycogen phosphorylase respectively. Neurons do not store glycogen apart from in some pathological states such as in Lafora disease (Gentry et al., 2018). Astrocytes do not possess the enzymes to break glycogen down into free glucose, rather it is broken down into pyruvate, showing that the by-products of glycogen breakdown are perhaps not intended for astrocytic use. Also, glycogen granules are most prevalent in areas that have high synaptic density (Brown and Ransom, 2007). These granules are more localised to excitatory axonal boutons that to dendritic spines (Cali et al., 2016). Such evidence supports the role of astrocytic glycogen in neuronal support.

Lastly, neuronal activity and subsequent glutamate release can also trigger glycolysis within neighbouring astrocytes, evidenced by levels of glucose phosphorylation. Blocking glutamate transporters prevented glucose phosphorylation, as did replacing the Na^+ in the cell media after stimulation with glutamate. This shows that astrocytes respond to glutamate release by metabolising glucose in a Na^+-dependent manner (Pellerin and Magistretti, 1994b). A later study showed that stimulating astrocytes with glutamate increased the activity of the astrocytic

Na^+/K^+-ATPase (Pellerin and Magistretti, 1997). This could be to compensate for the entry of Na^+ via the glutamate/Na^+ co-transporter; the Na^+/K^+-ATPase would need to remove Na^+ in order to maintain the Na^+ concentration gradient so that glutamate could continue to be taken up by the astrocyte in times of high neuronal activity. Neuronal activity also boosts astrocyte glucose metabolism in order to increase lactate export (Hasel et al., 2017).

1.13.6 Immune response

Astrocytes play a role in the immune system. Disease and traumatic injury can cause astrocytes to undergo a process called 'reactive astrogliosis'. Astrocyte reactivity has been found in neurodegenerative diseases, and reactive astrocytes form a glial scar in spinal cord injury (Fawcett and Asher, 1999). To make matters complicated, it is impossible to declare whether astrocytic reactivity results in a beneficial or detrimental effect on surrounding neurons. Many studies have shown how detrimental astrocytes can be to neurons when they are reactive, both in injury and disease states (Nagai et al., 2007). However, the presence of reactive astrocytes has been shown to be necessary to facilitate the healing of spinal cord injury in mice. Ablating reactive astrocytes resulted in neuronal death and demyelination in the spinal cord, resulting in motor deficits in the mice. This did not occur in the control mice (Faulkner et al., 2004). It could be that certain aspects of inflammation are beneficial, whilst others are not. A more targeted approach to modulating inflammation might be beneficial.

In a similar manner to how reactive microglia are classed (M1 or M2) (Cherry et al., 2014), astrocytes have also been proposed to have two reactive phenotypes: A1 or A2. A2 astrocytes are considered protective, and A1 harmful (Liddelow et al., 2017a). An A2 phenotype can be triggered by injured motor neurons in a stem cell model. The neurons upregulate ephrin type-B receptor 1, which stimulates STAT3 in astrocytes, resulting in upregulation of genes associated with beneficial inflammatory effects. In contrast, astrocytes stimulated with IL-6 which also activates the STAT3 pathway, resulted in upregulation of detrimental inflammatory genes. Notably, this protective response of astrocytes to upregulate ephrin type-B receptor 1 is absent in mouse models of ALS, as astrocytes failed to display any STAT3 activation (Tyzack et al., 2017).

A1 astrocytes can be triggered by reactive microglia releasing interleukin 1α (IL-1α), tumour necrosis factor α (TNFα) and C1q. These A1 astrocytes are not capable of sustaining synapses, with surviving synapses also displaying reduced mEPSCs. They are also powerfully neurotoxic, causing neuronal death in co-cultures and of astrocyte conditioned media (ACM)-treated neurons. A1 astrocytes are also prevalent in post-mortem tissue of brains affected by neurodegenerative diseases (Liddelow et al., 2017a). A triple knockout of IL-1α, THFα and C1q from microglia in a superoxide dismutase 1 $(SOD1)^{G93A}$ mouse model of amyotrophic lateral sclerosis prevented microglia from activating astrocytes, ultimately resulting in a

retardation of disease progression (Guttenplan et al., 2020). Such studies highlight the complexity of astrocyte reactivity and the role it can play in health and disease. The different inflammatory and phagocytic capabilities of astrocytes show further how heterogenous these cells are and how such responses can be altered by disease.

Few studies have been performed on the role of astrocytes in the immune responses in RTT, though studies have shown that RTT astrocytes express more GFAP (Kahanovitch et al., 2019), a marker associated with astrocytic reactivity (Sofroniew and Vinters, 2010). GFAP protein levels were significantly higher in RTT patient brains compared to controls' (Colantuoni et al., 2001), as well as in mutant MeCP2 mouse astrocytes (Okabe et al., 2012). This shows that astrocytic reactivity could play a role in RTT.

Similarly to microglia, astrocytes can also be phagocytic. *In vitro* models of brain injury have shown that astrocytes can phagocytose whole dead cells (Lööv et al., 2012), though are not as proficient at this as microglia (Magnus et al., 2002). In Alzheimer's Disease astrocytes have also shown they can phagocytose amyloid (Wyss-Coray et al., 2003). Studies have shown that the phagocytic ability of A1 astrocytes is also reduced compared to control astrocytes (Liddelow et al., 2017b). Such phagocytic activity of astrocytes is also important in synaptic pruning in the brain (Lee and Chung, 2019), which is vital for circuit development in the brain.

1.13.7 Synaptogenesis

Astrocytes are essential for the process of synaptogenesis in the CNS, with the main period of synaptogenesis occurring after the appearance and differentiation of astrocytes (Allen and Eroglu, 2017). Astrocytic processes are in very close proximity to synapses and can wrap around them. They are also able to cooperatively move with the dendritic spines, placing them in an ideal locale to be involved in synaptogenesis. The coverage of synapses by astrocytic processes can vary depending on the stage of development or injury state.

Studies have demonstrated the importance of astrocytes in synaptogenesis. For example, retinal ganglion cells form very few functional synapses when glia are absent. The addition of glia increased the functionality of these synapses (Pfrieger and Barres, 1997). Astrocytic contact and also factors secreted from astrocytes are involved in synaptogenesis. ACM added to retinal ganglion cells caused them to form ten times more excitatory synapses that those cultured without (Ullian et al., 2001, Nägler et al., 2001).

A number of these astrocyte-secreted factors have been identified and individually shown to contribute to synaptogenesis, such as apolipoproteins, cholesterol (van Deijk et al., 2017) and thrombospondins (Christopherson et al., 2005). Cholesterol is an integral part of the cell plasma membrane and is usually acquired from circulating lipoproteins in the blood. However, the brain must synthesise its own cholesterol *in situ* (Nagy and Ackerman, 2013) as cholesterol

cannot cross the blood brain barrier (Dietschy, 2009). Cholesterol treatment was found to increase synapse formation and mEPSC frequency in retinal ganglion cells by a similar level to treatment with glia-conditioned medium (GCM). Inhibiting cholesterol synthesis in these glial cultures prior to GCM collection resulted in reduced mEPSCs compared with GCM collected from non-treated glia. Supplementation of the cholesterol-deprived GCM with cholesterol rescued this negative effect (Mauch et al., 2001). Mice with specific SREBP2, an enzyme necessary for cholesterol synthesis (Brown and Goldstein, 2009), knockdown in astrocytes have reduced brain volume in the cortex and hippocampus, with a small decrease of PSD95 staining in cortical areas, indicating reduced synapse number (Ferris et al., 2017). Cholesterol derived from astrocytes is secreted with apolipoprotein E. Impairing this process *in vitro* results in an impairment in synaptic development and synaptic plasticity (van Deijk et al., 2017). Incubating induced pluripotent stem cell (iPSC)-derived neurons with thrombospondins and increasing concentrations of cholesterol resulted in an increase in PSD95 and VGLUT1 staining in a concentration-dependent manner, indicating presence of increased glutamatergic synapses (Klapper et al., 2019). Cholesterol is therefore a vital factor secreted from astrocytes for synapse formation.

Cholesterol metabolism has been implicated in RTT. The genes involved in cholesterol synthesis were found to be significantly upregulated in the brains of 1-month-old MeCP2 mutant mice, accompanied by increases in the total cholesterol concentration. Notably however, these levels returned to WT levels by D70, indicating that early perturbations in cholesterol metabolism may contribute to problems with synaptogenesis in young mice, potentially due to changes in membrane fluidity because of the aberrant cholesterol content. Treatment with statins helps to improve some of the symptoms of MeCP2 mutant mice, highlighting cholesterol synthesis as a potential treatment target in RTT (Nagy and Ackerman, 2013).

Thrombospondins are extracellular matrix (ECM) proteins that are expressed highly in astrocytes in the developing brain and promote the formation of structurally normal synapses by recruiting synaptic adhesion and scaffolding molecules. However, these synapses are silent without the presence of other astrocyte-secreted factors (Christopherson et al., 2005). The release of thrombospondins from astrocytes can be triggered *in vitro* by stimulating them with ATP (Tran and Neary, 2006). Little work has been done on the potential role of thrombospondins in RTT but they have been shown to have a role in Down Syndrome, a condition which shares some common features with RTT (Garcia et al., 2010).

Astrocytes can also release the synaptogenic molecule hevin and SPARC, which specifically antagonises hevin (Kucukdereli et al., 2011). Pre- and postsynaptic adhesion molecules (neurexins and neuroligins) interact with hevin suggesting that hevin might elicit its pro-

synaptogenic effects by clustering these adhesion molecules (Clarke and Barres, 2013). The expression of SPARC in mouse hippocampus peaks in astrocytes during the highest point of synaptogenesis with the expression downregulating in adulthood. Increasing neuronal activity using GABA receptor antagonists or with glutamate results in increased SPARC expression, showing that SPARC expression is regulated by activity levels and developmentally. SPARC-null mice have stronger synapses as shown by increased frequency and amplitude of mEPSCs, as a result of abnormal α-amino-3-hydroxy-5-methyl-4-isoxazolepropionic acid (AMPA) receptor clustering (Jones et al., 2011).

In order to form active synapses additional molecules are required. Glypicans are secreted from astrocytes and are sufficient to induce excitable synapse formation. The glypicans increase the surface expression and clustering of the GluA1 subunit of the AMPA receptor, resulting in a higher frequency of glutamatergic synaptic events (Allen et al., 2012). Glypican4-deficient mice have defective synapse formation (Allen et al., 2012). Astrocytic processes can also wrap around dendritic spines of neurons, and these astrocytic processes demonstrate dynamic remodelling behaviour that is cooperative with that is dendritic spines.

Astrocytes are also involved in synaptic pruning, a process that is as vital as synaptogenesis in order to refine connectivity in the brain. A transcriptome database shows that astrocytes are enriched for genes involved in phagocytosis, such as MEGF10 and MERTK (Cahoy et al., 2008), and can phagocytose synaptosomes. Astrocytes from MEGF10-/- and MERTK-/- mouse cortex have a 50% reduction in their ability to phagocytose synaptosomes (Chung et al., 2013).

Retinal ganglion cells upregulate C1q when exposed to a feeder-layer of immature, but not mature, astrocytes. C1q is a component of the innate immune system that can target cells for phagocytosis and found prevalently co-localised with PSD95 in the developing CNS (Stevens et al., 2007). The secreted astrocytic factor that causes the C1q upregulation in retinal ganglion cells is transforming growth factor β (TGF-β). Specifically blocking this pathway inhibited synaptic pruning (Bialas and Stevens, 2013). Blocking neuronal activity results in microglia phagocytosing weakened inputs, indicating that this synaptic pruning is at least partly regulated by activity. C1q knockout mice showed deficits in eye-specific segregation *in vivo* (Stevens et al., 2007). C1q was also present on synapses in the retina in mouse models of glaucoma resulting in synapse loss and retinal ganglion cell death. This shows that complement pathway mediated phagocytosis of synapses can be inappropriately activated in disease states in adulthood (Stevens et al., 2007). The role of astrocytes in synaptogenesis also shows that they are integral to the process of maturing circuits in the brain.

1.13.8 Circuit maturation

Astrocytes are vital for ensuring that mature functional networks can form. iPSC-derived glia and neuron cocultures demonstrate synchronised bursts of action potentials in neurons, visualised by increases in calcium, alongside spontaneous increases in neuronal intracellular calcium. Depleting glia from these cultures obliterated this spontaneous activity, in addition to impairing the maximum mean action potential frequency. A significant reduction in glutamatergic synapse density was observed in the cultures without glia, in addition to a prolonged AMPA mEPSC delay time. This delay time speeds up during development, so the slowing indicates a delay in synapse maturation (Klapper et al., 2019).

1.14 Modelling Rett Syndrome

As the roles of various cell types in the brain have been discussed, it is important to find the best model system with which to study them. As previously mentioned, data from rodents does not always translate well to humans, and human brain tissue from living patients is very scarce. Post-mortem brain tissue unfortunately can only provide information about the end stages of disease. Foetal primary cells can be used in order to study human primary cells, however these come with ethical implications due to them originating from aborted foetuses. Not all scientists would be comfortable working with such cells, and indeed these cells can also elicit a strong reaction from the public, as does research that uses animals. Such reactions could impact research funding as well as diminish public trust in the scientific process.

Human cell lines derived from cancers can also be used to model disease, such as the glioblastoma cell line, U-251, and the neuroblastoma cell line, SH-SY5Y. As these are cells derived from tumours they will not act in the same way as human primary brain cells, potentially limiting the translational information they can provide. Additionally, selection pressures can drive these cell lines to gain mutations and genetically drift from their tumour of origin, particularly if the cell line is not genotyped regularly. Furthermore, such cell lines are at risk of contamination, with the U-251 line being misidentified in some publications due to such contamination (Torsvik et al., 2014). Despite these limitations cell lines can be very helpful due to their very proliferative nature; they are cheap to maintain and can be used to optimise experimental procedures without needing to use more expensive and less robust cells.

Human cell lines from adults can also pose ethical implications. For example, the famous HeLa cell line derived without consent during a cervical cancer biopsy from Henrietta Lacks in the 1950s (Skloot and Company, 2010). Obtaining cells from Henrietta Lacks without her consent is indicative of consent laws at the time, and whether her race also played a part in her treatment remains controversial. Many scientists therefore are no longer comfortable using this cell line, and some members of the public also do wish it to be used. As a cancer cell line it also does not behave in a physiological way and contains mutations that allow such lines to

proliferate indefinitely. This means data obtained from such cell lines might not translate well to healthy primary cells. It does though add yet another reason why we need better and more ethical ways to model disease. Stem cell derived cells could provide the answer to this, building on the work of ESCs but without the ethical issues posed by them.

1.15 What are iPSCs?

iPSCs were developed in 2006 by Shinya Yamanaka, firstly using mice fibroblasts and subsequently with human fibroblasts. iPSCs are capable of generating cells from all three germ layers and form teratomas when engrafted (Takahashi and Yamanaka, 2006, Takahashi et al., 2007). Theoretically iPSCs can generate any cell type in the human body, removing the need for primary human tissue to generate cultures of cells. This is especially valuable for generating cells from particularly inaccessible parts of the body, such as the brain. They mark the beginning of huge new potential for disease modelling, as well as breaking the idea that terminally differentiated cells were incapable of turning back down their developmental pathway.

The researchers undertook a monumental amount of work in order to elucidate which genes could be used to turn fibroblasts back into pluripotent stem cells. The genes investigated were selected based on their role in maintaining the pluripotency and proliferation of embryonic stem cells, returning a list of 24 candidates. Any one of these 24 genes were incapable of forming stem cells from fibroblasts, yet all 24 genes together could. To pinpoint which of these were necessary, they managed to rule out ten of the 24 genes and then used different combinations of the remaining fourteen to determine four genes that were sufficient to reprogram fibroblasts into stem cells. These genes became known as the Yamanaka factors: octamer binding transcription factor 4 (Oct4), Sex determining Y box 2 (Sox2), Kruppel like factor 4 (Klf4) and c-myc (Takahashi and Yamanaka, 2006).

The uses of iPSCs include regenerative medicine and disease modelling. However, if cells are to be used as a transplantation treatment to replace lost tissue, in neurodegenerative diseases for example, it is important to consider that if retroviral transfection is used to deliver the Yamanaka factors to the fibroblasts the factors integrate into the genome, resulting in potential genomic alterations or mutations. iPSCs generated in this way are therefore unsuitable for potential therapeutic use in humans. Other methods that do not rely on genomic integration to generate ‘footprint-free’ iPSCs are available and are being developed. Such methods include using episomes (Matz et al., 2017) and non-integrating adenoviruses (Stadtfeld et al., 2008). These methods result in a transient expression of the factors and are an exciting development in the possibility of using iPSC-derived cells in medicine. It is also important to also consider that iPSCs are pluripotent, technically immortal cells. As such they are at high risk of developing chromosomal abnormalities and mutations, similarly to cell lines generated from

cancer cells. Several groups have noted that these abnormalities are often linked to cell-cycle regulation and cancer (Pera, 2011). It would therefore be vital to ensure that no iPSCs remained in cells being prepared for transplantation in case they formed cancerous tumours. Nonetheless, despite the current limitations for treatment-based uses of iPSCs it is undoubtable that iPSCs will prove to be an indispensable tool for disease modelling. After reprogramming, iPSCs still retain the original genotype of the somatic cell type such as fibroblasts or blood cells (DeRosa et al., 2012). As such, the generation of iPSCs provides a powerful approach to generate human cells and for modelling disease.

1.15.1 Generating NPCs

A range of protocols have been developed to generate various cell types from iPSCs. For the purpose of this thesis the main aim was to generate astrocytes from iPSCs. In order to generate these, an intermediate stem cell known as neural precursor cells (NPCs) must be generated first. Much has been learned about the generation of the CNS and cortex from developmental biology, and researchers have used these findings to generate protocols that can produce neurons and astrocytes from NPCs.

As previously described in section 1.11, the induction of the neuroectoderm is the result of exposure to BMP antagonists such as chordin and noggin. It is these molecules that prevent the ectoderm from forming skin, and direct it towards the neural fate. In culture this can be recapitulated using a BMP antagonist alongside a small molecule such as SB431542, which inhibits the transforming growth factor beta (TGFβ) pathway by preventing the phosphorylation of the Alk4, 5 and 7 receptors. BMP antagonists also inhibit SMAD. Combined, these molecules result in SMAD molecules being unable to dimerise and enter the nucleus to initiate transcription. iPSCs exposed to these molecules start to express NPC markers such as Pax6 after around 7 days, and intrinsically form rosette structures that are reminiscent of the developing neural tube (Chambers et al., 2009).

To generate NPCs from iPSCs in culture, multiple methods can be used such as embryoid body formation and culture using N2/B27 media to result in the generation of neural rosettes (Brennand et al., 2011). A benefit of this approach is that three-dimensional cell culture is more physiological than two-dimensional. However, it can be a technically challenging method as without using specific plates it can be difficult to generate embryoid bodies of consistent sizes, and other cell types alongside the NPCs are also generated.

1.15.2 Generating Astrocytes

Primary human astrocytes can be isolated from human foetal tissue. However, supplies of these are limited and also pose ethical considerations that could limit research potential. Astrocytes can also be generated from iPSC-derived NPCs, iPSCs or directly from fibroblasts (Caiazzo et al., 2015). To generate astrocytes directly from fibroblasts dox-inducible lentiviral

vectors can be used, containing the transcription factors NFIA, NFIB and Sox9. The generated cells stain positively for S100β and GFAP and were capable of taking up glutamate and generating calcium waves in response to thrombin (Caiazzo et al., 2015). Interestingly, RTT iPSCs were found to differentiate more readily into GFAP-positive cells than WT iPSCs (Andoh-Noda et al., 2015), potentially an advantageous feature for this project.

Other methods first generate NPCs from iPSCs, before generating astrocytes. Commonly used molecules used are ciliary neurotrophic factor (CNTF), heregulin and BMP4 (Shaltouki et al., 2013). Commercially available media can also be used from various sources to generate astrocytes from NPCs. Recent studies have demonstrated that astrocyte media (ScienCell) can be used to generate GFAP- and S100β-positive cells from NPCs (Tcw et al., 2017). Furthermore, suppliers such as Stem Cell Technologies and other companies have developed astrocyte induction kits, designed to generate astrocytes from NPCs. However, commercial media formulations are typically proprietary and therefore difficult to replicate 'in house'.

It is also noteworthy that GFAP is often used as an astrocytic marker but it is absent in some subsets of astrocytes (Sofroniew and Vinters, 2010). It is associated with reactivity or immaturity, and thus other markers are considered in some protocols, such as GLAST, Glt1 and 10-formyltetrahydrofolate dehydrogenase (Aldh1l1). Aldh1l1 has emerged as being potentially a better pan-astrocyte marker than GFAP (Cahoy et al., 2008, Barbar et al., 2020). Much work is needed to isolate and identify different astrocytic subtypes, as well as methods in to generate and characterise them.

The problem with reactive astrocytes is that they can lose their normal supportive physiological functions (Guttenplan et al., 2020). Serum-free conditions have been shown to reduce reactivity in iPSC-derived astrocyte cultures, however GFAP is still expressed in a number of these cells. The presence of serum also impacts the astrocytic gene expression (Perriot et al., 2018). It has been shown that adding FGF1 to immature astrocytes can increase the presence of Glt1 and GLAST, whilst downregulating GFAP. Such a phenotype is associated with mature and quiescent astrocytes (Roybon et al., 2013). In contrast, if studying astrocytic reactivity is desired, adding TNFα and IL-1α to iPSC-derived astrocytes can drive them to a more inflammatory phenotype, which in turn can prevent them from carrying out some of their normal physiological functions, such as glutamate clearance (Zhou et al., 2019, Roybon et al., 2013, Soubannier et al., 2020).

In addition to ensuring that generated astrocytes express expected markers it is also important to consider that they demonstrate normal astrocytic functions, such glutamate uptake and spontaneous calcium transients (Bazargani and Attwell, 2016). Generating functional iPSC-derived brain cells will revolutionise the way we study neurological disease.

1.16 Aims of this Thesis

Considering the advantages of iPSCs and the limitations of rodent-based models discussed in this chapter the development of an iPSC-derived model of RTT would hopefully provide a platform to generate translational data that will ultimately be of patient benefit. As the role of astrocytes in neurological disease is often overlooked, the model will focus on the part astrocytes play in RTT. Therefore, the overall aim of this thesis will be generate an iPSC-derived model to investigate the role of astrocytes in RTT. To achieve this aim, it will be broken down into smaller objectives:

1. To generate pure cultures of iPSC-derived astrocytes from a RTT iPSC line and two control iPSC lines. Cells will be characterised using immunocytochemistry and real time polymerase chain reaction (qPCR).
2. To functionally characterise the iPSC-derived astrocytes using calcium imaging and biochemical assays that investigate metabolic processes.
3. To investigate the effect that ACM from the RTT and control iPSC-derived astrocytes has on healthy iPSC-derived neurons using qPCR and calcium imaging.
4. To utilise RNA sequencing to investigate gene expression in RTT and control iPSC-derived astrocytes and analyse differential gene expression in order to identify biological pathways that may be altered.

Chapter Two: Generation and characterisation of RTT#27, RTT#37 and HipSci iPSC-derived astrocytes.

2.1 Introduction

Glial cells (astrocytes, oligodendrocytes and microglia) are thought to account for almost 50% of brain cells, though the ratio of neurons to glia varies across different brain structures (Herculano-Houzel, 2014). For example, the cerebellum is thought to contain 18.9% glial cells, compared to 58.4% glial cells in the grey matter of the cerebral cortex (Herculano-Houzel, 2014). Together, neurons and astrocytes interact in order to maintain brain homeostasis and preserve brain function. Numerous studies have demonstrated how vital astrocytes are to maintaining neuronal health (Bélanger and Magistretti, 2009). Studies using primary mouse neurons have shown that neurons grown along without glia have reduced viability, even if grown in the presence of ACM. This implies the presence of astrocytes is integral to supporting neurons through direct means (Whatley et al., 1981, Swanson and Choi, 1993). Three-dimensional astrocyte-neuron co-cultures have also demonstrated that neurons benefit from the presence of the astrocytes (Fang et al., 2019).

However, in contrast to their normal supportive role astrocytes have been found to exert negative effects on neurons in neurological diseases, such as Alzheimer's Disease, ALS and Huntington's Disease (Acosta et al., 2017, Pehar et al., 2017, Gray, 2019). For example, mice that only express $SOD1^{G93A}$ in their motor neurons do not develop motor deficits or develop disease (Lino et al., 2002), whereas transplanting $SOD1^{G93A}$ astrocytes into WT mice results in motor neuron degeneration and subsequent motor problems (Papadeas et al., 2011). This further illustrates the important role that astrocytes can play in neuronal and overall brain health. Thus, it is vital they are considered in models of brain disease.

Rodent models have been used to study many brain diseases, and we have gleaned much information from them. However, information from rodent species may not necessarily translate well to humans. As such it is worthwhile to consider other model systems with which to study these diseases. Human astrocytes are more complex, more heterogeneous and function differently to rodent astrocytes (Oberheim et al., 2009, Zhang et al., 2016). Therefore, a model that uses human astrocytes would be preferable to one which uses rodent. Unfortunately, primary brain tissue from humans is in limited supply, so other avenues must be considered.

iPSCs are an ideal tool to circumvent the issue of limited primary tissue supply. It is possible to theoretically generate and expand multiple cell types from one iPSC line, which can also be cultured either alone or in different combinations. iPSC-derived cells retain the genotype of the donor and can also be very beneficial for modelling sporadic forms of disease. Rodent models

tend to use rare familial mutations, such as the $SOD1^{G93A}$ mouse model of ALS, for example, whereas iPSC models do not have this limitation. In addition, iPSC models are therefore a powerful method of modelling human brain diseases *in vitro*.

Neurons and astrocytes can be generated from the same type of precursor cell, known as NPCs. To generate NPCs, *in vivo* neurodevelopment is replicated by using growth factors or small molecules that act on similar pathways involved in generating the neuroectoderm from the ectoderm. Noggin for example is a BMP inhibitor that is released from the organiser during neurodevelopment *in vivo*, and this is included in the original two-dimensional protocol for *in vitro* neural induction, alongside the small molecule SB431542 (Chambers et al., 2009). Other studies have used other small molecules, such as LDN193189 (Chambers et al., 2012) and dorsomorphin (Zhou et al., 2010). Combining these molecules results in efficient generation of NPCs.

Molecules such as CNTF are often found in astrocyte differentiation protocols, as this directly acts upon the astrogenic JAK-STAT pathway, discussed in chapter one (Hughes et al., 1988, Rajan and McKay, 1998, Shaltouki et al., 2013). Other important pathways can be acted upon also, such as using BMP4 to activate SMAD and cause heterodimerisation and translocation to the nucleus to initiate transcription of astrocyte genes. There are multiple methods of generating astrocytes from iPSC-derived NPCs (Roybon et al., 2013, Shaltouki et al., 2013, Serio et al., 2013, Krencik and Zhang, 2011).

To generate neurons NPCs can be treated with DAPT, a γ-secretase inhibitor (Dovey et al., 2001). The use of DAPT therefore prevents Notch signalling (Geling et al., 2002), forcing the NPCs towards a neuronal rather than glial fate. In stem cell models it has been shown to encourage neuronal differentiation (Crawford and Roelink, 2007). Once the cells are generated it is then important to characterise them both morphologically and functionally.

The overall aim of this chapter is to characterise the cells at each developmental stage: iPSCs, NPCs, neurons and astrocytes. It is imperative that cells are characterised prior to experimental use so that their identity can be confirmed, and purity of cultures assured. In this project iPSCs were obtained from a kind donation from Dr James Ellis (SickKids Hospital, Canada) and purchased from the Human Induced Pluripotent Cells Initiative (HipSci, Cambridge). Not all of the donated RTT iPSC lines survived the journey to the UK, so the disease line used in this project is the RTT#27 line. The disease line RTT#27 contains an 11 base pair deletion in exon one of the MeCP2 gene (c.47_57del; p.(Gly16Glufs*22)), resulting in frameshift and severely truncated exon1. The researchers ensured that the cell line was developed from fibroblasts which contained the mutant MeCP2 gene, rather than the wild-type (see section 1.4 on mosaic expression) (Djuric et al., 2015, Mnatzakanian et al., 2004). The

patient developed normally but had lost their vocabulary by 30 months old, developed ritualistic and repetitive behaviours, and seizures (Mnatzakanian et al., 2004).

The other surviving donated line is the RTT#37 line, an isogenic control of a MeCP2-null line, RTT#20 (Djuric et al., 2015, Cheung et al., 2011). The following table (table 2.1) includes all the RTT iPSC lines that were originally received and their mutations:

Cell Line	Type of Mutation	Specific Mutation
SK0019-002 #7	WT	-
RTT#27	Mutant	11bp deletion
RTT#39	Mutant	11bp deletion
RTT#48	Mutant	11bp deletion
RTT#20	Null	Exons 3 and 4 removed
RTT#37	WT (isogenic control of #20)	-

Table 2.1: All received RTT iPSC lines with mutations.

Cells were characterised at each stage in order to confirm their identity, with additional staining used to confirm the absence of unwanted cells. iPSCs were immunocytochemically stained for Oct4 and Sox2, NPCs for Sox2, Pax6, Nestin and Ki67. Oct4 is a pluripotency marker used to characterise stem cells (Zeineddine et al., 2014). Sox2 is an HMG box transcription factor that is expressed in NPCs (Ellis et al., 2004), whilst also being involved in the epigenetic reprogramming of differentiated cells to a pluripotent state, which is why it is also present in iPSCs (Zhang and Cui, 2014, Takahashi and Yamanaka, 2006). Pax6 demonstrates that the generated NPCs are dorsal, and thus involved in corticogenesis (Zhang et al., 2018a). Nestin is an intermediate filament protein specifically expressed in NPCs during development so this was also selected as a characterisation marker (Lendahl et al., 1990). Ki67 is a marker of cell proliferation and thus showed that the NPCs generated were proliferative (Scholzen and Gerdes, 2000). Astrocytes are stained for GFAP and S100β. GFAP is an intermediate filament present in astrocytes in the CNS, and is widely used as a marker for astrocytes (Eng et al., 2000). S100β is a calcium-binding protein (Donato, 2001) that is thought to be expressed in more mature astrocytes (Raponi et al., 2007). These markers were therefore all thought to be ideal to characterise the cells at each stage.

2.2 Aims

The overall aim of this chapter was to generate NPCs, astrocytes and neurons from the RTT#27, RTT#37 and HipSci iPSC lines. In order to achieve these aims the specific aims were to:

1. To optimise the generation of NPCs from control and RTT patient iPSCs using dual-SMAD inhibition.
2. To optimise the generation of astrocytes using a commercially available media formulation.
3. To optimise the generation of neuronal cells from the HipSci iPSCs by driving synchronous differentiation of NPCs by the addition of DAPT.
4. To characterise both precursor and differentiated cell types (iPSCs, NPCs, astrocytes and neurons) using morphological and immunocytochemical analysis.
5. To determine the expression of cell type specific genes using qPCR.

2.3 Methods and Materials

2.3.1 Control iPSC line culture

Healthy control iPSCs (HPSI1113i-podx_1) (HipSci.org) (herein referred to as the HipSci line) were cultured in vitronectin (ThermoFisher, USA)-coated T25 flasks (Corning, USA). Vitronectin was diluted to a concentration of 10µg/ml in sterile magnesium and calcium-free PBS (Sigma-Aldrich, USA) and 1ml/cm^2 was added to flasks. The flasks were incubated for 1 hour at room temperature before use. iPSCs were defrosted in a 37^{o}C water bath and then added to 4ml of DMEM. iPSCs were then centrifuged at 200G for 5 minutes at room temperature. The supernatant was then removed and the cell pellet resuspended in complete E8 media (ThermoFisher, USA), supplemented with 10µM Y-27632 (Tocris Bioscience, UK). The cell suspension was added to the vitronectin-coated flask and kept at 37^{o}C for 24 hours. A full media change was then performed with complete E8 media without Y-27632. Full media changes were then performed every day with complete E8 media until the larger colonies started to touch, at which point the iPSCs were passaged at a ratio of 1:3. In order to passage the cells they were washed twice with sterile PBS without magnesium or calcium before incubating for 4 minutes at 37^{o}C in 50µM EDTA in sterile PBS without magnesium or calcium (both Sigma-Aldrich, USA) until the colony edges started to detach. The EDTA solution was then removed and the cells were gently detached from the plate using a P1000 pipette with complete E8 media supplemented with 10µM Y-27632 (Tocris Bioscience, UK). They were then plated into new vitronectin-coated flasks. The media containing Y-27632 was removed after 24 hours. To freeze iPSCs the passaging protocol was performed as normal except cells were detached after EDTA treatment with 500µl of complete E8 media per 10cm^2 of confluent cells. The 500µl of cell suspension was then added to cryovials filled with 500µl of complete

E8 media with 20% DMSO. Cells were then frozen in a Mr Frosty (ThermoFisher Scientific, UK) for 24 hours at -80ºC before being transferred to liquid nitrogen.

2.3.2 RTT#27 and RTT#37 iPSC line culture

Two RTT patient lines (kindly donated by Professor James Ellis, SickKids Hospital, Toronto, Canada) were initially cultured on feeder cell cultures. 5000 cells/cm^2 of mitotically inhibited mouse fibroblasts were cultured on gelatin-coated flasks. Once visible colonies formed they were passaged with EDTA onto T25 flasks coated with Matrigel® (Corning) diluted in DMEM (ThermoFisher Scientific) according to the manufacturer's instructions. 1ml/10cm^2 of diluted Matrigel® was added to plates for 1 hour at room temperature. iPSCs were defrosted in a 37ºC water bath and then added to 4ml of DMEM. iPSCs were then centrifuged at 200G for 5 minutes at room temperature. The supernatant was removed and the cell pellet resuspended in mTeSR1 media (STEMCELL Technologies, Canada), supplemented with 10µM Y-27632 (Tocris Bioscience, UK). The cell suspension was added to the vitronectin-coated flask and kept at 37ºC for 24 hours. A full media change was then performed with mTeSR1 without Y-27632. Full media changes were performed every day with mTeSR1 (STEMCELL Technologies) until the larger colonies started to touch, at which point the iPSCs were passaged at a ratio of 1:3. In order to passage the cells they were washed twice with sterile PBS without magnesium and calcium before incubating for 4 minutes at 37ºC in 50µM EDTA until the colony edges started to detach. The EDTA was then removed and the cells were gently detached from the plate using a P1000 pipette with mTeSR1 supplemented with 10µM Y-27632 (Tocris Bioscience, UK). They were then plated into new Matrigel®-coated flasks. The media containing Y-27632 was removed after 24 hours. To freeze iPSCs the passaging protocol was performed as normal except cells were detached after EDTA treatment with 500µl of mTeSR1 media per 10cm^2 of confluent cells. The 500µl of cell suspension was then added to cryovials filled with 500µl of mTeSR1 with 20% DMSO. The vials were quickly added to a Mr Frosty and then frozen for 24 hours at -80ºC before being transferred to liquid nitrogen.

2.3.3 Passaging iPSCs for neural induction

To prepare cells for neural induction cells were allowed to grow until they reached almost 100% confluence. Media was then removed and the cells were washed twice with PBS without magnesium or calcium (Sigma-Aldrich, USA). 1ml of Accutase (ThermoFisher Scientific, USA) was added per 10cm^2 of cell culture area. iPSCs were incubated for 5 minutes at 37ºC. They were gently triturated with a P1000 pipette before the Accutase was diluted with 4ml of DMEM per 1ml of Accutase. The cell suspension was centrifuged at 200G for 5 minutes. The cell pellet was gently resuspended with 1ml of either complete E8 media or mTeSR1, depending on the cell line, with a P1000 pipette to achieve a single cell suspension. More stem cell media was added to make it up to the required volume and 10µM Y-27632 was added. This solution was then plated at a 1:1 ratio onto a vitronectin or Matrigel® coated plate depending on the cell

line. The plate or flask was then gently rocked forward and backwards, and side to side to ensure even attachment of cells to the surface. Cells were incubated at 37°C, 5% CO_2. Medium was replaced without Y-27632 after 24 hours.

2.3.4 Coating of cell culture surface (Poly-L-Ornithine and laminin)

Poly-l-ornithine (PORN) and laminin plates (both Sigma-Aldrich) were used to grow NPCs. PORN was diluted in sterile distilled water to a concentration of 20µg/ml. 150µl of this solution per cm^2 was added to the tissue culture surface. This was then incubated at 37°C for at least 2 hours. The PORN solution was then removed and the tissue culture surface was washed twice with sterile distilled water. Laminin was diluted in sterile distilled water to a concentration of 10µg/ml. 200µl per $10cm^2$ of this solution was added to the tissue culture surface. This was then incubated at 37°C overnight. The laminin was then removed and the cell culture surface washed once with sterile PBS without calcium or magnesium.

2.3.5 Neural induction

24 hours after iPSCs were seeded for neural induction (section 2.3.3) the cells were checked to ensure they were 100% confluent. Media was then exchanged with per $10cm^2$ of neural induction media A (NIM-A) (Axol Bioscience, UK), a commercially available media based on (Chambers et al., 2009). NIM-A was fully replaced every day for a maximum of 11 days or until the cells started to peel. The cells were maintained in this media and fed daily for a maximum of 11 days or until the cells started to peel. At this point the cells were passaged at a 1:1 ratio with Accutase. Cells were then resuspended and plated in commercially available Neural Induction Media B (NIM-B), based on N2/B27 formulation media. Cells had full media changes daily with NIM-B, until the cells formed very tight rosettes, with media changes daily. The neural rosettes were then passaged at a 1:2 ratio onto PORN/laminin coated plates. Passaging was performed with 1ml of Accutase per $10cm^2$ and incubated at 37°C, 5% CO_2 for 5 minutes. The detached cells were gently pipetted with P1000 with care taken to ensure the cells remained in clusters. The Accutase was diluted with 4ml of DMEM per 1 ml of Accutase and the cell suspension centrifuged at 200G for 5 minutes. The cell pellet was gently resuspended with a P1000 to avoid breaking up rosettes. Cells were seeded onto PORN/laminin-coated plates prepared the day before at a 1:2 ratio and maintained in neural maintenance media (NMM) (Axol Bioscience, UK) until the cells were ready for further passaging for experimental use or to be frozen down for future use (see section 2.3.6). For experimental use the rosettes were passaged with Accutase and seeded onto PORN/laminin plates at a density of 150-200,000 cells per cm^2 and maintained in NMM (Axol Bioscience, UK) with cells fed every other day.

2.3.6 Freezing NPCs

Freezing media was made up in advance consisting of 20% dimethyl sulphoxide (DMSO) and 80% NMM (Axol Bioscience, UK). 0.5ml of this was added to labelled 1.5ml cryovials (Corning, USA). Media was then removed from cells which were then washed twice with 2ml per $10cm^2$

of sterile PBS. 1ml of Accutase (Thermo Fisher Scientific, USA) was then added per 10cm^2 and incubated at 37^{o}C and 5% CO_2 for 5 minutes. When cells started to slightly peel at the edges a P1000 was use to gently dissociate the cells whilst keeping them in clumps. Single-cell dissociation was avoided in order to try and preserve the rosettes. 4ml of DMEM per 1ml of Accutase then added to neutralise the reaction. The cell suspension was added an appropriately sized falcon and they were spun at 200G for 5 minutes at room temperature. The pellet was gently resuspended in 1ml of NMM (Axol Bioscience, UK) with a P1000 pipette. This was then made up to at least 5ml with NMM (Axol Bioscience, UK). The cells were counted using Trypan Blue (Sigma-Aldrich, UK). The cell suspension was then made up with NMM (Axol Bioscience, UK) if necessary to a density of 5 x 10^6 cells per ml. 0.5ml of this suspension was then added to each cryovial containing the freezing media so that each contained around 2 x 10^6 NPCs. The cells were frozen in a Mr Frosty container at -80^{o}C before transferal to liquid nitrogen.

2.3.7 Generation of astrocytes from NPCs

NPCs derived from each control line (RTT#37 and HipSci) and the RTT#27 line (see section) were seeded at a density of 1.5 X 10^5 cells per cm^2 onto Matrigel®-coated plates, prepared as previously described. Astrocyte Differentiation and Maturation kits were used as per manufacturer's instructions (both from STEMCELL Technologies, Canada). After day 35, the end of the protocol, the astrocytes were maintained in Astrocyte Media (ScienCell, USA) until day 90+. Cells were passaged at least once a week from this point onto Matrigel®-coated plates at a density of 1-1.5 x 10^5 cells per cm^2.

2.3.8 Seeding NPCs at the end of neural induction

At day 17 the cells were passaged with Accutase. The media was removed and the cells rinsed with 2ml of sterile PBS without calcium or magnesium per 10cm^2. 1ml of Accutase (ThermoFisher Scientific, USA) was added per 10cm^2 to the cells. This was incubated at 37^{o}C with 5% CO_2 for 5. The cells were gently pipetted up and down with a P1000 pipette and the reaction then neutralised with 4ml of DMEM per 1ml of Accutase. This was then centrifuged at 200G for 5 minutes at room temperature. The cell pellet was gently resuspended with 1ml of NMM (Axol Bioscience, UK). The cells were split at a 1:2 ratio and seeded onto PORN/laminin coated plates containing NMM (Axol Bioscience, UK). The plate or flask was then moved forward and backwards, and side to side and left on the side for around 3 minutes to ensure even attachment of cells to the surface. They were then kept at 37^{o}C with 5% CO_2. The cells were fed with NMM (Axol Bioscience, UK) every two days. Once tightly packed neural rosette formation was observed the NPCs could be frozen down or passaged further for experimental use.

2.3.9 Seeding NPCs for experimental use or expansion

NPCs were passaged using Accutase, (see section 2.3.8) but instead of split in a 1:2 ratio they were seeded at a density of 130,000-150,000 cells per cm^2 onto PORN/laminin coated plates (see section 2.3.4). Passages higher than passage 3 were avoided due to the tendency of NPCs to start differentiating into neurons. The cells were fed every other day with NMM (Axol Bioscience, UK).

2.3.10 Synchronous neuronal differentiation NPCs to become neurons

NPCs were seeded at 150-180,000 cells/cm^2 onto PORN/laminin-coated plates or glass cover slips and fed with NMM (Axol Bioscience). Once they were confluent and forming rosettes their media was changed to BrainPhys™ Neuronal medium (STEMCELL Technologies) supplemented with, SM1 (STEMCELL Technologies), 0.00002mg/ml rh-BDNF (STEMCELL Technologies), 0.00002mg/ml rh-GDNF (STEMCELL Technologies) and 100µM DAPT (Abcam, UK), a gamma-secretase inhibitor. This media was changed every two days, for five days. After five days the media was changed to the same formulation without the DAPT. This method was optimised by Dr James Crowe (unpublished thesis).

2.3.11 Immunocytochemistry

For immunocytochemistry cells were grown on glass cover slips held in either 12 well or 24 well plates (Corning, USA). Media was removed from the cells and were washed twice with PBS without calcium or magnesium. They were then fixed with 4% paraformaldehyde (PFA) (Sigma-Aldrich, USA) for 12 minutes at room temperature. The PFA was then removed and the cells were washed twice with PBS. The fixed cells were stored at 4°C in 2ml of PBS per 10cm^2 until required. The cells were permeabilised with Triton X-100 (Sigma-Aldrich, UK) made up in PBS without calcium or magnesium to a final concentration of 0.2%. The cells were washed 3 times for 5 minutes at a time. After this, a blocking buffer (0.2% Triton and 2% BSA in PBS) was added for one hour to the cells. Following this the primary antibodies were added to the cells for one hour. All antibodies were diluted in blocking buffer to the required dilution with the exception of S100b (Dako, USA), which was ready-to-use. The dilutions for each antibody are shown in table 2.2. Following incubation with the primary antibody the solution was removed and the cells were washed 3 times for 5 minutes with blocking buffer. The secondary antibodies were then added for one hour with the dilutions shown in table 2.3. The solution was then removed and the cells were washed 3 times for 5 minutes with blocking buffer. Coverslips were then washed once with distilled water. The cells were mounted with ProLong Diamond antifade mountain with DAPI (Thermo Fisher Scientific) and left for 24 hours at room temperature in the dark before being stored at 4°C until imaging. Cells were imaged using a Zeiss Axiovert 200M epifluorescence microscope using Leica Application Suite Advanced Fluorescence software (Leica Microsystems, Milton Keynes, UK). Cells were imaged with a 20X lens (Nikon). For imaging three pictures were taken from three different

areas of each coverslip. These images were split into two fluorophore images and a DAPI image, which could then be overlaid. For analysis of staining images were opened as their separate channels with ImageJ (Fiji, NIH). They were converted to 16 bit and thresholded into black and white images. Analyse particles was then used in order to give a cell count. With stains where the morphology was too difficult to allow this, for example with GFAP staining, a total DAPI count was performed, and then GFAP-negative DAPI cells were counted from the merged image. This total was subtracted from the total DAPI, giving the number of GFAP-positive cells.

Antibody	Dilution	Species	Supplier
GFAP	1:400	Mouse	Millipore
S100b	1:1	Rabbit	Dako
Tuj	1:500	Mouse	Abcam
Pax6	1:300	Rabbit	Abcam
Sox2	1:200	Mouse	Abcam
Oct4	1:400	Rabbit	Abcam
Nestin	1:300	Mouse	Merck
Ki67	1:1000	Rabbit	Abcam

Table 2.2: Primary antibodies. Primary antibodies used for staining of iPSCs, NPCs and astrocytes alongside their dilution, species and supplier.

Antibody	Dilution	Supplier
Goat anti-rabbit	1:1000	Jackson Labs
Donkey anti-mouse	1:500	Jackson Labs

Table 2.3: Secondary antibodies. Secondary antibodies used against primary antibodies, alongside their dilution and supplier.

2.3.12 Realtime Polymerase Chain Reaction (RT PCR)

RNA was isolated from cells using the RNeasy kit (Qiagen, Germany) as per manufacturer's instructions. A DNase treatment was performed during this process using the RNase-Free DNase Set (Qiagen, Germany) as per manufacturer's instructions. RNA was quantified using a NanoDrop spectrophotometer (ThermoFisher Scientific, USA) and then stored at -80^{o}C. cDNA was synthesised from 500ng of RNA using Precision nanoScript2 Reverse Transcription Kit (Primer Design), as per manufacturer's instructions. cDNA was stored at -20^{o}C. qPCR was performed using primers and PrecisionPLUS qPCR Master Mix premixed with SYBRgreen (both from Primer Design) in Bright White real-time 96-well plates (Primer Design) using a Roche LightCycler 480 (Roche). Prevalidated primers were obtained from PrimerDesign for the following genes of interest: GFAP, S100β, MAP2, Tuj, Oct4, Sox2, Pax6, GLAST, Glt-1,

aquaporin 4 (AQP4), MCT1, MCT2, Aldh1l1, superoxide dismutase 2 (SOD2), glyceraldehyde 3-phosphate dehydrogenase (Gapdh), β-actin and tyrosine 3-monooxygenase/tryptophan 5-monooxygenase activation protein zeta (YWHAZ) (all Primer Design, UK). Each reaction was performed in duplicate and the components of each reaction were:

Component	Volume (µl)
cDNA	5
Primer	1
Water	4
SYBRgreen	10

Table 2.4: Table showing components of each individual qPCR reaction.

2.4 Results

In order to study the role of astrocytes in RTT it was necessary to optimise a protocol that generated relatively pure populations of 95%+ astrocytes from iPSCs. iPSCs first had to be differentiated to generate NPCs. These NPCs were then differentiated into neurons or astrocytes for further analysis and study. An overview of this process can be viewed in Figure 2.1.

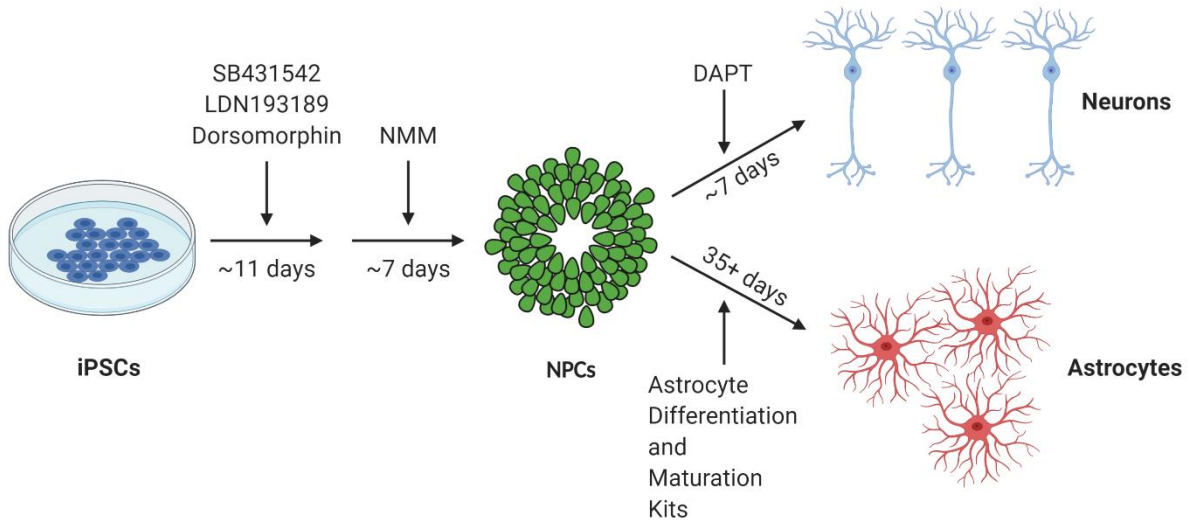

Figure 2.1: An overview of the process of generating astrocytes and neurons from iPSCs. Diagram shows an overview of methods and time scale for generating NPCs and subsequently neurons and astrocytes from iPSCs.

2.4.1 iPSCs form characteristic colonies and express Oct4 and Sox2

Two control iPSC lines (RTT#37 and HipSci) and one patient iPSC line (RTT#27) were cultured and expanded over a few weeks in order to bank sufficient cells for experimental use. Only one patient line was used due to extremely low viability (<5%, data not shown) of other cell lines on arrival (see table 2.1). Attempts to differentiate patient line RTT#20 was also unsuccessful as it did not differentiate during neural induction. Thus, it was only possible to use the RTT#27 line. To characterise these iPSCs immunocytochemistry (ICC) and real-time polymerase chain reaction (qPCR) were performed. As can be seen in Figure 2.2 all three iPSC lines express Oct4 and Sox2 as well as display the colony morphology characteristic of iPSCs, with clean edges and no differentiated cells. RTT#27 iPSCs were 97.44±2.50% positive for Oct4 and 97.76±1.78% positive for Sox2 (both n=3). RTT#37 iPSCs followed a similar trend (97.79±1.26% Oct4 and 97.09±1.10% Sox2 positive cells, n=3), as did the HipSci iPSC line (97.71±1.37% Oct4 and 97.70±1.39% Sox2, n=3). The iPSCs were then passaged for neural induction (see section 2.3.3) in order to generate NPCs.

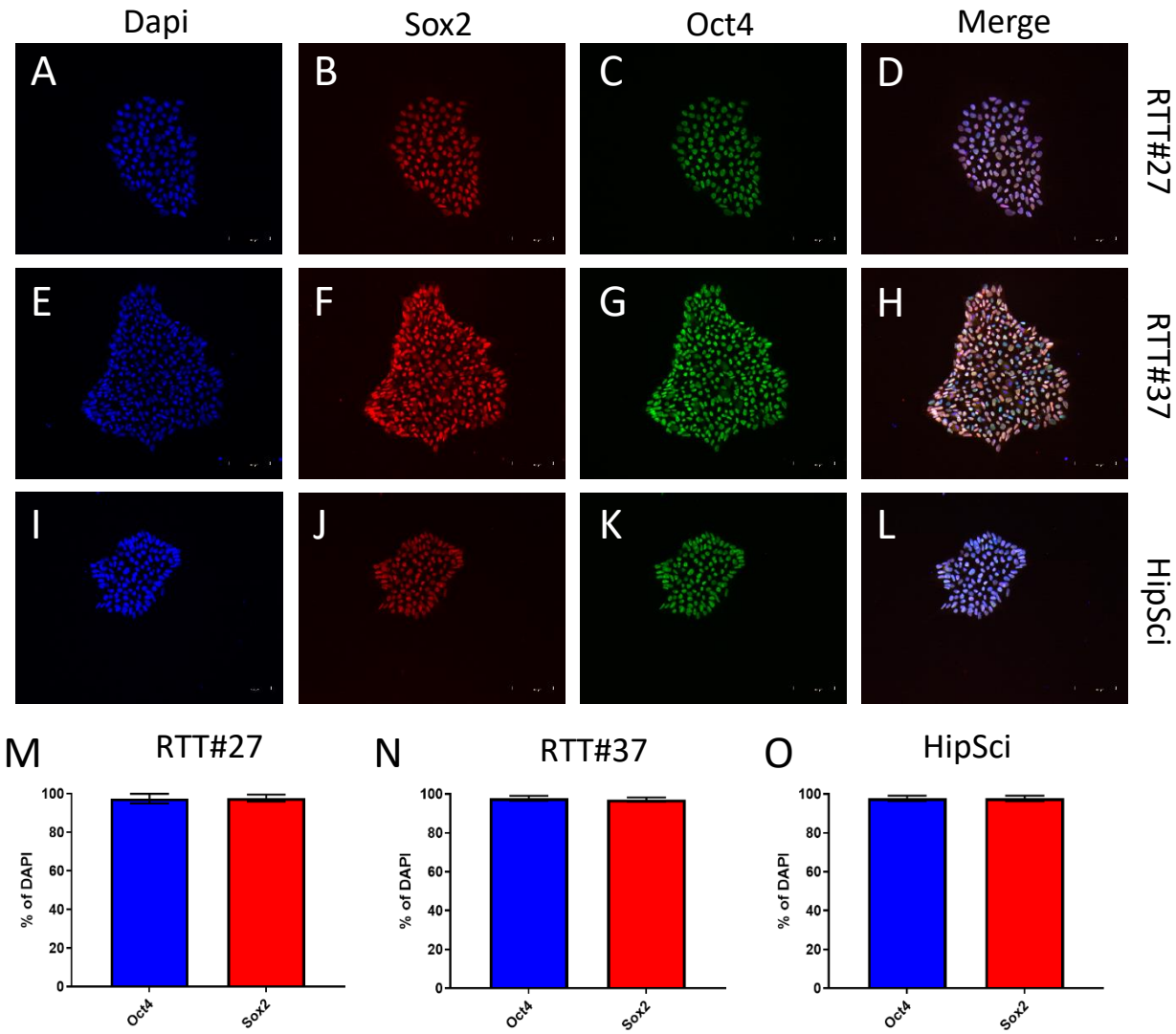

Figure 2.2: Representative immunocytochemistry staining and quantification of iPSC lines. Two control iPSC lines (RTT#37 and HipSci) and one disease iPSC line (RTT#27) were cultured and expanded before being characterised with iPSC markers, Oct4 (green) and Sox2 (red). **A), E) and I)** show nuclei staining with DAPI (blue), **B), F) and J)** show Sox2 staining, **C), G) and K)** staining show Oct4 staining and **D), H) and L)** show the merged images. The bar graphs **M), N) and O)** show the quantification of Oct4 and Sox2 for the RTT#27, RTT#37 and HipSci lines respectively n=3. Results are displayed as % of DAPI-positive cells ± standard deviation. Images are representative. Scale bars are 100µM.

2.4.2 NPCs form rosette structures and express the cortical markers Pax6 and Sox2 whilst not expressing the iPSC marker, Oct4.

All three iPSC lines underwent neural induction using the same method (see section 2.3.3) This method is known to generate NPCs by promoting the formation of neuroectoderm. These NPCs are then capable of differentiating into neurons and astrocytes.

To characterise the NPCs generated via neural induction they were stained for Sox2, Pax6, Nestin and Ki67. Quantification of Sox2 and Pax6 for each cell line can be seen in Figure 2.4 (RTT#27 Sox2 56.18±7.54%, Pax6 66.25±11.43%; RTT#37 Sox2 56.80±9.73%, Pax6 63.19±9.13%; HipSci Sox2 48.02±32.98, Pax6 59.14±17.72%; all n=3). iPSC-derived NPCs for all three lines were positive for Nestin, but due to the nature of the morphology of the staining it was not possible to quantify how many cells expressed Nestin. Ki67 was also used to show that the cells were proliferative. The iPSC marker, Oct4, was absent in all three cell lines (0±0% positive, n=3). The neuronal marker Tuj is also present in small amounts in the NPC populations. It can also be observed in Figure 2.4 that the NPCs form rosette structures, mimicking the neural tube formation during *in vivo* neurodevelopment.

The generation of NPCs from all three cell lines meant that they could then be differentiated towards either a neuronal or an astrogenic fate. Initial experiments attempted spontaneous differentiation methods to generate astrocytes, however this was very time consuming and did not yield very pure astrocyte populations due to neuronal contamination (data not shown). Therefore, another method to generate astrocytes from NPCs was attempted, using a commercially available kit (see section 2.3.7). Three neural inductions were performed for each iPSC line, and from each neural induction one astrocyte induction was performed. The HipSci line was also used to generate neurons; due to a material transfer agreement with SickKids Hospital neurons from the RTT#27 and RTT#37 lines were not made. An overview of this can be seen in Figure 2.3.

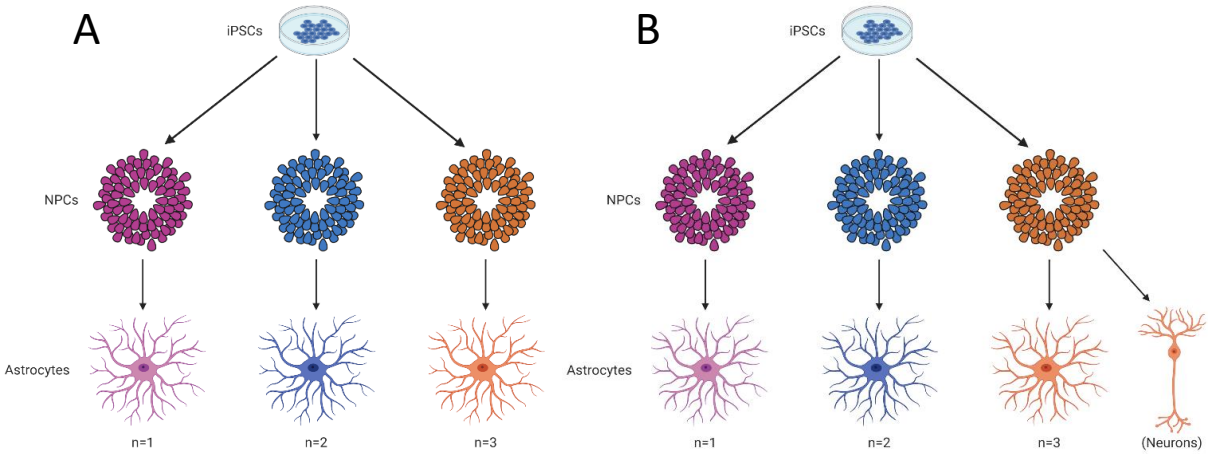

Figure 2.3: Overview of the generation of biological replicates for experiments. **A)** shows the biological replicates for the RTT#27 and RTT#37 lines. **B)** shows the biological replicates for the HipSci line, with an addition of neuron generation from the n=3 NPCs.

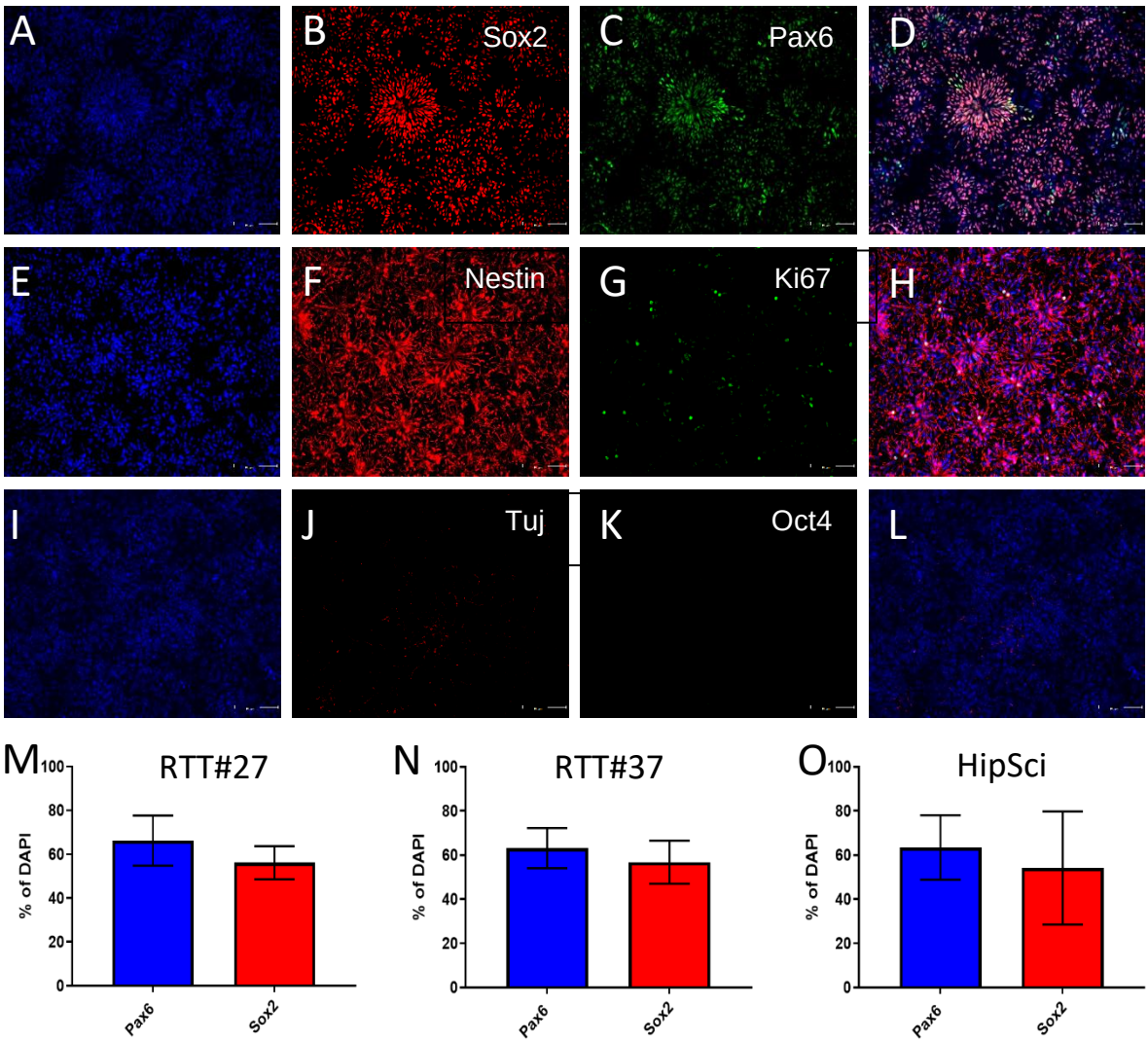

Figure 2.4: iPSC-derived NPCs are positive for Pax6, Sox2, Nestin and Ki67. Representative images of NPCs were chosen to depict immunocytochemistry of NPC markers and confirm absence of the iPSC marker, Oct4 (green). **A)** shows nuclei staining with DAPI (blue), **B)** Sox2 (red) staining, **C)** Pax6 (green) staining and **D)** shows the final merged image. The white arrows in **A)-D)** show a rosette structure. **E)** shows DAPI staining, **F)** shows Nestin (red) staining, **G)** shows Ki67 (green) staining and **H)** shows the merged image. **I)** shows DAPI nuclei staining, **J)** shows Tuj (red) staining, **K)** shows Oct4 staining, and **L)** shows the final merged image. Bar graphs **M), N) and O)** show quantification of Pax6- and Sox2-positive cells for the RTT#27, RTT#37 and HipSci line iPSC-derived NPCs respectively (n=3). Results are presented as % of DAPI-positive cells ± standard deviation. Images are representative. Scale bars are 100µM.

2.4.3 Astrocytes form relatively pure cultures and express GFAP with small amounts of S100b by day 60+.

Early attempts were made to generate astrocytes from NPCs using a previously described method from (Shaltouki et al., 2013) but this did not efficiently produce astrocytes (data not shown). Further experiments were conducted using a commercially available astrocyte differentiation kit from StemCell Technologies which was selected for use through the remainder of the project. Astrocytes generated from all cell lines were predominantly positive for GFAP after 9 weeks post-neural induction (Figure 2.5). S100β-positive cells were also detected at this time point. The RTT#27 line generated 97.27±0.97% GFAP-positive cells, and 28.76±11.22% S100β-positive cells (n=3). Similar figures were noted for the RTT#37 and HipSci lines (RTT#37 GFAP 96.77±2.11%, S100β 38.09±48.06%; HipSci GFAP 97.22±0.18%, S100β 20.20±8.12%; all n=3).

Neuronal contamination was also investigated with Tuj staining at 9 weeks post-neural induction. Levels of Tuj-positive cells were low, with RTT#27 (13.96±4.27%), RTT#37 (8.26±2.85%) and HipSci (9.26±2.37%). Owing to the nature of Tuj staining it was difficult to accurately quantify this.

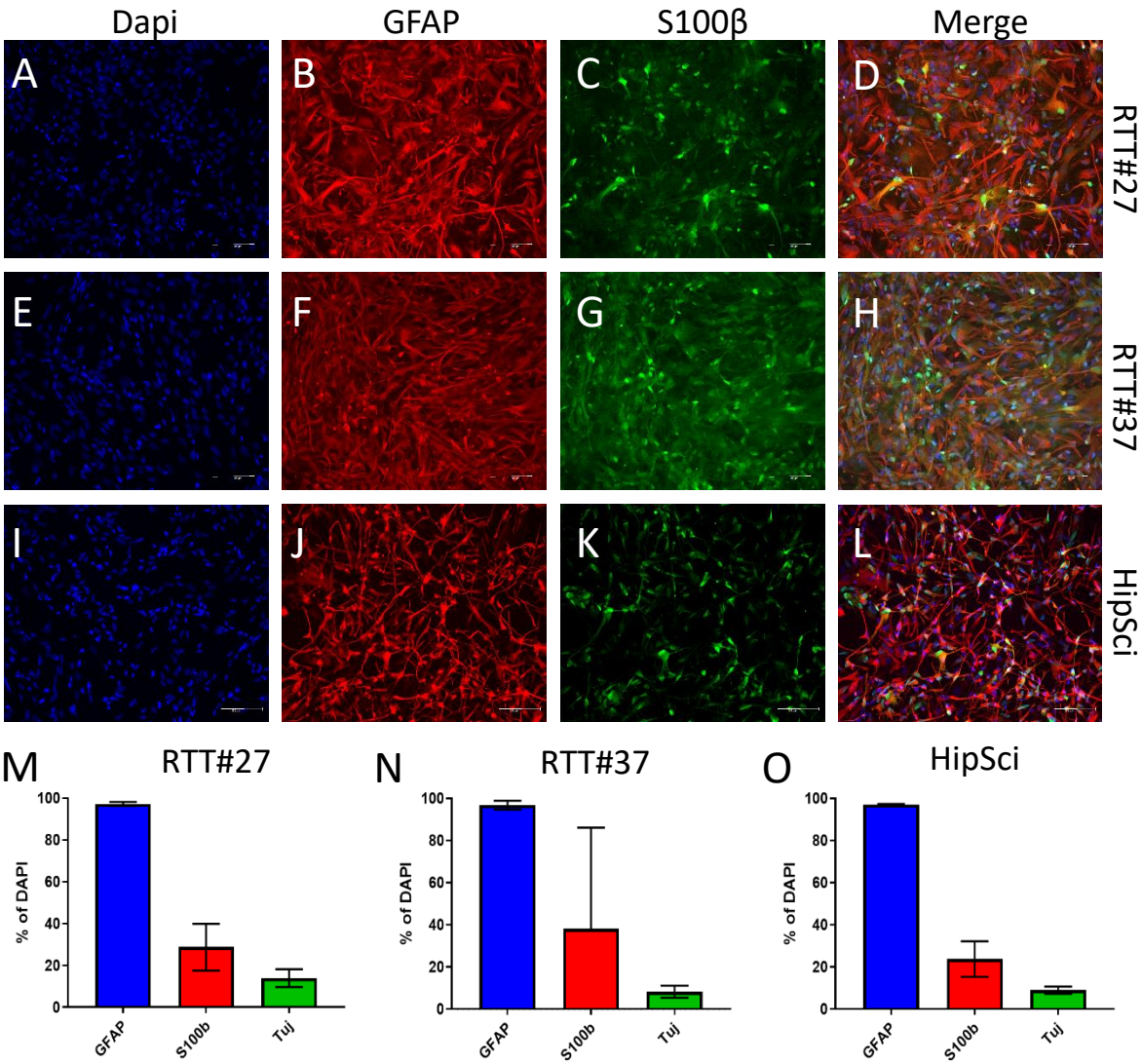

Figure 2.5: iPSC-derived astrocytes stain for GFAP and S100b, forming cultures with little neuronal contamination. Immunocytochemistry images demonstrate that astrocytes from all three cell lines were positive for the astrocyte markers GFAP and S100β. Panels **A), E) and I)** show DAPI staining for cell nuclei, **B), F) and J)** show GFAP staining, **C), G) and K)** show S100β staining, and **D), H) and L)** display the merged images for all three lines. The bar graphs **M), N) and O)** show the quantification of GFAP-, S100β- and Tuj-positive cells for RTT#27, RTT#37 and HipSci lines respectively. Data is expressed as % of total DAPI-positive cells ± standard deviation (n=3). Images are representative. Scale bars are 100µM.

2.4.4 DAPT treatment prevents Ki67-positive cells from appearing in neuronal cultures.

DAPT, a gamma-secretase inhibitor, was used to synchronise the differentiation of neurons and to induced cell cycle arrest (Dovey et al., 2001). This is a useful method for generating cultures of neurons without NPC or glial contamination. This method had been optimised previously by Dr James Crowe and Dr Alastair Grainger (personal communication, Aston University). DAPT treatment for 4 days led to the disappearance of Ki67 staining and therefore presence of proliferative cells. This treatment length was therefore selected for future work in which neurons were generated. ICC images showing Tuj and Ki67 staining for HipSci line-derived neurons can be seen in Figure 2.6. These neurons were used for later experiments (see chapter four).

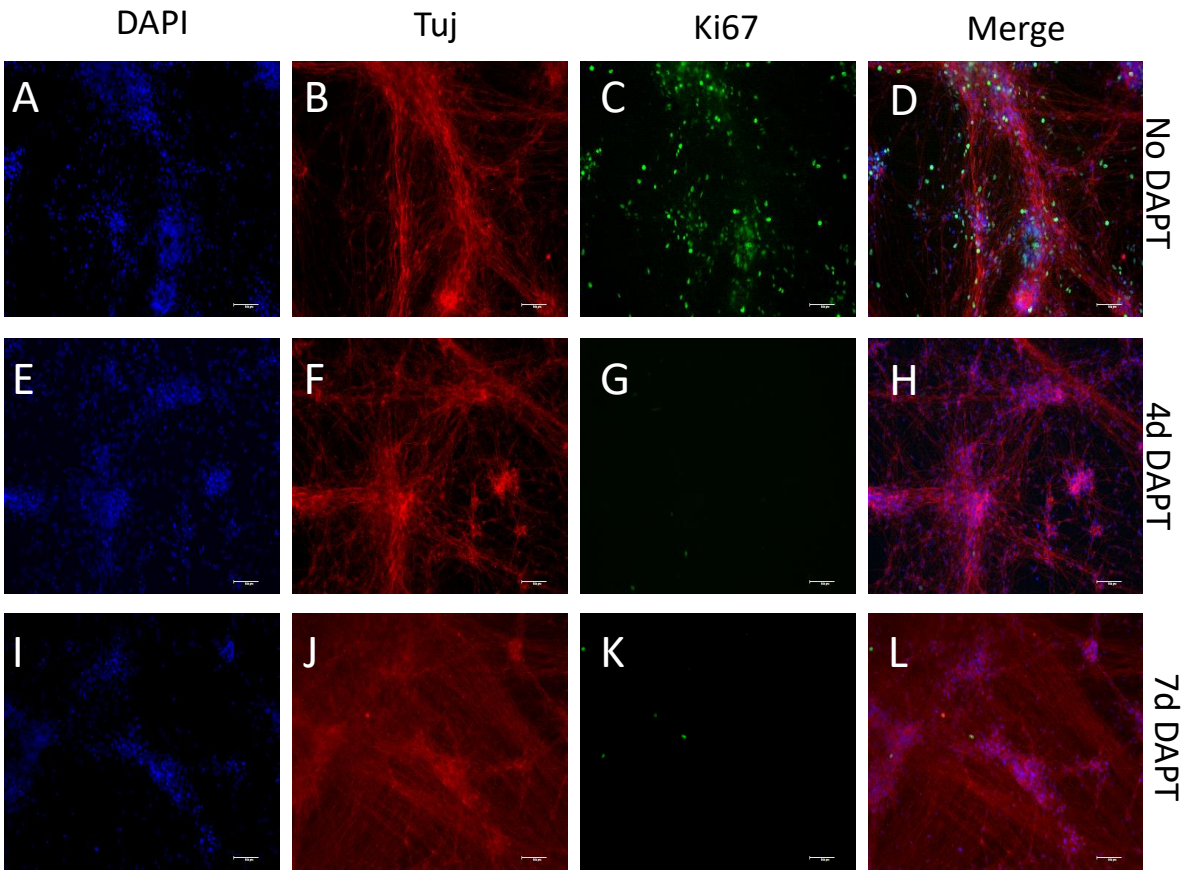

Figure 2.6: ICC images depict Tuj staining and Ki67 staining for HipSci line-derived neuronal cultures generated by treating NPCs with DAPT. Images **A)-D)** show **A)** DAPI (blue), **B)** Tuj (red), **C)** Ki67 (green) staining and **D)** shows the merged image for 4 days with no DAPT treatment post-neural induction. Images **E)-H)** show **E)** DAPI, **F)** Tuj, **G)** Ki67 staining and **H)** shows the merged image for 4 days with DAPT treatment post-neural induction. Images **I)-L)** show **I)** DAPI, **J)** Tuj, **K)** Ki67 staining and **L)** shows the merged image for 7 days with DAPT treatment post-neural induction (n=1). Images are representative. Scale bars are 100µM.

2.4.5 Cells downregulate Oct4 and upregulate GFAP throughout differentiation from iPSC to astrocytes.

In addition to ICC, qPCR was used as a method to further characterise cell types (see section 2.3.12). This method looks at gene expression so it can provide additional information to complement the protein expression analysis performed with ICC images. Pre-validated primers (Primer Design, UK) were used.

Oct4-positive staining was significantly reduced in NPCs in all three cell lines compared to iPSCs (n=3, P<0.05) (Figure 2.7). Oct4 gene expression was also significantly reduced in NPCs and astrocytes compared to iPSCs for all three lines (n=3, P<0.05) (Figure 2.7). Sox2-positive cells were significantly reduced from iPSCs to NPCs and astrocytes in all three cell lines (n=3, P<0.05), with the exception of RTT#27 iPSCs differentiated to RTT#27 astrocytes (Figure 2.8). Sox2 protein expression was seen in all astrocytes (data not shown). The expression of GFAP was also significantly increased in iPSC-derived astrocytes compared to iPSC-derived NPCs (n=3, p<0.05) (Figure 2.9). Genes were normalised to YWHAZ as its expression varied the least across all cell lines and cell types, compared to GAPDH and β-actin (see appendix A1).

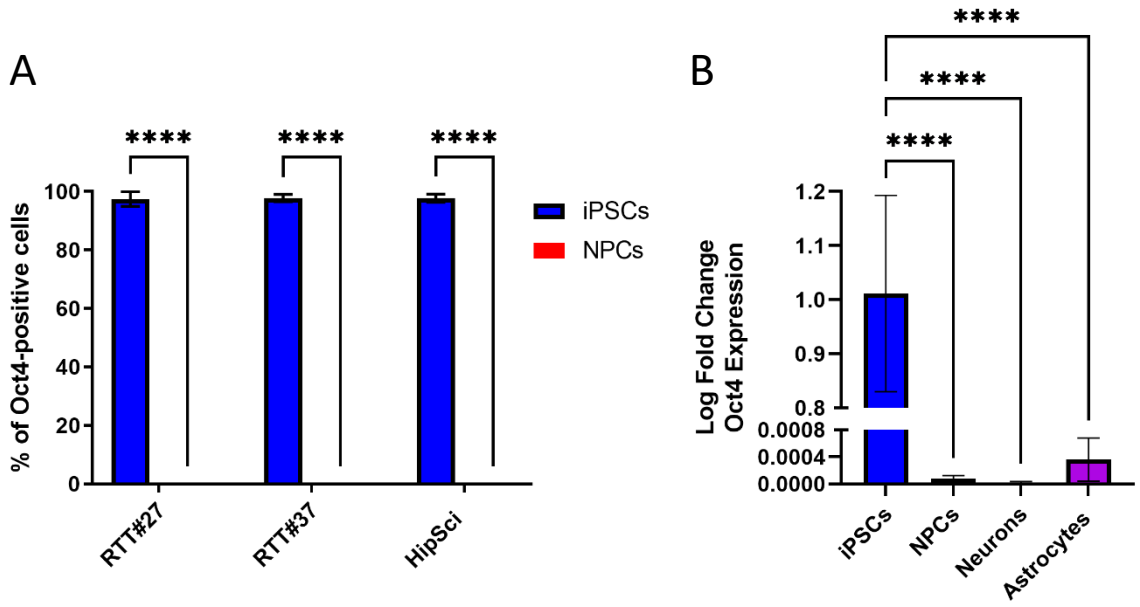

Figure 2.7: Immunocytochemistry quantification and qPCR showing changes in Oct4 protein and gene expression during differentiation. **A)** Shows ICC quantification of Oct4-positive cells in the RTT#27, RTT#37 and HipSci lines in iPSCs and then after differentiated to NPCs as % of Dapi ± standard deviation. **B)** Log fold change Oct4 gene expression after differentiation from iPSCs to NPCs, neurons and astrocytes in the HipSci line ± standard deviation (n=3, **** = p<0.0001, one-way ANOVA with Tukey's multiple comparison test).

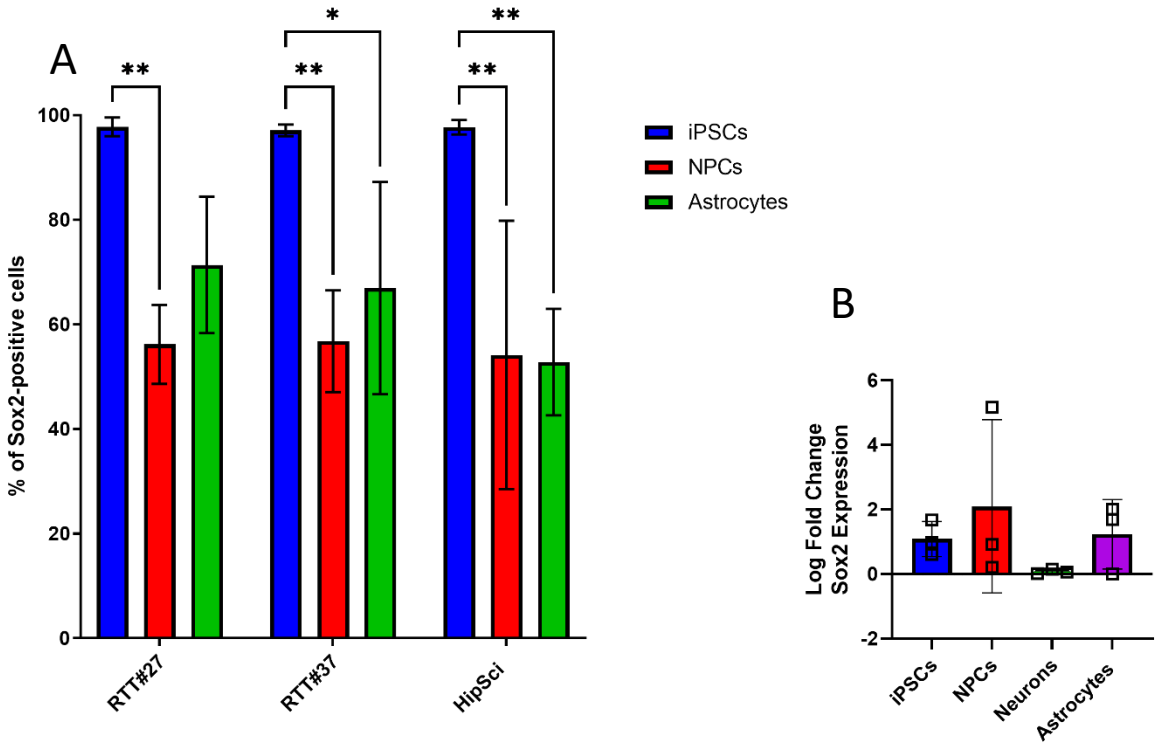

Figure 2.8: Immunocytochemistry quantification and qPCR showing changes in Sox2 protein and gene expression during differentiation. **A)** ICC quantification of Sox2-positive cells in the RTT#27, RTT#37 and HipSci lines in iPSCs, NPCs and astrocytes as % of total Dapi ± standard deviation (n=3, * is p=0.05, ** is p<0.01, two-way ANOVA with Tukey's multiple comparisons test). **B)** Log fold change Sox2 expression in HipSci line NPCs, neurons and astrocytes compared to iPSCs ± standard deviation. Genes normalised with YWHAZ.

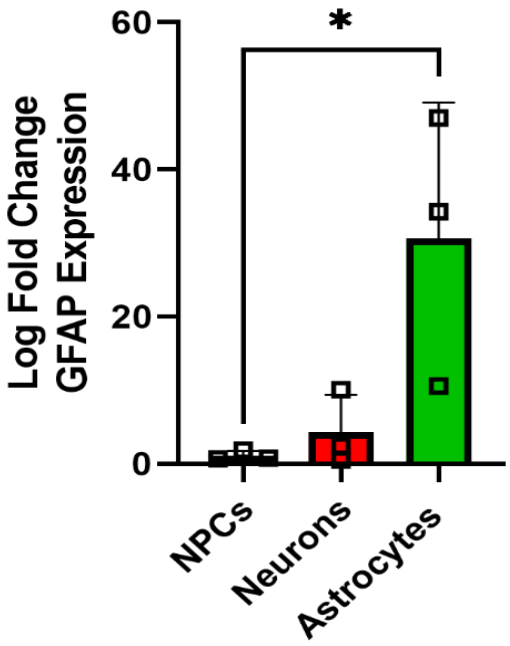

Figure 2.9: GFAP expression increases through the differentiation process from iPSC to astrocyte. Bar graph depicts the log fold gene expression changes for GFAP from differentiation of NPCs to neurons and to astrocytes for the HipSci line. Gene expression was normalised to the housekeeping gene YWHAZ. Results are expressed as log fold change ± standard deviation. * $p<0.05$, one-way ANOVA with Tukey's multiple comparison test, n=3).

2.5 Discussion

The results presented in this chapter demonstrated that NPCs, neurons and astrocytes can be generated from patient and RTT iPSC lines and can be morphologically characterised with ICC and qPCR analysis.

2.5.1 iPSCs can generate NPCs via Neural Induction

After confirming the pluripotent state of the iPSC lines with Oct4 and Sox2 staining cells were differentiated using commercially available media based on (Chambers et al., 2009). The decision to use two-dimensional neural induction as opposed to three-dimensional was that it initially proved successful, so for consistency it was decided to continue using this method for all neural inductions for all lines. However, some studies have suggested that three-dimensional neural inductions result in higher proportions of Pax6- and Nestin-positive cells that gave rise to neurons with longer neurites. It was shown that the neural rosettes generated were similar, and that functional studies such as patch-clamping in order to determine electrophysiological properties performed on the neurons gave similar results between the two methods (Chandrasekaran et al., 2017).

Sox2 is a transcription factor that is present in NPCs, and is one of the earliest markers of the developing CNS (Graham et al., 2003). It helps maintain the progenitor state of NPCs whilst inhibiting neuronal differentiation (Graham et al., 2003). Pax6 is also a transcription factor that is expressed in human neuroectoderm tissue and is thus another good marker for determining that NPCs have been generated (Zhang et al., 2010). NPCs generated for all three cell lines were not 100% Pax6 and Sox2 positive, ranging from 53-66%-positive for Pax6, and 56-67%-positive for Sox2 (see Figure 1.4), however the identity of the remaining cells is unknown. Other cover slips were stained for Nestin and Ki67, so it is plausible that the remaining cells were Nestin-positive but this could not be ascertained without staining for all three markers simultaneously. Due to the morphology of Nestin staining it was not possible to quantify this staining.

2.5.2 NPCs can generate neurons and astrocytes

For the purpose of this PhD it was necessary that NPCs were capable of differentiating into astrocytes, and from the proportions of cells generated that were GFAP-positive it seems this was successful (figure 2.5). At least 96% of cells were GFAP-positive, with variable proportions also being S100β-positive. GFAP gene expression also significantly increased from NPC through to astrocytes. Some neuronal contamination was observed by Tuj staining. This contamination could potentially be because Tuj can be co-expressed with GFAP in developing astrocytes (Dráberová et al., 2008) or because there some neurons in the culture. Another study that generated iPSC-derived astrocytes with the same method also observed 6% neuronal contamination (Hedegaard et al., 2020).

It is possible that the high percentage of GFAP-positive cells versus S100β-positive cells meant that fairly immature populations of astrocytes were generated, in contrast to a recent study that observed almost equally high proportions of S100β and GFAP-positive cells (Hedegaard et al., 2020). In order for more mature astrocytes to be made it would be ideal to grow them in more physiological conditions, for example in the presence of neurons, or maintain them in the astrocyte maturation media for a longer period. It has been shown that astrocytes grown with neurons upregulate more genes associated with maturity, for example components of the astrocyte-neuron lactate shuttle and those involved in neurotransmitter uptake, such as Glt1 and GLAST (Hasel et al., 2017). Removal could have been performed with immunopanning (Foo et al., 2011). However, introducing more cell types into culture increases the level of complexity, and due to time constraints, it was necessary to initially grow astrocytes in monoculture. RTT NPCs have been shown to be biased towards astrocyte lineage, however no differences in population purity of our astrocytes were observed (Andoh-Noda et al., 2015).

In order to gain a more comprehensive view of the potential heterogeneity of the astrocytes generated more diverse markers such as GLAST, Glt1 and AQP4 could have also been investigated. In addition to this it could have also provided more information about potential differences between the control lines and the disease line. qPCR could provide some information about these markers but ultimately gene expression does not always equate to protein expression. Additionally, RNA is collected from heterogenous populations of astrocytes and it is not possible to know exactly which subpopulations could be present. Single-cell RNA-sequencing (RNA-seq) could be a potential solution to learn more about particularly astrocytic populations generated by this method.

The neurons generated from the HipSci line were Tuj-positive, however due to the nature of the staining it was not possible to quantify this properly. To check the maturity of these neurons it might have been beneficial to co-stain Tuj with MAP2. MAPs bind to microtubules to stabilise them, and MAP2 is regarded as a marker for mature neurons (Cassimeris and Spittle, 2001). Further characterisation could have been done with VGLUT1 or glutamic acid decarboxylase 65 or 67, the enzymes that synthesise GABA from glutamate, in order to determine whether the neurons were glutamatergic or GABAergic respectively (Fremeau et al., 2004) (Soghomonian and Martin, 1998).

This chapter has shown that the required cells types can be generated from iPSCs, demonstrated by the reduction in the stem cell marker Oct4 and the emergence of astrocyte markers such as GFAP and S100β. The high percentage of GFAP-positive cells generated mean that it can be deduced that astrocytes were successfully produced and this method was therefore used to generate astrocyte for the remainder of the PhD.

As morphological and immunocytochemical analysis suggested that astrocytes were successfully generated the next stage of the project was to functionally characterise cells to investigate whether they perform typical astrocyte functions, and whether these functions vary between the disease line (RTT#27) and the two control lines (RTT#37 and HipSci).

Chapter Three – Functional characterisation of control and disease iPSC-derived astrocytes.

3.1 Introduction

Astrocytes exhibit many functions that are integral to neurodevelopment, synaptogenesis and neuronal health. As demonstrated in chapter 2, relatively pure populations of astrocytes were generated from both control and patient-derived iPSCs. Astrocytes have been implicated in the development of RTT and numerous studies have shown how they contribute to disease pathogenesis (Kahanovitch et al., 2019). It has also been shown that astrocytes can even spread MeCP2 deficiency throughout the syncytium via their gap junctions, meaning even astrocytes expressing WT MeCP2 can become affected by mutated MeCP2 (Maezawa et al., 2009). It is therefore important to determine any dysfunction that may be exhibited by these cells.

3.1.1 Calcium signalling

Astrocytes express many types of G-protein coupled receptors (GPCRs), such as purinergic, adrenergic, GABAergic and glutamatergic receptors, including many others (Agulhon et al., 2008). This means they are capable of responding to a variety of neurotransmitters such as glutamate and ATP with a rise in intracellular calcium (Cornell-Bell et al., 1990, Charles et al., 1991). They can also release neurotransmitters such as glutamate, ATP and D-serine in order to modulate synaptic activity, giving rise to the term “tripartite synapse”(Araque et al., 1999). Astrocytes *in situ* demonstrate spontaneous calcium oscillations (Parri et al., 2001), as do iPSC-derived astrocytes (Mizuno et al., 2018). Astrocytes can also respond to neurotransmitters such as glutamate and ATP. Astrocytic calcium activity has been shown to be abnormal in RTT (Dong et al., 2018). MeCP2^{R294X} iPSC-derived astrocytes had a significantly higher number of astrocytes that showed spontaneous oscillations compared to WT astrocytes. In addition, these astrocytes had a significantly higher amplitude in their responses to ATP stimulation. Expression of WT MeCP2 in the mutant astrocytes reduced the number that demonstrated oscillations. Such abnormalities were mediated by calcium overload in the endoplasmic reticulum, caused by store operated calcium entry. This effect is partly mediated by increased levels of transient receptor potential cation channel subfamily C member 4 (TRPC4). Such abnormal activity resulted in excessive activation of extrasynaptic NMDARs on neighbouring neurons (Dong et al., 2018).

3.1.2 Glutamate homeostasis

Astrocytes can also take up glutamate to maintain glutamate homeostasis in the brain (Mahmoud et al., 2019, Anderson and Swanson, 2000) (see section 1.13.2). CSF taken from RTT patients contained higher levels of glutamate compared to controls (Hamberger et al., 1992). Additionally, RTT patients often suffer from seizures, potentially due to hyperexcitability

of neurons caused by low basal levels of inhibitory activity (Zhang et al., 2008). This ties in with the finding excitatory/inhibitory balance is altered in RTT brains (Calfa et al., 2015, Banerjee et al., 2016). Additionally, visually evoked excitatory and inhibitory conductance is reduced in V1 pyramidal MeCP2 mutant mice (Banerjee et al., 2016). To further show the role that GABAergic neurons may play in RTT, knocking out MeCP2 from GABAergic neurons recapitulates many features of RTT. These neurons display reduced GABA quanta and reduced glutamic acid decarboxylase 1 and 2 levels in presynaptic locations (Chao et al., 2010). Thus, the role astrocytes play in glutamate homeostasis is an important consideration in RTT, as glutamate is the predominant excitatory neurotransmitter in the CNS and thus plays a key role in the excitatory and inhibitory balance of the brain.

This property of astrocytes has been suggested to be dysfunctional in RTT. Glutamate uptake of extracellular glutamate was shown to be altered in MeCP2-deficient astrocytes taken from mice. These cells removed more glutamate from media compared to WT astrocytes, due to impaired downregulation of Glt1 and GLAST in response to high glutamate concentrations (Okabe et al., 2012). Despite this finding being at odds with the increased concentration of glutamate found in RTT patients' CSF, it highlights that glutamate homeostasis is affected by mutant MeCP2 in astrocytes *in vitro*. Other cell types such as microglia may also display aberrant glutamate homeostasis that could contribute to the overall glutamate concentration in the CSF *in vivo*. This could lead to alterations in circuit formations or maturation of cells.

Glutamate uptake has also been postulated to trigger lactate release from astrocytes as part of the astrocyte-neuron lactate shuttle hypothesis (Pellerin and Magistretti, 1994b). Blocking glutamate transporters in astrocytes results in reduced glucose usage in response to synaptic stimulation, as well as impairing lactate release (Voutsinos-Porche et al., 2003). The link between glutamate uptake and lactate release in astrocytes has not been investigated in RTT.

3.1.5 Oxidative stress

The high levels of metabolism in the CNS in addition to the large presence of lipids means that the CNS is particularly vulnerable to oxidative stress. Astrocytes play an important role in protecting the CNS from oxidative stress (Chen et al., 2020). They can release glutathione (GSH) into the extracellular space which can protect neurons from nitric oxide, which can react with O_2^- to produce harmful reactive oxygen species (Chen et al., 2001b). Astrocytes are able to withstand intense oxidative stress whilst still maintaining their support role, protecting neurons in co-cultures from the same stress insult (Bhatia et al., 2019). Oxidative stress has also been observed in various models of RTT. Post-mortem studies of RTT brains have shown a significant reduction in vitamin C and GSH. It could be that mitochondria are defective in RTT, as there is increased lactate in the CSF of RTT patients and mitochondria have altered morphology (Lappalainen and Riikonen, 1994). MeCP2 knockout mice have shown increased

expression of the Uqcrc1 gene, which encodes a subunit of complex III in the electron transport chain. This results in an increase in mitochondrial respiration and a decrease in mitochondrial coupling, therefore increasing oxygen consumption and reactive oxygen species production. This can increase oxidative burden and therefore make the cells more vulnerable to damage (Filosa et al., 2015). Blood taken from RTT patients showed increased peroxidation damage to membrane lipids and decreased superoxide dismutase in red blood cells (Muller, 2019).

These functional capabilities of astrocytes must therefore be investigated and determined whether there is any difference between RTT and control astrocytes.

3.2 Aims

The overall aim of this chapter was to functionally characterise the iPSC-derived astrocytes generated from the RTT#27, RTT#37 and HipSci lines in chapter two. We hypothesise that the astrocytes would demonstrate normal astrocyte functions with the RTT#27 iPSC-derived astrocytes potentially functioning aberrantly compared to the control lines, RTT#37 and HipSci. In order to achieve these aims the specific aims were to:

1. To determine changes in the expression of genes associated with astrocyte characterisation and functions, such as glutamate uptake, lactate release and oxidative stress using qPCR to elucidate any potential differences in expression between the lines.
2. To determine if there are differences in spontaneous calcium activity in the astrocytes as well as responses to glutamate and ATP stimulation using fluorescent calcium imaging.
3. To determine if glutamate uptake is perturbed in RTT#27 iPSC-derived astrocytes using a fluorescent glutamate assay.
4. Determine whether the astrocytes release lactate in response to glutamate stimulation and if this process is aberrant in RTT#27 iPSC-derived astrocytes using a colourimetric lactate assay.
5. To investigate whether the RTT#27 iPSC-derived astrocytes display signs of oxidative stress by assaying protein carbonyl and isoprostane concentrations present in astrocytes and running a ferric reducing antioxidant power (FRAP) assay to determine antioxidant capacity.

3.3 Methods and Materials

3.3.1 Calcium imaging

Fluorescent calcium imaging was used to assess spontaneous calcium activity as well as invoked responses to 50µM ATP and 100µM glutamate in astrocyte monocultures and ACM-treated neuron monocultures. Astrocytes were grown at a density of 1-1.5 x 10^5 cells per cm^2 on Matrigel®-coated glass coverslips, and NPCs were synchronously differentiated using

DAPT (section 2.3.10) on PORN/laminin-coated glass cover slips (see section 2.3.4). Cells were incubated in 10µM membrane permeable Fluo4-acetoxymethyl ester (Fluo4-AM) (Molecular Probes, Eugene, Oregon, USA) in DMEM for 30 minutes at 37°C with 5% CO_2. Cells were then perfused with artificial cerebrospinal fluid (aCSF) (table 3.1). To maintain its pH, it was bubbled with carbogen gas (5% CO_2 and 95% O_2). Neurons were imaged every 2 seconds and astrocytes every 5 seconds with a 20X dipping lens (Nikon, UK) and a Fluo4 (470nm) filter cube (Chroma VT, USA). Images were acquired with an Orca CCD camera (Hamamatsu, Japan) with a 70ms exposure time. The fluorophore was excited at 470nm using an OptoLED power supply LED (Cairn, UK) and OptoMorph software (Molecular Devices, US). Cells were imaged to investigate spontaneous activity as well as responses to 50µM ATP and 100µM glutamate. Astrocytes were imaged every 5 seconds for 15 minutes and neurons were imaged every 2 seconds for 15 minutes. Spontaneous activity was recorded for 5 minutes before the addition of glutamate for 60 seconds in the astrocyte and neuron cultures. ATP was added at ten minutes for 60 seconds in the astrocyte cultures only.

aCSF component	Concentration (mM)
NaCl	126
KCl	2.5
$NaHCO_3$	26
Glucose	10
$MgSO_4$	10
$CaCl_2$	2
KH_2PO_4	1.25

Table 3.1: Table showing composition of aCSF.

3.3.2 Calcium imaging analysis – responses to neurotransmitters and spontaneous events

Analysis was performed using ImageJ. Videos were opened in image stacks and the brightness and contrast was adjusted. The images were corrected for any drift that occurred during imaging using the plugin Registration -> Linear Stack Alignment with SIFT. 40 regions of interest were chosen for astrocytes and 80 were chosen for neurons. The mean grey values were then calculated for each region of interest for each image. The raw values were transferred into Microsoft Excel and normalised to baseline using this equation: $\frac{\Delta F}{F} = \frac{F-F0}{F0}$. F0 is the value for the first frame in a video file. A cell was determined as responding to a neurotransmitter if the value of the peak was greater than $\frac{\Delta F}{F}$ + 2 standard deviations of the mean for every cell. A lag model was then created by subtracting the previous cell value from

each cell. Spontaneous events and active cells were then counted using the following equation to count peaks that were over 10% higher than baseline for neurons, or 5% for astrocytes:

=SUM((X2:X151>10)*(IFERROR((X2:X151>SUBTOTAL(4,OFFSET(X1,ROW(X2:X151)-2-1,0,2)))*(X2:X151>SUBTOTAL(4,OFFSET(X2,ROW(X2:X151),0,2))),0))

These values were chosen as they reflected the values where visual peaks could be seen by eye best for each cell type.

3.3.3 Glutamate uptake assay

Astrocytes were seeded at a density of 125,000 cells/cm^2 in a 12 well plate and one well was incubated for 30 minutes in Krebs'-Ringer-HEPES buffer (KR) (115mM NaCl, 5mM KCl, 1mM $MgCl_2$, 24mM $NaHCO_3$, 2.5mM $CaCl_2$-$2H_2O$, 25mM HEPES with 5.5mM D-Glucose) containing 200µM TBOA and two other wells were incubated with KR alone. After 30 minutes the KR wells were exchanged for KR containing either 30µM or 100µM glutamate, and the 200µM TBOA well was swapped for 30µM glutamate + 200µM TBOA. KR was then collected at 0 minutes, 30 minutes and 4 hours and immediately stored at -80^{o}C. Between sampling cells were stored at 37^{o}C and 5% CO_2. At 4 hours the cells were then scraped in 300µl of PBS and stored at -80^{o}C. To confirm glutamate did not degrade during the experiment 100µM was added to KR and added to an empty well containing no astrocytes. This was sampled at 0 minutes and 4 hours. The concentrations of glutamate in the samples and of the glutamate on its own were then determined using a fluorometric glutamate assay kit (Abcam) according to manufacturer's instructions (see appendix). The plates were then read in a Spectromax fluorescent plate reader.

3.3.4 Lactate release assay

Samples collected for the glutamate uptake assay (see section 3.3.3) were also used to quantify lactate release from cells. The samples taken at 0 minutes and 30 minutes were used. The lactate concentration in these samples were determined using a lactate assay (Abcam) according to manufacturer's instructions (see appendix). The plates were then read on a MultiSkan EX plate reader (ThermoFisher, USA).

3.3.4 Oxidative stress assays

Oxidative stress assays were kindly performed by Dr Richard Elsworthy (University of Birmingham, UK) on RTT#27, RTT#37 and HipSci iPSC-derived astrocyte lysates (n=3). The methods in this section are provided by Dr Richard Elsworthy.

3.3.4.1 Total 8-isoprostanes

Total 8-isoprostanes were measured using an ELISA kit to assess lipid peroxidation in cell lysates (516351, 8-isoprostane ELISA kit, Cayman Chemical). Immunoprecipitation was performed on cell lysates prior to the assay to ensure maximum specificity of antibody binding. Briefly, samples (100 µl) were added to the 8-isoprostane affinity sorbent (401113, 66 Cayman

Chemical) and incubated for 60 minutes with gentle mixing and then centrifuged at 1500xg for 30 seconds to sediment the sorbent. The supernatant was removed and discarded. Eicosanoid Column Affinity buffer (100µL, 400220, Cayman Chemical) was added and placed in the centrifuge at 1500xg for 30 seconds, the supernatant was then removed. This step was repeated by adding ultrapure water (100µL) before centrifugation and discarding the supernatant. Elution solution (100µL, 95% ethanol) was then added to the sediment and evaporated to dryness under nitrogen. Samples were suspended in the ELISA buffer (100µL). After immunoprecipitation of the samples, standards were prepared from the assay stock solution to create an 8-point standard curve ranging from 0/8 to 500pg/ml, a blank well was used as the 0pg/ml standard. Standard or sample (50µL) was added to the appropriate well with of 8-isoprostane tracer (50µL) and antiserum (50µL). This was incubated for 18hours at 4^{O}C. Ellman's reagent was added to each well (200µL) and left to incubate for 2 hours with gentle agitation. The plate was then read at 420nm (Fluostar Omega, BMG Labtech) and samples were calculated against the logit regression of standards (pg/ml) For cell assays, samples were normalised to total protein concentration of corresponding sample (pg/ml/mg).

3.3.4.2 Protein carbonyls

Modification of protein by formation of carbonyl groups was assessed by the method of (Carty et al., 2000). The preparation of carbonyl standards was carried out prior to the assay. Briefly, dialysis tubing was prepared by boiling in sodium bicarbonate (2% v/w) and EDTA (1mM, pH8). Tubing was rinsed and boiled for a further 10 min EDTA (1mM, pH8) before cooling and storing in ethanol at 4^{o}C. For oxidized BSA, BSA (10mg/ml) (50ml) was oxidized with AAPH (500mM) for 1 hour at 37^{o}C and dialysed against Tris-buffered saline (pH7) for 24 hours with frequent buffer changes. For reduced BSA, BSA (10mg/ml) was 67 added to sodium borohydride (1g) in TBS (50ml) and allowed to reduce overnight at 4^{o}C. The solution was then dialysed against TBS pH7, with frequent buffer changes. Protein concentration was then adjusted following BSA assay measurement and adjusted to equal concentrations (mg/ml). Oxidised and reduced standards were serially mixed to give a range of concentrations. Standards (500µl) were then added to DNPH (10mM, 500µl) and left for 1h with gentle agitation. Controls were made with HCl (2N, 500µl) added to DNPH (10mM, 500µl). Trichloroacetic acid (20%, 500µl) was then added to each standard and mixed before centrifugation for 3 min at 13000g. The supernatant was discarded, and the pellet washed 3 times with ethanol:ethyl acetate (1:1). Following washing, pellets were resuspended in guanidine HCl (1ml) and after vortexing left for 30 mins at 37^{o}C. Solutions were vortexed once more before centrifugation for 1min at 13000g. The supernatant was then removed, and absorbance read at 360nm (Fluostar Omega, BMG Labtech). Molarity of the solution was calculated ((abs-blanks)/22000) and normalized to protein content to give standard carbonyl content (nmol/mg). For determining carbonyl content samples (sodium carbonate 50mM, pH 9.2) were plated into 96 well plates (50µL at

0.05mg/ml). Protein was allowed to bind for 1h at 37o C before washing with TBS±Tween (300µL, 0.5%). DNPH was added in 2M HCl (1mM, 50µL) and allowed to react for 1h at room temperature before washing as before. Non-specific binding sites were blocked overnight at 4oC with TBS-tween (200µL, 1%). After washing, rabbit anti-DNPH primary antibody (50µL, 1:1000) was applied and incubated for 1h at 37OC and, following washing with TBS/Tween, anti-rabbit IgE conjugated to peroxidase (50µL, 1:5000) was also incubated at 37oC for 1h. The reaction was visualised by substrate solution (50µL; o-phenylenediamine tablets with hydrogen peroxide (8µl) in citrate-phosphate buffer (10ml) and stopped by addition of sulphuric acid (50µL, 2N). Absorbance was read at 490nm 68 (Fluostar Omega, BMG Labtech) and samples were calculated using linear regression. For cell assays, samples were normalised to total protein concentration of corresponding sample (mg/ml).

3.3.4.3 Total antioxidant capacity

Total antioxidant capacity was measured using a previously described method (Benzie and Strain, 1996). For blood plasma, samples were diluted 1:1 with ultrapure water (Millipore). For cell lysates, no dilution was utilised. Standards were freshly prepared using Ascorbic acid to create a 7-point standard curve ranging from 0µM to 1000µM. Sample or standard (10µl) was then added into wells a 96-well microtiter plate in duplicate. Next, the 'FRAP' reagent (300µl) was made by combining acetate buffer (30ml, 300mM), TPTZ solution (3ml, 10.6mM) and ferric chloride solution (3ml, 20mM) and added to each well. The plate was then incubated for 8 minutes at room temperature. Plate reading was completed at 650nm (Fluostar Omega, BMG Labtech) and values were calculated using linear regression. Values were expressed as µM of antioxidant power relative to ascorbic acid. For cell lysates assays, samples were normalised to total protein concentration of corresponding sample (µM /mg).

3.3.5 qPCR

See methods section 2.3.12.

3.4 Results

3.4.1 There is no significant difference in astrocyte gene expression between patient line and controls.

qPCR was performed on the disease line RTT#27 and the two control lines, RTT#37 and HipSci, in addition to a foetal primary astrocyte line. AQP4, GFAP and S100β were investigated but no significant differences in gene expression were found (Figure 3.1).

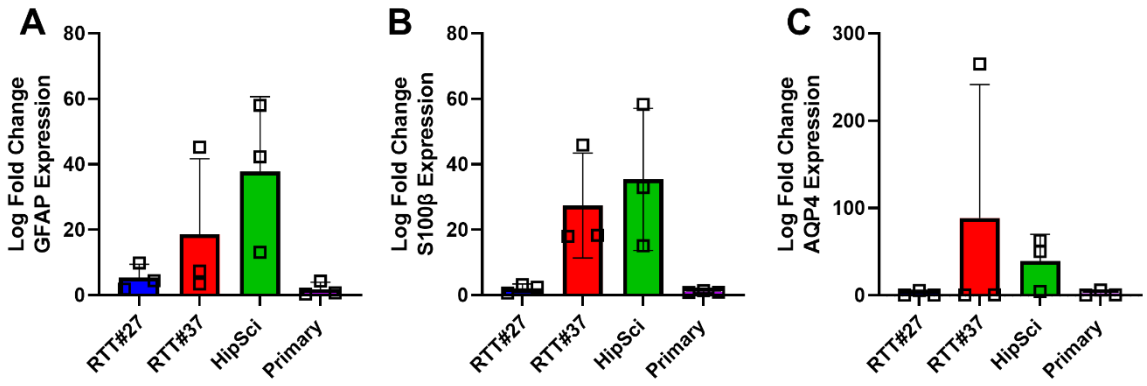

Figure 3.1: AQP4, GFAP or S100β gene expression in RTT#27, RTT#37, HipSci and Primary astrocytes. **A)** shows log fold change of AQP4 of RTT#27, RTT#37 and HipSci. **B)** shows log fold change of GFAP of RTT#27, RTT#37 and HipSci. **C)** shows log fold change of S100β of RTT#27, RTT#37 and HipSci (n=3). Results shown as log fold change ± standard deviation. One-way ANOVA with Tukey's multiple comparison test. Genes normalised with YWHAZ.

3.4.2 Astrocytes demonstrate spontaneous calcium oscillations and can respond to neurotransmitters such as glutamate and ATP.

In order to investigate whether the iPSC-derived astrocytes displayed functional characteristics of astrocytes *in vivo*, cells were assessed using calcium imaging to ascertain whether they demonstrated spontaneous calcium oscillations and responded to the neurotransmitters glutamate and ATP.

There was no significant difference in the percentage of cells showing spontaneous oscillations in the first five minutes pre-addition of glutamate between each cell line (RTT#27: 20.56±13.70%; RTT#37: 7.22±6.14%; HipSci: 29.17±30.16%, n=3, one-way ANOVA with Tukey's multiple comparison test). The total number of peaks counted was then divided by the number of cells displaying spontaneous oscillations in order to determine the average activity of the cells in each cell line. No significant differences were found (RTT#27: 1.23±0.82; RTT#37: 0.92±0.14; HipSci: 1.98±1.01, n=3, one-way ANOVA with Tukey's multiple comparison test, Figure 3.2).

There was no significant difference between the RTT#27, RTT#37 or HipSci lines in the percentage of cells that displayed spontaneous oscillations, determined by a 5% rise from

baseline (determined using method in section 3.3.3. In addition, the number of active cells were divided by the total number of peaks, but no significant difference was found.

To ascertain whether the iPSC-derived astrocytes could respond to neurotransmitters, 100µM of glutamate and 50µM ATP were added at 2.5 minutes and 10 minutes, respectively. Each neurotransmitter was added for one minute before being washed off with aCSF. Effects observed 2.5 minutes post-addition due to time taken for the neurotransmitters to pass through the perfusion system. No significant differences were found in the scale of the response to glutamate or ATP. RTT#27 iPSC-derived astrocytes responded to glutamate with a 15.95±11.35% increase in fluorescence, averaged from 40 cells per cover slip, with each biological differentiation having at least two cover slips. RTT#37 iPSC-derived astrocytes demonstrated an average 12.34±5.24% increase, and the HipSci iPSC-derived astrocytes had an average 32.99±26.57% increase (Figure 3.3). ATP also evoked responses in iPSC-derived astrocytes (RTT#27: 43.31±22.15%; RTT#37: 33.53±26.18%; HipSci 90.88±34.54%; n=3, Figure 3.2).

Next, the responses of each astrocyte line to glutamate, ATP or both were assessed. There was no significant difference in the response of HipSci (24.17±18.97%), RTT#27 (10.00±8.04%) or RTT#37 iPSC-derived astrocytes (15.28±7.47%) responses to glutamate. The percentage of HipSci iPSC-derived astrocytes that responded to ATP (90.00±1.25%) was significantly higher than the percentage of cells that responded to ATP from the RTT#27 (53.89±6.14%) and RTT#37 (57.64±9.92%) iPSC-derived astrocyte cultures (Figure 3.2).

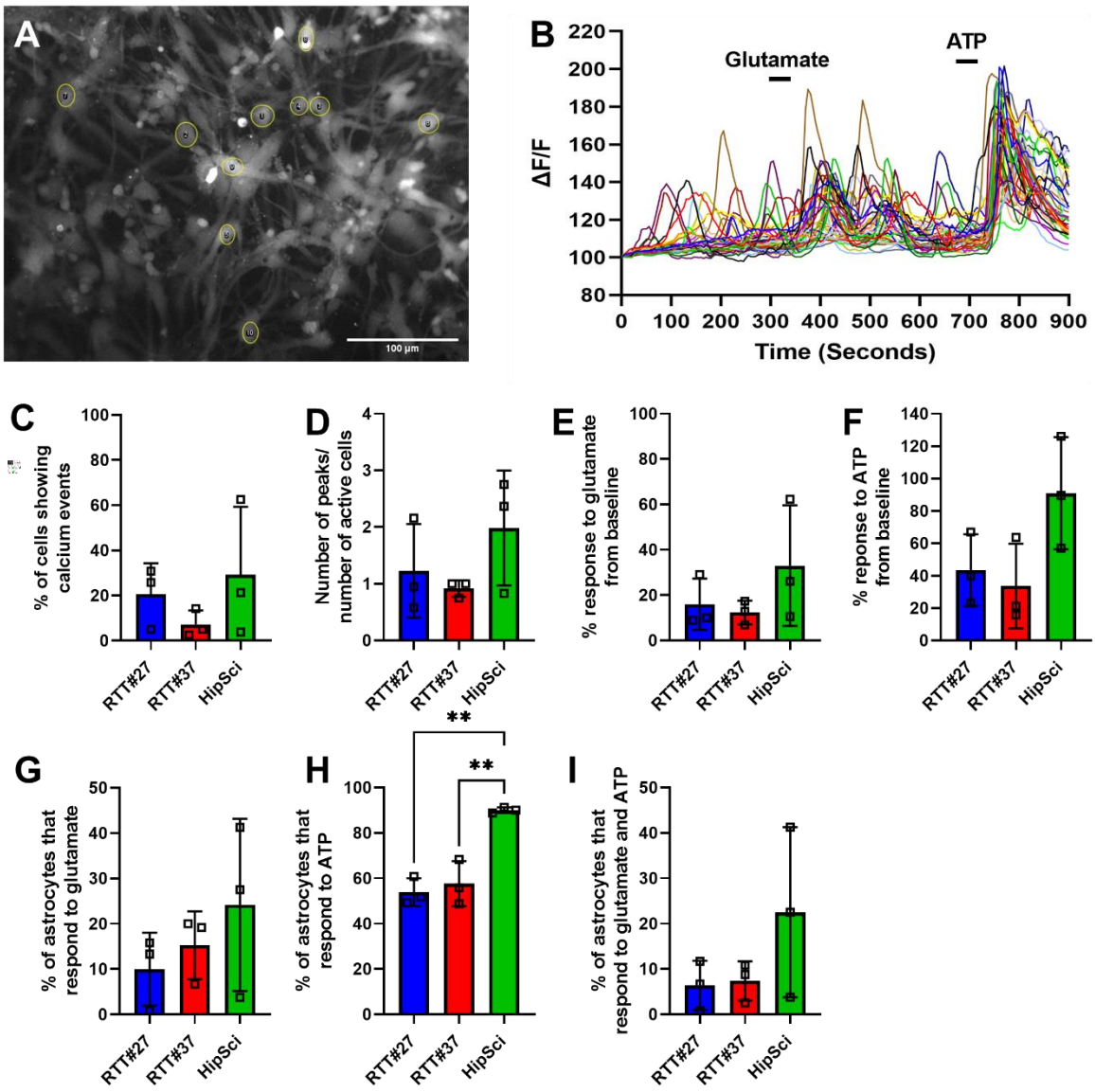

Figure 3.2: Astrocytes show spontaneous calcium events and can respond to glutamate and ATP. **A)** shows representative image of iPSC-derived astrocytes loaded with Fluo4-AM. **B)** shows a representative trace of calcium activity in iPSC-derived astrocytes loaded with Fluo4-AM. **C)** shows the percentage of cells that showed spontaneous oscillations in the first five minutes. **D)** shows the total number of peaks divide by the number of active cells. **E)** shows a bar graph of the % increase response to glutamate from baseline. **F)** shows % increase response to ATP from baseline. **G)** displays the percentage of astrocytes from each line that responded to glutamate. **H)** displays the % of astrocytes that respond to ATP. **I)** displays the percentage of astrocytes from each cell line that responded to both glutamate and ATP. 3 cover slips were imaged per each biological differentiation (n=3), 40 cells were analysed per cover slip, one-way ANOVA with Tukey's multiple-comparison test. Results expressed as % of cells ± standard deviation. One-way ANOVA with Tukey's multiple comparison test. ** = $p<0.01$.

3.4.3 Astrocytes can take up glutamate from their surroundings in an EAAT-dependent manner.

Astrocytes play a key role in glutamate homeostasis in the brain. In order to assess glutamate uptake in iPSC-derived astrocytes the three cell lines were subjected to two conditions. 30µM glutamate or 100µM glutamate was added to KR buffer and incubated with astrocytes over 240 minutes. The KR was sampled at 0 minutes, 30 minutes and 240 minutes. In the 30µM glutamate condition astrocytes from all three iPSC lines had removed glutamate from the KR after 30 minutes (RTT#27 0.018±0.005; RTT#37 0.030±0.0126; HipSci 0.023±0.016, calculated as µM/mg of protein ± standard deviation, n=3, Figure 3.3A). The uptake continued until 240 minutes (RTT#27 0.016±0.011; RTT#37 0.048±0.021; HipSci 0.031±0.015, calculated as µM/mg of protein ± standard deviation, n=3, Figure 3.3). After 240 minutes the RTT#37 iPSC-derived astrocytes had removed significantly more glutamate from the KR than the RTT#27 iPSC-derived astrocytes ($p<0.05$).

iPSC-derived astrocytes could also remove glutamate from the KR after incubation in 100µM glutamate. After 30 minutes all three lines had removed glutamate (RTT#27 0.054± 0.010; RTT#37 0.069± 0.054; HipSci 0.042± 0.024, calculated as µM/mg of protein ± standard deviation, n=3, Figure 3.3). Again, uptake continued until at least 240 minutes (RTT#27 0.086± 0.031; RTT#37 0.146± 0.069; HipSci 0.102± 0.018, calculated as µM/mg of protein ± standard deviation, n=3, Figure 3.3). 100µM glutamate was also added to KR and incubated at 37^{o}C without cells present to confirm glutamate does not degrade spontaneously, and a very small decrease in concentration was observed by 240 minutes (3.52%, n=1, Figure A2).

In order to assess whether the glutamate uptake by the iPSC-derived astrocytes was mediated by EAATs the global EAAT inhibitor, TBOA, was added with 30µM glutamate. TBOA significantly blocked glutamate uptake for 30 minutes in the RTT#37 iPSC-derived astrocytes, though this effect was reduced by 240 minutes. Despite a lack of significance in the RTT#27 and HipSci iPSC-derived astrocytes a reduction in glutamate uptake is still observed after 30 minutes (Figure 3.3).

qPCR was performed to assess the levels of gene expression of the glutamate transporters GLAST and Glt1 to investigate whether difference in expression could explain the glutamate uptake differences between the RTT#27 and RTT#37 iPSC-derived astrocytes. There was no significant difference in the expression of GLAST and Glt1 in all three iPSC-derived astrocyte lines or primary astrocytes (Figure 3.4).

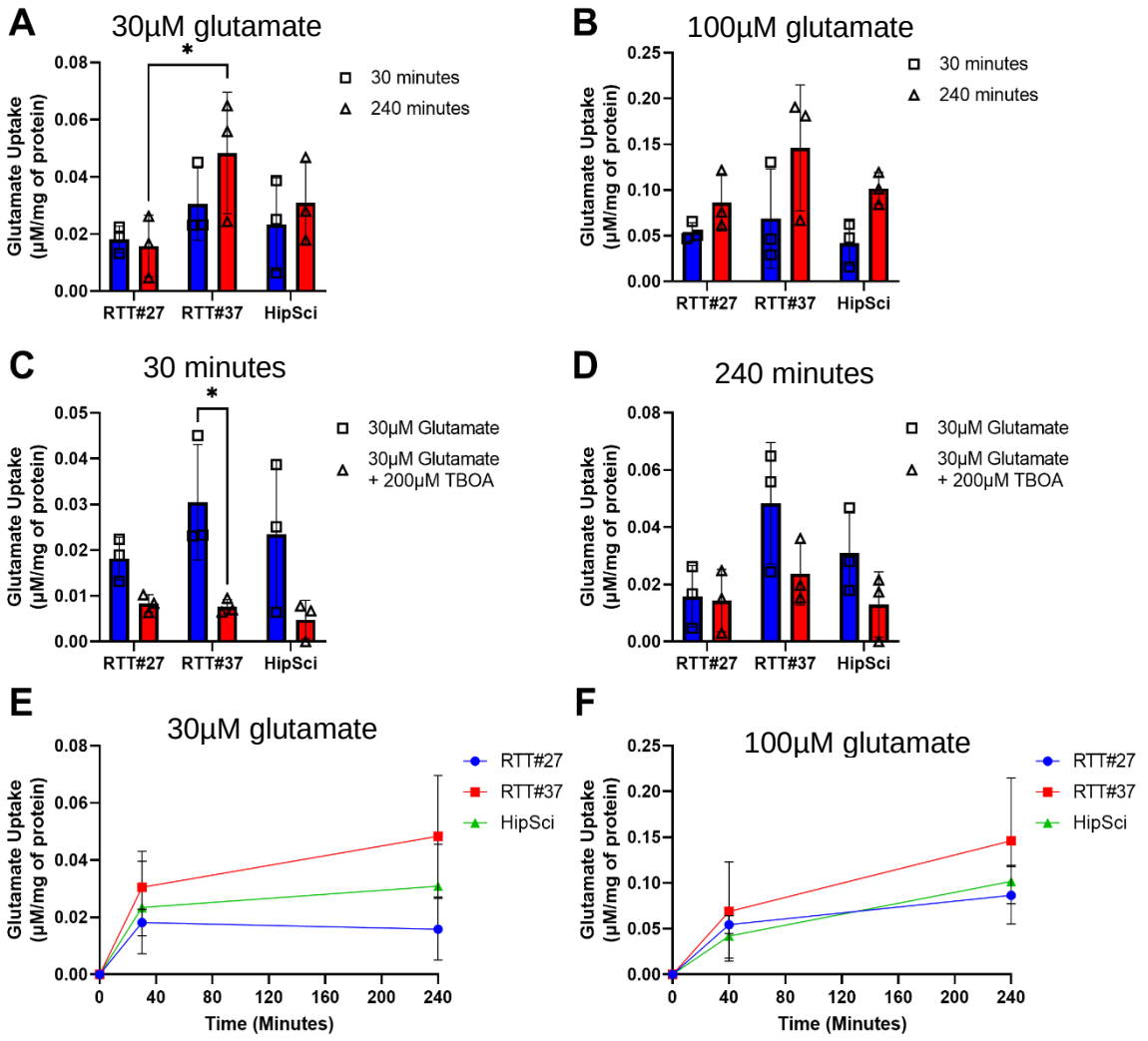

Figure 3.3: iPSC-derived astrocytes can remove glutamate from their surroundings. **A)** Bar graph showing glutamate removed from KR expressed as µM/mg of protein ± standard deviation over a 240 minute time period after incubation in 30µM glutamate. **B)** Bar graph showing glutamate removed from KR expressed as µM/mg of protein ± standard deviation over a 240 minute time period after incubation in 100µM. **C)** Bar graph showing glutamate removed from KR expressed as µM/mg of protein ± standard deviation after 30 minutes after incubation in 30µM glutamate and 200µM TBOA. **D)** Bar graph showing glutamate removed from KR expressed as µM/mg of protein ± standard deviation after 240 minutes after incubation in 30µM glutamate and 200µM TBOA. **E)** shows the time course of glutamate uptake after incubation in 30µM glutamate over the 240 minute time course. **F)** shows the time course of glutamate uptake after incubation in 100µM glutamate over the 240 minute time course. Error bars display standard deviation. All n=3, two-way ANOVA with Tukey's multiple comparison test. * = $p<0.05$.

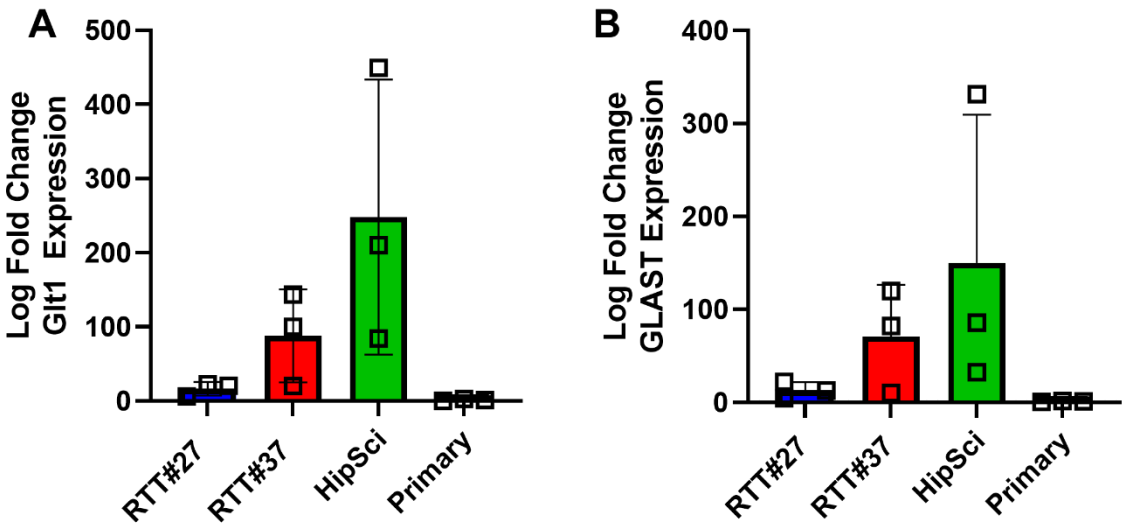

Figure 3.4: Glt1 and GLAST gene expression in iPSC-derived astrocytes. **A)** Log fold change of Glt1 gene expression shows Glt1 gene expression in RTT#27, RTT#37 and HipSci iPSC-derived astrocytes compared to primary astrocytes ± standard deviation. **B)** Log fold change of GLAST gene expression in RTT#27, RTT#37 and HipSci iPSC-derived astrocytes compared to primary astrocytes ± standard deviation. All n=3, one way ANOVA with Tukey's multiple comparison test. Genes normalised to YWHAZ.

3.4.4 Astrocytes release lactate in response to glutamate.

Glutamate has previously been shown to trigger lactate release from rodent astrocytes and embryocarcinoma-derived astrocytes (Pellerin and Magistretti, 1994b, Tarczyluk et al., 2013). Lactate concentration was therefore investigated in the KR after 30 minutes of glutamate treatment. This time point was chosen as results seen in Figure 3.3 demonstrated that TBOA was able to block glutamate at this point and therefore its impact on lactate could be assessed.

HipSci iPSC-derived astrocytes released significantly more lactate after 30 minutes in response to 30µM glutamate compared to RTT#27 iPSC-derived astrocytes (30µM glutamate RTT#27 0.02± 0.02((µM)(ml)/mg); HipSci 0.10± 0.02((µM)(ml)/mg), n=3, Figure 3.5).

In order to determine if lactate release was mediated by glutamate uptake, treatment with 30µM and 200µM TBOA treatment was also investigated. The addition of 200µM TBOA to the 30µM glutamate condition caused a decrease in lactate release which was significant ($p<0.01$) in the HipSci line iPSC-derived astrocytes compared to cells in 30µM glutamate alone (Figure 3.5).

Lactate is released from astrocytes via MCT1, as proposed by the astrocyte-neuron lactate shuttle hypothesis (Pellerin et al., 1998). Therefore, MCT1 expression was investigated in the astrocyte lines in order to see if there was a difference that could account for the discrepancies in lactate release between the RTT#27 and HipSci iPSC-derived astrocytes. No significant difference in gene expression was observed between the lines (Figure 3.5).

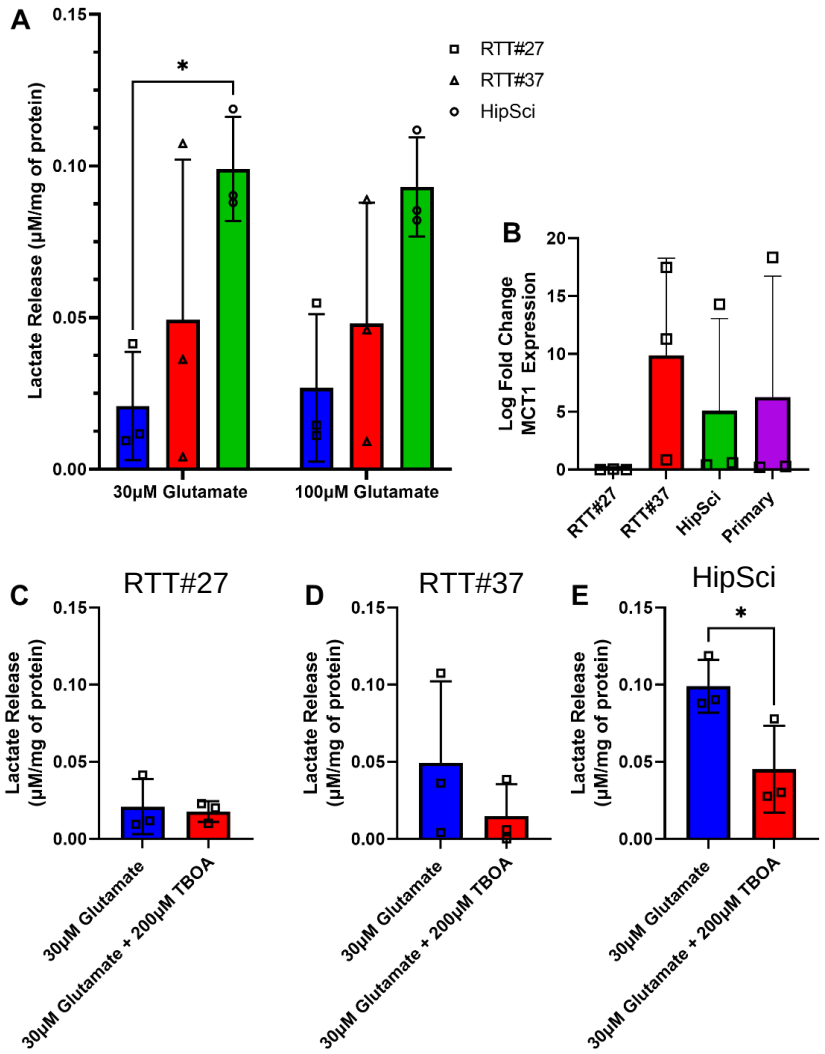

Figure 3.5: iPSC-derived astrocytes release lactate in response to glutamate which can be blocked by TBOA. **A)** Bar graph shows lactate release normalised to astrocyte protein levels after incubation in 30µM and 100µM glutamate expressed as µM/mg of protein ± standard deviation (two-way ANOVA with Tukey's multiple comparison, n=3, * = p<0.05). **B)** Log fold change of MCT1 gene expression shows Glt1 gene expression in RTT#27, RTT#37 and HipSci iPSC-derived astrocytes compared to primary astrocytes ± standard deviation (One-way ANOVA with Tukey's multiple comparison test, n=3, gene normalised to YWHAZ). **C)** Bar graph shows lactate release from RTT#27 iPSC-derived astrocytes normalised to astrocyte protein levels expressed as µM/mg of protein ± standard deviation after incubation in 30µM and 200µM TBOA. **D)** Bar graph shows lactate release from RTT#37 iPSC-derived astrocytes normalised to astrocyte protein levels expressed as µM/mg of protein ± standard deviation after incubation in 30µM and 200µM TBOA. **E)** Bar graph shows lactate release from HipSci iPSC-derived astrocytes normalised to astrocyte protein expressed as µM/mg of protein ± standard deviation levels after incubation in 30µM and 200µM TBOA. (unpaired T-test, n=3, * = p<0.05).

3.4.5 RTT#27 astrocytes do not show significant signs of oxidative stress.

In order to assess whether iPSC-derived astrocytes display signs of oxidative stress, the quantities of protein carbonyls, isoprostanes and antioxidant capacity of the cells were assessed. No significant differences in isoprostanes concentrations (RTT#27: 41.51±4.24pg/mL/mg; RTT#37: 48.58±23.11pg/mL/mg; HipSci: 31.48±2.07pg/mL/mg) or protein carbonyls concentrations (RTT#27: 58.34±8.23mg/mL/mg; RTT#37: 42.74±3.31mg/mL/mg; HipSci: 40.54± 11.83 mg/mL/mg). To assess antioxidant capacity a FRAP assay was performed, and no difference was observed between the cell lines (RTT#27: 1031.24± 134.30µM/mL/mg; RTT#37: 891.16± 269.95µM/mL/mg; 798.84± 134.71 µM/mL/mg). SOD2 expression was also investigated, but no significant differences in gene expression were observed across all cell lines (Figure 3.6).

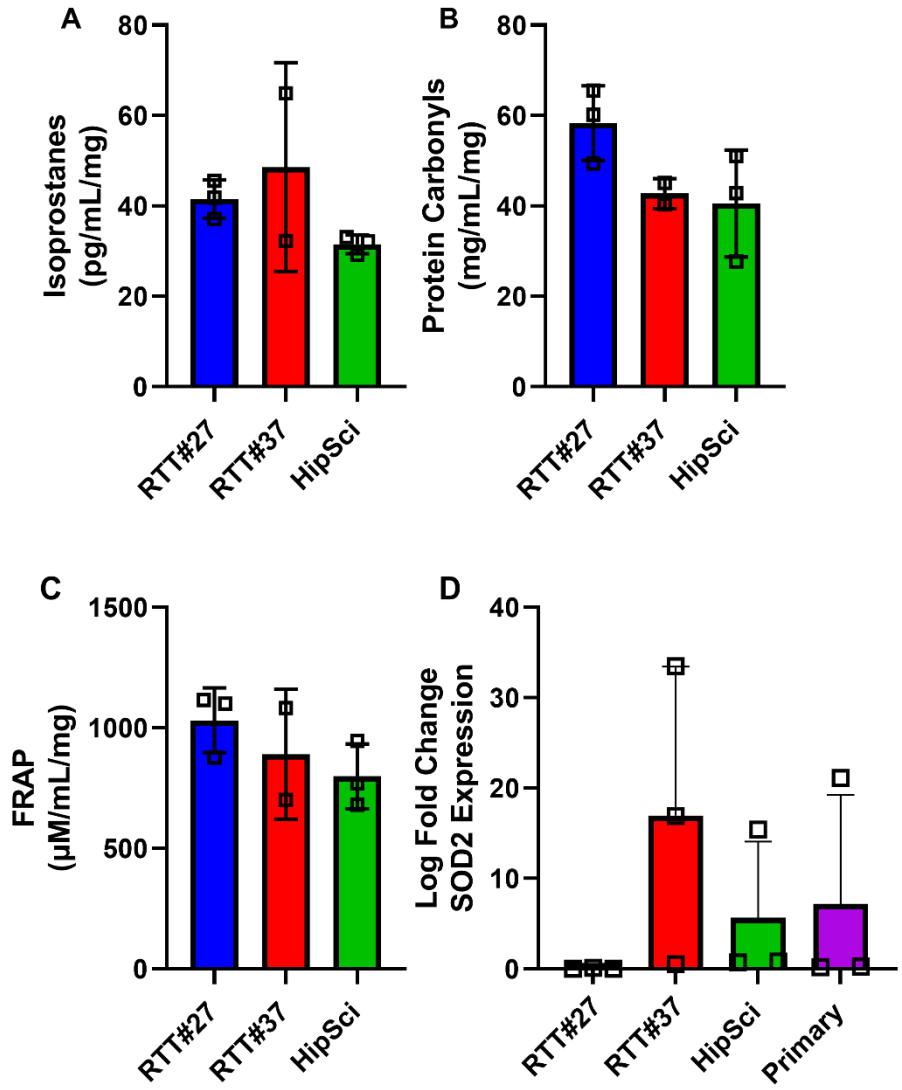

Figure 3.6: There are no significant differences in oxidative stress or SOD2 expression in RTT#27, RTT#37 and HipSci iPSC-derived astrocytes. **A)** depicts a bar graph displaying protein carbonyl concentrations normalised to astrocyte protein levels. **B)** shows isoprostanes concentrations normalised to astrocyte protein levels. **C)** shows the FRAP concentrations normalised to astrocyte protein levels. **D)** shows the log fold change in SOD2 expression in the RTT#27, RTT#37 and HipSci iPSC-derived astrocytes compared to primary astrocytes. Genes normalised to YWHAZ. (A-C RTT#27 and HipSci n=3, RTT#37 n=2, D) RTT#27, RTT#37 and HipSci n=3, one-way ANOVA with Tukey's multiple comparison test). Error bars show standard deviation.

3.5 Discussion

3.5.1 Gene Expression

qPCR was performed on iPSC-derived astrocytes in order to further characterise control and RTT#27 iPSC-derived astrocytes. No significant differences in gene expression were found for AQP4, GFAP or S100β in iPSC-derived astrocytes or primary astrocytes. This was unexpected as previous studies have demonstrated astrogliosis, a state associated with astrocytic reactivity and increased GFAP expression, in RTT brain cerebellum and cortex (Oldfors et al., 1990, Jellinger et al., 1988). Analysis of post-mortem RTT tissue has shown an increase in GFAP expression (Armstrong, 2005). Such an increase in GFAP expression has also been observed in MeCP2-deficient mice, in addition to increased S100β expression (Okabe et al., 2012). However, one RNA sequencing study noted that genes associated with astrogliosis were downregulated in whole cortex of MeCP2-deficient mice (Pacheco et al., 2017). Such differences in observation could be that the iPSC-derived astrocytes in our cultures were grown in monoculture and therefore did not develop alongside cells they would do *in vivo*, such as neurons, microglia and oligodendrocytes. There was also considerable variability in the qPCR data collected from the iPSC-derived astrocytes. Experimental procedures using iPSC-derived cells possibly require four or five repeats rather than the three in order to potentially reduce data spread. More disease lines would also need to be used alongside more control lines. These changes would narrow the confidence intervals and give a more precise estimate of data means, and would be more likely to show up statistically significant differences that are small as they would no longer be masked by wide data spread (Jones et al., 2003).

3.5.2 Calcium Activity

iPSC-derived astrocytes from all three lines responded to glutamate or ATP, with some responding to both. More astrocytes responded to ATP than to glutamate, potentially highlighting that the populations of astrocytes generated were heterogenous. A greater range of neurotransmitters could have been tested in order to elucidate whether the astrocytes populations expressed other receptors, such as GABA receptors. However, it is promising that populations of the astrocytes generate did indeed respond to both glutamate and ATP.

Spontaneous calcium oscillations were also observed, which has previously been demonstrated in astrocytes *ex vivo* and *in vitro* (Parri et al., 2001, Hill et al., 2012). No differences in spontaneous activity were observed between the cell lines, which is not in keeping with the literature. RTT astrocytes derived from iPSCs containing the R294X mutation showed more spontaneous calcium oscillations, and also displayed significantly higher responses to ATP stimulation than control iPSC-derived astrocytes (Dong et al., 2018). This was partly because of abnormally increased calcium load in the endoplasmic reticulum in the RTT astrocytes, alongside increased amplitude of calcium entry into astrocytes after ER calcium depletion with the drug Thapsigargin. The iPSC-derived astrocytes used in this chapter

had demonstrated no significant difference in level of spontaneous activity or in amplitude of ATP responses. This could be due to the difference in mutation in the RTT#27 line versus those by (Dong et al., 2018); R294X has been shown to be a one of the less severe mutations in MeCP2 that causes RTT (Bebbington et al., 2008). The age of the astrocytes in this paper were similar to those in this thesis, however the method of astrocyte differentiation was different. Dong et al., (2018) expanded their NPCs using a suspension culture of neural progenitor spheres. This methodological difference could lead to functional differences in the iPSC-derived astrocytes. Additionally, data shown in this thesis shows significant variability. Ideally more cover slips would have been imaged per biological differentiation, and potentially more differentiations should be performed in the future.

Results in chapter 2 demonstrated a small percentage of neuronal contamination. As such, tetrodotoxin (TTX) should have been administered to the cultures in order to block sodium channels in the neurons and prevent action potentials, in order to show that the calcium activity in the astrocytes was spontaneous and not due to neuronal activity. However, this is unlikely.

The results in this chapter suggest that these iPSC-derived astrocytes all have subpopulations that respond to glutamate and ATP. iPSC-derived astrocytes that respond to glutamate and ATP with intracellular calcium release have also been generated in other studies (Hedegaard et al., 2020). A higher proportion of all astrocytes responded to ATP rather than glutamate, however some astrocytes responded to both. This could reveal that our astrocytes were not mature enough to express the appropriate receptors in order to respond to glutamate and ATP. It could also mean that the astrocytes generated were very heterogeneous and could possibly be capable of responding to neurotransmitters that were not tried, such as GABA. Olfactory bulb astrocytes have been shown to respond to GABA uptake with calcium signalling (Doengi et al., 2009). Some astrocytic populations also express $GABA_A$ receptors; future experimental work could also investigate the effect of GABA on iPSC-derived astrocytes in RTT.

Further investigation could also reveal some more information about the heterogeneity of the astrocytes generated. Previous studies have investigated the effect of ATP on calcium in iPSC-derived astrocytes and characterised the responses according to four categories. These responses interestingly corresponded to region specific RNA-seq transcriptomes, showing that astrocytes from different parts of the brain could respond to ATP in different ways (Bradley et al., 2019). Such observations in iPSC-derived astrocytes could be a helpful way to generate or separate out astrocytes specific to certain brain regions, opening up more experimental possibilities and reducing data variability that could be obscuring notable observations.

Significantly more (~30%) HipSci line iPSC-derived astrocytes responded to ATP than from the RTT#27 and RTT#37 lines. This finding was interesting, as the RTT#37 line is also a control

line. qPCR could show whether there is higher ATP receptor expression in astrocytes derived from the HipSci line versus RTT#27 and RTT#37. Additionally, it could also be an effect of the way the iPSC lines are generated; the HipSci line might have had a different method of generation compared to the RTT#27 and RTT#37 lines.

3.5.3 Glutamate Uptake and Lactate Release

RTT#27, RTT#37 and HipSci iPSC-derived astrocytes all demonstrated glutamate uptake from their surroundings over a period of 30 minutes. Astrocytes incubated in 100µM of glutamate also continued to remove glutamate over a period of 4 hours. Further incubation could be performed in the future in order to discern when this uptake plateaus. The RTT#37 iPSC-derived astrocytes removed significantly more glutamate than the RTT#27 iPSC-derived astrocytes over a 240 minute period after incubation in 30µM glutamate. However, the qPCR data showed no significant differences in Glt1 or GLAST expression across the iPSC-derived astrocytes for all cell lines so it is uncertain whether this difference is due to aberrant glutamate transporter expression. Further work would also need to determine whether glutamate homeostasis within the astrocytes was dysfunctional, preventing further uptake in the RTT#27 astrocytes. Levels of the enzyme glutamine synthetase could be investigated, alongside glutamine levels, to determine whether the astrocytes are capable of metabolising the glutamate they take up. Differences in glutamate uptake in RTT models have also been observed in literature. Previous studies have noted that astrocytes from MeCP2-deficient mice were more adept at removing high concentrations of glutamate from media (Okabe et al., 2012), whereas the data in this chapter shows that the RTT#27 iPSC-derived astrocytes were less adept. However, the concentration used with the MeCP2-deficient astrocytes was 1mM, much higher than what was attempted in this chapter. Future work with higher concentrations of glutamate might reveal further functional differences in uptake. The same group noted that this high glutamate concentration prevented downregulation of the glutamate uptake genes, Glt1 and GLAST, in the MeCP2-deficient astrocytes (Okabe et al., 2012).

In order to discern whether this glutamate uptake was mediated by the EAATs, Glt1 and GLAST, the global EAAT inhibitor TBOA was used alongside 30µM glutamate. TBOA significantly blocked glutamate uptake in the RTT#37 iPSC-derived astrocytes for at least 30 minutes. The reason TBOA may not have had a significant effect on glutamate uptake in the RTT#27 iPSC-derived astrocytes is that these astrocytes removed less glutamate from their surroundings, therefore blocking it would not cause such a significant effect. This effect of the TBOA did not continue significantly to four hours in the RTT#37 iPSC-derived astrocytes, possibly because TBOA is a competitive, non-transportable blocker of EAATs. However, this shows that the glutamate uptake is mediated by EAATs in the RTT#37 iPSC-derived astrocytes. This finding is promising as the ability to take up glutamate is a sign that astrocytes

demonstrate some mature functions. Glutamate uptake *in vivo* by astrocytes allows them to isolate synapses and prevent glutamate spill over, controlling the efficiency of synapses and conserving the specificity of existing circuits (Dallérac et al., 2018). However, not all astrocytes are capable of removing glutamate, though due to the nature of the experiment it was not possible to determine whether any subpopulations of astrocytes were not removing glutamate (Israel et al., 2003).

Another notable finding from these uptake experiments is that a few data points revealed that by four hours some astrocytes were releasing glutamate back into the KR they were incubated in. This could show that they were releasing glutamate in response to stimulation, which has been observed in the literature (Dallérac et al., 2018, Jourdain et al., 2007). As observed from the calcium data (see section 3.4.2) some of the astrocytes generated in this chapter are capable of responding to glutamate, and thus could express glutamate receptors (mGluRs). qPCR or immunocytochemistry could confirm this in future experiments. Also, astrocytes have also been shown to contain VGLUT vesicles clustered around neuronal structures that correspondingly contain glutamate receptors (Bezzi et al., 2004). Stimulating astrocyte mGluRs resulted in calcium- and SNARE-dependent release of glutamate (Bezzi et al., 2004, Parpura et al., 1994). This glutamate release can modulate neighbouring neuronal activity (Parpura et al., 1994). Thus, is it possible that glutamate stimulation of astrocytes can cause them to release glutamate. However, this would require further experimental work in order to elucidate what is occurring in these data points.

To investigate whether glutamate uptake triggered lactate release in iPSC-derived astrocytes, the lactate concentration was determined after 30 minutes. This time point was chosen because TBOA was still effective at this time. HipSci iPSC-derived astrocytes released significantly more lactate in response to both 30µM and 100µM glutamate than RTT#27 iPSC-derived astrocytes. TBOA blocked this release significantly in HipSci iPSC-derived astrocytes, and non-significantly reduced lactate release in the RTT#27 and RTT#37 iPSC-derived astrocytes. The RTT#37 line was very variable. The lack of significance in the RTT#27 line might be because it released significantly less lactate in response to glutamate compared to the HipSci line, therefore blocking glutamate uptake might not have had an observable effect. However, TBOA blocking lactate release in response to glutamate in the HipSci line astrocytes shows that glutamate uptake into iPSC-derived astrocytes triggers lactate release, thus potentially showing the astrocyte-neuron lactate shuttle in an iPSC-derived system for the first time. As glutamate uptake a metabolically demanding process, future experiments could also assess differences in glucose uptake by the iPSC-derived astrocytes and ATP levels in cells as well as impact on glycogenolysis.

The increase in lactate release by the HipSci iPSC-derived astrocytes could not be explained by an increase in MCT1 expression, which has been found to be enriched in astrocytes (Bröer et al., 1997), as these data did not show any significant differences in its expression between the lines. The difference could be due to dysregulation of the glycolytic machinery in the RTT#27 astrocytes, preventing them from generating lactate to release. Differences in lactate levels have not always been observed in other model systems, with MeCP2-/y brains showing no difference in lactate levels compared to control mouse brains (Viola et al., 2007). As the levels were investigated across the whole brain it could be possible that regional differences are being masked.

Astrocytes are ideally placed to provide metabolic support, due to their positioning near capillaries and expression of the glucose transporter GLUT1 (Morgello et al., 1995). Thus, the role they might play in metabolic support for neurons in RTT is a worthwhile avenue for further study.

3.5.4 Oxidative Stress

The brain is particularly sensitive to oxidative stress because of its high lipid content and low concentration of antioxidants. Post-mortem studies on RTT brains have shown a severe reduction in vitamin C and GSH, and decreased SOD activity. Mitochondria could be dysfunctional in RTT, with increased lactate in CSF and altered morphology. In MeCP2 KO mice they have increased expression of Uqcrc1 gene (a subunit of complex III), resulting in increased mitochondrial respiration rates and increased oxygen consumption, leading to increase in ROS production. This increases the oxidative burden and the cells become more vulnerable to oxidative damage (Filosa et al., 2015). However, there were no significant differences in oxidative stress markers in cell lysates taken from RTT#27, RTT#37 and HipSci iPSC-derived astrocytes. Additionally, there were no significant differences in SOD2 expression across the lines.

As the astrocytes have been functionally characterised the impact they have on neurons will be assessed in chapter four. Media conditioned by RTT iPSC-derived astrocytes has been previously shown to have a negative effect on hippocampal neurons (Williams et al., 2014). Therefore, this will be investigated further using iPSC-derived neurons.

Chapter Four – Effect of RTT#27, RTT#37 and HipSci iPSC-derived ACM on HipSci iPSC-derived neurons.

4.1 Introduction

Astrocytes secrete many factors that can impact the cells around them, such as neurons and microglia. The effect that the astrocyte secretome has on neurons and synaptogenesis has been discussed in more detail in chapter one (section 1.13.7). Secreted factors from astrocytes have been implicated as being integral to pathogenesis in a number of diseases, including ALS and RTT (Nagai et al., 2007, Williams et al., 2014). Media conditioned by RTT iPSC-derived astrocytes has a negative impact on mouse neurons, resulting in reduced soma size and neurite length compared to media conditioned with WT iPSC-derived astrocytes. This effect could persist for 72 hours (Williams et al., 2014). Other studies have also shown that ACM from reactive astrocytes can be powerfully neurotoxic and result in significant neuronal death (Liddelow et al., 2017b). However, ACM can also be protective for neurons following certain conditions such as hypoxia (Yan et al., 2013). These studies show the variability in the effects that astrocytic state, whether in reactivity or disease, can have on their secretome and subsequently the effect on neurons.

Neurons express numerous receptors in order to respond to neurotransmitters such as glutamate. Glutamate is the most prevalent excitatory neurotransmitter in the CNS and its role in neuronal activation is implicated in a number of diseases due to excitotoxicity (Lewerenz and Maher, 2015). NMDA, AMPA and kainate receptors are the main families of ionotropic glutamate receptors that are present on the post-synaptic neuron. These types of receptors are ligand-gated ion channels. Stimulating these receptors with the appropriate ligand opens the ion pore, permitting the flow of sodium, potassium or calcium ions into the cell (Reiner and Levitz, 2018). NMDA receptors can be blocked by extracellular magnesium ions that block the channel, which can be removed when the neuron is sufficiently depolarised. Other types of glutamate receptors are metabotropic receptors, mGluRs, which are GPCRs. Activating these receptors triggers a metabolic cascade inside of the cell that result in various cellular processes (Reiner and Levitz, 2018).

Calcium activity can also occur in neurons in the absence of neurotransmitters (known as spontaneous events). These can occur before and after synapses form in development. Such events can regulate such processes as growth cone migration, dendritic spine arborization and can even regulate specification of neurotransmitter phenotype (Rosenberg and Spitzer, 2011). The pattern of calcium events, such as amplitude and interval, can differentially activate calcium-sensitive enzymes, such as calmodulin-dependent protein kinase II (CaMKII), that can ultimately affect transcription of specific genes that direct neuronal differentiation in development (Rosenberg and Spitzer, 2011). This spontaneous activity can become observed

throughout neighbouring cells, ultimately forming spontaneous activity that spreads across networks. Such activity is observed throughout nervous system development and can help coordinate activity (Blankenship and Feller, 2010).

Asynchronous calcium activity has been observed in immature cerebral organoids, as well as in networks formed after cerebral organoid dissociation. These calcium transients in the dissociated networks became synchronised over time, in line with network maturation, and could potentially be responsible for regulating long-range wiring in these networks (Sakaguchi et al., 2019). Network calcium activity has been observed to be dysregulated in conditions such as schizophrenia (Hamm et al., 2017), meaning that neuronal calcium activity in culture is worth investigating in disease.

Spontaneous calcium events can also drive cell differentiation during development. Neural crest cells in mice that display these spontaneous events preferentially differentiate into neurons (Carey and Matsumoto, 1999). Blocking calcium signalling in *Xenopus* embryos prevented neurogenesis from occurring (Jones et al., 1995). It has also been determined that a rise in intracellular calcium is also a direct cause in the initiation of neural induction in the *Pleurodeles waltl* embryo (Moreau et al., 1994). Spontaneous calcium activity is also involved in the maturation of cortical neurons *in vivo*. Post-migratory neurons were found to have a higher percentage of cells showing calcium transients, that were also more frequent, compare to neurons that were still migratory. Ectopic expression of a prokaryotic voltage-gated sodium channel was used to elevate neural activity in these neurons, also resulting in a significantly higher fraction of neurons displaying spontaneous calcium transients. This resulted in impeded neuronal migration and increased the branch formation of the neurons before they could reach their final destination (Bando et al., 2014). This shows the role of calcium in neuronal differentiation, migration and maturation. Therefore, it will be interesting to assess whether ACM from healthy and RTT iPSC-derived astrocytes differentially impact neuronal calcium activity and the potential implications this could have on neurodevelopment.

Astrocytes also secrete factors that activate the immune system, such as IL-6 (see section 1.13.6). Low concentrations of IL-6 secreted by astrocytes have been shown to be neuroprotective in neuron-astrocyte co-cultures treated with lipopolysaccharide (LPS). However, if astrocytes are excessively stimulated, the resultant high concentrations of IL-6 result in neuronal death (Li et al., 2009). Despite a lack of neuronal cell death observed in RTT patient brains, IL-6 has also been implicated in neurodevelopmental disorders such as schizophrenia and autism (Smith et al., 2007). Therefore, the role of inflammatory cytokines such as IL-6 may worthy of investigation in RTT.

Investigating the effect of ACM on healthy iPSC-derived neurons would perhaps provide some insight about the effect of the astrocyte secretome on functional aspects of development.

4.2 Aims

The hypothesis of this chapter is that ACM generated from RTT#27 iPSC-derived astrocytes will have a negative effect on iPSC-derived neurons in terms of calcium activity and gene expression compared to ACM from RTT#37 and HipSci iPSC-derived astrocytes. As such the overall aim of this chapter was to assess the effect of RTT iPSC-derived astrocyte conditioned media on HipSci iPSC-derived neurons. To achieve this aim the specific objectives were to:

1. To generate astrocyte conditioned media from the RTT#27, RTT#37 and HipSci lines.
2. Determine if ACM displayed any differences in IL-6 concentration between the RTT#27, RTT#37 and HipSci lines.
3. To generate iPSC-derived neurons from the HipSci line and treat these with astrocyte conditioned media from the RTT#27, RTT#37 and HipSci lines to determine impact of neuronal growth and morphology, as well as expression of markers such as SOD2.
4. To perform calcium imaging of neurons treated with ACM to determine if there are any differences in spontaneous activity or in response to glutamate.

4.3 Methods and Materials

4.3.1 Cell culture

For culture of iPSCs, NPCs and astrocytes see chapter 2, section 2.3.

4.3.2 Generation of Astrocyte Conditioned Media (ACM)

Astrocytes were seeded at density of 1-1.5 x 10^5 cells/cm^2 on Matrigel®-coated plates. Once the cells reached 100% confluence their astrocyte media (ScienCell) was switched to NMM (Axol Bioscience) for 72 hours. After 72 hours the media was collected and centrifuged at 300G to remove dead cells. The supernatant was collected in 15ml falcon tubes and stored at -20^{o}C until required. Astrocytes were all used between 12-14 weeks post-neural induction.

4.3.3 Treatment of iPSC-derived neurons with ACM

iPSC-derived neurons were generated from the HipSci line as described in section 2.3.10. Post DAPT treatment, the neurons remained in BrainPhys™ Neuronal medium (STEMCELL Technologies) supplemented with, SM1 (STEMCELL Technologies), 20pg/ml rh-BDNF (STEMCELL Technologies), 20pg/ml rh-GDNF (STEMCELL Technologies) for two days. Following this, the cells were treated with either NMM, RTT#27 ACM or HipSci ACM (generated as described in section 4.3.2) for 72 hours. After this time the cells were assessed using calcium imaging (section 3.3.1), or their RNA was collected for qPCR (section 2.3.12) for assessment of changes in gene expression for the following genes of interest: SOD2, MAP2, Tuj, MCT2, GRIN1 and GRIN2b (all PrimerDesign, UK).

4.3.4 IL-6 ELISA

A human IL-6 DuoSet ELISA (R&D Systems, USA) was performed to measure the IL-6 concentration in ACM generated by RTT#27, RTT#37 and HipSci iPSC-derived astrocytes (see section 4.3.2) according to manufacturer's instructions. The plate was read using a MultiSkan EX plate reader (Thermo Fisher, USA).

4.3.5 Calcium imaging

Calcium imaging experiments were performed as described in section 3.3.1.

4.4 Results

4.4.1 RTT#27 astrocytes release significantly more IL-6 than RTT#37 or HipSci astrocytes at basal levels.

ACM collected from RTT#27 iPSC-derived astrocytes contained significantly more IL-6 than medium collected from the RTT#37 and HipSci iPSC-derived astrocytes (RTT#27: 104.16±59.35pg/ul; RTT#37: 4.78±7.93pg/ul; HipSci: 10.77±13.43pg/ul, n=3) (Figure 4.1).

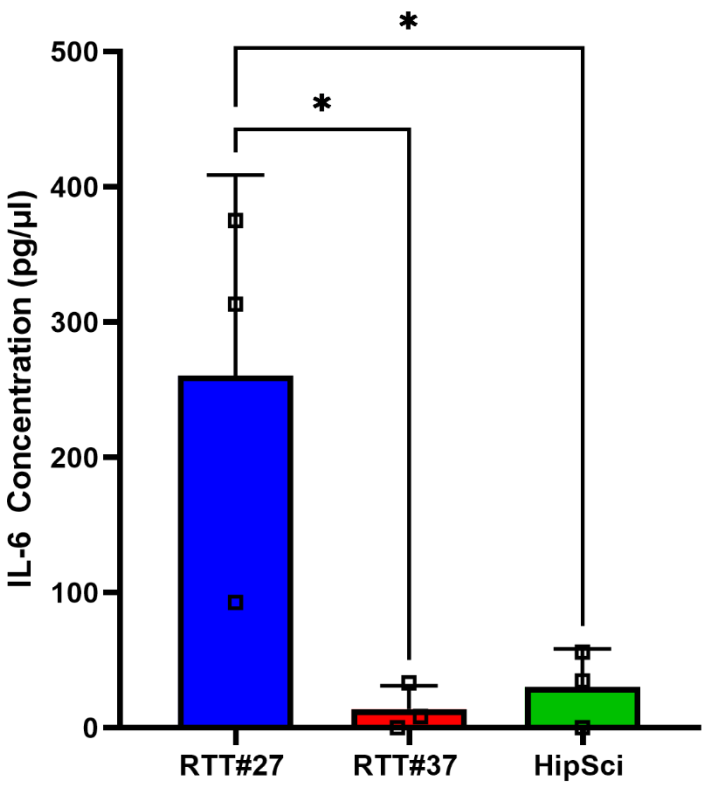

Figure 4.1: Unstimulated RTT#27 iPSC-derived astrocytes release significantly more IL-6 than RTT#37 or HipSci iPSC-derived astrocytes. Bar graph shows IL-6 concentration (pg/µl) in the astrocyte conditioned media (ACM) collected from RTT#27, RTT#37 and HipSci iPSC-derived astrocytes. Results are expressed as concentration pg/µl ± standard deviation (n=3, one-way ANOVA with Tukey's multiple comparison test, * = $p<0.05$).

4.4.2 No significant difference in gene expression is found between HipSci iPSC-derived neurons after treatment with astrocyte conditioned medium.

To assess whether the ACM from different cell lines altered gene expression in the HipSci iPSC-derived neurons the neurons were collected after treatment for analysis with qPCR. The RTT#37-treated neurons were excluded as due to time constraints only an n=2 was collected. No significant differences in SOD2, MCT2, MAP2 or Tuj expression was observed after 72 hours of treatment.

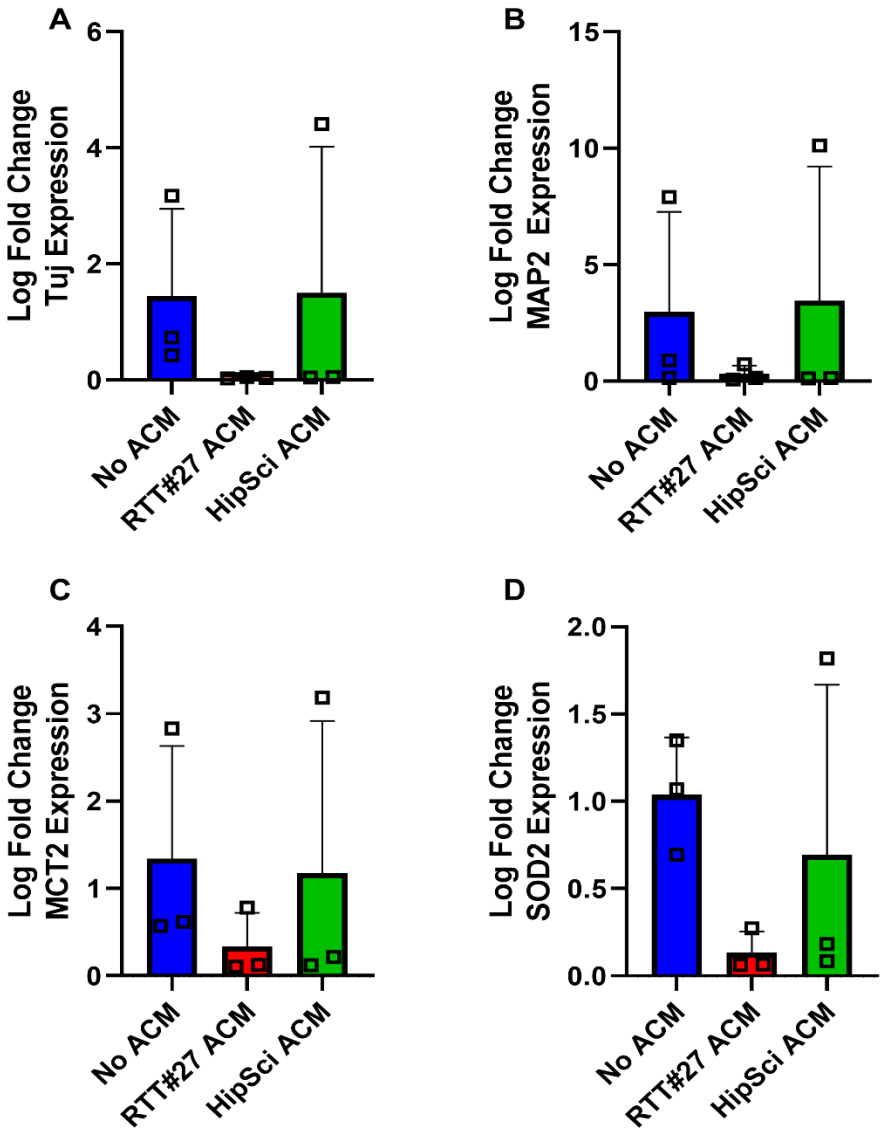

Figure 4.2: No significant difference found in gene expression in HipSci iPSC-derived neurons after treatment with astrocyte conditioned media. **A)** shows log fold change Tuj expression between neurons grown with no ACM or treated with RTT#27 or HipSci ACM. **B)** shows log fold change MAP2 expression between neurons grown with no ACM or treated with RTT#27 or HipSci ACM. **C)** shows log fold change MCT2 expression between neurons grown with no ACM or treated with RTT#27 or HipSci ACM. **D)** shows log fold change SOD2 expression between neurons grown with no ACM or treated with RTT#27 or HipSci ACM. Results shown as log fold change ± standard deviation (n=3, one way ANOVA with Tukey's multiple comparison test). Gene expression was normalised to YWHAZ.

4.4.3 HipSci ACM-treated iPSC-derived neurons have an increased response to glutamate compared to no ACM, RTT#27 and RTT#37 ACM-treated iPSC-derived neurons.

iPSC-derived neurons derived from the HipSci line were investigated using calcium imaging after treatment with either NMM or ACM. Spontaneous activity was observed by the presence of peaks in the absence of neurotransmitters for the first 300 seconds of recording, before the addition of glutamate at 300 seconds (Figure 4.3). Glutamate was added for at least one minute before being washed off with aCSF. Glutamate elicited a noticeable increase in fluorescence in the iPSC-derived neurons which was attenuated once removed. The spontaneous activity of the neurons then resumed.

iPSC-derived neurons treated with RTT#37 ACM had a higher percentage of cells that displayed spontaneous activity compared to those treated with RTT#27 ACM (RTT#27: 10.28±2.10%; RTT#37: 32.50±3.54%; HipSci: 25.63±5.12%; No ACM: 19.31±10.72%; all n=3 except RTT#37 (n=2)). No significant differences were found in the number of peaks shown per cell. HipSci ACM resulted in iPSC-derived neurons responding more robustly to glutamate than cells treated with NMM, RTT#27 or RTT#37 ACM (RTT#27: 110.08±11.40%; RTT#37: 61.94%; HipSci: 235.82±6.67%; No ACM: 95.95±25.30%, RTT#27 and No ACM n=3, RTT#37 n=1, HipSci n=2). Sufficient quantities of RTT#37 ACM were available for an n=2, however the cells for the second experiment were not viable as they had mostly detached from the glass cover slips. The glutamate response for the n=3 for the HipSci was unsuccessful twice so was not included, meaning that the HipSci ACM was only an n=2. This was later found out to be because the bath in which the cover slip was imaged had to be changed and had increased in volume, meaning the glutamate needed to be added for a longer time period than it was for this final n=3. Statistical analysis was not performed on these samples due to insufficient replicates.

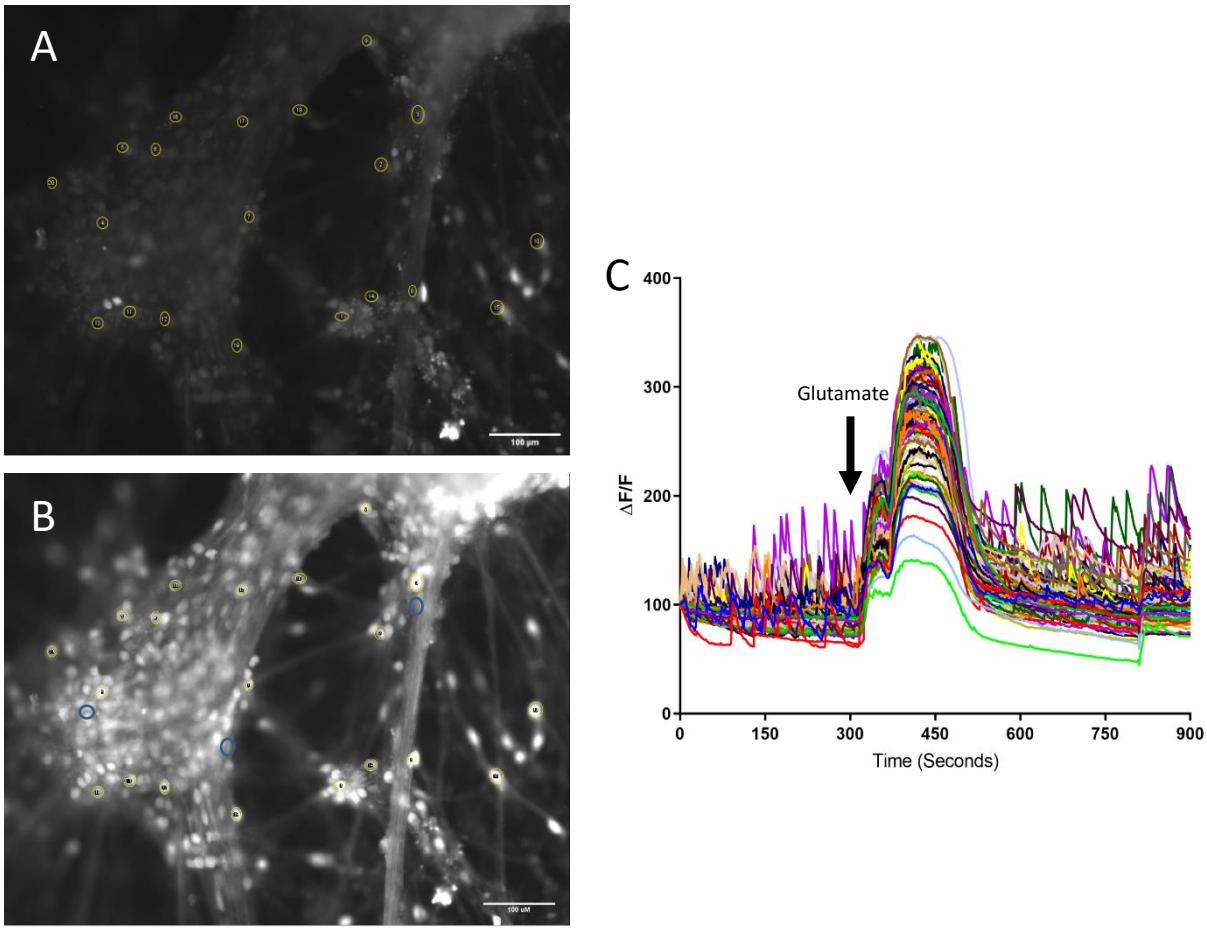

Figure 4.3: HipSci iPSC-derived neurons respond to glutamate. **A)** shows a representative image of iPSC-derived neurons loaded with Fluo4-AM overlaid with 20 example ROIs. **B)** shows the same iPSC-derived neurons during a response to 100µM glutamate overlaid with 20 example ROIs. **C)** shows a representative trace of 80 regions of interest taken from iPSC-derived neurons during periods of spontaneous activity and after the addition of glutamate at 300 seconds for 90 seconds. The values are normalised to the baseline fluorescence and displayed as ΔF/F. Cells were imaged for a total of 900 seconds with an image taken every 2 seconds. iPSC-derived neurons were imaged at 2-3 weeks post-NPC. Scale bars are 100µm.

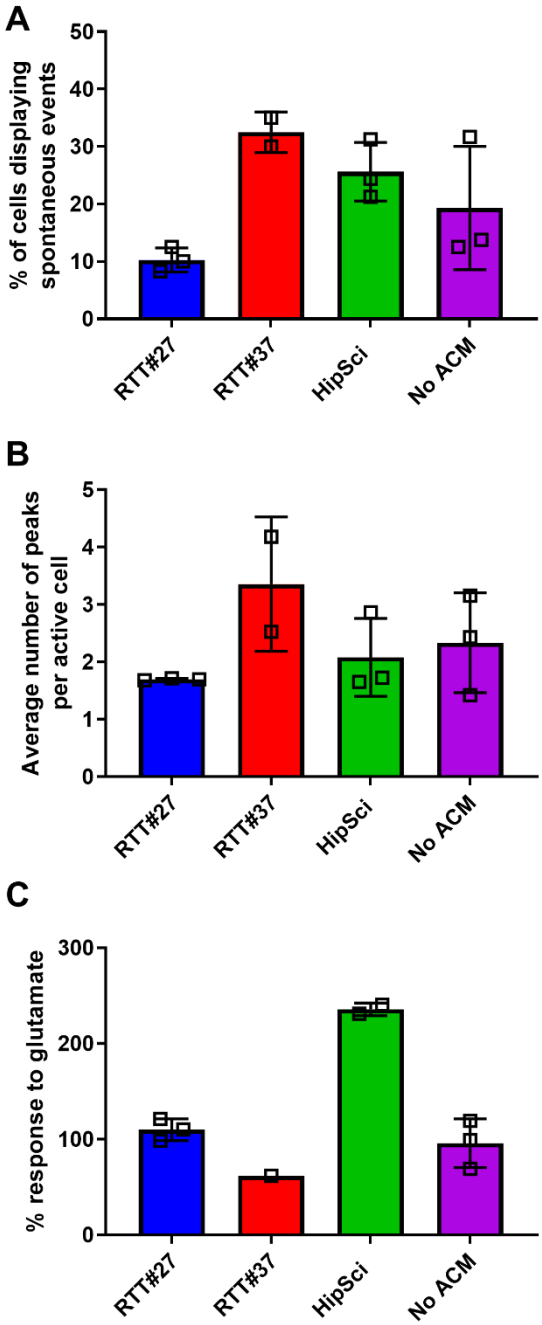

Figure 4.4: Calcium activity of HipSci iPSC-derived neurons treated with ACM from different lines. **A)** shows the percentage of cells that display spontaneous events as determined by rises in fluorescence 10% above baseline (RTT#27, HipSci and No ACM n=3, RTT#37 n=2). **B)** shows the average number of peaks per active cell for iPSC-derived neurons. **C)** shows percentage responses to glutamate from baseline. (RTT#27 and No ACM n=3, RTT#37 n=1, HipSci n=2). Results are expressed ± standard deviation.

4.4.4 There is no significant difference in expression of GRIN1 and GRIN2b between iPSC-derived neurons treated with ACM generated from different cell lines.

As the ACM derived from HipSci astrocytes had a significant effect on the response of iPSC-derived neurons to glutamate the expression of specific NMDA receptor subunits was investigated in HipSci iPSC-derived neurons. However, no difference in expression of GRIN1 or GRIN2b was found using qPCR (Figure 4.5) following treatment with ACM.

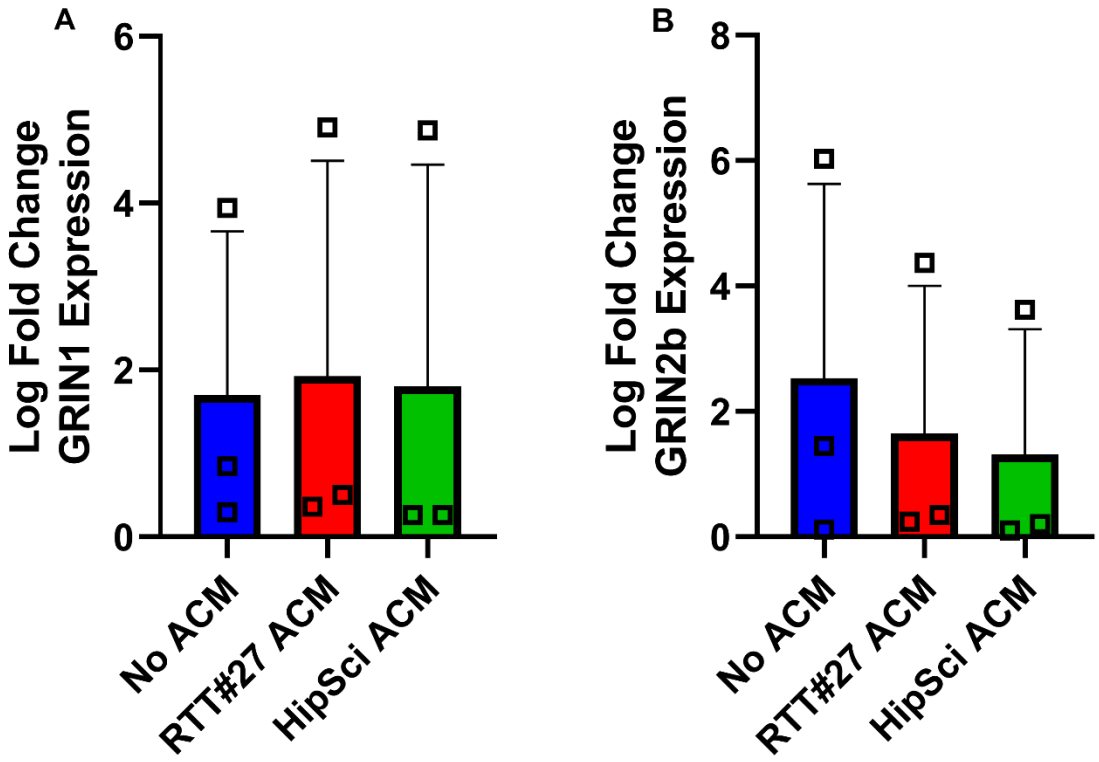

Figure 4.5: There is no significant difference in GRIN1 or GRIN2b expression in neurons treated with ACM from different cell lines. **A)** shows gene expression of GRIN1 in iPSC-derived neurons treated with either RTT#27, RTT#37, HipSci ACM, or with no ACM. **B)** shows gene expression of GRIN2b in iPSC-derived neurons treated with either RTT#27, RTT#37, HipSci ACM, or with no ACM. (all n=3 except RTT#37 ACM which is n=2). One-way ANOVA with Tukey's multiple comparison test. Results expressed as log fold change ± standard deviation.

4.5 Discussion

Previous studies have shown that RTT ACM has a detrimental effect on neuronal morphology (Williams et al., 2014). However, the mechanism that leads to this change in morphology has not been uncovered. ACM collected from primary MeCP$^{-/y}$ and MeCP2$^{-/+}$ mouse astrocytes secreted over 200% more BDNF than WT astrocytes (Maezawa et al., 2009), although overall levels of BDNF in MeCP$^{-/y}$ brains are lower than in WT (Chang et al., 2006).

4.5.1 IL-6

RTT#27 iPSC-derived astrocytes secreted significantly more IL-6 than RTT#37 or HipSci iPSC-derived astrocytes at basal levels, indicating that they are more reactive than their healthy counterparts. Whether this reactivity is beneficial or detrimental to neighbouring cell types was not explored in this thesis (see section 1.13.6). IL-6 specifically has been shown to promote axonal regrowth after spinal cord injury with accompanying functional recovery, thus showing that the increase in IL-6 may be not serving a negative effect, however this would need to be further investigated (Yang et al., 2012). Following trauma in mice, overexpression of IL-6 and of the IL-6 receptor resulted in accelerated nerve regrowth compared to non-transgenic mice (Hirota et al., 1996). This increased release of IL-6 from RTT#27 astrocytes could therefore be a protective response. Applying neutralising IL-6 antibodies to the RTT#27 ACM prior to iPSC-derived neuron application could provide more information about the role IL-6, if any, has on the neuronal function. Additionally, further work could include the application of proinflammatory factors such as LPS, TNFα and IL-1β to the astrocytes in order to see how IL-6 release is affected by immune activation, as well as potentially anti-inflammatory factors such as arginase 1.

Previous studies have demonstrated that there is no difference in the secretion of IL6 in astrocytes from MeCP2 KO mice compared to WT mice. However, the MeCP2 KO astrocytes released less IL-6 in response to LPS stimulation compared to WT astrocytes (Maezawa et al., 2009). The MeCP2 KO astrocytes also released significantly less IL-1β in response to LPS stimulation. It was suggested that this could be due to their p38 MAPK being constitutively hyperphosphorylated. It could be possible that therefore the pathway is hyperactivated, and potentially may be hyporesponsive to further stimulation by LPS (Maezawa et al., 2009). This study also demonstrated that MeCP2-deficient astrocytes express and released BDNF at higher levels than WT astrocytes (Maezawa et al., 2009). A BDNF ELISA was performed with the ACM samples collected from RTT astrocytes within this project, however the levels were all below the detection limit of the assay (data not shown).

Despite the positive effects described above, the impact of immune responses during pregnancy caused by maternal infection are associated with diseases like schizophrenia and conditions such as autism spectrum disorders due to a possible impact on neurodevelopment.

Maternal immune activation in mice produces offspring that present with gene expression and behaviours that are associated with schizophrenia and autism. It has been suggested that IL-6 specifically is responsible for some of these changes (Smith et al., 2007). Future work could assess the role IL-6 plays in RTT in early stages of development. In addition, further work could also include analysing the ACM in all conditions for other inflammatory factors, such as TNFα.

4.5.2 Calcium Imaging

Significantly more neurons treated with RTT#37 ACM displayed spontaneous events than those treated with RTT#27 ACM. In order to determine if these events were independent of action potential activity, the sodium channel blocker TTX should have been applied. Further analysis at higher magnification or at lower cell densities could have been used to spatially analyse calcium activity in the neurons, in order to determine whether activity varied throughout axons or somas in the different treated conditions. The ability of calcium to elicit different effects is thought to be due to the spatial profile of calcium. Calcium can form microdomains that are situated very close to either calcium channels or to calcium-sensitive proteins. This means that very targeted responses to calcium increases can be elicited, resulting in a very diverse set of responses. It is important to note that calcium activity and electrical activity are not the same, and future experiments could make use of a multielectrode array in order to investigate electrical activity.

Neurons treated with HipSci ACM displayed significantly higher responses to glutamate than those treated with RTT#27, RTT#37, or no ACM. In order to elucidate more about the receptor expression on the neurons more targeted neurotransmitters could have been used, such as (S)-3,5-Dihydroxyphenylglycine (DHPG) to target mGluR1 and mGluR5. Agonists such as NMDA and AMPA could have been used to selectively target subfamilies of ionotropic glutamate receptors also. This could have provided more information regarding the heterogeneity of glutamate receptors present on the neurons, and whether any differences appeared depending on ACM treatment.

It must also be considered that the iPSC-derived neurons in this chapter were derived from a healthy individual. In RTT where there is mosaic expression of mutant MeCP2 (see section 1.4), some neurons would express mutant MeCP2. Therefore, their response to ACM from multiple iPSC lines would need to be assessed, as well as the influence that the populations of mutant MeCP2 and WT MeCP2-expressing neurons would have on each other.

4.5.3 qPCR

All of the qPCR data in this chapter demonstrates wide data spread. It could be that the differentiation of iPSC-derived cells results in considerable biological variability between differentiations, in which case more cell lines would need to be investigated and with higher numbers of repeats in order to hopefully reduce the standard deviation. However, it could also

be that there were issues with the cDNA synthesis. Re-synthesising cDNA after re-quantifying the RNA from certain samples altered the CT values considerably after it was noted that they were all strangely high. It could have been that concentration readings that were measured using the Nanodrop (ThermoFisher Scientific) were too high, resulting in too low a concentration of RNA being used to synthesise cDNA. However, due to time constraints it was not possible to re-synthesise all of the cDNA again and subsequently run all of the qPCR experiments. Further experiments are required to repeat these experiments with cDNA synthesised after re-quantifying the RNA.

Following the significant increase in glutamate response caused by treating iPSC-derived neurons with HipSci ACM, the expression of NMDA subunits was investigated. No significant differences were found in GRIN1 or GRIN2b expression between the conditions. Mutations in GRIN1 and GRIN2a have been linked RTT-like disorders, those where the symptoms and phenotype appear to be similar but without the classic MeCP2 mutation (Frankel et al., 2020). *De novo* mutations in GRIN2a and GRIN2b have been found to cause sporadic cases of schizophrenia and autism spectrum disorders, disorders where glutamate transmission is altered (Tarabeux et al., 2011). Whether such changes are also found in classic RTT is unknown, but due to the issues with qPCR and also only investigating the effect of ACM on healthy iPSC-derived neurons this could not be deduced in this thesis but would be interesting to investigate further.

4.5.4 Neuronal Morphology

Neuronal morphology is abnormal in RTT, characterised by small somas and reduced dendrite length (Williams et al., 2014). Neurons were stained for Tuj after treatment with the different ACM conditions, but due to the density it was not possibly to assess morphology (Figure 4.6). Cells were plated at this density as this was part of the optimised protocol (see section 2.3.10). However, in future work NPCs should perhaps be seeded a much lower density for the purpose of ICC and assessing morphology. This way it would be possible to quantify neuronal soma size and count dendritic branching, in addition to measuring neurite length. This would provide much more information about the effect of RTT and healthy ACM on iPSC-derived neurons.

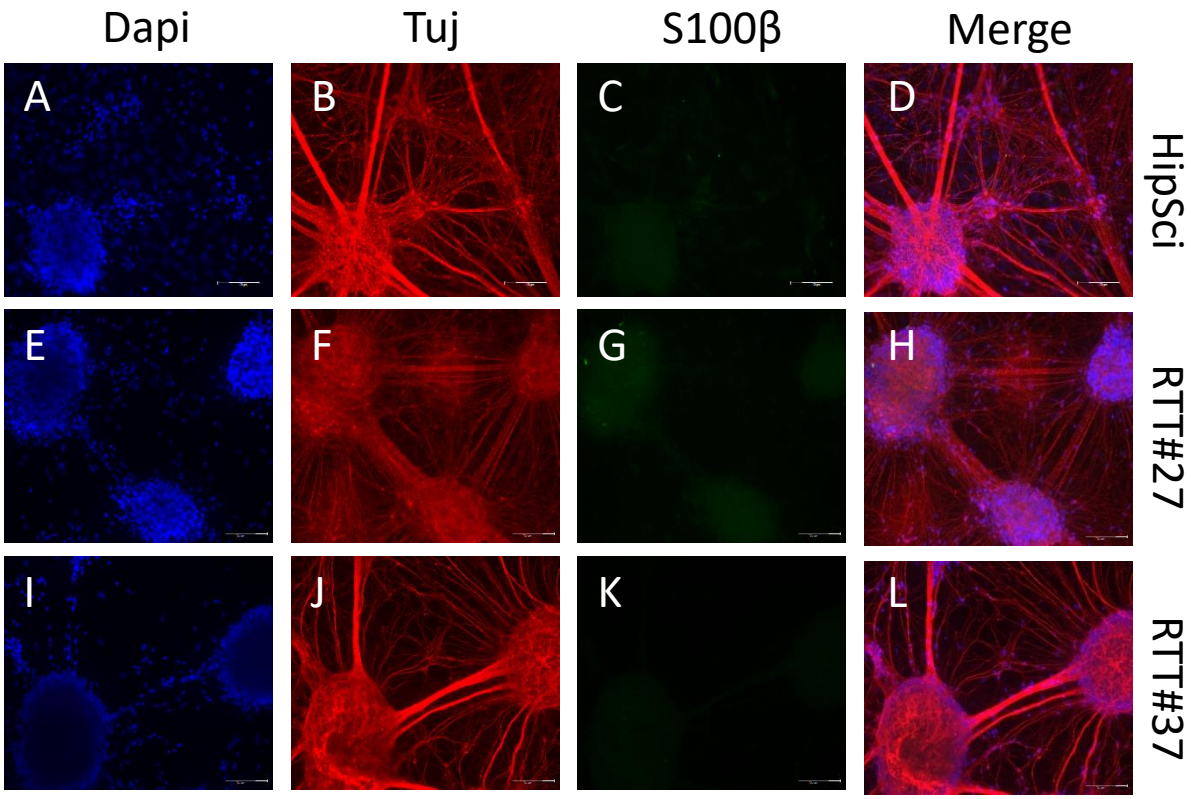

Figure 4.6: Representative images of HipSci, RTT#27 and RTT#37 ACM-treated HipSci iPSC-derived neurons. **A-D)** show Dapi, Tuj, S100β and merged images for HipSci ACM-treated HipSci iPSC-derived neurons. **E-H)** show Dapi, Tuj, S100β and merged images for RTT#27 ACM-treated HipSci iPSC-derived neurons. **I-L)** show Dapi, Tuj, S100β and merged images for RTT#37 ACM-treated HipSci iPSC-derived neurons. Scale bars are 100µM.

This chapter has determined that ACM from RTT#27 astrocytes secrete significantly higher concentrations of IL-6 compared with ACM from RTT#37 or HipSci astrocytes. In addition, neurons treated with ACM from HipSci astrocytes display significantly higher responses to glutamate compared to neurons treated with ACM from RTT#27 astrocytes. This suggests that the secretome of astrocytes in RTT could be dysregulated, potentially contributing to an abnormal inflammatory environment. Further work to explore the whole secretome of RTT astrocytes and its effect on neuronal development and behaviour would provide a greater insight in RTT.

A beneficial first step to investigating pathways that are impacted in RTT iPSC-derived astrocytes compared to healthy iPSC-derived astrocytes would be to perform RNA-seq on these astrocytes. This would provide information about all of the genes that are expressed in these astrocytes, and will highlight any differences and the pathways that these dysregulated genes are most involved in. Such information would then provide specific genes to target and investigate in RTT, allowing a more focussed approach to design future experiments.

Chapter Five – RNA sequencing of RTT#27 and HipSci iPSC-derived astrocytes.

5.1 Introduction

The previous chapters have demonstrated differences in the functional capabilities between RTT#27 and HipSci iPSC-derived astrocytes, for example differences in lactate release in response to glutamate. However, in many experiments no significant differences were observed. A potential approach to try and uncover pathways and genes that might contribute to RTT pathology and symptoms would be to perform RNA-seq. This would reveal dysregulated pathways that could ultimately link to the symptoms of RTT and the role that astrocytes may play in this disease.

RNA-seq is a high throughput method of quantifying and mapping a cell's transcriptome (Wang et al., 2009). The transcriptome shows the complete set of gene transcripts present in a cell, and their quantities. It can be highly specific depending on cell type and can be altered by various physiological conditions.

Multiple methods are available to perform RNA-seq. The three main methods are: Illumina, Pacific Biosciences and the Oxford Nanopore. In the Illumina method cDNA molecules are clustered on a flow cell and is sequenced with fluorescently labelled nucleotides, which are then imaged to generate reads between 50-500 base pairs (bp) long. Pacific Biosciences workflow works by attaching a polymerase to the bottom of a nanowell and fluorescently labelled nucleotides are incorporated into the strand and then detected. The Oxford Nanopore method uses a motor protein to translocate the RNA strand through the nanopore, which causes a change in current which is then detected and generates 1-10kb reads (Stark et al., 2019).

RNA-seq has provided invaluable data about the differences between human and mouse astrocytes, as well as the differences between progenitor and mature astrocytes (Zhang et al., 2016). The study by Zhang et al. (2016) also revealed that astrocytes grown in serum upregulate genes associated with reactivity, compared to astrocytes grown without (Zhang et al., 2016). Analysing the expression of thousands of genes and comparing them between different cell conditions is a hugely powerful tool, particularly in terms of health, aging and disease (Pan et al., 2020). Additionally, RNA-seq has also provided information about characterising changes in astrocyte gene expression throughout disease, showing how the cells change and the impact this can have on their function (Diaz-Castro et al., 2019). RNA-seq of astrocytes isolated from Huntington's Disease brain tissue has shown upregulation of genes of reactivity genes associated with the A1 neurotoxic type of astrocyte, such as serglycin and guanylate binding protein 2 (Liddelow et al., 2017a, Al-Dalahmah et al., 2020).

Single cell RNA-seq can also be utilised to provide gene expression information that are specific to certain cell types, which can then be helpful in cell characterisation (Al-Dalahmah et al., 2020). Brain region-specific cell characterisation can be determined in this way also, providing cells with region-specific genetic signatures (Herrero-Navarro et al., 2020). Knowledge about specific genes that are expressed by certain populations of cells will be helpful for isolating these cells from mixed cultures or tissues, giving researchers the chance to characterise subtypes of cells.

RNA-seq has been performed on motor cortex and cerebellar autopsy samples from RTT patients, but not on astrocyte monocultures. Studies have shown that genes affected were mostly associated with long term potentiation and axon guidance, and an acetylcholine receptor (M4) also showing a significantly decreased expression (Gogliotti et al., 2018). This gene is also implicated in Alzheimer's Disease and schizophrenia. Single-cell RNA-seq has also been used to exploit the mosaicism in RTT by assessing each cell's XCI status in addition to gene expression. This meant that mutant and WT cells from the same individual could be sequenced. The study did include astrocytes but did not display data as it was deemed to be underpowered compared to other cell types. However, in excitatory neurons dysregulated genes by MeCP2 were found to be enriched in pathways that controlled metabolism or nervous system development (Renthal et al., 2018). Other gene expression analysis technologies show that RTT patient brain samples show an increased expression of glial-specific cell markers such as GFAP and EAAT1 (Colantuoni et al., 2001). As discussed in chapter three, EAAT1 is involved in glutamate clearance, which is a mechanism implicated in RTT (Okabe et al., 2012). A review of transcriptome analysis performed on RTT human samples concluded that the main dysregulated pathways were in dendritic connectivity and synapse regulation, mitochondrial dysfunction, and glial cell activity (Shovlin and Tropea, 2018).

Differentially regulated gene sets determined between two conditions can also then be used for gene ontology analysis, showing which pathways these genes are enriched in. This can provide a dataset on which to plan new targeted experiments and learn more about the effects or potential causes of disease.

5.2 Aims

We hypothesised that RTT#27 iPSC-derived astrocytes would have dysregulated pathways involved in lactate release and neurodevelopment, based on results from previous chapters. The aim of this chapter was to perform RNA-seq on RTT#27 and HipSci iPSC-derived astrocytes in order to:

1. Extract RNA from RTT#27 and HipSci iPSC-derived astrocytes for Illumina sequencing.

2. Analysis RNA-seq data using usegalaxy.org, using programmes such as DESeq2 to investigate differential gene expression.
3. To confirm which biological pathways are predicted to be differentially regulated based on altered gene expression.
4. To compare gene expression of the RTT#27 and HipSci iPSC-derived astrocytes with other RNA-seq studies of iPSC-derived astrocytes in order to confirm their identity.

5.3 Methods and Materials

5.3.1 RNA collection

RNA was isolated from RTT#27 and HipSci iPSC-derived astrocytes at week 9-10 using the RNeasy kit (Qiagen, Germany) as per manufacturer's instructions (see appendix). A DNase treatment was performed during this process using the RNase-Free DNase Set (Qiagen, Germany) as per manufacturer's instructions (see appendix). RNA was quantified using the NanoDrop spectrophotometer (ThermoFisher Scientific, USA) and then stored at -80oC. 30µl of each sample was then sent to Novogene Europe, Cambridge for library preparation and RNA-seq (en.novogene.com). Novogene also assessed RNA quality to confirm its suitability for RNA-seq.

5.3.2 RNA-seq

Illumina NovaSeq performed by Novogene Europe, Cambridge. The library prep was 250-300 base pair insert paired end reads.

5.3.3 Data analysis

The online RNA-seq programme Galaxy was used (https://usegalaxy.org/) (Afgan et al., 2018). Quality of the FASTQ files was assessed with FastQC. HISAT2 was then used to obtain the number of aligned reads to the reference genome Human (homo sapiens) (b37):hg 19. The following table lists the percentages of uniquely mapped reads:

Sample	Uniquely mapped reads (%)
HipSci n=1	89.88
HipSci n=2	89.72
HipSci n=3	87.78
RTT#27 n=1	90.97
RTT#27 n=2	90.01
RTT#27 n=3	91.21

Table 5.1: Percentages of uniquely mapped reads to reference genome Human (homo sapiens) (b37):hg 19.

The BAM files were then filtered to only include reads of Phred quality score of 20 or higher. The programme featureCounts was then used to count number of reads mapped to each gene.

DESeq2 was then performed which normalises the number of reads to the length of the gene and compares gene expression between the RTT#27 and HipSci samples. The most differentially expressed genes as determined by those with a p-adjusted value less than 0.05 and a log fold change of at least 1 were then visualised as a heatmap, using Heatmap2. These differentially expressed genes were then put into the gene ontology programme, GOrilla (http://cbl-gorilla.cs.technion.ac.il/) (Eden et al., 2009).

5.3.4 Quality control on RNA samples collected for RNA-seq.

At least 400ng of total RNA per sample was required in at least a 20µl volume. Quality control was performed by Novogene on the RNA samples. All six samples passed quality control checks so were sent for library preparation. The FastQC programme was run on Galaxy to assess the quality of the reads. All six samples scored high base quality scores across the reads (Figure 5.1).

5.4 Results

5.4.1 Quality control on the RNA-seq reads using FastQC

To assess the quality of the reads across each sample the programme FastQC was run, which displays the quality scores for each read position in the read. All positions had a score of 20 or higher, as indicated by the y axis (figure 5.1). This score means that each base pair has a presumed accuracy read of at least 99%.

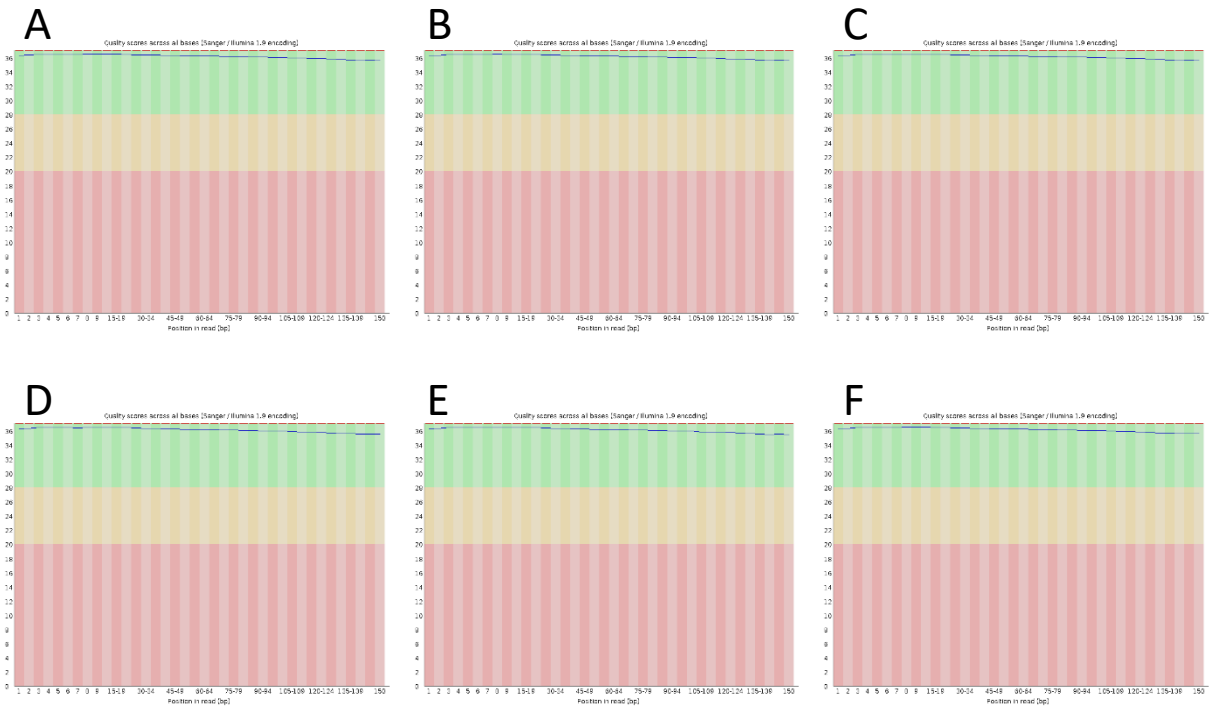

Figure 5.1: Quality scores across all bases using Sanger/Illumina 9 scoring. **A-C)** show the quality score across reads for each base position in the read for the RTT#27 n=1-3 samples. **D-F)** show the quality score across reads for each base position in the read for the HipSci n=1-3 samples. The x axis shows base position, and the y axis shows the quality score.

5.4.2 RNA-seq on RTT#27 and HipSci iPSC-derived astrocytes.

To attempt to learn more about gene expression that could reveal more about the differences between the RTT#27 and HipSci iPSC-derived astrocytes RNA-seq was performed. Following principal component analysis included in the DESeq2 programme on Galaxy one replicate sample for the HipSci line was excluded as it did not cluster with the other two samples and it might have skewed the results (Figure 5.2). The hierarchical clustering analysis and heat map (Figure 5.3) shows that the RTT#27 samples are most similar to each other and the HipSci samples are most similar to each other also. A number of genes are significantly differentially expressed between the two samples (Figure 5.3). The principal component analysis shows that the samples from each patient line cluster together after removal of the HipSci n=3 replicate (Figure 5.3).

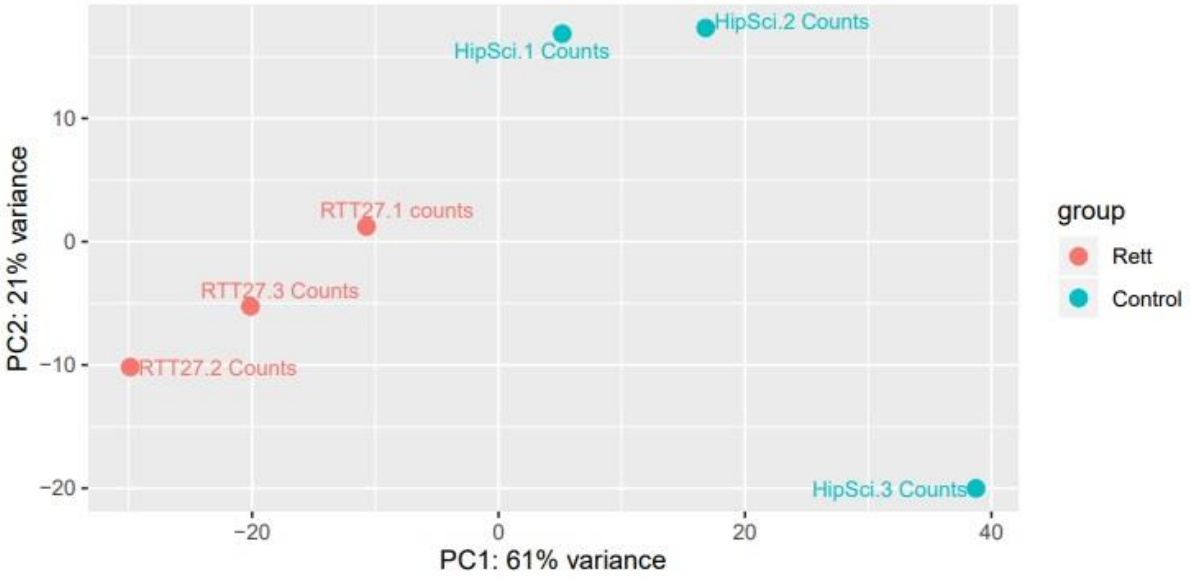

Figure 5.2: Principal component analysis for all iPSC-derived astrocyte samples.

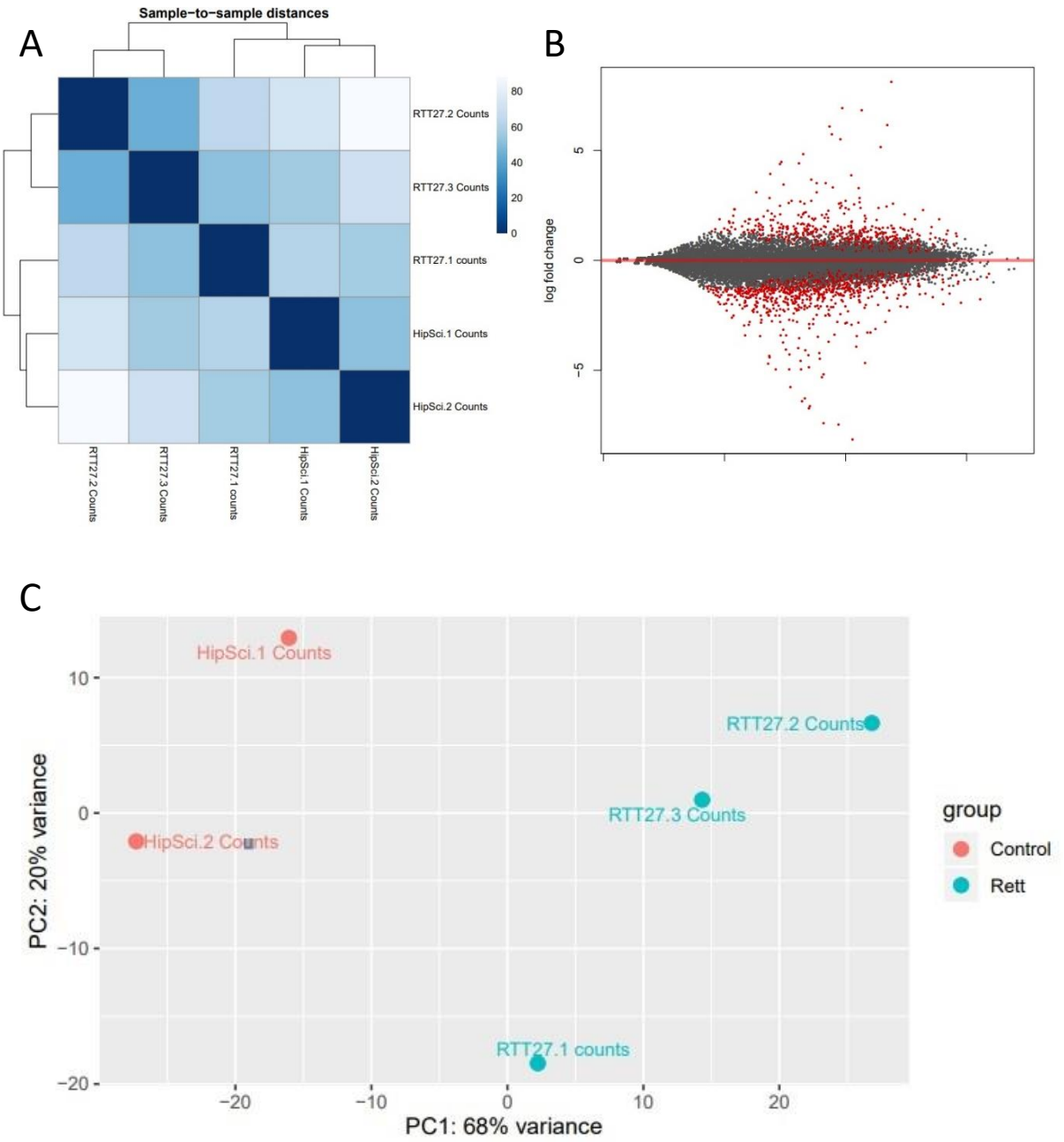

Figure 5.3: RNA-seq of RTT#27 and HipSci iPSC-derived astrocytes. **A)** Heatmap and dendogram of hierarchical clustering of RNA sequencing of HipSci.1, HipSci.2, RTT#27.1, RTT#27.2 and RTT#27.3 iPSC-derived astrocytes. **B)** Scatter MA plot of gene log2 fold change of normalised gene counts between the RTT#27 and HipSci iPSC-derived astrocyte samples. The red points are those whose p value is less than 0.1. **C)** the principal component analysis for all samples.

5.4.3 Differentially expressed gene analysis on RNA-seq data

Heatmap2 was used to visualise the top differentially expressed genes based on normalised counts for the most differentially expressed genes. Figure 5.4 shows that the samples derived from each cell line cluster together, showing that they are more similar to each other than the other cell line.

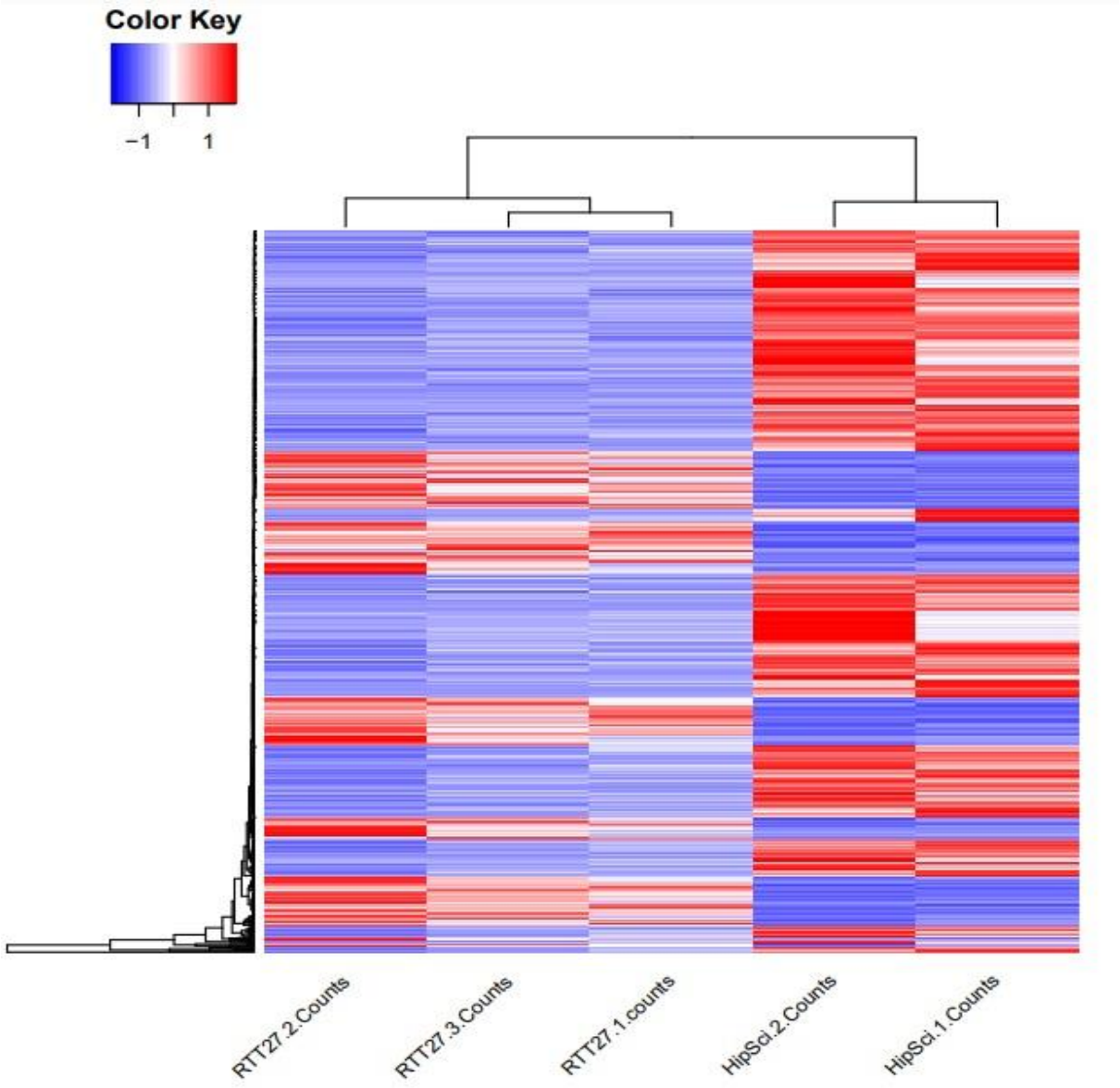

Figure 5.4: Heatmap of differentially expressed genes across RTT#27 and HipSci iPSC-derived astrocytes. Figure displays hierarchical clustering of differentially expressed genes across the astrocyte samples. The RTT#27 samples are the first three columns (n=3) and the HipSci samples are the last two columns (n=2). Red indicates upregulation of genes with blue showing downregulation. Scale bar in top left.

Comparison of gene expression between control (HipSci) and RTT#27 iPSC-derived astrocytes demonstrate that 19,975 genes are commonly expressed. 740 genes are uniquely expressed in the RTT#27 iPSC-derived astrocytes that are not in the HipSci iPSC-derived astrocytes. 935 genes are uniquely expressed in the HipSci iPSC-derived astrocytes that are not in the RTT#27 iPSC-derived astrocytes. This is visualised in the Venn diagram in figure 5.5. The full list of uniquely expressed genes can be seen in table A2.

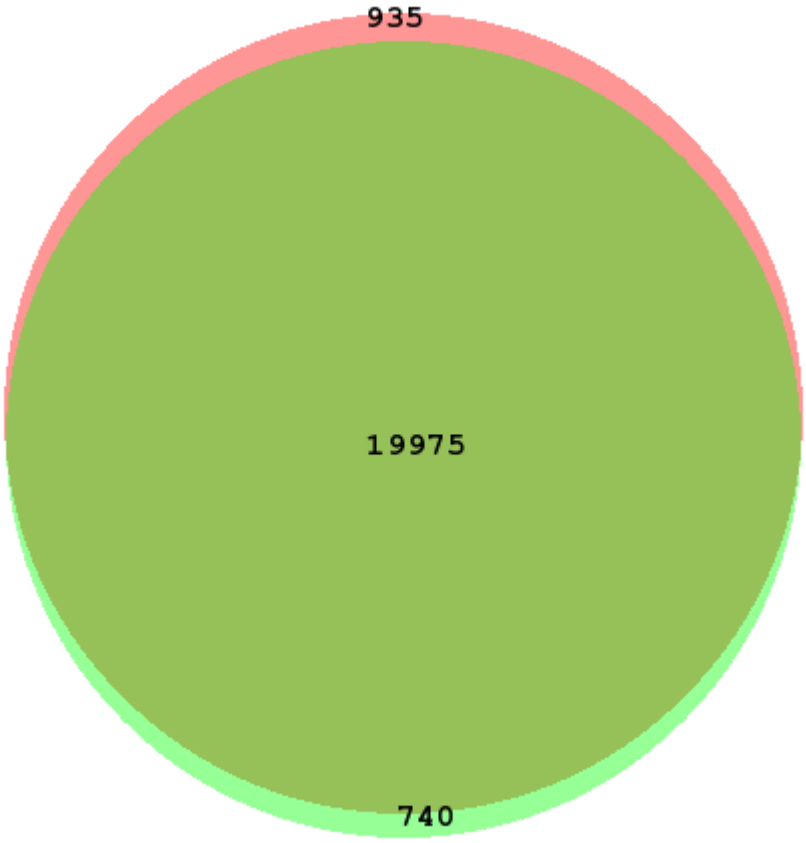

Figure 5.5: Venn diagram depicting overlap of commonly expressed genes between RTT#27 and HipSci iPSC-derived astrocytes. 19,975 are commonly expressed by astrocytes derived from both cell lines. 935 genes are uniquely expressed by the HipSci iPSC-derived astrocytes (red), and 740 uniquely expressed genes are expressed by the RTT#27 iPSC-derived astrocytes. Created with BioVenn (Hulsen et al., 2008).

The gene ontology pathways that the differentially expressed genes are involved in was investigated using GOrilla (Figure 5.6). The pathway with the most differentially expressed genes is the ECM organisation with a p value of 3.38E-18, followed by extracellular structure organisation, biological adhesion and developmental process. The full list of genes involved in the top ten pathways can be found in the appendix (table A1).

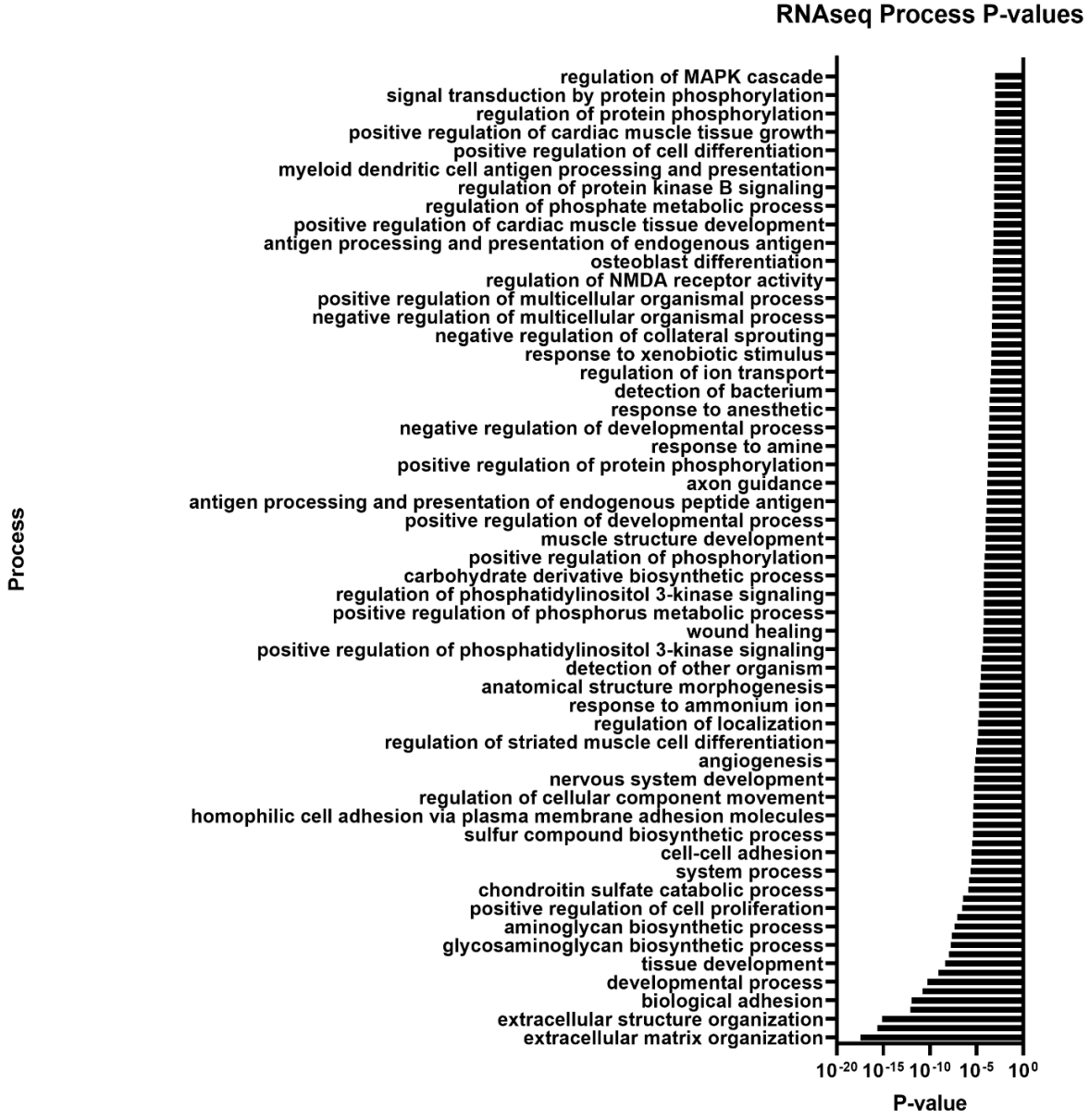

Figure 5.6: Gene ontology analysis of pathways differentially regulated genes are involved in. Bar graph showing the list of biological pathways differentially regulated genes are most involved in between the RTT#27 and HipSci iPSC-derived astrocytes.

To assess whether the samples expressed astrocyte-specific genes a list was consulted based on RNA-seq data from (Al-Dalahmah et al., 2020). Analysis revealed that the samples expressed many of these genes, as can be seen in table 5.2. 82% of the astrocyte specific genes in the list were expressed by 100% of the samples.

Gene	Hip. 1	Hip. 2	RTT27. 1	RTT27. 2	RTT27. 3	%
Solute carrier family 1 member 2	1	1	1	1	1	100
Glutamate-ammonia ligase	1	1	1	1	1	100
clusterin	1	1	1	1	1	100
paraoxonase 2	1	1	1	1	1	100
Metallothionein 2A	1	1	1	1	1	100
Nuclear Paraspeckle Assembly Transcript 1	1	1	1	1	1	100
apolipoprotein E	1	1	1	1	1	100
Solute carrier family 1 member 3	1	1	1	1	1	100
Collagen alpha-3(V) chain	0	0	0	0	0	0
ATPase Na+/K+ Transporting Subunit Beta 2	1	1	1	1	1	100
Prostaglandin-H2 D-isomerase	0	0	0	0	0	0
cystatin 3	0	0	0	0	0	0
Neurotrimin	1	1	1	1	1	100
Carboxypeptidase E	1	1	1	1	1	100
Chromosome 1 Open Reading Frame 61	1	1	1	1	1	100
ATPase Na+/K+ Transporting Subunit Alpha 2	1	1	1	1	1	100
Adhesion G Protein-Coupled Receptor V1	1	1	1	1	1	100
aquaporin 4	1	1	1	1	1	100
Metallothionein 3	1	1	1	1	1	100
Metallothionein 1E	1	1	1	1	1	100
Empty Spiracles Homeobox 2	1	1	1	1	1	100
Gap Junction Protein Alpha 1	1	1	1	1	1	100
Creatine Kinase B	0	0	0	0	0	0

Family With Sequence Similarity 171 Member B	1	1	1	1	1	100
NMYC downstream-regulated gene 2	0	0	0	0	0	0
Metallothionein 1G	0	0	1	1	0	40
Neurotrophic Receptor Tyrosine Kinase 2	1	1	1	1	1	100
glial fibrillary acidic protein	1	1	1	1	1	100
Tweety Family Member 1	1	1	1	1	1	100
Fibroblast Growth Factor Receptor 3	1	1	1	1	1	100
Metallothionein 1F	1	1	1	1	1	100
Sideroflexin 5	1	1	1	1	1	100
SPARC Like 1	1	1	1	1	1	100
DEAD-Box Helicase 17	1	1	1	1	1	100
Hypoxia Inducible Factor 3 Subunit Alpha	1	1	1	1	1	100
Metallothionein 1M	0	0	1	1	0	40
Tubulin Beta 2B Class IIb	1	1	1	1	1	100
Dystonin	1	1	1	1	1	100
Metastasis Associated Lung Adenocarcinoma Transcript 1	1	1	1	1	1	100

Table 5.2: Table shows whether the RNA-seq samples from the RTT#27 or HipSci iPSC-derived astrocytes express the astrocyte-specific genes determined by (Al-Dalahmah et al., 2020). 1 corresponds to expression and 0 means no expression. The final column shows the percentage of samples that express the given gene.

5.4.4 The 11 base pair deletion in exon 1 of the MeCP2 gene truncates the MeCP2 protein in the RTT#27 iPSC-derived astrocytes.

Visualising the mapped reads from HISAT2 in the integrated genome browser shows that the deletion mutation in exon 1 seems to severely truncate the MeCP2 protein (figure 5.7) as the mapping of the read stops.

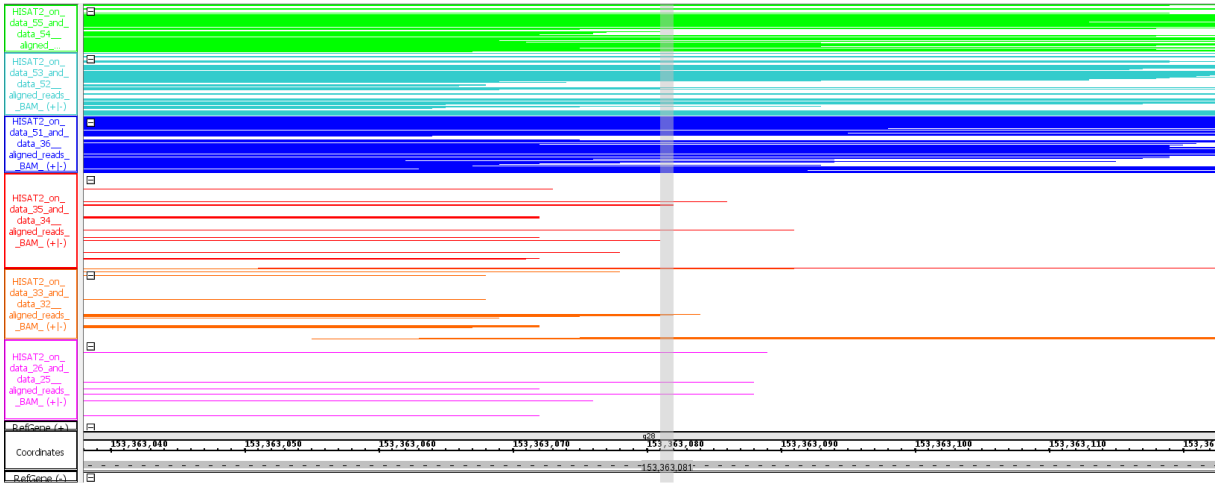

Figure 5.7: The mapped reads of iPSC-derived astrocyte samples visualised in the integrated genome browser. Figure shows the mapped reads from the iPSC-derived astrocyte samples at the location of the 11 base pair deletion in the MeCP2 gene. The green, teal and blue reads are from the HipSci iPSC-derived astrocytes, and the red, orange and pink reads are from the RTT#27 iPSC-derived astrocytes.

5.5 Discussion

RNA-seq was performed on RTT#27 and HipSci iPSC-derived astrocytes in order to find out whether any genes are differentially expressed between these cells, and to find out if these genes are enriched in any biological pathways. This could provide information for a more targeted approach for finding new pathways to investigate in RTT.

The preliminary data in this chapter has shown that there is differential gene expression between the RTT#27 and HipSci iPSC-derived astrocytes. Whilst RNA-seq has previously been performed before in RTT, this has usually been on whole human brain tissue rather than on specific human cell types (Shovlin and Tropea, 2018, Gogliotti et al., 2018), or on whole MeCP2-deficient mouse brains (Pacheco et al., 2017). However, to the author's knowledge, no RNA-seq analysis has been performed on RTT patient-derived iPSC-derived astrocytes. Thus, the data in this chapter could provide a good foundation for further experiments to perform with RTT iPSC-derived astrocytes. MeCP2 itself was not differentially expressed between the RTT#27 and HipSci iPSC-derived astrocytes.

A significant number of genes that were differentially expressed between the two conditions were found to be involved in ECM organisation. Interestingly, this was also demonstrated in RNA-seq studies performed on microglia from WT and MeCP2-deficient mice (Zhao et al., 2017). This indicates that the selection of genes involved in these pathways (see appendix Table A1) are worthy of future investigation, particularly considering the ECM's role in development and synaptogenesis (Ferrer-Ferrer and Dityatev, 2018). Other biological pathways that have been implicated in RTT mouse models are synaptic dysfunction and neuronal transmission, inflammation and mitochondrial function (Krishnaraj et al., 2019)

The ECM has not been widely investigated in RTT, even though the ECM forms the scaffold for all cell types of the brain and accounts for 20% of the adult brain volume (Nicholson and Syková, 1998, Oohashi et al., 2015). Matrix metalloproteinases (MMPs) are enzymes that are capable of digesting components of the ECM and are therefore involved in tissue remodelling, such as that that occurs during development (Stamenkovic, 2003). Aberrant levels of MMPs have been found in a number of neurological conditions, such as ALS (Łukaszewicz-Zając et al., 2014). It has been found that circulating levels of MMP2 and 9 are higher in RTT patients (Carmeli et al., 2011). These, alongside MMP7, are associated with the breakdown of the blood brain barrier. Notably, two MMPs (MMP7 and 14) are highlighted in the list of genes associated with the ECM organisation pathway in this study (Table A1). MMP7 is thought to facilitate immune cell access to the brain in an experimental mouse model of multiple sclerosis by increase the permeability of the blood brain barrier (Buhler et al., 2009). The role MMP7 could play in ECM organisation and blood brain barrier integrity might be a worthwhile subject of investigation in RTT. Transcriptome analysis of $MeCP^{+/-}$ microglia also yielded ECM

components as being high on the list of differentially expressed genes (Zhao et al., 2017). Finally, RNA-seq performed on dorsal root ganglia of MeCP2 mutant rats also demonstrated differentially regulated genes enriched in pathways associated with the ECM and axon outgrowth (Bhattacherjee et al., 2017).

Thrombospondin 2 was found to be dysregulated in the RTT#27 iPSC-derived astrocytes, and is implicated in the cell adhesion and biological adhesion pathways. It is also involved in synaptogenesis (see section 1.13.7). Mice deficient in thrombospondin 2 demonstrate a leaky BBB and display altered ECM remodelling during injury (Tian et al., 2011). Decorin also appears in the list of dysregulated genes in the ECM organisation pathway. It is an ECM protein expressed by astrocytes and neurons (Zhang et al., 2018b). Decorin can promote axon growth even in the presence of inhibitory molecules such as chondroitin sulphate proteoglycans (Minor et al., 2008). Interestingly, a number of chondroitin sulphate proteoglycans are also in the list of dysregulated genes, such as neurocan, veriscan and brevican. They inhibit axon outgrowth and are upregulated during CNS injury, expressed by reactive astrocytes (McKeon et al., 1999, Asher et al., 2002). Considering the negative effect that RTT iPSC-derived ACM has on cultured hippocampal neuron dendrite outgrowth (Williams et al., 2014), these molecules would be worth investigating in RTT.

The hyaluronan and proteoglycan link protein (Hapln) 1 and hyaluronan synthase (Has) 3 are also dysregulated in the ECM organisation pathway. Haplns are part of ECM structures known as perineuronal nets, which surround the cell bodies of inhibitory neurons (Oohashi et al., 2015), and Has3 is one of the enzymes that synthesise hyaluronans, the main component of the ECM in the brain (Itano et al., 1999). Astrocytes are known to produce hyaluronans, and this production increases throughout age in macaque brains. CD44 expression also increased alongside it, a hyaluronan receptor which is associated with reactive astrocytes in brain lesions (Girgrah et al., 1991, Cargill et al., 2012). Hyaluronan production is also increased during CNS injury and astrogliosis (Struve et al., 2005). Furthermore, reduction in hyaluronan levels reduces the volume of the extracellular space in the brain, a phenomenon which exacerbates seizures in *in vitro* models of epilepsy (Perkins et al., 2017). The role of hyaluronan could also therefore be investigated in the role of seizures in RTT. It is noteworthy that these genes are associated with CNS injury, aging and astrogliosis. The dysregulation of these genes in RTT may therefore be contributing to a brain environment that does not support neural cell types, potentially leading to their dysfunction. Considering also that ECM components in the brain are involved in neural plasticity, the ECM in RTT is definitely a treatment target worth investigating (Miyata and Kitagawa, 2017).

RNA-seq on iPSC-derived neurons would have been good to compare purity and cell specific markers (Zhang et al., 2016). In addition, one of the HipSci biological replicates had to be

excluded from analysis as it did not cluster with its counterparts in the principal component analysis (data not shown) as it might have skewed results. Therefore, this sample would have to be repeated, and other control and disease lines would have to be included to add power to the data. However, 82% of the astrocyte specific genes in the list were expressed by 100% of the samples.

As MeCP2 has such a significant role in transcriptional regulation and development (see sections 1.5 and 1.6) more work investigating the outputs of RNA-seq will be invaluable to further understanding RTT, and indeed other conditions where MeCP2 is involved such as MeCP2 duplication syndrome (Ramocki et al., 2010). A MeCP2 interaction map can be seen in figure 5.8 to showcase further pathways of interest.

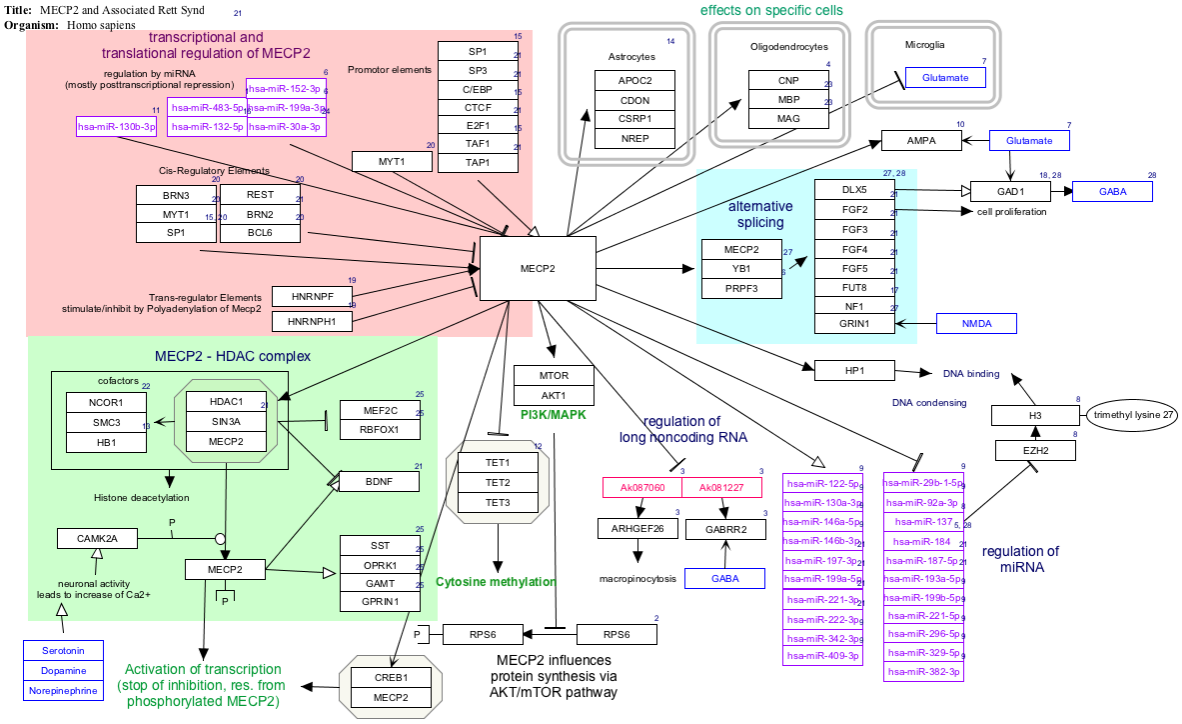

Figure 5.8: MeCP2 interaction map. Map shows upstream regulators of MeCP2 and the downstream effectors of MeCP2, with the effects it has on molecular pathways. Image taken from: MeCP2 and Associated Rett Syndrome pathways (Homo sapiens) http://www.wikipathways.org/instance/WP3584. (Ehrhart et al., 2016)

Chapter Six: Discussion and Future Work

Research on RTT has been dominated by rodent models containing either mutated MeCP2 or knockout MeCP2. Human iPSCs provide an opportunity to explore RTT using human patient-derived cells that contain physiologically relevant mutations whilst also being human in origin. It is hoped this could provide more translational data that could lead to findings and future treatments for RTT. The purpose of this discussion is to summarise the main findings of this thesis, to discuss broader issues that have not been included in the individual discussions, and to pose suggestions for future work.

The aim of this thesis was to test the hypothesis that astrocytes derived from RTT patient iPSCs display functional differences that contribute to disease pathogenesis. In addition, it was also investigated whether this impacted the function of healthy iPSC-derived neurons. The specific aims of this thesis were to:

1. Generate astrocyte cultures from healthy and RTT iPSC lines.
2. Determine the functional properties of iPSC-derived astrocytes and investigate if the healthy and disease lines exhibit differences.
3. Determine the effect RTT iPSC-derived astrocytes can have on healthy iPSC-derived neurons to investigate the non-cell autonomous effects of astrocytes on neuronal function.

6.1 Summary of Experimental Findings

6.1.1 Chapter Two

Experiments performed in chapter two demonstrated that 95%+ astrocyte monocultures could be generated from RTT#27, RTT#37 and HipSci iPSCs, quantified by GFAP staining. NPCs were generated as an intermediate cell type using a dual-SMAD inhibition neural induction method, and these cells displayed rosette morphology and were positive for Sox2 and Pax6 (Chambers et al., 2009). The cells downregulated gene expression of the pluripotency marker Oct4 throughout the differentiation from iPSC to NPCs, neurons and astrocytes (see Figure 1.6). The expression of Oct4 protein was undetectable at the end of the neural induction process. A small amount of neuronal contamination (<15%, see Figure 1.5) was observed in these cultures however the high percentage of astrocytes meant that these cultures were deemed acceptable for future use.

6.1.2 Chapter Three

The astrocytes generated and characterised in chapter two were functionally characterised to ensure that the cells produced could provide a physiologically meaningful model system. The iPSC-derived astrocytes displayed spontaneous calcium events with populations of astrocytes also responding to the neurotransmitters glutamate and ATP. In addition, the iPSC-derived astrocytes could also remove glutamate from their surroundings, and this uptake was

prevented for at least 30 minutes with the glutamate transport inhibitor, TBOA. Astrocytes also demonstrated a functional ANLS system. In response to glutamate uptake the astrocytes could release lactate as previously described in rodent (Pellerin and Magistretti, 1994a) and human astrocytes (Tarczyluk et al., 2013). These findings demonstrate that iPSC-derived astrocytes demonstrate physiological properties that have been observed *in vitro* and *in vivo* (Sofroniew and Vinters, 2010). In response to 30µM glutamate, the healthy control HipSci iPSC-derived astrocytes released significantly more lactate compared to the RTT#27 iPSC-derived astrocytes. TBOA significantly prevented this lactate release in HipSci iPSC-derived astrocytes, demonstrating that the glutamate uptake was at least partially driving the lactate release. This difference between healthy and disease astrocytes has not been noted in the literature before, making this a novel finding worthy of further investigation. No differences were noted in oxidative stress markers between the RTT#27, RTT#37 and HipSci iPSC-derived astrocytes. This data was very variable however, which will be discussed further in section 6.3.1.2.

6.1.3 Chapter Four

Previous work has shown that ACM from RTT iPSC-derived astrocytes has a negative effect on mouse hippocampal neurons; the cells have shorter dendrites and smaller soma (Williams et al., 2014). In order to investigate the effect that the astrocyte secretome has on iPSC-derived neurons ACM was collected from RTT#27, RTT#37 and HipSci iPSC-derived astrocytes which was then used to treat neurons. Investigation of ACM using ELISA demonstrated that RTT#27 ACM contained a significantly higher concentration of IL-6 than RTT#37 or HipSci ACM.

Fluorescent calcium imaging of neurons incubated with ACM demonstrated that cells treated with ACM from the HipSci iPSC-derived astrocytes demonstrated significantly increased responses to glutamate compared to neurons not treated with ACM or with ACM from RTT#27 or RTT#37 astrocytes. RTT#37 ACM induced a significantly higher level of spontaneous activity compared to neurons treated with RTT#27 ACM. This suggests that the secretome from the RTT astrocytes impact the activity of healthy iPSC-derived neurons.

6.1.4 Chapter Five

RNA-seq was performed on iPSC-derived astrocytes from the HipSci and RTT#27 lines. Two biological replicates were included from the HipSci line and three were included from the RTT#27 line. Samples from each line clustered together in the principal component analysis and in the heat map of samples. This shows that the biological samples within each line were more similar to each other than they were to samples from the other line. Differentially expressed genes were analysed, and GO analysis demonstrated that the pathway that was most highly dysregulated was ECM organisation. This therefore would be a promising area of

further study. Further data analysis could be performed on this RNA-seq data and might yield more pathways to explore in the future.

As only astrocytes were included in this thesis it was not possible to determine a list of astrocyte-specific genes compared to other neural cell types. However, using a list from a previously published paper (Al-Dalahmah et al., 2020) it was shown that the astrocytes in this paper express genes specifically associated with astrocytes. RNA-seq has not been performed on RTT iPSC-derived astrocytes, meaning these data are a point of novelty in this thesis.

6.2 General Discussion

6.2.1 Astrocyte Markers

A key focus of this thesis was to generate iPSC-derived astrocytes. Therefore, the marker used to characterise these cells must be appropriate. GFAP was selected as an astrocytic marker in this thesis as it has been used extensively throughout the literature since its discovery in 1969 (Eng et al., 2000). However, GFAP has been criticised as a pan-astrocytic marker as it tends to be positive in reactive astrocytes rather than quiescent astrocytes (Sofroniew and Vinters, 2010). Thus, it could be possible that non-reactive astrocytes are missed. Aldh1l1 has been found to a better global astrocyte marker than GFAP, being more broadly expressed in astrocyte populations (Cahoy et al., 2008). Another potential pan-astrocyte marker is CD49f, which has been found to be expressed in human foetal astrocytes and in iPSC-derived astrocytes (Barbar et al., 2020). These two markers might have been a better choice to characterise the astrocytic populations. Further to this, other markers, such as Glt1, GLAST, AQP4 and Kir4.1, could have been used to provide more information about the possible heterogeneity of the astrocyte cultures and aided in the characterisation of cells (Chaudhry et al., 1995, Nielsen et al., 1997, Poopalasundaram et al., 2000). Whilst qPCR was performed on these markers, as well as S100β, there were issues with the qPCR data as discussed in chapter three.

The astrocyte populations in this thesis were almost 100% positive for GFAP, potentially indicating that reactive astrocytes had been generated. Future studies could consider the addition of FGF2 to astrocyte cultures, as this has been shown to reduce reactivity and revert astrocytes to a quiescent state (Roybon et al., 2013). The media that the astrocytes were maintained in after day 35 of astrocyte induction also contains 2% serum. Serum has been shown to trigger reactivity in astrocytes; other studies investigating astrocyte reactivity ensure they use serum-free media (Liddelow et al., 2017b), although some studies use serum levels as high as 10% (Hedegaard et al., 2020). It is worth noting that whilst Hedegaard et al. (2020) had high levels of GFAP-positive astrocytes they also had a high proportion of S100β-positive astrocytes, indicative of a more mature population. Reactive astrocytes have altered functions and can release more inflammatory factors, which could potentially impact studying their

functions at later points (Liddelow et al., 2017b) . Additionally, as discussed in Chapter One, reactive astrocytes encompass a range of physiological effects, with some being beneficial to surrounding neurons and others harmful. If non-reactive astrocytes were generated from both healthy and RTT lines, future work could distinguish the effects these astrocytes had on iPSC-derived neurons.

6.2.2 Functional Characterisation of Astrocytes

The astrocytes generated in this thesis demonstrated the ability to remove glutamate from their surroundings and release lactate in response. This is a strong indication that the iPSC-derived astrocytes generated display some astrocytic functions as previously described (Mahmoud et al., 2019, Cho and Bannai, 1990). Lactate release in response to glutamate uptake has not been observed in iPSC-derived astrocytes and indicates the potential of these cells to contribute to and model the ANLS as discussed in section 1.13.5. RTT#27 iPSC-derived astrocytes released significantly less lactate than the HipSci iPSC-derived astrocytes in response to glutamate. This could indicate that astrocytes in RTT are not able to efficiently transfer metabolites to neurons in times of high neuronal activity or stress. This could have a negative impact on neuronal function. Release of lactate from astrocytes has been shown to be critical for long term memory formation as it is critical for the energy-intensive process of mRNA translation (Buttgereit and Brand, 1995, Suzuki et al., 2011). Disrupting the expression of astrocytic MCT4 or MCT1 causes amnesia in rats which can be rescued by lactate, however lactate cannot rescue amnesia caused by disruption of neuronal MCT2 expression (Suzuki et al., 2011). It has been demonstrated that the release of lactate from astrocytes is critical for long term memory formation as it provides the necessary energy for neurons to translate mRNA during learning (Descalzi et al., 2019). CSF levels of lactate are higher in RTT patients, though this is thought to be a secondary consequence of hyperventilation rather than evidence of metabolic dysfunction (Lappalainen and Riikonen, 1994).

To investigate this further, neurons could either be cultured in direct contact with RTT iPSC-derived astrocytes. Or iPSC-derived neurons could be treated with media containing lactate levels of stimulated astrocytes from both healthy and disease lines. The neurons could then be stimulated, either electrophysiologically or pharmacologically to determine the impact on neuronal activity, such as amplitude, frequency and duration of mEPSCs. The impact on cellular health and viability could also be considered, in order to try and determine the effect of this reduced lactate release by RTT astrocytes.

Due to the previously discussed issues with the qPCR data, immunocytochemical analysis of the Glt1 and GLAST transporters could be performed in the future. This could give information about the localisation of these transporters and indeed quantification of them. To further investigate, total levels of these proteins could be investigated with Western Blot or nuclear

magnetic resonance spectroscopy. The same studies could be performed with the lactate transporter, MCT1, in order to investigate whether it is lower levels of this transporter that is responsible for the lower release of lactate. Enzymes responsible for synthesising lactate in astrocytes, such as lactate dehydrogenase 5 (LDH5), could also be considered for investigation. LDH5 is specifically expressed in astrocytes whereas other isoforms such as LDH1 are expressed in neurons (Venkov et al., 1976, Bittar et al., 1996).

The astrocytes produced in this thesis also responded to glutamate and ATP, further showing that they display functional characteristics of astrocytes. More neurotransmitters such as GABA or DHPG could have been used. Genetically encoded calcium indicator (GECI) iPSC lines would also be a good tool to use in co-cultures, as the impact of one cell type on another could be functionally investigated without the need for calcium dyes. For morphological analysis in co-cultures, a GFP-tagged line could also mean that morphology of specific cell types could be assessed to see how different cell types affect one another. Such a line could also be visualised without the need for fixing or staining the cells, meaning that changes could be visualised live over time. Indeed, such work has been performed in this lab by Dr James Crowe (unpublished thesis, 2020).

6.2.3 Electrophysiological Cell Characterisation

Additional functional characterisation could have been performed with whole cell patch clamping. This could have provided information about the membrane properties of iPSC-derived astrocytes and neurons, such as resting membrane potential or their permeability to certain ions. Compared to neurons, astrocytes have a hyperpolarised resting membrane potential of ~-80mV and lower resistance (~4-20MΩ) (Dallérac et al., 2013). Astrocytic membranes are very permeable to potassium, indicated by their membrane potential being very close to the Nernst potential for potassium (Somjen, 1975). Electrophysiology properties of the iPSC-derived astrocytes could have been used as further characterisation to distinguish them from neurons, as well as potentially providing information about healthy astrocytes compared with those from RTT iPSC-derived astrocytes. Indeed, MeCP2 mutant mice display a ~50% reduction in Kir4.1 protein, which translates with a reduction in Kir4.1-mediated currents (Nwaobi et al., 2016). As Kir4.1 is a key astrocytic protein which is also implicated in RTT (see section 1.13.1) this would be worth investigating in iPSC-derived models of RTT.

Furthermore, a single astrocyte could also have been filled with a fluorescent dye in order to see whether it can spread throughout the syncytium of cultured astrocytes. Treatment then with a gap junction blocker such as carbenoxolone could show that the iPSC-derived astrocytes form a syncytium connected by gap junctions, akin to astrocytes *in vivo* (Pacholko et al., 2020). The presence of gap junctions could also be investigated using immunocytochemistry using staining for connexin 30 (Cx30) and connexin 43 (Cx43). This has

been previously been demonstrated in NT2.D1 derived neuronal cells (Tarczyluk et al., 2013) and in iPSC-derived astrocytes (Dr James Crowe, unpublished thesis).

6.2.4 Cell Maturity

Synaptic staining of the markers PSD95 and synaptophysin in iPSC-derived neuronal cultures in this thesis did not demonstrate positive staining after 2 weeks in culture (data not shown). Synapsin staining has been observed in iPSC-derived neurons after 4-5 weeks in cultures, in addition these neurons were grown on rat glial feeder layers (Kim et al., 2011). This suggests that neuronal cultures were not mature enough at the point of staining and would benefit from additional time in culture with the presence of astrocytes. Despite treatment with ACM synapses did not form in these cultures, though glial-derived factors have shown to promote synapse formation in retinal ganglion cells cultured from rat (Nägler et al., 2001). As retinal ganglion cells are primary cells that have benefited from normal development it could be that these cells were more mature than the iPSC-derived neuronal monocultures used in this thesis. Future work should aim to allow iPSC-derived neurons to reach a later timepoint before synaptic staining is attempted. MAP2 staining should also have been used rather than solely relying on Tuj, as MAP2 is a marker of mature neurons. The presence of astrocytes also aids neuronal and synapse maturation (see section 1.13.7), with neurons also aiding astrocyte maturation (Hasel et al., 2017). Co-cultures of neurons and astrocytes would therefore be the next step in optimising this model of RTT. Such co-cultures were attempted but had a low success rate due to over-proliferation of astrocytes causing the cultures to die. An attempt was made to culture the cells for a shorter time period, with RTT#37 iPSC-derived astrocytes stained for GFAP in order to assess whether even a short time in co-culture (72 hours) could impact astrocytic morphology. Unfortunately, there was not time to repeat this experiment with all cell lines, however it can be seen from the images in Figure 6.1, that the iPSC-derived astrocytes co-cultured with iPSC-derived neurons exhibit different morphology to those derived in monoculture. Further optimisation and analysis could confirm the morphological differences and assess whether healthy iPSC-derived astrocytes grow differently in co-culture to RTT iPSC-derived astrocytes.

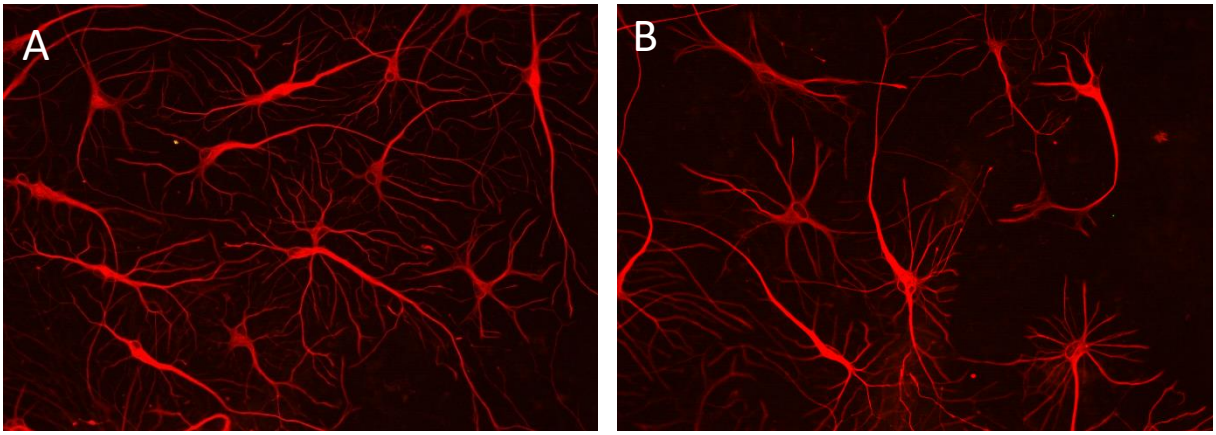

Figure 6.1: Immunocytochemistry image of iPSC-derived astrocytes grown with iPSC-derived neurons. **A)** and **B)** both depict RTT#37 iPSC-derived astrocytes stained for GFAP co-cultured with iPSC-derived neurons (unstained).

6.2.5 ACM

As it was determined that ACM from RTT#27 iPSC-derived astrocytes contained significantly more IL-6 than the RTT#37 or HipSci ACM it is important to investigate a broader panel of inflammatory markers using ELISAs, such as TNFα in future studies. In addition, the astrocytes could have been investigated after being stimulated by factors such as LPS in order to deduce whether there is a difference in reactivity between the RTT astrocytes compared to healthy controls. As astrocytes also release factors that are integral to synaptogenesis such as thrombospondins (see section 1.13.7) it would have been useful to investigate the presence of these in the ACM (Christopherson et al., 2005). In conjunction with synaptic staining of neurons after ACM treatment this could provide information about the effect the astrocyte secretome has on synaptogenesis in RTT. Thrombospondins are secreted by astrocytes and are involved in synaptogenesis in the CNS (see section 1.13.7) Thrombospondin 2 (TSP2) is dysregulated in RTT#27 iPSC-derived astrocytes. Treatment of retinal ganglion cells with TSP2 significantly increases synapse number (Eroglu et al., 2009). Levels of this protein in RTT#27 and HipSci iPSC-derived ACM could be investigated in future work as well the impact on synaptogenesis.

Further work could also seek to investigate the effect the ACM had on iPSC-derived neuronal morphology. The neurons in this thesis were plated at too high a density for dendritic analysis to be possible. For the purposes of such analysis the seeding density of NPCs prior to synchronisation should be lower than that used for functional studies such as calcium imaging.

6.2.6 RNA-Seq

RNA-seq was performed on two biological replicates from the HipSci iPSC-derived astrocytes and on three of the RTT#27 iPSC-derived astrocytes. The third biological replicate from the HipSci line was excluded as it did not cluster with the other two biological replicates from that line and it was thought it might skew results. In the future another sample from a different

biological differentiation would have be sequenced. In addition, more control and disease lines should be sequenced to add power to the data.

Once the biological replicate was removed from analysis it the HipSci samples and RTT#27 samples clustered together. They also had differentially expressed genes which were put into a gene ontology analysis programme to see which terms were enriched for the differentially expressed genes. The most enriched term was for ECM organisation. The top ten terms and their corresponding genes can be seen in the appendix (table A1). As this ECM organisation term has also been found to be enriched in differentially expressed genes between WT and MeCP2-deficient mice microglia it is definitely a future direction worth pursuing. Few studies have performed RNA-seq in RTT models, with most being performed on whole brain tissue from patients or MeCP2-deficient mice. Thus, performing RNA-seq specifically on iPSC-derived astrocytes in this thesis might provide some novel data about their role RTT.

The iPSC-derived astrocytes used in this study were found to express a number of genes that are considered to be astrocyte-specific according to the literature (Al-Dalahmah et al., 2020). This further confirms that iPSC-derived astrocytes have been generated in this thesis. In future experiments it would be beneficial to perform RNA-seq on iPSCs, NPCs, iPSC-derived neurons and microglia in order to compare gene expression between different iPSC-derived neural cell types at each stage of development.

6.3 Are iPSC-derived cells a good way to study RTT?

As the main aspect of this thesis was to generate an iPSC-derived system for modelling RTT it is important to consider whether it was successful in achieving this. In the section below, some limitations and benefits of the model will be discussed.

6.3.1 Limitations of the Model

6.3.1.1 Mosaicism

Due to random somatic X chromosome inactivation patients with RTT do not express mutant MeCP2 in all of their cells. Some cells will still contain the WT allele of MeCP2. Experiments in this thesis that used RTT#27 line had 100% of these astrocytes present. In order to more accurately model RTT an isogenic control of the RTT#27 that contained WT MeCP2 could be generated in order to grow cultures that contain 50% mutant MeCP2 and 50% WT MeCP2. ACM could have been generated from these cultures also.

Indeed, due to the nature of RTT a WT MeCP2 line could be generated from the same patient as a mutant MeCP2 line. This would result in data that is far more reflective of the disease, and may indeed demonstrate in iPSC-derived systems how mutant MeCP2 can spread throughout an astrocytic syncytium as it has in the literature (Maezawa et al., 2009).

6.3.1.2 iPSC-derived Cell Variability

A difficulty that was observed across the experimental work in this thesis is the variability in iPSC-derived cells. This variability was observed across the different biological differentiations for each cell line, as well as between the two control cell lines (RTT#37 and HipSci). This issue has been addressed and discussed in the field (Volpato and Webber, 2020). One suggested reason is that iPSC lines acquire mutations throughout the process of cell culture, particularly those that benefit cell culture. Mutations in the tumour suppressor gene, p53, have been noted to be common as mutations in this gene restrict the regulation on cell division and apoptosis (Merkle et al., 2017). Such mutations could alter the function of the generated cells and could even be dangerous if iPSC-derived cells were to be used clinically. Genetic testing therefore has been suggested to compensate for this. Mutations would also not be consistent across cell lines, introducing variability that is out of the control of the researcher. This could also amplify differences in cell lines that are independent of what is being studied, potentially masking significant results or disease differences. Karyotyping to identify potential chromosomal abnormalities should have also been performed prior to and during iPSC use, as iPSCs can acquire chromosomal abnormalities during culture (Liang and Zhang, 2013).

A simpler reason for the variability can also be due to the researcher. Experience and knowledge vary greatly between researchers, and also within the same researcher as a project progresses. Subtle changes in treatment of cells could manifest in experimental results, adding to the biological variability observed in this thesis.

The RTT#37 iPSC-derived astrocytes were in particular very variable across the differentiations in functional studies and did not always correlate with results from the HipSci control line. For future work, more disease lines and more control lines would need to be used. Additionally, to reduce variability within the lines it is possible that an n=3 is not sufficient and that an n=5 might be more useful for statistical analysis.

6.3.1.3 Two-dimensional Culture System

The iPSC-derived astrocytes generated in this thesis were differentiated and cultured as monocultures. This means that the cells were not grown in a physiological condition as they would *in vivo*, which contains other cell types such as microglia, oligodendrocytes and neurons, all of which aid in the functional maturation of the cell types. Astrocytes for example downregulate genes associated with maturity if they are removed from neuronal cultures (Hasel et al., 2017). The astrocytes could possibly therefore not demonstrate the full complement of astrocytic functions or perform them in a way that would be seen *in vivo*. Thus for future work it would be beneficial to consider the introduction of other cell types into these cultures, either as co-cultures or as a three-dimensional culture system such as a cerebral organoid (Lancaster et al., 2013). Due to the more spontaneous assembly of cerebral

organoids that replicate *in vivo* development and also demonstrate the layered structure of the cerebral cortex, these are invaluable tools for studying neurodevelopmental disorders such as RTT in a way not possible in other culture systems. Cerebral organoids can also be kept in culture for a very long time, some up to 20 months (Sloan et al., 2017). This sort of time scale would also mean that the cells would mature in a temporal manner and provide more translational data, particularly in diseases of aging like Alzheimer's Disease. However, if organoids become too large it is difficult for media and nutrients to perfuse, leading to a necrotic centre. The introduction of vasculature to these organoids would help solve this as well as provide an extra level of physiological relevance. Recent studies have generated vascularised cerebral organoids which could provide useful model systems (Pham et al., 2018).

Recent work has generated RTT iPSC-derived organoids that demonstrate premature cortical plate neuron formation (Gomes et al., 2020), showing that these models are indeed starting to be used to investigate RTT.

6.3.1.4 Reliance on Commercially Available Media

Commercially available media was used throughout this thesis. The use of commercial media may not be idea as formulations are often proprietary and often change. This may potentially impact reproducibility of experimental work. The price of these media can also be prohibitive to increases numbers of experiments and to the scalability of work. However, optimising protocols for generating cell types can take a lot of time and effort. This can be limiting for smaller labs where there might be only one person working on a single project. The availability of these media therefore free researcher time to commit to experimental design and come up with new ideas. In addition, these medias will have been rigorously tested and are also often used in other publications.

6.3.2 Benefits of the model

6.3.2.1 Enriched cultures of iPSC-derived astrocytes

The iPSC-derived astrocyte cultures in this thesis were very enriched for astrocytes as evidenced by GFAP staining. This enrichment was observed across all three cell lines and in each biological differentiation for each, meaning that cell sorted methods such as fluorescent-activated cell sorting (FACS) or immunopanning (Foo et al., 2011) were not necessary, making the method easier and cheaper. The astrocytes were also able to be frozen down at multiple time points past day 35, meaning that they could be banked and used in the future. This means that the process of iPSC to astrocyte would not have to be repeated once sufficient astrocytes had been generated. In addition to this, the astrocytes proliferated *in vitro* which meant that they could be expanded. The RNA-seq data also shows that the generated astrocytes expressed genes that are specific to astrocytes (Al-Dalahmah et al., 2020).

6.3.2.2 iPSC-derived astrocytes demonstrated astrocytic functions found in vivo.

The astrocytes generated in this thesis demonstrated numerous astrocytic functions that have been described *in vivo*. They displayed spontaneous calcium events and could respond to neurotransmitters such as glutamate and ATP. In addition, they were able to remove glutamate from their surroundings and release lactate in response to this uptake. This functional characterisation has assessed more astrocytic functions than is usually covered in the literature, so the knowledge that human iPSC-derived astrocytes are a viable replacement to foetal primary astrocytes or mouse astrocytes is a promising finding. As the RTT#27 iPSC-derived astrocytes also showed these functions it means that iPSC-derived astrocytes are worthwhile way to study astrocytes in disease. These functional properties have not been observed in iPSC-derived astrocytes in RTT so these findings could be considered novel.

6.3.2.3 Two-dimensional cultures.

Using a two-dimensional cell culture system is one of the simplest ways to model disease. This means that is easy to deduce results from and also for complexity to be added by adding extra cell types. It also means that it is an easy system to replicate by other researchers. Even though the two-dimensional system offers simplicity it also means that physiological relevance is compromised. However, this thesis has demonstrated that astrocytes grown in two-dimensional in monoculture do demonstrate functions of astrocytes *in vivo*.

6.3.2.4 Cell banking at each stage.

By generating astrocytes from iPSCs via NPCs it enables each cell type to be expanded and frozen at multiple stages. This reduces the time taken to generate astrocytes from iPSCs again if necessary. Furthermore, freezing and banking NPCs means that if different neural cell types are required, such as neurons or oligodendrocytes, they can be generated without having to start differentiation from the iPSC stage.

6.3.2.5 The future of disease modelling.

This thesis represents a completely iPSC-derived model, meaning that it is human in origin and contains the MeCP2 mutation that is found in the donor patient, as well as their unique genetic background. Results from iPSC-derived models are therefore very translational meaning that any findings could hopefully reflect human disease more than other model systems, such as primary mouse cell culture, would. Ultimately this will lead to breakthroughs in neurological diseases such as RTT and provide new treatment targets or cures in the future.

Brain diseases are notoriously difficult to study and discover drugs for. Alzheimer's Disease has a failure rate of over 99% for new drug discovery (Cummings et al., 2019), with the only drugs currently available merely alleviating symptoms for a limited period of time (Huang et al., 2020). RTT also currently has no cures, and treatments are limited to symptom management. As RTT neurological symptoms were successfully reversed in a mouse model of RTT it is

hopeful that similar effects could be achieved in human patients, particularly as RTT does not present with any neurodegeneration (Guy et al., 2007). Whilst this is very promising, it is important to note that therapies that target the MeCP2 gene may have unintended side effects; brain volume might increase in patients, which could be a problem as patients with RTT have smaller heads (Clarke and Abdala Sheikh, 2018). Another factor to consider is that not all those affected by brain disorders want to see a cure, rather an improvement in the facilities and support for themselves or their loved one (Clarke and Abdala Sheikh, 2018). However, if there could be a treatment that benefited the lives of those with neurological disorders, or indeed could reverse symptoms, then it is worth continuing to search for one. Understanding how the brain functions and how pathogenesis is initiated and spreads in the brain is an important step in doing this, therefore it is imperative that new models are continuously developed for modelling brain diseases that provide translational data to ultimately benefit patients' lives.

6.4 Conclusion

Human iPSC-derived astrocytes and neurons were generated in this thesis from one RTT line and from two control lines. All three lines were capable of neural induction and consistent subsequent differentiation to highly enriched cultures of astrocytes. These astrocytes demonstrated functions that are characteristic of astrocytes *in vivo*. Such functions were consistently observed across all cell lines, showing that the method used in this thesis for generating functional astrocytes was reproducible and reliable. To optimise this further, mixed cultures of mutant and WT MeCP2 astrocytes should be considered. Further complexity could also be added by co-culturing different cell types derived from iPSCs, such as interneurons, microglia and oligodendrocytes, in the future. This thesis demonstrated that iPSC-derived astrocytes can possible model a functional ANLS, and that this could be impaired in astrocytes derived from RTT iPSCs. This has not been shown in the literature before, so is an exciting point of novelty worthy of further study. In addition, the RNA-seq performed on RTT iPSC-derived astrocytes to compare them with healthy iPSC-derived astrocytes has also not been seen in the literature. The data from these experiments are also novel findings that have shown potentially dysregulated genes and pathways in RTT, which will definitely be worth considering in future work.

References

ACAMPA, M. & GUIDERI, F. 2006. Cardiac disease and Rett syndrome. *Arch Dis Child,* 91**,** 440-3.

ACOSTA, C., ANDERSON, H. D. & ANDERSON, C. M. 2017. Astrocyte dysfunction in Alzheimer disease. *J Neurosci Res,* 95**,** 2430-2447.

AFGAN, E., BAKER, D., BATUT, B., VAN DEN BEEK, M., BOUVIER, D., ČECH, M., CHILTON, J., CLEMENTS, D., CORAOR, N., GRÜNING, B. A., GUERLER, A., HILLMAN-JACKSON, J., HILTEMANN, S., JALILI, V., RASCHE, H., SORANZO, N., GOECKS, J., TAYLOR, J., NEKRUTENKO, A. & BLANKENBERG, D. 2018. The Galaxy platform for accessible, reproducible and collaborative biomedical analyses: 2018 update. *Nucleic Acids Research,* 46**,** W537-W544.

AGULHON, C., PETRAVICZ, J., MCMULLEN, A. B., SWEGER, E. J., MINTON, S. K., TAVES, S. R., CASPER, K. B., FIACCO, T. A. & MCCARTHY, K. D. 2008. What is the role of astrocyte calcium in neurophysiology? *Neuron,* 59**,** 932-946.

AL-DALAHMAH, O., SOSUNOV, A. A., SHAIK, A., OFORI, K., LIU, Y., VONSATTEL, J. P., ADORJAN, I., MENON, V. & GOLDMAN, J. E. 2020. Single-nucleus RNA-seq identifies Huntington disease astrocyte states. *Acta Neuropathologica Communications,* 8**,** 19.

ALLEN, N. J., BENNETT, M. L., FOO, L. C., WANG, G. X., CHAKRABORTY, C., SMITH, S. J. & BARRES, B. A. 2012. Astrocyte glypicans 4 and 6 promote formation of excitatory synapses via GluA1 AMPA receptors. *Nature,* 486**,** 410-4.

ALLEN, N. J. & EROGLU, C. 2017. Cell Biology of Astrocyte-Synapse Interactions. *Neuron,* 96**,** 697-708.

AMIR, R. E., VAN DEN VEYVER, I. B., WAN, M., TRAN, C. Q., FRANCKE, U. & ZOGHBI, H. Y. 1999. Rett syndrome is caused by mutations in X-linked MECP2, encoding methyl-CpG-binding protein 2. *Nat Genet,* 23**,** 185-8.

ANDERSON, C. M. & SWANSON, R. A. 2000. Astrocyte glutamate transport: review of properties, regulation, and physiological functions. *Glia,* 32**,** 1-14.

ANDOH-NODA, T., AKAMATSU, W., MIYAKE, K., MATSUMOTO, T., YAMAGUCHI, R., SANOSAKA, T., OKADA, Y., KOBAYASHI, T., OHYAMA, M., NAKASHIMA, K., KUROSAWA, H., KUBOTA, T. & OKANO, H. 2015. Differentiation of multipotent neural stem cells derived from Rett syndrome patients is biased toward the astrocytic lineage. *Mol Brain,* 8**,** 31.

ARAQUE, A., PARPURA, V., SANZGIRI, R. P. & HAYDON, P. G. 1999. Tripartite synapses: glia, the unacknowledged partner. *Trends Neurosci,* 22**,** 208-15.

ARCHER, H., EVANS, J., LEONARD, H., COLVIN, L., RAVINE, D., CHRISTODOULOU, J., WILLIAMSON, S., CHARMAN, T., BAILEY, M. E., SAMPSON, J., DE KLERK, N. & CLARKE, A. 2007. Correlation between clinical severity in patients with Rett syndrome with a p.R168X or p.T158M MECP2 mutation, and the direction and degree of skewing of X-chromosome inactivation. *J Med Genet,* 44**,** 148-52.

ARIANI, F., HAYEK, G., RONDINELLA, D., ARTUSO, R., MENCARELLI, M. A., SPANHOL-ROSSETO, A., POLLAZZON, M., BUONI, S., SPIGA, O., RICCIARDI, S., MELONI, I., LONGO, I., MARI, F., BROCCOLI, V., ZAPPELLA, M. & RENIERI, A. 2008. FOXG1 is responsible for the congenital variant of Rett syndrome. *Am J Hum Genet,* 83**,** 89-93.

ARMSTRONG, D. D. 1992. The neuropathology of the Rett syndrome. *Brain Dev,* 14 Suppl**,** S89-98.

ARMSTRONG, D. D. 2005. Neuropathology of Rett syndrome. *J Child Neurol,* 20**,** 747-53.

ASHER, R. A., MORGENSTERN, D. A., SHEARER, M. C., ADCOCK, K. H., PESHEVA, P. & FAWCETT, J. W. 2002. Versican Is Upregulated in CNS Injury and Is a Product of Oligodendrocyte Lineage Cells. *The Journal of Neuroscience,* 22**,** 2225-2236.

ASZTELY, F., ERDEMLI, G. & KULLMANN, D. M. 1997. Extrasynaptic glutamate spillover in the hippocampus: dependence on temperature and the role of active glutamate uptake. *Neuron,* 18**,** 281-93.

ATTWELL, D., BUCHAN, A. M., CHARPAK, S., LAURITZEN, M., MACVICAR, B. A. & NEWMAN, E. A. 2010. Glial and neuronal control of brain blood flow. *Nature,* 468**,** 232-43.

AZEVEDO, F. A., CARVALHO, L. R., GRINBERG, L. T., FARFEL, J. M., FERRETTI, R. E., LEITE, R. E., JACOB FILHO, W., LENT, R. & HERCULANO-HOUZEL, S. 2009. Equal numbers of neuronal and

nonneuronal cells make the human brain an isometrically scaled-up primate brain. *J Comp Neurol,* 513**,** 532-41.

BALMER, D., GOLDSTINE, J., RAO, Y. M. & LASALLE, J. M. 2003. Elevated methyl-CpG-binding protein 2 expression is acquired during postnatal human brain development and is correlated with alternative polyadenylation. *J Mol Med (Berl),* 81**,** 61-8.

BANDO, Y., IRIE, K., SHIMOMURA, T., UMESHIMA, H., KUSHIDA, Y., KENGAKU, M., FUJIYOSHI, Y., HIRANO, T. & TAGAWA, Y. 2014. Control of Spontaneous Ca2+ Transients Is Critical for Neuronal Maturation in the Developing Neocortex. *Cerebral Cortex,* 26**,** 106-117.

BANERJEE, A., RIKHYE, R. V., BRETON-PROVENCHER, V., TANG, X., LI, C., LI, K., RUNYAN, C. A., FU, Z., JAENISCH, R. & SUR, M. 2016. Jointly reduced inhibition and excitation underlies circuit-wide changes in cortical processing in Rett syndrome. *Proc Natl Acad Sci U S A,* 113**,** E7287-e7296.

BARBAR, L., JAIN, T., ZIMMER, M., KRUGLIKOV, I., SADICK, J. S., WANG, M., KALPANA, K., ROSE, I. V. L., BURSTEIN, S. R., RUSIELEWICZ, T., NIJSURE, M., GUTTENPLAN, K. A., DI DOMENICO, A., CROFT, G., ZHANG, B., NOBUTA, H., HÉBERT, J. M., LIDDELOW, S. A. & FOSSATI, V. 2020. CD49f Is a Novel Marker of Functional and Reactive Human iPSC-Derived Astrocytes. *Neuron,* 107**,** 436-453.e12.

BAZARGANI, N. & ATTWELL, D. 2016. Astrocyte calcium signaling: the third wave. *Nat Neurosci,* 19**,** 182-9.

BEBBINGTON, A., ANDERSON, A., RAVINE, D., FYFE, S., PINEDA, M., DE KLERK, N., BEN-ZEEV, B., YATAWARA, N., PERCY, A., KAUFMANN, W. E. & LEONARD, H. 2008. Investigating genotype-phenotype relationships in Rett syndrome using an international data set. *Neurology,* 70**,** 868-75.

BÉLANGER, M. & MAGISTRETTI, P. J. 2009. The role of astroglia in neuroprotection. *Dialogues Clin Neurosci,* 11**,** 281-95.

BELICHENKO, P. V., OLDFORS, A., HAGBERG, B. & DAHLSTROM, A. 1994. Rett syndrome: 3-D confocal microscopy of cortical pyramidal dendrites and afferents. *Neuroreport,* 5**,** 1509-13.

BELLOT-SAEZ, A., KEKESI, O., MORLEY, J. W. & BUSKILA, Y. 2017. Astrocytic modulation of neuronal excitability through K(+) spatial buffering. *Neurosci Biobehav Rev,* 77**,** 87-97.

BENZIE, I. F. & STRAIN, J. J. 1996. The ferric reducing ability of plasma (FRAP) as a measure of "antioxidant power": the FRAP assay. *Anal Biochem,* 239**,** 70-6.

BEZZI, P., GUNDERSEN, V., GALBETE, J. L., SEIFERT, G., STEINHÄUSER, C., PILATI, E. & VOLTERRA, A. 2004. Astrocytes contain a vesicular compartment that is competent for regulated exocytosis of glutamate. *Nature Neuroscience,* 7**,** 613-620.

BHATIA, T. N., PANT, D. B., ECKHOFF, E. A., GONGAWARE, R. N., DO, T., HUTCHISON, D. F., GLEIXNER, A. M. & LEAK, R. K. 2019. Astrocytes Do Not Forfeit Their Neuroprotective Roles After Surviving Intense Oxidative Stress. *Frontiers in Molecular Neuroscience,* 12.

BHATTACHERJEE, A., MU, Y., WINTER, M. K., KNAPP, J. R., EGGIMANN, L. S., GUNEWARDENA, S. S., KOBAYASHI, K., KATO, S., KRIZSAN-AGBAS, D. & SMITH, P. G. 2017. Neuronal cytoskeletal gene dysregulation and mechanical hypersensitivity in a rat model of Rett syndrome. *Proceedings of the National Academy of Sciences,* 114**,** E6952-E6961.

BIALAS, A. R. & STEVENS, B. 2013. TGF-β signaling regulates neuronal C1q expression and developmental synaptic refinement. *Nature neuroscience,* 16**,** 1773-1782.

BIENVENU, T., VILLARD, L., DE ROUX, N., BOURDON, V., FONTES, M., BELDJORD, C., TARDIEU, M., JONVEAUX, P. & CHELLY, J. 2002. Spectrum of MECP2 mutations in Rett syndrome. *Genet Test,* 6**,** 1-6.

BITTAR, P. G., CHARNAY, Y., PELLERIN, L., BOURAS, C. & MAGISTRETTI, P. J. 1996. Selective distribution of lactate dehydrogenase isoenzymes in neurons and astrocytes of human brain. *J Cereb Blood Flow Metab,* 16**,** 1079-89.

BLANKENSHIP, A. G. & FELLER, M. B. 2010. Mechanisms underlying spontaneous patterned activity in developing neural circuits. *Nat Rev Neurosci,* 11**,** 18-29.

BOCKENHAUER, D., FEATHER, S., STANESCU, H. C., BANDULIK, S., ZDEBIK, A. A., REICHOLD, M., TOBIN, J., LIEBERER, E., STERNER, C., LANDOURE, G., ARORA, R., SIRIMANNA, T., THOMPSON, D., CROSS, J. H., VAN'T HOFF, W., AL MASRI, O., TULLUS, K., YEUNG, S., ANIKSTER, Y., KLOOTWIJK, E., HUBANK, M., DILLON, M. J., HEITZMANN, D., ARCOS-BURGOS, M., KNEPPER, M. A., DOBBIE, A., GAHL, W. A., WARTH, R., SHERIDAN, E. & KLETA, R. 2009. Epilepsy, ataxia, sensorineural deafness, tubulopathy, and KCNJ10 mutations. *N Engl J Med,* 360**,** 1960-70.

BOGGIO, E. M., LONETTI, G., PIZZORUSSO, T. & GIUSTETTO, M. 2010. Synaptic determinants of rett syndrome. *Front Synaptic Neurosci,* 2**,** 28.

BOND, A. M., BHALALA, O. G. & KESSLER, J. A. 2012. The dynamic role of bone morphogenetic proteins in neural stem cell fate and maturation. *Developmental neurobiology,* 72**,** 1068-1084.

BONNI, A., SUN, Y., NADAL-VICENS, M., BHATT, A., FRANK, D. A., ROZOVSKY, I., STAHL, N., YANCOPOULOS, G. D. & GREENBERG, M. E. 1997. Regulation of gliogenesis in the central nervous system by the JAK-STAT signaling pathway. *Science,* 278**,** 477-83.

BRADLEY, R. A., SHIREMAN, J., MCFALLS, C., CHOI, J., CANFIELD, S. G., DONG, Y., LIU, K., LISOTA, B., JONES, J. R., PETERSEN, A., BHATTACHARYYA, A., PALECEK, S. P., SHUSTA, E. V., KENDZIORSKI, C. & ZHANG, S.-C. 2019. Regionally specified human pluripotent stem cell-derived astrocytes exhibit different molecular signatures and functional properties. *Development,* 146**,** dev170910.

BRENNAND, K. J., SIMONE, A., JOU, J., GELBOIN-BURKHART, C., TRAN, N., SANGAR, S., LI, Y., MU, Y., CHEN, G., YU, D., MCCARTHY, S., SEBAT, J. & GAGE, F. H. 2011. Modelling schizophrenia using human induced pluripotent stem cells. *Nature,* 473**,** 221-225.

BRÖER, S., RAHMAN, B., PELLEGRI, G., PELLERIN, L., MARTIN, J. L., VERLEYSDONK, S., HAMPRECHT, B. & MAGISTRETTI, P. J. 1997. Comparison of lactate transport in astroglial cells and monocarboxylate transporter 1 (MCT 1) expressing Xenopus laevis oocytes. Expression of two different monocarboxylate transporters in astroglial cells and neurons. *J Biol Chem,* 272**,** 30096-102.

BROOKER, G. J., KALLONIATIS, M., RUSSO, V. C., MURPHY, M., WERTHER, G. A. & BARTLETT, P. F. 2000. Endogenous IGF-1 regulates the neuronal differentiation of adult stem cells. *J Neurosci Res,* 59**,** 332-41.

BROWN, A. M. & RANSOM, B. R. 2007. Astrocyte glycogen and brain energy metabolism. *Glia,* 55**,** 1263-71.

BROWN, A. M., SICKMANN, H. M., FOSGERAU, K., LUND, T. M., SCHOUSBOE, A., WAAGEPETERSEN, H. S. & RANSOM, B. R. 2005. Astrocyte glycogen metabolism is required for neural activity during aglycemia or intense stimulation in mouse white matter. *J Neurosci Res,* 79**,** 74-80.

BROWN, K., SELFRIDGE, J., LAGGER, S., CONNELLY, J., DE SOUSA, D., KERR, A., WEBB, S., GUY, J., MERUSI, C., KOERNER, M. V. & BIRD, A. 2016. The molecular basis of variable phenotypic severity among common missense mutations causing Rett syndrome. *Hum Mol Genet,* 25**,** 558-70.

BROWN, M. S. & GOLDSTEIN, J. L. 2009. Cholesterol feedback: from Schoenheimer's bottle to Scap's MELADL. *J Lipid Res,* 50 Suppl**,** S15-27.

BUHLER, L. A., SAMARA, R., GUZMAN, E., WILSON, C. L., KRIZANAC-BENGEZ, L., JANIGRO, D. & ETHELL, D. W. 2009. Matrix metalloproteinase-7 facilitates immune access to the CNS in experimental autoimmune encephalomyelitis. *BMC Neurosci,* 10**,** 17.

BUSHONG, E. A., MARTONE, M. E., JONES, Y. Z. & ELLISMAN, M. H. 2002. Protoplasmic astrocytes in CA1 stratum radiatum occupy separate anatomical domains. *J Neurosci,* 22**,** 183-92.

BUTTGEREIT, F. & BRAND, M. D. 1995. A hierarchy of ATP-consuming processes in mammalian cells. *Biochemical Journal,* 312**,** 163-167.

CAHOY, J. D., EMERY, B., KAUSHAL, A., FOO, L. C., ZAMANIAN, J. L., CHRISTOPHERSON, K. S., XING, Y., LUBISCHER, J. L., KRIEG, P. A., KRUPENKO, S. A., THOMPSON, W. J. & BARRES, B. A. 2008. A

transcriptome database for astrocytes, neurons, and oligodendrocytes: a new resource for understanding brain development and function. *J Neurosci,* 28**,** 264-78.
CAIAZZO, M., GIANNELLI, S., VALENTE, P., LIGNANI, G., CARISSIMO, A., SESSA, A., COLASANTE, G., BARTOLOMEO, R., MASSIMINO, L., FERRONI, S., SETTEMBRE, C., BENFENATI, F. & BROCCOLI, V. 2015. Direct conversion of fibroblasts into functional astrocytes by defined transcription factors. *Stem Cell Reports,* 4**,** 25-36.
CALFA, G., LI, W., RUTHERFORD, J. M. & POZZO-MILLER, L. 2015. Excitation/inhibition imbalance and impaired synaptic inhibition in hippocampal area CA3 of Mecp2 knockout mice. *Hippocampus,* 25**,** 159-68.
CALFA, G., PERCY, A. K. & POZZO-MILLER, L. 2011. Experimental models of Rett syndrome based on Mecp2 dysfunction. *Exp Biol Med (Maywood),* 236**,** 3-19.
CALI, C., BAGHABRA, J., BOGES, D. J., HOLST, G. R., KRESHUK, A., HAMPRECHT, F. A., SRINIVASAN, M., LEHVASLAIHO, H. & MAGISTRETTI, P. J. 2016. Three-dimensional immersive virtual reality for studying cellular compartments in 3D models from EM preparations of neural tissues. *J Comp Neurol,* 524**,** 23-38.
CAREY, M. B. & MATSUMOTO, S. G. 1999. Spontaneous calcium transients are required for neuronal differentiation of murine neural crest. *Dev Biol,* 215**,** 298-313.
CARGILL, R., KOHAMA, S. G., STRUVE, J., SU, W., BANINE, F., WITKOWSKI, E., BACK, S. A. & SHERMAN, L. S. 2012. Astrocytes in aged nonhuman primate brain gray matter synthesize excess hyaluronan. *Neurobiology of Aging,* 33**,** 830.e13-830.e24.
CARMELI, E., BACHAR, A. & BEIKER, R. 2011. Expression of global oxidative stress and matrix metalloproteinases is associated with rett syndrome. *Neurochemical Journal,* 5**,** 141-145.
CARTER, J. C., LANHAM, D. C., PHAM, D., BIBAT, G., NAIDU, S. & KAUFMANN, W. E. 2008. Selective cerebral volume reduction in Rett syndrome: a multiple-approach MR imaging study. *AJNR. American journal of neuroradiology,* 29**,** 436-441.
CASSIMERIS, L. & SPITTLE, C. 2001. Regulation of microtubule-associated proteins. *Int Rev Cytol,* 210**,** 163-226.
CASTRO, J., GARCIA, R. I., KWOK, S., BANERJEE, A., PETRAVICZ, J., WOODSON, J., MELLIOS, N., TROPEA, D. & SUR, M. 2014. Functional recovery with recombinant human IGF1 treatment in a mouse model of Rett Syndrome. *Proc Natl Acad Sci U S A,* 111**,** 9941-6.
CHAMBERS, S. M., FASANO, C. A., PAPAPETROU, E. P., TOMISHIMA, M., SADELAIN, M. & STUDER, L. 2009. Highly efficient neural conversion of human ES and iPS cells by dual inhibition of SMAD signaling. *Nat Biotechnol,* 27**,** 275-80.
CHAMBERS, S. M., QI, Y., MICA, Y., LEE, G., ZHANG, X. J., NIU, L., BILSLAND, J., CAO, L., STEVENS, E., WHITING, P., SHI, S. H. & STUDER, L. 2012. Combined small-molecule inhibition accelerates developmental timing and converts human pluripotent stem cells into nociceptors. *Nat Biotechnol,* 30**,** 715-20.
CHANDRASEKARAN, A., AVCI, H. X., OCHALEK, A., RÖSINGH, L. N., MOLNÁR, K., LÁSZLÓ, L., BELLÁK, T., TÉGLÁSI, A., PESTI, K., MIKE, A., PHANTHONG, P., BÍRÓ, O., HALL, V., KITIYANANT, N., KRAUSE, K.-H., KOBOLÁK, J. & DINNYÉS, A. 2017. Comparison of 2D and 3D neural induction methods for the generation of neural progenitor cells from human induced pluripotent stem cells. *Stem Cell Research,* 25**,** 139-151.
CHANG, Q., KHARE, G., DANI, V., NELSON, S. & JAENISCH, R. 2006. The disease progression of Mecp2 mutant mice is affected by the level of BDNF expression. *Neuron,* 49**,** 341-8.
CHAO, H. T., CHEN, H., SAMACO, R. C., XUE, M., CHAHROUR, M., YOO, J., NEUL, J. L., GONG, S., LU, H. C., HEINTZ, N., EKKER, M., RUBENSTEIN, J. L., NOEBELS, J. L., ROSENMUND, C. & ZOGHBI, H. Y. 2010. Dysfunction in GABA signalling mediates autism-like stereotypies and Rett syndrome phenotypes. *Nature,* 468**,** 263-9.
CHAO, H. T., ZOGHBI, H. Y. & ROSENMUND, C. 2007. MeCP2 controls excitatory synaptic strength by regulating glutamatergic synapse number. *Neuron,* 56**,** 58-65.

CHAPLEAU, C. A., CALFA, G. D., LANE, M. C., ALBERTSON, A. J., LARIMORE, J. L., KUDO, S., ARMSTRONG, D. L., PERCY, A. K. & POZZO-MILLER, L. 2009. Dendritic spine pathologies in hippocampal pyramidal neurons from Rett syndrome brain and after expression of Rett-associated MECP2 mutations. *Neurobiol Dis,* 35**,** 219-33.

CHARLES, A. C., MERRILL, J. E., DIRKSEN, E. R. & SANDERSON, M. J. 1991. Intercellular signaling in glial cells: calcium waves and oscillations in response to mechanical stimulation and glutamate. *Neuron,* 6**,** 983-92.

CHAUDHRY, F. A., LEHRE, K. P., VAN LOOKEREN CAMPAGNE, M., OTTERSEN, O. P., DANBOLT, N. C. & STORM-MATHISEN, J. 1995. Glutamate transporters in glial plasma membranes: highly differentiated localizations revealed by quantitative ultrastructural immunocytochemistry. *Neuron,* 15**,** 711-20.

CHEN, R. Z., AKBARIAN, S., TUDOR, M. & JAENISCH, R. 2001a. Deficiency of methyl-CpG binding protein-2 in CNS neurons results in a Rett-like phenotype in mice. *Nat Genet,* 27**,** 327-31.

CHEN, W. G., CHANG, Q., LIN, Y., MEISSNER, A., WEST, A. E., GRIFFITH, E. C., JAENISCH, R. & GREENBERG, M. E. 2003. Derepression of BDNF transcription involves calcium-dependent phosphorylation of MeCP2. *Science,* 302**,** 885-9.

CHEN, Y., QIN, C., HUANG, J., TANG, X., LIU, C., HUANG, K., XU, J., GUO, G., TONG, A. & ZHOU, L. 2020. The role of astrocytes in oxidative stress of central nervous system: A mixed blessing. *Cell Proliferation,* 53**,** e12781.

CHEN, Y., VARTIAINEN, N. E., YING, W., CHAN, P. H., KOISTINAHO, J. & SWANSON, R. A. 2001b. Astrocytes protect neurons from nitric oxide toxicity by a glutathione-dependent mechanism. *J Neurochem,* 77**,** 1601-10.

CHERRY, J. D., OLSCHOWKA, J. A. & O'BANION, M. K. 2014. Neuroinflammation and M2 microglia: the good, the bad, and the inflamed. *Journal of Neuroinflammation,* 11**,** 98.

CHEUNG, A. Y., HORVATH, L. M., GRAFODATSKAYA, D., PASCERI, P., WEKSBERG, R., HOTTA, A., CARREL, L. & ELLIS, J. 2011. Isolation of MECP2-null Rett Syndrome patient hiPS cells and isogenic controls through X-chromosome inactivation. *Hum Mol Genet,* 20**,** 2103-15.

CHEVER, O., DJUKIC, B., MCCARTHY, K. D. & AMZICA, F. 2010. Implication of Kir4.1 channel in excess potassium clearance: an in vivo study on anesthetized glial-conditional Kir4.1 knock-out mice. *J Neurosci,* 30**,** 15769-77.

CHO, Y. & BANNAI, S. 1990. Uptake of glutamate and cysteine in C-6 glioma cells and in cultured astrocytes. *J Neurochem,* 55**,** 2091-7.

CHRISTOPHERSON, K. S., ULLIAN, E. M., STOKES, C. C., MULLOWNEY, C. E., HELL, J. W., AGAH, A., LAWLER, J., MOSHER, D. F., BORNSTEIN, P. & BARRES, B. A. 2005. Thrombospondins are astrocyte-secreted proteins that promote CNS synaptogenesis. *Cell,* 120**,** 421-33.

CHUNG, W.-S., CLARKE, L. E., WANG, G. X., STAFFORD, B. K., SHER, A., CHAKRABORTY, C., JOUNG, J., FOO, L. C., THOMPSON, A., CHEN, C., SMITH, S. J. & BARRES, B. A. 2013. Astrocytes mediate synapse elimination through MEGF10 and MERTK pathways. *Nature,* 504**,** 394-400.

CLARKE, A. J. & ABDALA SHEIKH, A. P. 2018. A perspective on "cure" for Rett syndrome. *Orphanet Journal of Rare Diseases,* 13**,** 44.

CLARKE, L. E. & BARRES, B. A. 2013. Emerging roles of astrocytes in neural circuit development. *Nat Rev Neurosci,* 14**,** 311-21.

COLANTUONI, C., JEON, O. H., HYDER, K., CHENCHIK, A., KHIMANI, A. H., NARAYANAN, V., HOFFMAN, E. P., KAUFMANN, W. E., NAIDU, S. & PEVSNER, J. 2001. Gene expression profiling in postmortem Rett Syndrome brain: differential gene expression and patient classification. *Neurobiol Dis,* 8**,** 847-65.

CORNELL-BELL, A. H., FINKBEINER, S. M., COOPER, M. S. & SMITH, S. J. 1990. Glutamate induces calcium waves in cultured astrocytes: long-range glial signaling. *Science,* 247**,** 470-3.

COSTALES, J. & KOLEVZON, A. 2016. The therapeutic potential of insulin-like growth factor-1 in central nervous system disorders. *Neuroscience & Biobehavioral Reviews,* 63**,** 207-222.

CRAWFORD, T. Q. & ROELINK, H. 2007. The notch response inhibitor DAPT enhances neuronal differentiation in embryonic stem cell-derived embryoid bodies independently of sonic hedgehog signaling. *Dev Dyn,* 236**,** 886-92.
CUMMINGS, J., FELDMAN, H. H. & SCHELTENS, P. 2019. The “rights” of precision drug development for Alzheimer’s disease. *Alzheimer's Research & Therapy,* 11**,** 76.
DALLÉRAC, G., CHEVER, O. & ROUACH, N. 2013. How do astrocytes shape synaptic transmission? Insights from electrophysiology. *Front Cell Neurosci,* 7**,** 159.
DALLÉRAC, G., ZAPATA, J. & ROUACH, N. 2018. Versatile control of synaptic circuits by astrocytes: where, when and how? *Nat Rev Neurosci,* 19**,** 729-743.
DANI, J. W., CHERNJAVSKY, A. & SMITH, S. J. 1992. Neuronal activity triggers calcium waves in hippocampal astrocyte networks. *Neuron,* 8**,** 429-40.
DANI, V. S., CHANG, Q., MAFFEI, A., TURRIGIANO, G. G., JAENISCH, R. & NELSON, S. B. 2005. Reduced cortical activity due to a shift in the balance between excitation and inhibition in a mouse model of Rett syndrome. *Proc Natl Acad Sci U S A,* 102**,** 12560-5.
DEITMER, J. W., THEPARAMBIL, S. M., RUMINOT, I., NOOR, S. I. & BECKER, H. M. 2019. Energy Dynamics in the Brain: Contributions of Astrocytes to Metabolism and pH Homeostasis. *Frontiers in neuroscience,* 13**,** 1301-1301.
DENEEN, B., HO, R., LUKASZEWICZ, A., HOCHSTIM, C. J., GRONOSTAJSKI, R. M. & ANDERSON, D. J. 2006. The transcription factor NFIA controls the onset of gliogenesis in the developing spinal cord. *Neuron,* 52**,** 953-68.
DEROSA, B. A., VAN BAAREN, J. M., DUBEY, G. K., LEE, J. M., CUCCARO, M. L., VANCE, J. M., PERICAK-VANCE, M. A. & DYKXHOORN, D. M. 2012. Derivation of autism spectrum disorder-specific induced pluripotent stem cells from peripheral blood mononuclear cells. *Neurosci Lett,* 516**,** 9-14.
DESCALZI, G., GAO, V., STEINMAN, M. Q., SUZUKI, A. & ALBERINI, C. M. 2019. Lactate from astrocytes fuels learning-induced mRNA translation in excitatory and inhibitory neurons. *Communications Biology,* 2**,** 247.
DIAZ-CASTRO, B., GANGWANI, M. R., YU, X., COPPOLA, G. & KHAKH, B. S. 2019. Astrocyte molecular signatures in Huntington’s disease. *Science Translational Medicine,* 11**,** eaaw8546.
DIETSCHY, J. M. 2009. Central nervous system: cholesterol turnover, brain development and neurodegeneration. *Biol Chem,* 390**,** 287-93.
DJUKIC, B., CASPER, K. B., PHILPOT, B. D., CHIN, L. S. & MCCARTHY, K. D. 2007. Conditional knock-out of Kir4.1 leads to glial membrane depolarization, inhibition of potassium and glutamate uptake, and enhanced short-term synaptic potentiation. *J Neurosci,* 27**,** 11354-65.
DJURIC, U., CHEUNG, A. Y. L., ZHANG, W., MOK, R. S., LAI, W., PIEKNA, A., HENDRY, J. A., ROSS, P. J., PASCERI, P., KIM, D.-S., SALTER, M. W. & ELLIS, J. 2015. MECP2e1 isoform mutation affects the form and function of neurons derived from Rett syndrome patient iPS cells. *Neurobiology of Disease,* 76**,** 37-45.
DOENGI, M., HIRNET, D., COULON, P., PAPE, H.-C., DEITMER, J. W. & LOHR, C. 2009. GABA uptake-dependent Ca²⁺ signaling in developing olfactory bulb astrocytes. *Proceedings of the National Academy of Sciences,* 106**,** 17570.
DONATO, R. 2001. S100: a multigenic family of calcium-modulated proteins of the EF-hand type with intracellular and extracellular functional roles. *The International Journal of Biochemistry & Cell Biology,* 33**,** 637-668.
DONG, Q., LIU, Q., LI, R., WANG, A., BU, Q., WANG, K. H. & CHANG, Q. 2018. Mechanism and consequence of abnormal calcium homeostasis in Rett syndrome astrocytes. *Elife,* 7.
DONG, X. X., WANG, Y. & QIN, Z. H. 2009. Molecular mechanisms of excitotoxicity and their relevance to pathogenesis of neurodegenerative diseases. *Acta Pharmacol Sin,* 30**,** 379-87.
DOVEY, H. F., JOHN, V., ANDERSON, J. P., CHEN, L. Z., DE SAINT ANDRIEU, P., FANG, L. Y., FREEDMAN, S. B., FOLMER, B., GOLDBACH, E., HOLSZTYNSKA, E. J., HU, K. L., JOHNSON-WOOD, K. L., KENNEDY, S. L., KHOLODENKO, D., KNOPS, J. E., LATIMER, L. H., LEE, M., LIAO, Z.,

LIEBERBURG, I. M., MOTTER, R. N., MUTTER, L. C., NIETZ, J., QUINN, K. P., SACCHI, K. L., SEUBERT, P. A., SHOPP, G. M., THORSETT, E. D., TUNG, J. S., WU, J., YANG, S., YIN, C. T., SCHENK, D. B., MAY, P. C., ALTSTIEL, L. D., BENDER, M. H., BOGGS, L. N., BRITTON, T. C., CLEMENS, J. C., CZILLI, D. L., DIECKMAN-MCGINTY, D. K., DROSTE, J. J., FUSON, K. S., GITTER, B. D., HYSLOP, P. A., JOHNSTONE, E. M., LI, W. Y., LITTLE, S. P., MABRY, T. E., MILLER, F. D. & AUDIA, J. E. 2001. Functional gamma-secretase inhibitors reduce beta-amyloid peptide levels in brain. *J Neurochem,* 76**,** 173-81.

DRÁBEROVÁ, E., DEL VALLE, L., GORDON, J., MARKOVÁ, V., SMEJKALOVÁ, B., BERTRAND, L., DE CHADARÉVIAN, J. P., AGAMANOLIS, D. P., LEGIDO, A., KHALILI, K., DRÁBER, P. & KATSETOS, C. D. 2008. Class III beta-tubulin is constitutively coexpressed with glial fibrillary acidic protein and nestin in midgestational human fetal astrocytes: implications for phenotypic identity. *J Neuropathol Exp Neurol,* 67**,** 341-54.

DU, F., NGUYEN, M. V., KARTEN, A., FELICE, C. A., MANDEL, G. & BALLAS, N. 2016. Acute and crucial requirement for MeCP2 function upon transition from early to late adult stages of brain maturation. *Hum Mol Genet,* 25**,** 1690-702.

EDEN, E., NAVON, R., STEINFELD, I., LIPSON, D. & YAKHINI, Z. 2009. GOrilla: a tool for discovery and visualization of enriched GO terms in ranked gene lists. *BMC Bioinformatics,* 10**,** 48.

EHRHART, F., COORT, S. L. M., CIRILLO, E., SMEETS, E., EVELO, C. T. & CURFS, L. M. G. 2016. Rett syndrome – biological pathways leading from MECP2 to disorder phenotypes. *Orphanet Journal of Rare Diseases,* 11**,** 158.

ELLIS, P., FAGAN, B. M., MAGNESS, S. T., HUTTON, S., TARANOVA, O., HAYASHI, S., MCMAHON, A., RAO, M. & PEVNY, L. 2004. SOX2, a persistent marker for multipotential neural stem cells derived from embryonic stem cells, the embryo or the adult. *Dev Neurosci,* 26**,** 148-65.

ENG, L. F., GHIRNIKAR, R. S. & LEE, Y. L. 2000. Glial fibrillary acidic protein: GFAP-thirty-one years (1969-2000). *Neurochem Res,* 25**,** 1439-51.

ERBSLOH, F., BERNSMEIER, A. & HILLESHEIM, H. 1958. [The glucose consumption of the brain & its dependence on the liver]. *Arch Psychiatr Nervenkr Z Gesamte Neurol Psychiatr,* 196**,** 611-26.

EROGLU, C., ALLEN, N. J., SUSMAN, M. W., O'ROURKE, N. A., PARK, C. Y., OZKAN, E., CHAKRABORTY, C., MULINYAWE, S. B., ANNIS, D. S., HUBERMAN, A. D., GREEN, E. M., LAWLER, J., DOLMETSCH, R., GARCIA, K. C., SMITH, S. J., LUO, Z. D., ROSENTHAL, A., MOSHER, D. F. & BARRES, B. A. 2009. Gabapentin receptor alpha2delta-1 is a neuronal thrombospondin receptor responsible for excitatory CNS synaptogenesis. *Cell,* 139**,** 380-92.

ETHELL, I. M. & YAMAGUCHI, Y. 1999. Cell surface heparan sulfate proteoglycan syndecan-2 induces the maturation of dendritic spines in rat hippocampal neurons. *J Cell Biol,* 144**,** 575-86.

FABIO, R. A., COLOMBO, B., RUSSO, S., COGLIATI, F., MASCIADRI, M., FOGLIA, S., ANTONIETTI, A. & TAVIAN, D. 2014. Recent insights into genotype-phenotype relationships in patients with Rett syndrome using a fine grain scale. *Res Dev Disabil,* 35**,** 2976-86.

FALCONER, D. S. 1951. Two new mutants, 'trembler' and 'reeler', with neurological actions in the house mouse (Mus musculus L.). *J Genet,* 50**,** 192-201.

FAN, G., MARTINOWICH, K., CHIN, M. H., HE, F., FOUSE, S. D., HUTNICK, L., HATTORI, D., GE, W., SHEN, Y., WU, H., TEN HOEVE, J., SHUAI, K. & SUN, Y. E. 2005. DNA methylation controls the timing of astrogliogenesis through regulation of JAK-STAT signaling. *Development,* 132**,** 3345-56.

FANG, A., LI, D., HAO, Z., WANG, L., PAN, B., GAO, L., QU, X. & HE, J. 2019. Effects of astrocyte on neuronal outgrowth in a layered 3D structure. *BioMedical Engineering OnLine,* 18**,** 74.

FARINA, C., ALOISI, F. & MEINL, E. 2007. Astrocytes are active players in cerebral innate immunity. *Trends Immunol,* 28**,** 138-45.

FATATIS, A. & RUSSELL, J. T. 1992. Spontaneous changes in intracellular calcium concentration in type I astrocytes from rat cerebral cortex in primary culture. *Glia,* 5**,** 95-104.

FAULKNER, J. R., HERRMANN, J. E., WOO, M. J., TANSEY, K. E., DOAN, N. B. & SOFRONIEW, M. V. 2004. Reactive astrocytes protect tissue and preserve function after spinal cord injury. *J Neurosci,* 24**,** 2143-55.

FAWCETT, J. W. & ASHER, R. A. 1999. The glial scar and central nervous system repair. *Brain Res Bull,* 49**,** 377-91.

FERRER-FERRER, M. & DITYATEV, A. 2018. Shaping Synapses by the Neural Extracellular Matrix. *Front Neuroanat,* 12**,** 40.

FERRIS, H. A., PERRY, R. J., MOREIRA, G. V., SHULMAN, G. I., HORTON, J. D. & KAHN, C. R. 2017. Loss of astrocyte cholesterol synthesis disrupts neuronal function and alters whole-body metabolism. *Proc Natl Acad Sci U S A,* 114**,** 1189-1194.

FILOSA, J. A., MORRISON, H. W., IDDINGS, J. A., DU, W. & KIM, K. J. 2016. Beyond neurovascular coupling, role of astrocytes in the regulation of vascular tone. *Neuroscience,* 323**,** 96-109.

FILOSA, S., PECORELLI, A., D'ESPOSITO, M., VALACCHI, G. & HAJEK, J. 2015. Exploring the possible link between MeCP2 and oxidative stress in Rett syndrome. *Free Radic Biol Med,* 88**,** 81-90.

FINEBERG, N. A., HADDAD, P. M., CARPENTER, L., GANNON, B., SHARPE, R., YOUNG, A. H., JOYCE, E., ROWE, J., WELLSTED, D., NUTT, D. J. & SAHAKIAN, B. J. 2013. The size, burden and cost of disorders of the brain in the UK. *J Psychopharmacol,* 27**,** 761-70.

FOLEY, K. R., DOWNS, J., BEBBINGTON, A., JACOBY, P., GIRDLER, S., KAUFMANN, W. E. & LEONARD, H. 2011. Change in gross motor abilities of girls and women with rett syndrome over a 3- to 4-year period. *J Child Neurol,* 26**,** 1237-45.

FOO, L. C., ALLEN, N. J., BUSHONG, E. A., VENTURA, P. B., CHUNG, W. S., ZHOU, L., CAHOY, J. D., DANEMAN, R., ZONG, H., ELLISMAN, M. H. & BARRES, B. A. 2011. Development of a method for the purification and culture of rodent astrocytes. *Neuron,* 71**,** 799-811.

FRANKEL, E., DODSON, J., SHARIFI, M., PILLAI, R., RAMSEY, K., GUPTA, R., BRZEZINSKI, M., VENUGOPAL, P., LLACI, L., GERALD, B., MILLS, G., BELNAP, N., SANCHEZ-CASTILLO, M., BALAK, C. D., CLAASEN, A. M., SZELINGER, S., JEPSEN, W. M., SINIARD, A. L., RICHHOLT, R., DE BOTH, M., NAYMIK, M., SCHRAUWEN, I., PIRAS, I. S., CRAIG, D. W., HUENTELMAN, M. J., NARAYANAN, V. & RANGASAMY, S. 2020. Complex genetic network underlying the convergent of Rett Syndrome like (RTT-L) phenotype in neurodevelopmental disorders. *bioRxiv***,** 2020.01.11.899658.

FREMEAU, R. T., JR., VOGLMAIER, S., SEAL, R. P. & EDWARDS, R. H. 2004. VGLUTs define subsets of excitatory neurons and suggest novel roles for glutamate. *Trends Neurosci,* 27**,** 98-103.

FU, C., ARMSTRONG, D., MARSH, E., LIEBERMAN, D., MOTIL, K., WITT, R., STANDRIDGE, S., NUES, P., LANE, J., DINKEL, T., COENRAADS, M., VON HEHN, J., JONES, M., HALE, K., SUTER, B., GLAZE, D., NEUL, J., PERCY, A. & BENKE, T. 2020. Consensus guidelines on managing Rett syndrome across the lifespan. *BMJ Paediatrics Open,* 4**,** e000717.

FUJITA, T., CHEN, M. J., LI, B., SMITH, N. A., PENG, W., SUN, W., TONER, M. J., KRESS, B. T., WANG, L., BENRAISS, A., TAKANO, T., WANG, S. & NEDERGAARD, M. 2014. Neuronal Transgene Expression in Dominant-Negative SNARE Mice. *The Journal of Neuroscience,* 34**,** 16594.

GAO, H., BU, Y., WU, Q., WANG, X., CHANG, N., LEI, L., CHEN, S., LIU, D., ZHU, X., HU, K. & XIONG, J. W. 2015. Mecp2 regulates neural cell differentiation by suppressing the Id1 to Her2 axis in zebrafish. *J Cell Sci,* 128**,** 2340-50.

GARCIA, O., TORRES, M., HELGUERA, P., COSKUN, P. & BUSCIGLIO, J. 2010. A role for thrombospondin-1 deficits in astrocyte-mediated spine and synaptic pathology in Down's syndrome. *PLoS One,* 5**,** e14200.

GARTLER, S. M., DYER, K. A., GRAVES, J. A. & ROCCHI, M. 1985. A two step model for mammalian X-chromosome inactivation. *Prog Clin Biol Res,* 198**,** 223-35.

GELING, A., STEINER, H., WILLEM, M., BALLY-CUIF, L. & HAASS, C. 2002. A gamma-secretase inhibitor blocks Notch signaling in vivo and causes a severe neurogenic phenotype in zebrafish. *EMBO Rep,* 3**,** 688-94.

GENTRY, M. S., GUINOVART, J. J., MINASSIAN, B. A., ROACH, P. J. & SERRATOSA, J. M. 2018. Lafora disease offers a unique window into neuronal glycogen metabolism. *J Biol Chem,* 293**,** 7117-7125.

GHOSH, A. & GREENBERG, M. E. 1995. Distinct roles for bFGF and NT-3 in the regulation of cortical neurogenesis. *Neuron,* 15**,** 89-103.

GIRGRAH, N., LETARTE, M., BECKER, L. E., CRUZ, T. F., THERIAULT, E. & MOSCARELLO, M. A. 1991. Localization of the CD44 glycoprotein to fibrous astrocytes in normal white matter and to reactive astrocytes in active lesions in multiple sclerosis. *J Neuropathol Exp Neurol,* 50**,** 779-92.

GOGLIOTTI, R. G., FISHER, N. M., STANSLEY, B. J., JONES, C. K., LINDSLEY, C. W., CONN, P. J. & NISWENDER, C. M. 2018. Total RNA Sequencing of Rett Syndrome Autopsy Samples Identifies the M(4) Muscarinic Receptor as a Novel Therapeutic Target. *J Pharmacol Exp Ther,* 365**,** 291-300.

GOLDMAN, S. & TEMUDO, T. 2012. Hand stereotypies distinguish Rett syndrome from autism disorder. *Mov Disord,* 27**,** 1060-2.

GOMES, A. R., FERNANDES, T. G., VAZ, S. H., SILVA, T. P., BEKMAN, E. P., XAPELLI, S., DUARTE, S., GHAZVINI, M., GRIBNAU, J., MUOTRI, A. R., TRUJILLO, C. A., SEBASTIÃO, A. M., CABRAL, J. M. S. & DIOGO, M. M. 2020. Modeling Rett Syndrome With Human Patient-Specific Forebrain Organoids. *Frontiers in Cell and Developmental Biology,* 8.

GÖTZ, M., STOYKOVA, A. & GRUSS, P. 1998. Pax6 controls radial glia differentiation in the cerebral cortex. *Neuron,* 21**,** 1031-44.

GRAHAM, V., KHUDYAKOV, J., ELLIS, P. & PEVNY, L. 2003. SOX2 Functions to Maintain Neural Progenitor Identity. *Neuron,* 39**,** 749-765.

GRAY, M. 2019. Astrocytes in Huntington's Disease. *Adv Exp Med Biol,* 1175**,** 355-381.

GUTTENPLAN, K. A., WEIGEL, M. K., ADLER, D. I., COUTHOUIS, J., LIDDELOW, S. A., GITLER, A. D. & BARRES, B. A. 2020. Knockout of reactive astrocyte activating factors slows disease progression in an ALS mouse model. *Nature Communications,* 11**,** 3753.

GUY, J., GAN, J., SELFRIDGE, J., COBB, S. & BIRD, A. 2007. Reversal of neurological defects in a mouse model of Rett syndrome. *Science,* 315**,** 1143-7.

HAAS, R. H. 1988. The history and challenge of Rett syndrome. *J Child Neurol,* 3 Suppl**,** S3-5.

HAGBERG, B., AICARDI, J., DIAS, K. & RAMOS, O. 1983. A progressive syndrome of autism, dementia, ataxia, and loss of purposeful hand use in girls: Rett's syndrome: report of 35 cases. *Ann Neurol,* 14**,** 471-9.

HAMBERGER, A., GILLBERG, C., PALM, A. & HAGBERG, B. 1992. Elevated CSF Glutamate in Rett Syndrome. *Neuropediatrics,* 23**,** 212-213.

HAMM, J. P., PETERKA, D. S., GOGOS, J. A. & YUSTE, R. 2017. Altered Cortical Ensembles in Mouse Models of Schizophrenia. *Neuron,* 94**,** 153-167.e8.

HAN, X., CHEN, M., WANG, F., WINDREM, M., WANG, S., SHANZ, S., XU, Q., OBERHEIM, N. A., BEKAR, L., BETSTADT, S., SILVA, A. J., TAKANO, T., GOLDMAN, S. A. & NEDERGAARD, M. 2013. Forebrain engraftment by human glial progenitor cells enhances synaptic plasticity and learning in adult mice. *Cell Stem Cell,* 12**,** 342-53.

HANSEN, J. C., WEXLER, B. B., ROGERS, D. J., HITE, K. C., PANCHENKO, T., AJITH, S. & BLACK, B. E. 2011. DNA binding restricts the intrinsic conformational flexibility of methyl CpG binding protein 2 (MeCP2). *J Biol Chem,* 286**,** 18938-48.

HASEL, P., DANDO, O., JIWAJI, Z., BAXTER, P., TODD, A. C., HERON, S., MÁRKUS, N. M., MCQUEEN, J., HAMPTON, D. W., TORVELL, M., TIWARI, S. S., MCKAY, S., ERASO-PICHOT, A., ZORZANO, A., MASGRAU, R., GALEA, E., CHANDRAN, S., WYLLIE, D. J. A., SIMPSON, T. I. & HARDINGHAM, G. E. 2017. Neurons and neuronal activity control gene expression in astrocytes to regulate their development and metabolism. *Nature Communications,* 8**,** 15132.

HAWKINS, J. & AHMAD, S. 2016. Why Neurons Have Thousands of Synapses, a Theory of Sequence Memory in Neocortex. *Frontiers in Neural Circuits,* 10.

HECKMAN, L. D., CHAHROUR, M. H. & ZOGHBI, H. Y. 2014. Rett-causing mutations reveal two domains critical for MeCP2 function and for toxicity in MECP2 duplication syndrome mice. *Elife,* 3.

HEDEGAARD, A., MONZÓN-SANDOVAL, J., NEWEY, S. E., WHITELEY, E. S., WEBBER, C. & AKERMAN, C. J. 2020. Pro-maturational Effects of Human iPSC-Derived Cortical Astrocytes upon iPSC-Derived Cortical Neurons. *Stem Cell Reports,* 15**,** 38-51.

HEITHOFF, B. P., GEORGE, K. K., PHARES, A. N., ZUIDHOEK, I. A., MUNOZ-BALLESTER, C. & ROBEL, S. 2020. Astrocytes are necessary for blood-brain barrier maintenance in the adult mouse brain. *Glia*.

HERCULANO-HOUZEL, S. 2014. The glia/neuron ratio: how it varies uniformly across brain structures and species and what that means for brain physiology and evolution. *Glia,* 62**,** 1377-91.

HERRERO-NAVARRO, Á., PUCHE-AROCA, L., MORENO-JUAN, V., SEMPERE-FERRÀNDEZ, A., ESPINOSA, A., SUSÍN, R., TORRES-MASJOAN, L., LEYVA-DÍAZ, E., KAROW, M., FIGUERES-OÑATE, M., LÓPEZ-MASCARAQUE, L., LÓPEZ-ATALAYA, J. P., BERNINGER, B. & LÓPEZ-BENDITO, G. 2020. Astrocytes and neurons share brain region-specific transcriptional signatures. *bioRxiv***,** 2020.04.21.038737.

HILL, E. J., JIMÉNEZ-GONZÁLEZ, C., TARCZYLUK, M., NAGEL, D. A., COLEMAN, M. D. & PARRI, H. R. 2012. NT2 derived neuronal and astrocytic network signalling. *PLoS One,* 7**,** e36098.

HIRABAYASHI, Y., SUZKI, N., TSUBOI, M., ENDO, T. A., TOYODA, T., SHINGA, J., KOSEKI, H., VIDAL, M. & GOTOH, Y. 2009. Polycomb limits the neurogenic competence of neural precursor cells to promote astrogenic fate transition. *Neuron,* 63**,** 600-13.

HIRASE, H., QIAN, L., BARTHO, P. & BUZSAKI, G. 2004. Calcium dynamics of cortical astrocytic networks in vivo. *PLoS Biol,* 2**,** E96.

HIROTA, H., KIYAMA, H., KISHIMOTO, T. & TAGA, T. 1996. Accelerated Nerve Regeneration in Mice by upregulated expression of interleukin (IL) 6 and IL-6 receptor after trauma. *Journal of Experimental Medicine,* 183**,** 2627-2634.

HODGKIN, A. L. & HUXLEY, A. F. 1939. Action Potentials Recorded from Inside a Nerve Fibre. *Nature,* 144**,** 710-711.

HODGKIN, A. L. & HUXLEY, A. F. 1952. A quantitative description of membrane current and its application to conduction and excitation in nerve. *J Physiol,* 117**,** 500-44.

HODGKIN, A. L., HUXLEY, A. F. & KATZ, B. 1952. Measurement of current-voltage relations in the membrane of the giant axon of Loligo. *J Physiol,* 116**,** 424-48.

HOLT, L. M., HERNANDEZ, R. D., PACHECO, N. L., TORRES CEJA, B., HOSSAIN, M. & OLSEN, M. L. 2019. Astrocyte morphogenesis is dependent on BDNF signaling via astrocytic TrkB.T1. *Elife,* 8.

HUANG, L.-K., CHAO, S.-P. & HU, C.-J. 2020. Clinical trials of new drugs for Alzheimer disease. *Journal of Biomedical Science,* 27**,** 18.

HUGHES, S. M., LILLIEN, L. E., RAFF, M. C., ROHRER, H. & SENDTNER, M. 1988. Ciliary neurotrophic factor induces type-2 astrocyte differentiation in culture. *Nature,* 335**,** 70-73.

HULSEN, T., DE VLIEG, J. & ALKEMA, W. 2008. BioVenn – a web application for the comparison and visualization of biological lists using area-proportional Venn diagrams. *BMC Genomics,* 9**,** 488.

ISHIBASHI, M., ANG, S. L., SHIOTA, K., NAKANISHI, S., KAGEYAMA, R. & GUILLEMOT, F. 1995. Targeted disruption of mammalian hairy and Enhancer of split homolog-1 (HES-1) leads to up-regulation of neural helix-loop-helix factors, premature neurogenesis, and severe neural tube defects. *Genes Dev,* 9**,** 3136-48.

ISRAEL, J. M., SCHIPKE, C. G., OHLEMEYER, C., THEODOSIS, D. T. & KETTENMANN, H. 2003. GABAA receptor-expressing astrocytes in the supraoptic nucleus lack glutamate uptake and receptor currents. *Glia,* 44**,** 102-10.

ITANO, N., SAWAI, T., YOSHIDA, M., LENAS, P., YAMADA, Y., IMAGAWA, M., SHINOMURA, T., HAMAGUCHI, M., YOSHIDA, Y., OHNUKI, Y., MIYAUCHI, S., SPICER, A. P., MCDONALD, J. A. & KIMATA, K. 1999. Three Isoforms of Mammalian Hyaluronan Synthases Have Distinct Enzymatic Properties*. *Journal of Biological Chemistry,* 274**,** 25085-25092.

JANKNECHT, R., WELLS, N. J. & HUNTER, T. 1998. TGF-beta-stimulated cooperation of smad proteins with the coactivators CBP/p300. *Genes Dev,* 12**,** 2114-9.
JELLINGER, K., ARMSTRONG, D., ZOGHBI, H. Y. & PERCY, A. K. 1988. Neuropathology of Rett syndrome. *Acta Neuropathol,* 76**,** 142-58.
JIN, X.-R., CHEN, X.-S. & XIAO, L. 2017. MeCP2 Deficiency in Neuroglia: New Progress in the Pathogenesis of Rett Syndrome. *Frontiers in Molecular Neuroscience,* 10.
JONES, E. V., BERNARDINELLI, Y., TSE, Y. C., CHIERZI, S., WONG, T. P. & MURAI, K. K. 2011. Astrocytes control glutamate receptor levels at developing synapses through SPARC-beta-integrin interactions. *J Neurosci,* 31**,** 4154-65.
JONES, P. L., VEENSTRA, G. J., WADE, P. A., VERMAAK, D., KASS, S. U., LANDSBERGER, N., STROUBOULIS, J. & WOLFFE, A. P. 1998. Methylated DNA and MeCP2 recruit histone deacetylase to repress transcription. *Nat Genet,* 19**,** 187-91.
JONES, S. M., HOFMANN, A. D., LIEBER, J. L. & RIBERA, A. B. 1995. Overexpression of potassium channel RNA: in vivo development rescues neurons from suppression of morphological differentiation in vitro. *J Neurosci,* 15**,** 2867-74.
JONES, S. R., CARLEY, S. & HARRISON, M. 2003. An introduction to power and sample size estimation. *Emergency Medicine Journal,* 20**,** 453.
JOURDAIN, P., BERGERSEN, L. H., BHAUKAURALLY, K., BEZZI, P., SANTELLO, M., DOMERCQ, M., MATUTE, C., TONELLO, F., GUNDERSEN, V. & VOLTERRA, A. 2007. Glutamate exocytosis from astrocytes controls synaptic strength. *Nat Neurosci,* 10**,** 331-9.
KADAM, S. D., SULLIVAN, B. J., GOYAL, A., BLUE, M. E. & SMITH-HICKS, C. 2019. Rett Syndrome and CDKL5 Deficiency Disorder: From Bench to Clinic. *Int J Mol Sci,* 20.
KAGEYAMA, R. & OHTSUKA, T. 1999. The Notch-Hes pathway in mammalian neural development. *Cell Res,* 9**,** 179-88.
KAHANOVITCH, U., PATTERSON, K. C., HERNANDEZ, R. & OLSEN, M. L. 2019. Glial Dysfunction in MeCP2 Deficiency Models: Implications for Rett Syndrome. *Int J Mol Sci,* 20.
KALSCHEUER, V. M., TAO, J., DONNELLY, A., HOLLWAY, G., SCHWINGER, E., KUBART, S., MENZEL, C., HOELTZENBEIN, M., TOMMERUP, N., EYRE, H., HARBORD, M., HAAN, E., SUTHERLAND, G. R., ROPERS, H. H. & GECZ, J. 2003. Disruption of the serine/threonine kinase 9 gene causes severe X-linked infantile spasms and mental retardation. *Am J Hum Genet,* 72**,** 1401-11.
KANG, J., JIANG, L., GOLDMAN, S. A. & NEDERGAARD, M. 1998. Astrocyte-mediated potentiation of inhibitory synaptic transmission. *Nat Neurosci,* 1**,** 683-92.
KANG, P., LEE, H. K., GLASGOW, S. M., FINLEY, M., DONTI, T., GABER, Z. B., GRAHAM, B. H., FOSTER, A. E., NOVITCH, B. G., GRONOSTAJSKI, R. M. & DENEEN, B. 2012. Sox9 and NFIA coordinate a transcriptional regulatory cascade during the initiation of gliogenesis. *Neuron,* 74**,** 79-94.
KANSKI, R., VAN STRIEN, M. E., VAN TIJN, P. & HOL, E. M. 2014. A star is born: new insights into the mechanism of astrogenesis. *Cellular and Molecular Life Sciences,* 71**,** 433-447.
KERR, B., SOTO, C. J., SAEZ, M., ABRAMS, A., WALZ, K. & YOUNG, J. I. 2012. Transgenic complementation of MeCP2 deficiency: phenotypic rescue of Mecp2-null mice by isoform-specific transgenes. *Eur J Hum Genet,* 20**,** 69-76.
KESSARIS, N., PRINGLE, N. & RICHARDSON, W. D. 2008. Specification of CNS glia from neural stem cells in the embryonic neuroepithelium. *Philos Trans R Soc Lond B Biol Sci,* 363**,** 71-85.
KIM, J.-E., O'SULLIVAN, M. L., SANCHEZ, C. A., HWANG, M., ISRAEL, M. A., BRENNAND, K., DEERINCK, T. J., GOLDSTEIN, L. S. B., GAGE, F. H., ELLISMAN, M. H. & GHOSH, A. 2011. Investigating synapse formation and function using human pluripotent stem cell-derived neurons. *Proceedings of the National Academy of Sciences,* 108**,** 3005-3010.
KLAPPER, S. D., GARG, P., DAGAR, S., LENK, K., GOTTMANN, K. & NIEWEG, K. 2019. Astrocyte lineage cells are essential for functional neuronal differentiation and synapse maturation in human iPSC-derived neural networks. *Glia,* 67**,** 1893-1909.
KRENCIK, R. & ZHANG, S. C. 2011. Directed differentiation of functional astroglial subtypes from human pluripotent stem cells. *Nat Protoc,* 6**,** 1710-7.

KRIAUCIONIS, S. & BIRD, A. 2004. The major form of MeCP2 has a novel N-terminus generated by alternative splicing. *Nucleic Acids Res,* 32**,** 1818-23.
KRISHNARAJ, R., HAASE, F., COOREY, B., LUCA, E. J., WONG, I., BOYLING, A., ELLAWAY, C., CHRISTODOULOU, J. & GOLD, W. A. 2019. Genome-wide transcriptomic and proteomic studies of Rett syndrome mouse models identify common signaling pathways and cellular functions as potential therapeutic targets. *Hum Mutat,* 40**,** 2184-2196.
KUCUKDERELI, H., ALLEN, N. J., LEE, A. T., FENG, A., OZLU, M. I., CONATSER, L. M., CHAKRABORTY, C., WORKMAN, G., WEAVER, M., SAGE, E. H., BARRES, B. A. & EROGLU, C. 2011. Control of excitatory CNS synaptogenesis by astrocyte-secreted proteins Hevin and SPARC. *Proc Natl Acad Sci U S A,* 108**,** E440-9.
LANCASTER, M. A., RENNER, M., MARTIN, C.-A., WENZEL, D., BICKNELL, L. S., HURLES, M. E., HOMFRAY, T., PENNINGER, J. M., JACKSON, A. P. & KNOBLICH, J. A. 2013. Cerebral organoids model human brain development and microcephaly. *Nature,* 501**,** 373-379.
LAPPALAINEN, R. & RIIKONEN, R. S. 1994. Elevated CSF lactate in the Rett syndrome: cause or consequence? *Brain Dev,* 16**,** 399-401.
LARSEN, B. R., STOICA, A. & MACAULAY, N. 2016a. Managing Brain Extracellular K(+) during Neuronal Activity: The Physiological Role of the Na(+)/K(+)-ATPase Subunit Isoforms. *Frontiers in physiology,* 7**,** 141-141.
LARSEN, B. R., STOICA, A. & MACAULAY, N. 2016b. Managing Brain Extracellular K+ during Neuronal Activity: The Physiological Role of the Na+/K+-ATPase Subunit Isoforms. *Frontiers in Physiology,* 7.
LAURVICK, C. L., DE KLERK, N., BOWER, C., CHRISTODOULOU, J., RAVINE, D., ELLAWAY, C., WILLIAMSON, S. & LEONARD, H. 2006. Rett syndrome in Australia: a review of the epidemiology. *J Pediatr,* 148**,** 347-52.
LEE, E. & CHUNG, W. S. 2019. Glial Control of Synapse Number in Healthy and Diseased Brain. *Front Cell Neurosci,* 13**,** 42.
LEE, S., YOON, B.-E., BERGLUND, K., OH, S.-J., PARK, H., SHIN, H.-S., AUGUSTINE, G. J. & LEE, C. J. 2010. Channel-Mediated Tonic GABA Release from Glia. *Science,* 330**,** 790-796.
LENDAHL, U., ZIMMERMAN, L. B. & MCKAY, R. D. G. 1990. CNS stem cells express a new class of intermediate filament protein. *Cell,* 60**,** 585-595.
LEWERENZ, J. & MAHER, P. 2015. Chronic Glutamate Toxicity in Neurodegenerative Diseases—What is the Evidence? *Frontiers in Neuroscience,* 9.
LEWIS, J. D., MEEHAN, R. R., HENZEL, W. J., MAURER-FOGY, I., JEPPESEN, P., KLEIN, F. & BIRD, A. 1992. Purification, sequence, and cellular localization of a novel chromosomal protein that binds to methylated DNA. *Cell,* 69**,** 905-14.
LI, H., ZHONG, X., CHAU, K. F., SANTISTEVAN, N. J., GUO, W., KONG, G., LI, X., KADAKIA, M., MASLIAH, J., CHI, J., JIN, P., ZHANG, J., ZHAO, X. & CHANG, Q. 2014. Cell cycle-linked MeCP2 phosphorylation modulates adult neurogenesis involving the Notch signalling pathway. *Nat Commun,* 5**,** 5601.
LI, X.-Z., BAI, L.-M., YANG, Y.-P., LUO, W.-F., HU, W.-D., CHEN, J.-P., MAO, C.-J. & LIU, C.-F. 2009. Effects of IL-6 secreted from astrocytes on the survival of dopaminergic neurons in lipopolysaccharide-induced inflammation. *Neuroscience Research,* 65**,** 252-258.
LIANG, G. & ZHANG, Y. 2013. Genetic and epigenetic variations in iPSCs: potential causes and implications for application. *Cell stem cell,* 13**,** 149-159.
LIANG, J. S., SHIMOJIMA, K., TAKAYAMA, R., NATSUME, J., SHICHIJI, M., HIRASAWA, K., IMAI, K., OKANISHI, T., MIZUNO, S., OKUMURA, A., SUGAWARA, M., ITO, T., IKEDA, H., TAKAHASHI, Y., OGUNI, H., IMAI, K., OSAWA, M. & YAMAMOTO, T. 2011. CDKL5 alterations lead to early epileptic encephalopathy in both genders. *Epilepsia,* 52**,** 1835-42.
LIDDELOW, S. A., GUTTENPLAN, K. A., CLARKE, L. E., BENNETT, F. C., BOHLEN, C. J., SCHIRMER, L., BENNETT, M. L., MÜNCH, A. E., CHUNG, W.-S., PETERSON, T. C., WILTON, D. K., FROUIN, A., NAPIER, B. A., PANICKER, N., KUMAR, M., BUCKWALTER, M. S., ROWITCH, D. H., DAWSON, V.

L., DAWSON, T. M., STEVENS, B. & BARRES, B. A. 2017a. Neurotoxic reactive astrocytes are induced by activated microglia. *Nature,* 541**,** 481-487.

LIDDELOW, S. A., GUTTENPLAN, K. A., CLARKE, L. E., BENNETT, F. C., BOHLEN, C. J., SCHIRMER, L., BENNETT, M. L., MUNCH, A. E., CHUNG, W. S., PETERSON, T. C., WILTON, D. K., FROUIN, A., NAPIER, B. A., PANICKER, N., KUMAR, M., BUCKWALTER, M. S., ROWITCH, D. H., DAWSON, V. L., DAWSON, T. M., STEVENS, B. & BARRES, B. A. 2017b. Neurotoxic reactive astrocytes are induced by activated microglia. *Nature,* 541**,** 481-487.

LINO, M. M., SCHNEIDER, C. & CARONI, P. 2002. Accumulation of SOD1 mutants in postnatal motoneurons does not cause motoneuron pathology or motoneuron disease. *J Neurosci,* 22**,** 4825-32.

LIOY, D. T., GARG, S. K., MONAGHAN, C. E., RABER, J., FOUST, K. D., KASPAR, B. K., HIRRLINGER, P. G., KIRCHHOFF, F., BISSONNETTE, J. M., BALLAS, N. & MANDEL, G. 2011. A role for glia in the progression of Rett's syndrome. *Nature,* 475**,** 497-500.

LÖÖV, C., HILLERED, L., EBENDAL, T. & ERLANDSSON, A. 2012. Engulfing astrocytes protect neurons from contact-induced apoptosis following injury. *PloS one,* 7**,** e33090-e33090.

ŁUKASZEWICZ-ZAJĄC, M., MROCZKO, B. & SŁOWIK, A. 2014. Matrix metalloproteinases (MMPs) and their tissue inhibitors (TIMPs) in amyotrophic lateral sclerosis (ALS). *J Neural Transm (Vienna),* 121**,** 1387-97.

MACKAY, J., DOWNS, J., WONG, K., HEYWORTH, J., EPSTEIN, A. & LEONARD, H. 2017. Autonomic breathing abnormalities in Rett syndrome: caregiver perspectives in an international database study. *J Neurodev Disord,* 9**,** 15.

MAEZAWA, I. & JIN, L. W. 2010. Rett syndrome microglia damage dendrites and synapses by the elevated release of glutamate. *J Neurosci,* 30**,** 5346-56.

MAEZAWA, I., SWANBERG, S., HARVEY, D., LASALLE, J. M. & JIN, L. W. 2009. Rett syndrome astrocytes are abnormal and spread MeCP2 deficiency through gap junctions. *J Neurosci,* 29**,** 5051-61.

MAGISTRETTI, P. J., PELLERIN, L., ROTHMAN, D. L. & SHULMAN, R. G. 1999. Energy on demand. *Science,* 283**,** 496-7.

MAGNUS, T., CHAN, A., LINKER, R. A., TOYKA, K. V. & GOLD, R. 2002. Astrocytes are less efficient in the removal of apoptotic lymphocytes than microglia cells: implications for the role of glial cells in the inflamed central nervous system. *J Neuropathol Exp Neurol,* 61**,** 760-6.

MAHMOUD, S., GHARAGOZLOO, M., SIMARD, C. & GRIS, D. 2019. Astrocytes Maintain Glutamate Homeostasis in the CNS by Controlling the Balance between Glutamate Uptake and Release. *Cells,* 8.

MANGIA, S., SIMPSON, I. A., VANNUCCI, S. J. & CARRUTHERS, A. 2009. The in vivo neuron-to-astrocyte lactate shuttle in human brain: evidence from modeling of measured lactate levels during visual stimulation. *J Neurochem,* 109 Suppl 1**,** 55-62.

MARÍN, O. & RUBENSTEIN, J. L. 2001. A long, remarkable journey: tangential migration in the telencephalon. *Nat Rev Neurosci,* 2**,** 780-90.

MATHIISEN, T. M., LEHRE, K. P., DANBOLT, N. C. & OTTERSEN, O. P. 2010. The perivascular astroglial sheath provides a complete covering of the brain microvessels: an electron microscopic 3D reconstruction. *Glia,* 58**,** 1094-103.

MATZ, P., WRUCK, W., FAULER, B., HEREBIAN, D., MIELKE, T. & ADJAYE, J. 2017. Footprint-free human fetal foreskin derived iPSCs: A tool for modeling hepatogenesis associated gene regulatory networks. *Scientific Reports,* 7**,** 6294.

MAUCH, D. H., NAGLER, K., SCHUMACHER, S., GORITZ, C., MULLER, E. C., OTTO, A. & PFRIEGER, F. W. 2001. CNS synaptogenesis promoted by glia-derived cholesterol. *Science,* 294**,** 1354-7.

MCGRAW, C. M., SAMACO, R. C. & ZOGHBI, H. Y. 2011. Adult neural function requires MeCP2. *Science,* 333**,** 186.

MCKENNA, M. C., STRIDH, M. H., MCNAIR, L. F., SONNEWALD, U., WAAGEPETERSEN, H. S. & SCHOUSBOE, A. 2016. Glutamate oxidation in astrocytes: Roles of glutamate dehydrogenase and aminotransferases. *J Neurosci Res,* 94**,** 1561-1571.

MCKEON, R. J., JURYNEC, M. J. & BUCK, C. R. 1999. The chondroitin sulfate proteoglycans neurocan and phosphacan are expressed by reactive astrocytes in the chronic CNS glial scar. *J Neurosci,* 19**,** 10778-88.

MERKLE, F. T., GHOSH, S., KAMITAKI, N., MITCHELL, J., AVIOR, Y., MELLO, C., KASHIN, S., MEKHOUBAD, S., ILIC, D., CHARLTON, M., SAPHIER, G., HANDSAKER, R. E., GENOVESE, G., BAR, S., BENVENISTY, N., MCCARROLL, S. A. & EGGAN, K. 2017. Human pluripotent stem cells recurrently acquire and expand dominant negative P53 mutations. *Nature,* 545**,** 229-233.

MINOR, K., TANG, X., KAHRILAS, G., ARCHIBALD, S. J., DAVIES, J. E. & DAVIES, S. J. 2008. Decorin promotes robust axon growth on inhibitory CSPGs and myelin via a direct effect on neurons. *Neurobiol Dis,* 32**,** 88-95.

MIYATA, S. & KITAGAWA, H. 2017. Formation and remodeling of the brain extracellular matrix in neural plasticity: Roles of chondroitin sulfate and hyaluronan. *Biochimica et Biophysica Acta (BBA) - General Subjects,* 1861**,** 2420-2434.

MIZUNO, G. O., WANG, Y., SHI, G., WANG, Y., SUN, J., PAPADOPOULOS, S., BROUSSARD, G. J., UNGER, E. K., DENG, W., WEICK, J., BHATTACHARYYA, A., CHEN, C. Y., YU, G., LOOGER, L. L. & TIAN, L. 2018. Aberrant Calcium Signaling in Astrocytes Inhibits Neuronal Excitability in a Human Down Syndrome Stem Cell Model. *Cell Rep,* 24**,** 355-365.

MNATZAKANIAN, G. N., LOHI, H., MUNTEANU, I., ALFRED, S. E., YAMADA, T., MACLEOD, P. J. M., JONES, J. R., SCHERER, S. W., SCHANEN, N. C., FRIEZ, M. J., VINCENT, J. B. & MINASSIAN, B. A. 2004. A previously unidentified MECP2 open reading frame defines a new protein isoform relevant to Rett syndrome. *Nature Genetics,* 36**,** 339-341.

MOLOFSKY, A. V., KRENCIK, R., ULLIAN, E. M., TSAI, H. H., DENEEN, B., RICHARDSON, W. D., BARRES, B. A. & ROWITCH, D. H. 2012. Astrocytes and disease: a neurodevelopmental perspective. *Genes Dev,* 26**,** 891-907.

MONTANA, V., NI, Y., SUNJARA, V., HUA, X. & PARPURA, V. 2004. Vesicular glutamate transporter-dependent glutamate release from astrocytes. *J Neurosci,* 24**,** 2633-42.

MOREAU, M., LECLERC, C., GUALANDRIS-PARISOT, L. & DUPRAT, A. M. 1994. Increased internal Ca2+ mediates neural induction in the amphibian embryo. *Proc Natl Acad Sci U S A,* 91**,** 12639-43.

MORGELLO, S., USON, R. R., SCHWARTZ, E. J. & HABER, R. S. 1995. The human blood-brain barrier glucose transporter (GLUT1) is a glucose transporter of gray matter astrocytes. *Glia,* 14**,** 43-54.

MOTIL, K. J., SCHULTZ, R. J., BROWNING, K., TRAUTWEIN, L. & GLAZE, D. G. 1999. Oropharyngeal dysfunction and gastroesophageal dysmotility are present in girls and women with Rett syndrome. *J Pediatr Gastroenterol Nutr,* 29**,** 31-7.

MULLER, M. 2019. Disturbed redox homeostasis and oxidative stress: Potential players in the developmental regression in Rett syndrome. *Neurosci Biobehav Rev,* 98**,** 154-163.

MURPHY-ROYAL, C., DUPUIS, J., GROC, L. & OLIET, S. H. R. 2017. Astroglial glutamate transporters in the brain: Regulating neurotransmitter homeostasis and synaptic transmission. *J Neurosci Res,* 95**,** 2140-2151.

NADARAJAH, B. & PARNAVELAS, J. G. 2002. Modes of neuronal migration in the developing cerebral cortex. *Nat Rev Neurosci,* 3**,** 423-32.

NAGAI, M., RE, D. B., NAGATA, T., CHALAZONITIS, A., JESSELL, T. M., WICHTERLE, H. & PRZEDBORSKI, S. 2007. Astrocytes expressing ALS-linked mutated SOD1 release factors selectively toxic to motor neurons. *Nature Neuroscience,* 10**,** 615-622.

NÄGLER, K., MAUCH, D. H. & PFRIEGER, F. W. 2001. Glia-derived signals induce synapse formation in neurones of the rat central nervous system. *J Physiol,* 533**,** 665-79.

NAGY, G. & ACKERMAN, S. L. 2013. Cholesterol metabolism and Rett syndrome pathogenesis. *Nature Genetics,* 45**,** 965-967.

NAKASHIMA, K., YANAGISAWA, M., ARAKAWA, H., KIMURA, N., HISATSUNE, T., KAWABATA, M., MIYAZONO, K. & TAGA, T. 1999. Synergistic Signaling in Fetal Brain by STAT3-Smad1 Complex Bridged by p300. *Science,* 284**,** 479-482.

NAN, X., CAMPOY, F. J. & BIRD, A. 1997. MeCP2 is a transcriptional repressor with abundant binding sites in genomic chromatin. *Cell,* 88**,** 471-81.
NAN, X., NG, H. H., JOHNSON, C. A., LAHERTY, C. D., TURNER, B. M., EISENMAN, R. N. & BIRD, A. 1998. Transcriptional repression by the methyl-CpG-binding protein MeCP2 involves a histone deacetylase complex. *Nature,* 393**,** 386-9.
NEUL, J. L., FANG, P., BARRISH, J., LANE, J., CAEG, E. B., SMITH, E. O., ZOGHBI, H., PERCY, A. & GLAZE, D. G. 2008. Specific mutations in methyl-CpG-binding protein 2 confer different severity in Rett syndrome. *Neurology,* 70**,** 1313-21.
NGUYEN, M. V., DU, F., FELICE, C. A., SHAN, X., NIGAM, A., MANDEL, G., ROBINSON, J. K. & BALLAS, N. 2012. MeCP2 is critical for maintaining mature neuronal networks and global brain anatomy during late stages of postnatal brain development and in the mature adult brain. *J Neurosci,* 32**,** 10021-34.
NICHOLSON, C. & SYKOVÁ, E. 1998. Extracellular space structure revealed by diffusion analysis. *Trends in Neurosciences,* 21**,** 207-215.
NIELSEN, S., NAGELHUS, E. A., AMIRY-MOGHADDAM, M., BOURQUE, C., AGRE, P. & OTTERSEN, O. P. 1997. Specialized membrane domains for water transport in glial cells: high-resolution immunogold cytochemistry of aquaporin-4 in rat brain. *J Neurosci,* 17**,** 171-80.
NWAOBI, S. E., CUDDAPAH, V. A., PATTERSON, K. C., RANDOLPH, A. C. & OLSEN, M. L. 2016. The role of glial-specific Kir4.1 in normal and pathological states of the CNS. *Acta neuropathologica,* 132**,** 1-21.
OBERHEIM, N. A., TAKANO, T., HAN, X., HE, W., LIN, J. H. C., WANG, F., XU, Q., WYATT, J. D., PILCHER, W., OJEMANN, J. G., RANSOM, B. R., GOLDMAN, S. A. & NEDERGAARD, M. 2009. Uniquely Hominid Features of Adult Human Astrocytes. *The Journal of Neuroscience,* 29**,** 3276.
OHNO, Y. 2018. Astrocytic Kir4.1 potassium channels as a novel therapeutic target for epilepsy and mood disorders. *Neural Regen Res,* 13**,** 651-652.
OHTSUKA, T., ISHIBASHI, M., GRADWOHL, G., NAKANISHI, S., GUILLEMOT, F. & KAGEYAMA, R. 1999. Hes1 and Hes5 as notch effectors in mammalian neuronal differentiation. *Embo j,* 18**,** 2196-207.
OKABE, Y., TAKAHASHI, T., MITSUMASU, C., KOSAI, K., TANAKA, E. & MATSUISHI, T. 2012. Alterations of gene expression and glutamate clearance in astrocytes derived from an MeCP2-null mouse model of Rett syndrome. *PLoS One,* 7**,** e35354.
OLDFORS, A., SOURANDER, P., ARMSTRONG, D. L., PERCY, A. K., WITT-ENGERSTRÖM, I. & HAGBERG, B. A. 1990. Rett syndrome: cerebellar pathology. *Pediatr Neurol,* 6**,** 310-4.
OLSON, C. O., ZACHARIAH, R. M., EZEONWUKA, C. D., LIYANAGE, V. R. & RASTEGAR, M. 2014. Brain region-specific expression of MeCP2 isoforms correlates with DNA methylation within Mecp2 regulatory elements. *PLoS One,* 9**,** e90645.
OOHASHI, T., EDAMATSU, M., BEKKU, Y. & CARULLI, D. 2015. The hyaluronan and proteoglycan link proteins: Organizers of the brain extracellular matrix and key molecules for neuronal function and plasticity. *Experimental Neurology,* 274**,** 134-144.
OPERTO, F. F., MAZZA, R., PASTORINO, G. M. G., VERROTTI, A. & COPPOLA, G. 2019. Epilepsy and genetic in Rett syndrome: A review. *Brain Behav,* 9**,** e01250.
PACHECO, N. L., HEAVEN, M. R., HOLT, L. M., CROSSMAN, D. K., BOGGIO, K. J., SHAFFER, S. A., FLINT, D. L. & OLSEN, M. L. 2017. RNA sequencing and proteomics approaches reveal novel deficits in the cortex of Mecp2-deficient mice, a model for Rett syndrome. *Mol Autism,* 8**,** 56.
PACHOLKO, A. G., WOTTON, C. A. & BEKAR, L. K. 2020. Astrocytes—The Ultimate Effectors of Long-Range Neuromodulatory Networks? *Frontiers in Cellular Neuroscience,* 14.
PAN, J., MA, N., YU, B., ZHANG, W. & WAN, J. 2020. Transcriptomic profiling of microglia and astrocytes throughout aging. *Journal of Neuroinflammation,* 17**,** 97.
PAPADEAS, S. T., KRAIG, S. E., O'BANION, C., LEPORE, A. C. & MARAGAKIS, N. J. 2011. Astrocytes carrying the superoxide dismutase 1 (SOD1G93A) mutation induce wild-type motor neuron degeneration in vivo. *Proc Natl Acad Sci U S A,* 108**,** 17803-8.

PARIDAEN, J. T. & HUTTNER, W. B. 2014. Neurogenesis during development of the vertebrate central nervous system. *EMBO Rep,* 15**,** 351-64.
PARPURA, V., BASARSKY, T. A., LIU, F., JEFTINIJA, K., JEFTINIJA, S. & HAYDON, P. G. 1994. Glutamate-mediated astrocyte-neuron signalling. *Nature,* 369**,** 744-7.
PARRI, H. R. & CRUNELLI, V. 2003. The role of Ca2+ in the generation of spontaneous astrocytic Ca2+ oscillations. *Neuroscience,* 120**,** 979-92.
PARRI, H. R., GOULD, T. M. & CRUNELLI, V. 2001. Spontaneous astrocytic Ca2+ oscillations in situ drive NMDAR-mediated neuronal excitation. *Nat Neurosci,* 4**,** 803-12.
PASCUAL, O., CASPER, K. B., KUBERA, C., ZHANG, J., REVILLA-SANCHEZ, R., SUL, J. Y., TAKANO, H., MOSS, S. J., MCCARTHY, K. & HAYDON, P. G. 2005. Astrocytic purinergic signaling coordinates synaptic networks. *Science,* 310**,** 113-6.
PATTEN, I. & PLACZEK, M. 2000. The role of Sonic hedgehog in neural tube patterning. *Cell Mol Life Sci,* 57**,** 1695-708.
PEHAR, M., HARLAN, B. A., KILLOY, K. M. & VARGAS, M. R. 2017. Role and Therapeutic Potential of Astrocytes in Amyotrophic Lateral Sclerosis. *Curr Pharm Des,* 23**,** 5010-5021.
PELLERIN, L. & MAGISTRETTI, P. J. 1994a. Glutamate uptake into astrocytes stimulates aerobic glycolysis: a mechanism coupling neuronal activity to glucose utilization. *Proceedings of the National Academy of Sciences,* 91**,** 10625.
PELLERIN, L. & MAGISTRETTI, P. J. 1994b. Glutamate uptake into astrocytes stimulates aerobic glycolysis: a mechanism coupling neuronal activity to glucose utilization. *Proceedings of the National Academy of Sciences of the United States of America,* 91**,** 10625-10629.
PELLERIN, L. & MAGISTRETTI, P. J. 1997. Glutamate uptake stimulates Na+,K+-ATPase activity in astrocytes via activation of a distinct subunit highly sensitive to ouabain. *J Neurochem,* 69**,** 2132-7.
PELLERIN, L., PELLEGRI, G., MARTIN, J.-L. & MAGISTRETTI, P. J. 1998. Expression of monocarboxylate transporter mRNAs in mouse brain: Support for a distinct role of lactate as an energy substrate for the neonatal vs. adult brain. *Proceedings of the National Academy of Sciences,* 95**,** 3990.
PERA, M. F. 2011. The dark side of induced pluripotency. *Nature,* 471**,** 46-47.
PERKINS, K. L., ARRANZ, A. M., YAMAGUCHI, Y. & HRABETOVA, S. 2017. Brain extracellular space, hyaluronan, and the prevention of epileptic seizures. *Rev Neurosci,* 28**,** 869-892.
PERRIOT, S., MATHIAS, A., PERRIARD, G., CANALES, M., JONKMANS, N., MERIENNE, N., MEUNIER, C., EL KASSAR, L., PERRIER, A. L., LAPLAUD, D. A., SCHLUEP, M., DÉGLON, N. & DU PASQUIER, R. 2018. Human Induced Pluripotent Stem Cell-Derived Astrocytes Are Differentially Activated by Multiple Sclerosis-Associated Cytokines. *Stem Cell Reports,* 11**,** 1199-1210.
PFRIEGER, F. W. & BARRES, B. A. 1997. Synaptic efficacy enhanced by glial cells in vitro. *Science,* 277**,** 1684-7.
PHAM, M. T., POLLOCK, K. M., ROSE, M. D., CARY, W. A., STEWART, H. R., ZHOU, P., NOLTA, J. A. & WALDAU, B. 2018. Generation of human vascularized brain organoids. *Neuroreport,* 29**,** 588-593.
PIERRE, K., PELLERIN, L., DEBERNARDI, R., RIEDERER, B. M. & MAGISTRETTI, P. J. 2000. Cell-specific localization of monocarboxylate transporters, MCT1 and MCT2, in the adult mouse brain revealed by double immunohistochemical labeling and confocal microscopy. *Neuroscience,* 100**,** 617-27.
PINI, G., SCUSA, M. F., CONGIU, L., BENINCASA, A., MORESCALCHI, P., BOTTIGLIONI, I., DI MARCO, P., BORELLI, P., BONUCCELLI, U., DELLA-CHIESA, A., PRINA-MELLO, A. & TROPEA, D. 2012. IGF1 as a Potential Treatment for Rett Syndrome: Safety Assessment in Six Rett Patients. *Autism Res Treat,* 2012**,** 679801.
POOPALASUNDARAM, S., KNOTT, C., SHAMOTIENKO, O. G., FORAN, P. G., DOLLY, J. O., GHIANI, C. A., GALLO, V. & WILKIN, G. P. 2000. Glial heterogeneity in expression of the inwardly rectifying K(+) channel, Kir4.1, in adult rat CNS. *Glia,* 30**,** 362-72.

PORTER, J. T. & MCCARTHY, K. D. 1996. Hippocampal astrocytes in situ respond to glutamate released from synaptic terminals. *J Neurosci,* 16**,** 5073-81.
RAICHLE, M. E. & GUSNARD, D. A. 2002. Appraising the brain's energy budget. *Proceedings of the National Academy of Sciences,* 99**,** 10237.
RAJAN, P. & MCKAY, R. D. G. 1998. Multiple Routes to Astrocytic Differentiation in the CNS. *The Journal of Neuroscience,* 18**,** 3620.
RAMOCKI, M. B., TAVYEV, Y. J. & PETERS, S. U. 2010. The MECP2 duplication syndrome. *Am J Med Genet A,* 152a**,** 1079-88.
RAPONI, E., AGENES, F., DELPHIN, C., ASSARD, N., BAUDIER, J., LEGRAVEREND, C. & DELOULME, J.-C. 2007. S100B expression defines a state in which GFAP-expressing cells lose their neural stem cell potential and acquire a more mature developmental stage. *Glia,* 55**,** 165-177.
REINER, A. & LEVITZ, J. 2018. Glutamatergic Signaling in the Central Nervous System: Ionotropic and Metabotropic Receptors in Concert. *Neuron,* 98**,** 1080-1098.
REISS, A. L., FARUQUE, F., NAIDU, S., ABRAMS, M., BEATY, T., BRYAN, R. N. & MOSER, H. 1993. Neuroanatomy of Rett syndrome: a volumetric imaging study. *Ann Neurol,* 34**,** 227-34.
RENTHAL, W., BOXER, L. D., HRVATIN, S., LI, E., SILBERFELD, A., NAGY, M. A., GRIFFITH, E. C., VIERBUCHEN, T. & GREENBERG, M. E. 2018. Characterization of human mosaic Rett syndrome brain tissue by single-nucleus RNA sequencing. *Nature Neuroscience,* 21**,** 1670-1679.
ROSENBERG, S. S. & SPITZER, N. C. 2011. Calcium signaling in neuronal development. *Cold Spring Harb Perspect Biol,* 3**,** a004259.
ROTHSTEIN, J. D., DYKES-HOBERG, M., PARDO, C. A., BRISTOL, L. A., JIN, L., KUNCL, R. W., KANAI, Y., HEDIGER, M. A., WANG, Y., SCHIELKE, J. P. & WELTY, D. F. 1996. Knockout of glutamate transporters reveals a major role for astroglial transport in excitotoxicity and clearance of glutamate. *Neuron,* 16**,** 675-86.
ROYBON, L., LAMAS, N. J., GARCIA, A. D., YANG, E. J., SATTLER, R., LEWIS, V. J., KIM, Y. A., KACHEL, C. A., ROTHSTEIN, J. D., PRZEDBORSKI, S., WICHTERLE, H. & HENDERSON, C. E. 2013. Human stem cell-derived spinal cord astrocytes with defined mature or reactive phenotypes. *Cell Rep,* 4**,** 1035-1048.
SAHARA, S. & O'LEARY, D. D. 2009. Fgf10 regulates transition period of cortical stem cell differentiation to radial glia controlling generation of neurons and basal progenitors. *Neuron,* 63**,** 48-62.
SAKAGUCHI, H., OZAKI, Y., ASHIDA, T., MATSUBARA, T., OISHI, N., KIHARA, S. & TAKAHASHI, J. 2019. Self-Organized Synchronous Calcium Transients in a Cultured Human Neural Network Derived from Cerebral Organoids. *Stem Cell Reports,* 13**,** 458-473.
SANSOM, S. N., GRIFFITHS, D. S., FAEDO, A., KLEINJAN, D. J., RUAN, Y., SMITH, J., VAN HEYNINGEN, V., RUBENSTEIN, J. L. & LIVESEY, F. J. 2009. The level of the transcription factor Pax6 is essential for controlling the balance between neural stem cell self-renewal and neurogenesis. *PLoS Genet,* 5**,** e1000511.
SAVTCHOUK, I. & VOLTERRA, A. 2018. Gliotransmission: Beyond Black-and-White. *The Journal of Neuroscience,* 38**,** 14-25.
SCHOLZEN, T. & GERDES, J. 2000. The Ki-67 protein: from the known and the unknown. *J Cell Physiol,* 182**,** 311-22.
SCHWARTZMAN, J. S., BERNARDINO, A., NISHIMURA, A., GOMES, R. R. & ZATZ, M. 2001. Rett syndrome in a boy with a 47,XXY karyotype confirmed by a rare mutation in the MECP2 gene. *Neuropediatrics,* 32**,** 162-4.
SCHWIENING, C. J. 2012. A brief historical perspective: Hodgkin and Huxley. *The Journal of physiology,* 590**,** 2571-2575.
SELKIRK, J. V., NOTTEBAUM, L. M., VANA, A. M., VERGE, G. M., MACKAY, K. B., STIEFEL, T. H., NAEVE, G. S., POMEROY, J. E., PETROSKI, R. E., MOYER, J., DUNLOP, J. & FOSTER, A. C. 2005. Role of the GLT-1 subtype of glutamate transporter in glutamate homeostasis: the GLT-1-preferring

inhibitor WAY-855 produces marginal neurotoxicity in the rat hippocampus. *Eur J Neurosci,* 21**,** 3217-28.
SERIO, A., BILICAN, B., BARMADA, S. J., ANDO, D. M., ZHAO, C., SILLER, R., BURR, K., HAGHI, G., STORY, D., NISHIMURA, A. L., CARRASCO, M. A., PHATNANI, H. P., SHUM, C., WILMUT, I., MANIATIS, T., SHAW, C. E., FINKBEINER, S. & CHANDRAN, S. 2013. Astrocyte pathology and the absence of non-cell autonomy in an induced pluripotent stem cell model of TDP-43 proteinopathy. *Proc Natl Acad Sci U S A,* 110**,** 4697-702.
SETOGUCHI, H., NAMIHIRA, M., KOHYAMA, J., ASANO, H., SANOSAKA, T. & NAKASHIMA, K. 2006. Methyl-CpG binding proteins are involved in restricting differentiation plasticity in neurons. *J Neurosci Res,* 84**,** 969-79.
SHAHBAZIAN, M. D., ANTALFFY, B., ARMSTRONG, D. L. & ZOGHBI, H. Y. 2002. Insight into Rett syndrome: MeCP2 levels display tissue- and cell-specific differences and correlate with neuronal maturation. *Human Molecular Genetics,* 11**,** 115-124.
SHALTOUKI, A., PENG, J., LIU, Q., RAO, M. S. & ZENG, X. 2013. Efficient generation of astrocytes from human pluripotent stem cells in defined conditions. *Stem Cells,* 31**,** 941-52.
SHELDON, A. L. & ROBINSON, M. B. 2007. The role of glutamate transporters in neurodegenerative diseases and potential opportunities for intervention. *Neurochem Int,* 51**,** 333-55.
SHOVLIN, S. & TROPEA, D. 2018. Transcriptome level analysis in Rett syndrome using human samples from different tissues. *Orphanet J Rare Dis,* 13**,** 113.
SIRIANNI, N., NAIDU, S., PEREIRA, J., PILLOTTO, R. F. & HOFFMAN, E. P. 1998. Rett syndrome: confirmation of X-linked dominant inheritance, and localization of the gene to Xq28. *Am J Hum Genet,* 63**,** 1552-8.
SKENE, P. J., ILLINGWORTH, R. S., WEBB, S., KERR, A. R., JAMES, K. D., TURNER, D. J., ANDREWS, R. & BIRD, A. P. 2010. Neuronal MeCP2 is expressed at near histone-octamer levels and globally alters the chromatin state. *Mol Cell,* 37**,** 457-68.
SKLOOT, R. & COMPANY, M. 2010. Immortal Life of Henrietta Lacks, the.
SLEZAK, M., GROSCHE, A., NIEMIEC, A., TANIMOTO, N., PANNICKE, T., MÜNCH, T. A., CROCKER, B., ISOPE, P., HÄRTIG, W., BECK, S. C., HUBER, G., FERRACCI, G., PERRAUT, M., REBER, M., MIEHE, M., DEMAIS, V., LÉVÊQUE, C., METZGER, D., SZKLARCZYK, K., PRZEWLOCKI, R., SEELIGER, M. W., SAGE-CIOCCA, D., HIRRLINGER, J., REICHENBACH, A., REIBEL, S. & PFRIEGER, F. W. 2012. Relevance of exocytotic glutamate release from retinal glia. *Neuron,* 74**,** 504-16.
SLOAN, S. A. & BARRES, B. A. 2014. Looks can be deceiving: reconsidering the evidence for gliotransmission. *Neuron,* 84**,** 1112-5.
SLOAN, S. A., DARMANIS, S., HUBER, N., KHAN, T. A., BIREY, F., CANEDA, C., REIMER, R., QUAKE, S. R., BARRES, B. A. & PAŞCA, S. P. 2017. Human Astrocyte Maturation Captured in 3D Cerebral Cortical Spheroids Derived from Pluripotent Stem Cells. *Neuron,* 95**,** 779-790.e6.
SMITH, S. E. P., LI, J., GARBETT, K., MIRNICS, K. & PATTERSON, P. H. 2007. Maternal Immune Activation Alters Fetal Brain Development through Interleukin-6. *The Journal of Neuroscience,* 27**,** 10695.
SMRT, R. D., EAVES-EGENES, J., BARKHO, B. Z., SANTISTEVAN, N. J., ZHAO, C., AIMONE, J. B., GAGE, F. H. & ZHAO, X. 2007. Mecp2 deficiency leads to delayed maturation and altered gene expression in hippocampal neurons. *Neurobiol Dis,* 27**,** 77-89.
SOFRONIEW, M. V. & VINTERS, H. V. 2010. Astrocytes: biology and pathology. *Acta Neuropathol,* 119**,** 7-35.
SOGHOMONIAN, J.-J. & MARTIN, D. L. 1998. Two isoforms of glutamate decarboxylase: why? *Trends in Pharmacological Sciences,* 19**,** 500-505.
SOMJEN, G. G. 1975. Electrophysiology of neuroglia. *Annu Rev Physiol,* 37**,** 163-90.
SOMJEN, G. G. 1979. Extracellular potassium in the mammalian central nervous system. *Annu Rev Physiol,* 41**,** 159-77.
SONNEWALD, U., WESTERGAARD, N., PETERSEN, S. B., UNSGÅRD, G. & SCHOUSBOE, A. 1993. Metabolism of [U-13C]Glutamate in Astrocytes Studied by 13C NMR Spectroscopy:

Incorporation of More Label into Lactate than into Glutamine Demonstrates the Importance of the Tricarboxylic Acid Cycle. *Journal of Neurochemistry,* 61**,** 1179-1182.
SOUBANNIER, V., MAUSSION, G., CHAINEAU, M., SIGUTOVA, V., ROULEAU, G., DURCAN, T. M. & STIFANI, S. 2020. Characterization of human iPSC-derived astrocytes with potential for disease modeling and drug discovery. *Neurosci Lett,* 731**,** 135028.
STADTFELD, M., NAGAYA, M., UTIKAL, J., WEIR, G. & HOCHEDLINGER, K. 2008. Induced pluripotent stem cells generated without viral integration. *Science,* 322**,** 945-9.
STAMENKOVIC, I. 2003. Extracellular matrix remodelling: the role of matrix metalloproteinases. *J Pathol,* 200**,** 448-64.
STARK, R., GRZELAK, M. & HADFIELD, J. 2019. RNA sequencing: the teenage years. *Nat Rev Genet,* 20**,** 631-656.
STEVENS, B., ALLEN, N. J., VAZQUEZ, L. E., HOWELL, G. R., CHRISTOPHERSON, K. S., NOURI, N., MICHEVA, K. D., MEHALOW, A. K., HUBERMAN, A. D., STAFFORD, B., SHER, A., LITKE, A. M., LAMBRIS, J. D., SMITH, S. J., JOHN, S. W. & BARRES, B. A. 2007. The classical complement cascade mediates CNS synapse elimination. *Cell,* 131**,** 1164-78.
STILES, J. & JERNIGAN, T. L. 2010a. The basics of brain development. *Neuropsychology review,* 20**,** 327-348.
STILES, J. & JERNIGAN, T. L. 2010b. The basics of brain development. *Neuropsychol Rev,* 20**,** 327-48.
STOLT, C. C., LOMMES, P., SOCK, E., CHABOISSIER, M. C., SCHEDL, A. & WEGNER, M. 2003. The Sox9 transcription factor determines glial fate choice in the developing spinal cord. *Genes Dev,* 17**,** 1677-89.
STRUVE, J., MAHER, P. C., LI, Y. Q., KINNEY, S., FEHLINGS, M. G., KUNTZ, C. T. & SHERMAN, L. S. 2005. Disruption of the hyaluronan-based extracellular matrix in spinal cord promotes astrocyte proliferation. *Glia,* 52**,** 16-24.
SUN, Y., NADAL-VICENS, M., MISONO, S., LIN, M. Z., ZUBIAGA, A., HUA, X., FAN, G. & GREENBERG, M. E. 2001. Neurogenin promotes neurogenesis and inhibits glial differentiation by independent mechanisms. *Cell,* 104**,** 365-76.
SUZUKI, A., STERN, S. A., BOZDAGI, O., HUNTLEY, G. W., WALKER, R. H., MAGISTRETTI, P. J. & ALBERINI, C. M. 2011. Astrocyte-neuron lactate transport is required for long-term memory formation. *Cell,* 144**,** 810-23.
SWANSON, R. A. & CHOI, D. W. 1993. Glial glycogen stores affect neuronal survival during glucose deprivation in vitro. *J Cereb Blood Flow Metab,* 13**,** 162-9.
TAKAHASHI, K., TANABE, K., OHNUKI, M., NARITA, M., ICHISAKA, T., TOMODA, K. & YAMANAKA, S. 2007. Induction of pluripotent stem cells from adult human fibroblasts by defined factors. *Cell,* 131**,** 861-72.
TAKAHASHI, K. & YAMANAKA, S. 2006. Induction of pluripotent stem cells from mouse embryonic and adult fibroblast cultures by defined factors. *Cell,* 126**,** 663-76.
TAKOUDA, J., KATADA, S. & NAKASHIMA, K. 2017. Emerging mechanisms underlying astrogenesis in the developing mammalian brain. *Proc Jpn Acad Ser B Phys Biol Sci,* 93**,** 386-398.
TARABEUX, J., KEBIR, O., GAUTHIER, J., HAMDAN, F. F., XIONG, L., PITON, A., SPIEGELMAN, D., HENRION, É., MILLET, B., FATHALLI, F., JOOBER, R., RAPOPORT, J. L., DELISI, L. E., FOMBONNE, É., MOTTRON, L., FORGET-DUBOIS, N., BOIVIN, M., MICHAUD, J. L., DRAPEAU, P., LAFRENIÈRE, R. G., ROULEAU, G. A., KREBS, M. O. & TEAM, S. D. 2011. Rare mutations in N-methyl-D-aspartate glutamate receptors in autism spectrum disorders and schizophrenia. *Translational Psychiatry,* 1**,** e55-e55.
TARCZYLUK, M. A., NAGEL, D. A., O'NEIL, J. D., PARRI, H. R., TSE, E. H., COLEMAN, M. D. & HILL, E. J. 2013. Functional astrocyte-neuron lactate shuttle in a human stem cell-derived neuronal network. *J Cereb Blood Flow Metab,* 33**,** 1386-93.
TARQUINIO, D. C., MOTIL, K. J., HOU, W., LEE, H. S., GLAZE, D. G., SKINNER, S. A., NEUL, J. L., ANNESE, F., MCNAIR, L., BARRISH, J. O., GEERTS, S. P., LANE, J. B. & PERCY, A. K. 2012. Growth failure and outcome in Rett syndrome: specific growth references. *Neurology,* 79**,** 1653-61.

TCHIEU, J., CALDER, E. L., GUTTIKONDA, S. R., GUTZWILLER, E. M., AROMOLARAN, K. A., STEINBECK, J. A., GOLDSTEIN, P. A. & STUDER, L. 2019. NFIA is a gliogenic switch enabling rapid derivation of functional human astrocytes from pluripotent stem cells. *Nat Biotechnol,* 37**,** 267-275.

TCW, J., WANG, M., PIMENOVA, A. A., BOWLES, K. R., HARTLEY, B. J., LACIN, E., MACHLOVI, S. I., ABDELAAL, R., KARCH, C. M., PHATNANI, H., SLESINGER, P. A., ZHANG, B., GOATE, A. M. & BRENNAND, K. J. 2017. An Efficient Platform for Astrocyte Differentiation from Human Induced Pluripotent Stem Cells. *Stem Cell Reports,* 9**,** 600-614.

TIAN, W., SAWYER, A., KOCAOGLU, F. B. & KYRIAKIDES, T. R. 2011. Astrocyte-derived thrombospondin-2 is critical for the repair of the blood-brain barrier. *Am J Pathol,* 179**,** 860-8.

TILLOTSON, R. & BIRD, A. 2019. The Molecular Basis of MeCP2 Function in the Brain. *J Mol Biol*.

TORSVIK, A., STIEBER, D., ENGER, P., GOLEBIEWSKA, A., MOLVEN, A., SVENDSEN, A., WESTERMARK, B., NICLOU, S. P., OLSEN, T. K., CHEKENYA ENGER, M. & BJERKVIG, R. 2014. U-251 revisited: genetic drift and phenotypic consequences of long-term cultures of glioblastoma cells. *Cancer Med,* 3**,** 812-24.

TRAN, M. D. & NEARY, J. T. 2006. Purinergic signaling induces thrombospondin-1 expression in astrocytes. *Proc Natl Acad Sci U S A,* 103**,** 9321-6.

TYZACK, G. E., HALL, C. E., SIBLEY, C. R., CYMES, T., FOROSTYAK, S., CARLINO, G., MEYER, I. F., SCHIAVO, G., ZHANG, S.-C., GIBBONS, G. M., NEWCOMBE, J., PATANI, R. & LAKATOS, A. 2017. A neuroprotective astrocyte state is induced by neuronal signal EphB1 but fails in ALS models. *Nature Communications,* 8**,** 1164.

ULLIAN, E. M., SAPPERSTEIN, S. K., CHRISTOPHERSON, K. S. & BARRES, B. A. 2001. Control of synapse number by glia. *Science,* 291**,** 657-61.

VAN DEIJK, A. F., CAMARGO, N., TIMMERMAN, J., HEISTEK, T., BROUWERS, J. F., MOGAVERO, F., MANSVELDER, H. D., SMIT, A. B. & VERHEIJEN, M. H. 2017. Astrocyte lipid metabolism is critical for synapse development and function in vivo. *Glia,* 65**,** 670-682.

VANNUCCI, S. J., MAHER, F. & SIMPSON, I. A. 1997. Glucose transporter proteins in brain: delivery of glucose to neurons and glia. *Glia,* 21**,** 2-21.

VEGAS, N., CAVALLIN, M., MAILLARD, C., BODDAERT, N., TOULOUSE, J., SCHAEFER, E., LERMAN-SAGIE, T., LEV, D., MAGALIE, B., MOUTTON, S., HAAN, E., ISIDOR, B., HERON, D., MILH, M., RONDEAU, S., MICHOT, C., VALENCE, S., WAGNER, S., HULLY, M., MIGNOT, C., MASUREL, A., DATTA, A., ODENT, S., NIZON, M., LAZARO, L., VINCENT, M., COGNE, B., GUERROT, A. M., ARPIN, S., PEDESPAN, J. M., CAUBEL, I., PONTIER, B., TROUDE, B., RIVIER, F., PHILIPPE, C., BIENVENU, T., SPITZ, M. A., BERY, A. & BAHI-BUISSON, N. 2018. Delineating FOXG1 syndrome: From congenital microcephaly to hyperkinetic encephalopathy. *Neurol Genet,* 4**,** e281.

VENKOV, L., ROSENTAL, L. & MANOLOVA, M. 1976. Subcellular distribution of LDH isoenzymes in neuronal- and glial-enriched fractions. *Brain Research,* 109**,** 323-333.

VERBICH, D., PRENOSIL, G. A., CHANG, P. K., MURAI, K. K. & MCKINNEY, R. A. 2012. Glial glutamate transport modulates dendritic spine head protrusions in the hippocampus. *Glia,* 60**,** 1067-77.

VIOLA, A., SAYWELL, V., VILLARD, L., COZZONE, P. J. & LUTZ, N. W. 2007. Metabolic fingerprints of altered brain growth, osmoregulation and neurotransmission in a Rett syndrome model. *PLoS One,* 2**,** e157.

VOLPATO, V. & WEBBER, C. 2020. Addressing variability in iPSC-derived models of human disease: guidelines to promote reproducibility. *Disease Models & Mechanisms,* 13**,** dmm042317.

VOUTSINOS-PORCHE, B., BONVENTO, G., TANAKA, K., STEINER, P., WELKER, E., CHATTON, J. Y., MAGISTRETTI, P. J. & PELLERIN, L. 2003. Glial glutamate transporters mediate a functional metabolic crosstalk between neurons and astrocytes in the mouse developing cortex. *Neuron,* 37**,** 275-86.

WANG, Z., GERSTEIN, M. & SNYDER, M. 2009. RNA-Seq: a revolutionary tool for transcriptomics. *Nat Rev Genet,* 10**,** 57-63.

WHATLEY, S. A., HALL, C. & LIM, L. 1981. Hypothalamic neurons in dissociated cell culture: the mechanism of increased survival times in the presence of non-neuronal cells. *J Neurochem,* 36**,** 2052-6.

WILLIAMS, E. C., ZHONG, X., MOHAMED, A., LI, R., LIU, Y., DONG, Q., ANANIEV, G. E., MOK, J. C., LIN, B. R., LU, J., CHIAO, C., CHERNEY, R., LI, H., ZHANG, S. C. & CHANG, Q. 2014. Mutant astrocytes differentiated from Rett syndrome patients-specific iPSCs have adverse effects on wild-type neurons. *Hum Mol Genet,* 23**,** 2968-80.

WYSS-CORAY, T., LOIKE, J. D., BRIONNE, T. C., LU, E., ANANKOV, R., YAN, F., SILVERSTEIN, S. C. & HUSEMANN, J. 2003. Adult mouse astrocytes degrade amyloid-beta in vitro and in situ. *Nat Med,* 9**,** 453-7.

XU, X. & POZZO-MILLER, L. 2013. A novel DNA-binding feature of MeCP2 contributes to Rett syndrome. *Frontiers in Cellular Neuroscience,* 7.

YAN, J. W., TAN, T. Y. & HUANG, Q. L. 2013. Protective effect of astrocyte-conditioned medium on neurons following hypoxia and mechanical injury. *Chin J Traumatol,* 16**,** 3-9.

YANG, P., WEN, H., OU, S., CUI, J. & FAN, D. 2012. IL-6 promotes regeneration and functional recovery after cortical spinal tract injury by reactivating intrinsic growth program of neurons and enhancing synapse formation. *Exp Neurol,* 236**,** 19-27.

YUAN, Z.-F., MAO, S.-S., SHEN, J., JIANG, L.-H., XU, L., XU, J.-L. & GAO, F. 2020. Insulin-Like Growth Factor-1 Down-Regulates the Phosphorylation of FXYD1 and Rescues Behavioral Deficits in a Mouse Model of Rett Syndrome. *Frontiers in Neuroscience,* 14.

ZEINEDDINE, D., HAMMOUD, A. A., MORTADA, M. & BOEUF, H. 2014. The Oct4 protein: more than a magic stemness marker. *Am J Stem Cells,* 3**,** 74-82.

ZHANG, L., HE, J., JUGLOFF, D. G. M. & EUBANKS, J. H. 2008. The MeCP2-null mouse hippocampus displays altered basal inhibitory rhythms and is prone to hyperexcitability. *Hippocampus,* 18**,** 294-309.

ZHANG, M., NGO, J., PIROZZI, F., SUN, Y.-P. & WYNSHAW-BORIS, A. 2018a. Highly efficient methods to obtain homogeneous dorsal neural progenitor cells from human and mouse embryonic stem cells and induced pluripotent stem cells. *Stem Cell Research & Therapy,* 9**,** 67.

ZHANG, Q., PANGRSIC, T., KREFT, M., KRZAN, M., LI, N., SUL, J. Y., HALASSA, M., VAN BOCKSTAELE, E., ZOREC, R. & HAYDON, P. G. 2004. Fusion-related release of glutamate from astrocytes. *J Biol Chem,* 279**,** 12724-33.

ZHANG, S. & CUI, W. 2014. Sox2, a key factor in the regulation of pluripotency and neural differentiation. *World J Stem Cells,* 6**,** 305-11.

ZHANG, W., GE, Y., CHENG, Q., ZHANG, Q., FANG, L. & ZHENG, J. 2018b. Decorin is a pivotal effector in the extracellular matrix and tumour microenvironment. *Oncotarget,* 9**,** 5480-5491.

ZHANG, X., HUANG, C. T., CHEN, J., PANKRATZ, M. T., XI, J., LI, J., YANG, Y., LAVAUTE, T. M., LI, X. J., AYALA, M., BONDARENKO, G. I., DU, Z. W., JIN, Y., GOLOS, T. G. & ZHANG, S. C. 2010. Pax6 is a human neuroectoderm cell fate determinant. *Cell Stem Cell,* 7**,** 90-100.

ZHANG, Y., CHEN, K., SLOAN, S. A., BENNETT, M. L., SCHOLZE, A. R., O'KEEFFE, S., PHATNANI, H. P., GUARNIERI, P., CANEDA, C., RUDERISCH, N., DENG, S., LIDDELOW, S. A., ZHANG, C., DANEMAN, R., MANIATIS, T., BARRES, B. A. & WU, J. Q. 2014. An RNA-sequencing transcriptome and splicing database of glia, neurons, and vascular cells of the cerebral cortex. *J Neurosci,* 34**,** 11929-47.

ZHANG, Y., SLOAN, S. A., CLARKE, L. E., CANEDA, C., PLAZA, C. A., BLUMENTHAL, P. D., VOGEL, H., STEINBERG, G. K., EDWARDS, M. S., LI, G., DUNCAN, J. A., 3RD, CHESHIER, S. H., SHUER, L. M., CHANG, E. F., GRANT, G. A., GEPHART, M. G. & BARRES, B. A. 2016. Purification and Characterization of Progenitor and Mature Human Astrocytes Reveals Transcriptional and Functional Differences with Mouse. *Neuron,* 89**,** 37-53.

ZHAO, D., MOKHTARI, R., PEDROSA, E., BIRNBAUM, R., ZHENG, D. & LACHMAN, H. M. 2017. Transcriptome analysis of microglia in a mouse model of Rett syndrome: differential expression of genes associated with microglia/macrophage activation and cellular stress. *Mol Autism,* 8**,** 17.

ZHAO, N., MA, D., LEONG, W. Y., HAN, J., VANDONGEN, A., CHEN, T. & GOH, E. L. K. 2015. The methyl-CpG-binding domain (MBD) is crucial for MeCP2's dysfunction-induced defects in adult newborn neurons. *Frontiers in Cellular Neuroscience,* 9**,** 158.

ZHOU, J., SU, P., LI, D., TSANG, S., DUAN, E. & WANG, F. 2010. High-efficiency induction of neural conversion in human ESCs and human induced pluripotent stem cells with a single chemical inhibitor of transforming growth factor beta superfamily receptors. *Stem Cells,* 28**,** 1741-50.

ZHOU, Q., VIOLLET, C., EFTHYMIOU, A., KHAYRULLINA, G., MORITZ, K. E., WILKERSON, M. D., SUKUMAR, G., DALGARD, C. L. & DOUGHTY, M. L. 2019. Neuroinflammatory astrocytes generated from cord blood-derived human induced pluripotent stem cells. *Journal of Neuroinflammation,* 16**,** 164.

Appendix

A1. Housekeeping gene selection

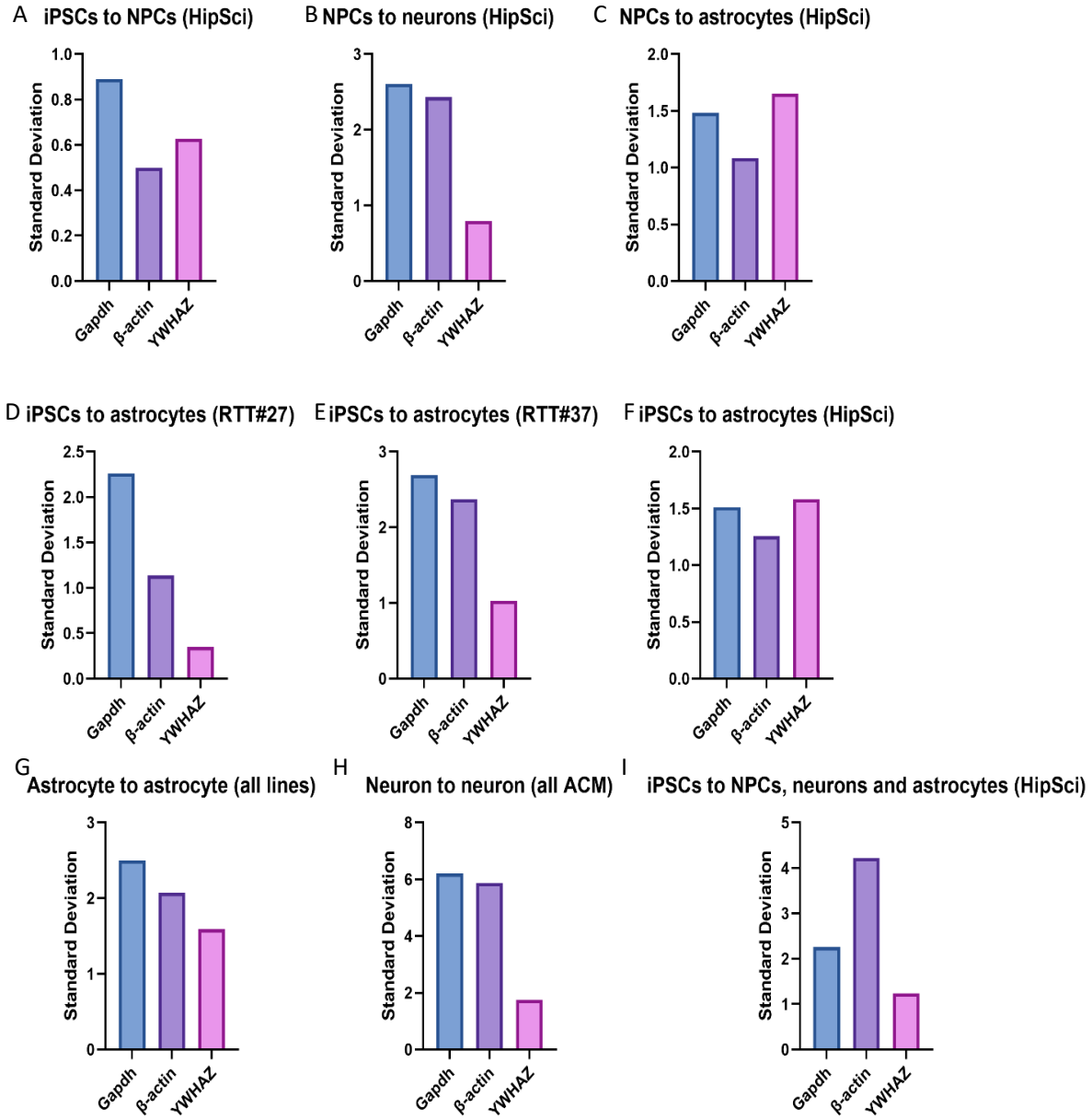

Figure A1: Standard deviation of Ct values for housekeeping genes between samples. **A)-I)** Bar graphs depict the standard deviation of Ct values for the housekeeping genes Gapdh, β-actin and YWHAZ. The housekeeping gene with the lowest standard deviation was selected to normalise genes when comparing between the labelled conditions.

A.2 Glutamate in Kreb's Ringer alone

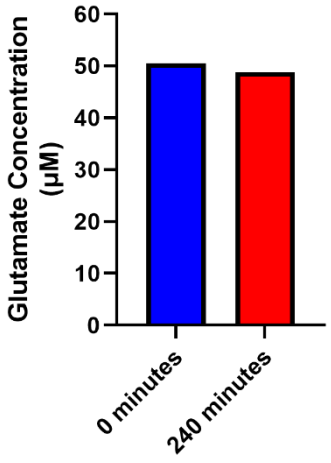

Figure A2: Glutamate does not degrade in Kreb's Ringer solution.

A.3 Genes involved in top ten GO pathway analysis

Description	P-value	Genes
ECM organization	3.38E-18	PDGFA - platelet-derived growth factor alpha polypeptide ADAMTS4 - adam metallopeptidase with thrombospondin type 1 motif, 4 TIMP2 - timp metallopeptidase inhibitor 2 FN1 - fibronectin 1 HAPLN1 - hyaluronan and proteoglycan link protein 1 DDR2 - discoidin domain receptor tyrosine kinase 2 SPP1 - secreted phosphoprotein 1 TLL2 - tolloid-like 2 HAS3 - hyaluronan synthase 3 COL1A2 - collagen, type i, alpha 2 COL3A1 - collagen, type iii, alpha 1 ITGA11 - integrin, alpha 11 CCDC80 - coiled-coil domain containing 80 DCN - decorin

		ADAM8 - adam metallopeptidase domain 8 NR2E1 - nuclear receptor subfamily 2, group e, member 1 CYP1B1 - cytochrome p450, family 1, subfamily b, polypeptide 1 EMILIN1 - elastin microfibril interfacer 1 COL7A1 - collagen, type vii, alpha 1 MMP7 - matrix metallopeptidase 7 (matrilysin, uterine) BGN - biglycan TGFBI - transforming growth factor, beta-induced, 68kda OLFML2A - olfactomedin-like 2a LAMC2 - laminin, gamma 2 COL6A3 - collagen, type vi, alpha 3 COL9A3 - collagen, type ix, alpha 3 COL8A2 - collagen, type viii, alpha 2 COL4A5 - collagen, type iv, alpha 5 FLRT2 - fibronectin leucine rich transmembrane protein 2 NTNG1 - netrin g1 MMP14 - matrix metallopeptidase 14 (membrane-inserted) COL4A6 - collagen, type iv, alpha 6 COL5A1 - collagen, type v, alpha 1 SULF2 - sulfatase 2 BCAN - brevican COL12A1 - collagen, type xii, alpha 1 FBN1 - fibrillin 1 VCAN - versican LAMA3 - laminin, alpha 3 COL27A1 - collagen, type xxvii, alpha 1 NCAN - neurocan COL10A1 - collagen, type x, alpha 1 COL16A1 - collagen, type xvi, alpha 1 POSTN - periostin, osteoblast specific factor

		COL15A1 - collagen, type xv, alpha 1 THSD4 - thrombospondin, type i, domain containing 4
anatomical structure development	2.2E-16	IFITM5 - interferon induced transmembrane protein 5 GFRA1 - gdnf family receptor alpha 1 CASZ1 - castor zinc finger 1 FN1 - fibronectin 1 GFRA2 - gdnf family receptor alpha 2 HSF4 - heat shock transcription factor 4 MITF - microphthalmia-associated transcription factor GDF10 - growth differentiation factor 10 PAX3 - paired box 3 SPP1 - secreted phosphoprotein 1 POU6F2 - pou class 6 homeobox 2 SPEG - speg complex locus NAIP - nlr family, apoptosis inhibitory protein INHBA - inhibin, beta a DCT - dopachrome tautomerase NRN1 - neuritin 1 RCN3 - reticulocalbin 3, ef-hand calcium binding domain DCN - decorin EN2 - engrailed homeobox 2 ENG - endoglin CTTNBP2 - cortactin binding protein 2 BGN - biglycan TENM1 - teneurin transmembrane protein 1 WISP1 - wnt1 inducible signaling pathway protein 1 CPS1 - carbamoyl-phosphate synthase 1, mitochondrial HPRT1 - hypoxanthine phosphoribosyltransferase 1 CLDN3 - claudin 3 MMP14 - matrix metallopeptidase 14 (membrane-

		inserted) ACRV1 - acrosomal vesicle protein 1 TMEM132E - transmembrane protein 132e GDF6 - growth differentiation factor 6 CYTL1 - cytokine-like 1 CRH - corticotropin releasing hormone JPH1 - junctophilin 1 RGS4 - regulator of g-protein signaling 4 CALCRL - calcitonin receptor-like MICALCL - mical c-terminal like IL7R - interleukin 7 receptor POSTN - periostin, osteoblast specific factor PAQR5 - progestin and adipoq receptor family member v AQP2 - aquaporin 2 (collecting duct) PDGFA - platelet-derived growth factor alpha polypeptide ADAMTS4 - adam metallopeptidase with thrombospondin type 1 motif, 4 NEBL - nebulette FGF13 - fibroblast growth factor 13 PAX8 - paired box 8 TSPEAR - thrombospondin-type laminin g domain and ear repeats DDR2 - discoidin domain receptor tyrosine kinase 2 SPHK1 - sphingosine kinase 1 FGF5 - fibroblast growth factor 5 FGF7 - fibroblast growth factor 7 NTRK2 - neurotrophic tyrosine kinase, receptor, type 2 COL1A2 - collagen, type i, alpha 2 CA2 - carbonic anhydrase ii POU3F4 - pou class 3 homeobox 4 COL3A1 - collagen, type iii, alpha 1 CDSN - corneodesmosin MEF2C - myocyte enhancer factor 2c

		EDIL3 - egf-like repeats and discoidin i-like domains 3 SCN5A - sodium channel, voltage-gated, type v, alpha subunit EGF - epidermal growth factor CYP1B1 - cytochrome p450, family 1, subfamily b, polypeptide 1 BARX1 - barx homeobox 1 CNTN1 - contactin 1 AMIGO2 - adhesion molecule with ig-like domain 2 COL7A1 - collagen, type vii, alpha 1 COL6A3 - collagen, type vi, alpha 3 LAMC2 - laminin, gamma 2 COL9A3 - collagen, type ix, alpha 3 UNC5C - unc-5 homolog c (c. elegans) EBF1 - early b-cell factor 1 ADCYAP1 - adenylate cyclase activating polypeptide 1 (pituitary) OSGIN1 - oxidative stress induced growth inhibitor 1 PCSK2 - proprotein convertase subtilisin/kexin type 2 ASS1 - argininosuccinate synthase 1 SLC25A27 - solute carrier family 25, member 27 TBX1 - t-box 1 SNAI2 - snail family zinc finger 2 COL5A1 - collagen, type v, alpha 1 SULF2 - sulfatase 2 EDNRA - endothelin receptor type a IRX5 - iroquois homeobox 5 STC2 - stanniocalcin 2 DAB2 - dab, mitogen-responsive phosphoprotein, homolog 2 (drosophila) ZIC4 - zic family member 4 COL27A1 - collagen, type xxvii, alpha 1 FBN1 - fibrillin 1

		LAMA3 - laminin, alpha 3 COL10A1 - collagen, type x, alpha 1 COLEC11 - collectin sub-family member 11 NRCAM - neuronal cell adhesion molecule NR2E3 - nuclear receptor subfamily 2, group e, member 3 PCDHA11 - protocadherin alpha 11 PCDHA10 - protocadherin alpha 10 TIMP2 - timp metallopeptidase inhibitor 2 MAL - mal, t-cell differentiation protein PCDHA6 - protocadherin alpha 6 PCDHA5 - protocadherin alpha 5 PGM5 - phosphoglucomutase 5 PCDHA4 - protocadherin alpha 4 WDR72 - wd repeat domain 72 PCDHA3 - protocadherin alpha 3 NKX2-5 - nk2 homeobox 5 CHST2 - carbohydrate (n-acetylglucosamine-6-o) sulfotransferase 2 TMEM119 - transmembrane protein 119 HILS1 - histone linker h1 domain, spermatid-specific 1, pseudogene WNT10B - wingless-type mmtv integration site family, member 10b HLA-DRB1 - major histocompatibility complex, class ii, dr beta 1 NOV - nephroblastoma overexpressed CLMP - cxadr-like membrane protein TLL2 - tolloid-like 2 INA - internexin neuronal intermediate filament protein, alpha HLF - hepatic leukemia factor TLR4 - toll-like receptor 4 CHL1 - cell adhesion molecule l1-like NR2E1 - nuclear receptor subfamily 2, group e, member 1

		VDR - vitamin d (1,25- dihydroxyvitamin d3) receptor MXRA8 - matrix-remodelling associated 8 CALB1 - calbindin 1, 28kda NGFR - nerve growth factor receptor NTNG1 - netrin g1 IRX2 - iroquois homeobox 2 PCDHB15 - protocadherin beta 15 EXTL1 - exostosin-like glycosyltransferase 1 CREB3L1 - camp responsive element binding protein 3-like 1 NRG1 - neuregulin 1 DSP - desmoplakin NKX2-2 - nk2 homeobox 2 XYLT1 - xylosyltransferase i VAMP5 - vesicle-associated membrane protein 5 DDX39B - dead (asp-glu-ala-asp) box polypeptide 39b ATP8B1 - atpase, aminophospholipid transporter, class i, type 8b, member 1 TEK - tek tyrosine kinase, endothelial TSHZ3 - teashirt zinc finger homeobox 3 PAPSS2 - 3'-phosphoadenosine 5'-phosphosulfate synthase 2 OSR1 - odd-skipped related 1 (drosophila) TDRD6 - tudor domain containing 6 HAPLN1 - hyaluronan and proteoglycan link protein 1 EYA4 - eyes absent homolog 4 (drosophila) TFAP2B - transcription factor ap-2 beta (activating enhancer binding protein 2 beta) CHRDL1 - chordin-like 1 MICAL2 - microtubule associated monooxygenase, calponin and lim domain containing 2 ERG - v-ets avian erythroblastosis virus e26 oncogene homolog

		NR2F2 - nuclear receptor subfamily 2, group f, member 2 LYN - v-yes-1 yamaguchi sarcoma viral related oncogene homolog NR2F1 - nuclear receptor subfamily 2, group f, member 1 ITGA11 - integrin, alpha 11 SSTR3 - somatostatin receptor 3 DAAM2 - dishevelled associated activator of morphogenesis 2 AMBN - ameloblastin (enamel matrix protein) NFATC2 - nuclear factor of activated t-cells, cytoplasmic, calcineurin-dependent 2 FOXD3 - forkhead box d3 HNMT - histamine n-methyltransferase IGF1 - insulin-like growth factor 1 (somatomedin c) SEMA7A - semaphorin 7a, gpi membrane anchor (john milton hagen blood group) SOHLH2 - spermatogenesis and oogenesis specific basic helix-loop-helix 2 KLF4 - kruppel-like factor 4 (gut) EPHA7 - eph receptor a7 BCAN - brevican POTEE - pote ankyrin domain family, member e SGCA - sarcoglycan, alpha (50kda dystrophin-associated glycoprotein) EPHB6 - eph receptor b6 PLXDC1 - plexin domain containing 1 SGCD - sarcoglycan, delta (35kda dystrophin-associated glycoprotein) ERBB3 - v-erb-b2 avian erythroblastic leukemia viral oncogene homolog 3 ERBB4 - v-erb-b2 avian erythroblastic leukemia viral oncogene homolog 4 HMOX1 - heme oxygenase (decycling) 1 VCAN - versican

		NCAN - neurocan HMX1 - h6 family homeobox 1
extracellular structure organization	6.84E-16	PDGFA - platelet-derived growth factor alpha polypeptide ADAMTS4 - adam metallopeptidase with thrombospondin type 1 motif, 4 TIMP2 - timp metallopeptidase inhibitor 2 FN1 - fibronectin 1 HAPLN1 - hyaluronan and proteoglycan link protein 1 DDR2 - discoidin domain receptor tyrosine kinase 2 SPP1 - secreted phosphoprotein 1 TLL2 - tolloid-like 2 HAS3 - hyaluronan synthase 3 COL1A2 - collagen, type i, alpha 2 COL3A1 - collagen, type iii, alpha 1 CCDC80 - coiled-coil domain containing 80 ITGA11 - integrin, alpha 11 DCN - decorin ADAM8 - adam metallopeptidase domain 8 NR2E1 - nuclear receptor subfamily 2, group e, member 1 CYP1B1 - cytochrome p450, family 1, subfamily b, polypeptide 1 EMILIN1 - elastin microfibril interfacer 1 COL7A1 - collagen, type vii, alpha 1 BGN - biglycan MMP7 - matrix metallopeptidase 7 (matrilysin, uterine) TGFBI - transforming growth factor, beta-induced, 68kda OLFML2A - olfactomedin-like 2a LAMC2 - laminin, gamma 2 COL6A3 - collagen, type vi, alpha 3 COL9A3 - collagen, type ix, alpha 3 COL8A2 - collagen, type viii, alpha 2

		COL4A5 - collagen, type iv, alpha 5 FLRT2 - fibronectin leucine rich transmembrane protein 2 NTNG1 - netrin g1 MMP14 - matrix metallopeptidase 14 (membrane-inserted) COL4A6 - collagen, type iv, alpha 6 COL5A1 - collagen, type v, alpha 1 SULF2 - sulfatase 2 BCAN - brevican COL12A1 - collagen, type xii, alpha 1 FBN1 - fibrillin 1 LAMA3 - laminin, alpha 3 COL27A1 - collagen, type xxvii, alpha 1 VCAN - versican NCAN - neurocan COL10A1 - collagen, type x, alpha 1 COL16A1 - collagen, type xvi, alpha 1 POSTN - periostin, osteoblast specific factor COL15A1 - collagen, type xv, alpha 1 THSD4 - thrombospondin, type i, domain containing 4
cell adhesion	8.15E-13	PCDHA11 - protocadherin alpha 11 PCDHA10 - protocadherin alpha 10 NCAM2 - neural cell adhesion molecule 2 PCDHA6 - protocadherin alpha 6 PCDHA5 - protocadherin alpha 5 PGM5 - phosphoglucomutase 5 FN1 - fibronectin 1 PCDHA4 - protocadherin alpha 4 PCDHA3 - protocadherin alpha 3 SPP1 - secreted phosphoprotein 1 NOV - nephroblastoma overexpressed PLXNB3 - plexin b3 LRFN5 - leucine rich repeat and fibronectin type iii domain containing 5

		CHL1 - cell adhesion molecule l1-like EMILIN1 - elastin microfibril interfacer 1 ROBO3 - roundabout, axon guidance receptor, homolog 3 (drosophila) ENG - endoglin MXRA8 - matrix-remodelling associated 8 PCDHGA10 - protocadherin gamma subfamily a, 10 PCDH10 - protocadherin 10 TENM1 - teneurin transmembrane protein 1 WISP1 - wnt1 inducible signaling pathway protein 1 FLRT2 - fibronectin leucine rich transmembrane protein 2 CLDN3 - claudin 3 NTNG1 - netrin g1 PCDHB15 - protocadherin beta 15 CLDN2 - claudin 2 DSP - desmoplakin RAC2 - ras-related c3 botulinum toxin substrate 2 (rho family, small gtp binding protein rac2) POSTN - periostin, osteoblast specific factor TEK - tek tyrosine kinase, endothelial NLGN4Y - neuroligin 4, y-linked HAPLN1 - hyaluronan and proteoglycan link protein 1 DDR2 - discoidin domain receptor tyrosine kinase 2 MYBPC1 - myosin binding protein c, slow type PCDHGC4 - protocadherin gamma subfamily c, 4 COL3A1 - collagen, type iii, alpha 1 CDSN - corneodesmosin PCDHGB7 - protocadherin gamma subfamily b, 7 EDIL3 - egf-like repeats and discoidin i-like domains 3 ADAM8 - adam metallopeptidase domain 8 SSPN - sarcospan ITGA11 - integrin, alpha 11

		PCDHGB5 - protocadherin gamma subfamily b, 5 AMBN - ameloblastin (enamel matrix protein) CYP1B1 - cytochrome p450, family 1, subfamily b, polypeptide 1 EMB - embigin CNTN1 - contactin 1 AMIGO2 - adhesion molecule with ig-like domain 2 COL7A1 - collagen, type vii, alpha 1 TGFBI - transforming growth factor, beta-induced, 68kda COL6A3 - collagen, type vi, alpha 3 LAMC2 - laminin, gamma 2 COL8A2 - collagen, type viii, alpha 2 HMCN1 - hemicentin 1 COL4A6 - collagen, type iv, alpha 6 COL5A1 - collagen, type v, alpha 1 BCAN - brevican THBS2 - thrombospondin 2 COL12A1 - collagen, type xii, alpha 1 FBN1 - fibrillin 1 LAMA3 - laminin, alpha 3 VCAN - versican NCAN - neurocan COL16A1 - collagen, type xvi, alpha 1 COL15A1 - collagen, type xv, alpha 1 NRCAM - neuronal cell adhesion molecule
biological adhesion	1.11E-12	PCDHA11 - protocadherin alpha 11 PCDHA10 - protocadherin alpha 10 NCAM2 - neural cell adhesion molecule 2 PCDHA6 - protocadherin alpha 6 PCDHA5 - protocadherin alpha 5 PGM5 - phosphoglucomutase 5 FN1 - fibronectin 1 PCDHA4 - protocadherin alpha 4 PCDHA3 - protocadherin alpha 3 SPP1 - secreted phosphoprotein 1

		NOV - nephroblastoma overexpressed PLXNB3 - plexin b3 LRFN5 - leucine rich repeat and fibronectin type iii domain containing 5 CHL1 - cell adhesion molecule l1-like EMILIN1 - elastin microfibril interfacer 1 ROBO3 - roundabout, axon guidance receptor, homolog 3 (drosophila) ENG - endoglin MXRA8 - matrix-remodelling associated 8 PCDHGA10 - protocadherin gamma subfamily a, 10 PCDH10 - protocadherin 10 TENM1 - teneurin transmembrane protein 1 WISP1 - wnt1 inducible signaling pathway protein 1 FLRT2 - fibronectin leucine rich transmembrane protein 2 CLDN3 - claudin 3 NTNG1 - netrin g1 PCDHB15 - protocadherin beta 15 CLDN2 - claudin 2 DSP - desmoplakin RAC2 - ras-related c3 botulinum toxin substrate 2 (rho family, small gtp binding protein rac2) POSTN - periostin, osteoblast specific factor TEK - tek tyrosine kinase, endothelial NLGN4Y - neuroligin 4, y-linked HAPLN1 - hyaluronan and proteoglycan link protein 1 DDR2 - discoidin domain receptor tyrosine kinase 2 MYBPC1 - myosin binding protein c, slow type PCDHGC4 - protocadherin gamma subfamily c, 4 COL3A1 - collagen, type iii, alpha 1 CDSN - corneodesmosin PCDHGB7 - protocadherin gamma subfamily b, 7 EDIL3 - egf-like repeats and discoidin i-like

		domains 3 ADAM8 - adam metallopeptidase domain 8 SSPN - sarcospan ITGA11 - integrin, alpha 11 PCDHGB5 - protocadherin gamma subfamily b, 5 AMBN - ameloblastin (enamel matrix protein) CYP1B1 - cytochrome p450, family 1, subfamily b, polypeptide 1 EMB - embigin CNTN1 - contactin 1 AMIGO2 - adhesion molecule with ig-like domain 2 COL7A1 - collagen, type vii, alpha 1 TGFBI - transforming growth factor, beta-induced, 68kda COL6A3 - collagen, type vi, alpha 3 LAMC2 - laminin, gamma 2 COL8A2 - collagen, type viii, alpha 2 HMCN1 - hemicentin 1 COL4A6 - collagen, type iv, alpha 6 COL5A1 - collagen, type v, alpha 1 BCAN - brevican THBS2 - thrombospondin 2 COL12A1 - collagen, type xii, alpha 1 FBN1 - fibrillin 1 LAMA3 - laminin, alpha 3 VCAN - versican NCAN - neurocan COL16A1 - collagen, type xvi, alpha 1 COL15A1 - collagen, type xv, alpha 1 NRCAM - neuronal cell adhesion molecule
system development	1.51E-11	PCDHA11 - protocadherin alpha 11 PCDHA10 - protocadherin alpha 10 MAL - mal, t-cell differentiation protein TIMP2 - timp metallopeptidase inhibitor 2 GFRA1 - gdnf family receptor alpha 1 PCDHA6 - protocadherin alpha 6

		GFRA2 - gdnf family receptor alpha 2 FN1 - fibronectin 1 PCDHA5 - protocadherin alpha 5 PCDHA4 - protocadherin alpha 4 PCDHA3 - protocadherin alpha 3 NKX2-5 - nk2 homeobox 5 GDF10 - growth differentiation factor 10 PAX3 - paired box 3 POU6F2 - pou class 6 homeobox 2 NAIP - nlr family, apoptosis inhibitory protein INHBA - inhibin, beta a NRN1 - neuritin 1 NR2E1 - nuclear receptor subfamily 2, group e, member 1 TENM1 - teneurin transmembrane protein 1 NGFR - nerve growth factor receptor MMP14 - matrix metallopeptidase 14 (membrane-inserted) PCDHB15 - protocadherin beta 15 EXTL1 - exostosin-like glycosyltransferase 1 NRG1 - neuregulin 1 XYLT1 - xylosyltransferase i TEK - tek tyrosine kinase, endothelial ADAMTS4 - adam metallopeptidase with thrombospondin type 1 motif, 4 OSR1 - odd-skipped related 1 (drosophila) PAPSS2 - 3'-phosphoadenosine 5'-phosphosulfate synthase 2 FGF13 - fibroblast growth factor 13 HAPLN1 - hyaluronan and proteoglycan link protein 1 PAX8 - paired box 8 TFAP2B - transcription factor ap-2 beta (activating enhancer binding protein 2 beta) CHRDL1 - chordin-like 1 FGF5 - fibroblast growth factor 5

		COL1A2 - collagen, type i, alpha 2 MEF2C - myocyte enhancer factor 2c COL3A1 - collagen, type iii, alpha 1 NR2F1 - nuclear receptor subfamily 2, group f, member 1 BARX1 - barx homeobox 1 IGF1 - insulin-like growth factor 1 (somatomedin c) PCSK2 - proprotein convertase subtilisin/kexin type 2 TBX1 - t-box 1 SULF2 - sulfatase 2 BCAN - brevican EDNRA - endothelin receptor type a ERBB3 - v-erb-b2 avian erythroblastic leukemia viral oncogene homolog 3 ERBB4 - v-erb-b2 avian erythroblastic leukemia viral oncogene homolog 4 ZIC4 - zic family member 4 VCAN - versican FBN1 - fibrillin 1 COL10A1 - collagen, type x, alpha 1 NCAN - neurocan NRCAM - neuronal cell adhesion molecule
developmental process	5.76E-11	IFITM5 - interferon induced transmembrane protein 5 GFRA1 - gdnf family receptor alpha 1 HSF4 - heat shock transcription factor 4 GFRA2 - gdnf family receptor alpha 2 CASZ1 - castor zinc finger 1 GDF10 - growth differentiation factor 10 SPP1 - secreted phosphoprotein 1 SPEG - speg complex locus NAIP - nlr family, apoptosis inhibitory protein NRN1 - neuritin 1 EN2 - engrailed homeobox 2 ENG - endoglin

		MDGA2 - mam domain containing glycosylphosphatidylinositol anchor 2 BGN - biglycan TENM1 - teneurin transmembrane protein 1 HPRT1 - hypoxanthine phosphoribosyltransferase 1 CPS1 - carbamoyl-phosphate synthase 1, mitochondrial WISP1 - wnt1 inducible signaling pathway protein 1 CLDN3 - claudin 3 ACRV1 - acrosomal vesicle protein 1 CRH - corticotropin releasing hormone JPH1 - junctophilin 1 RGS4 - regulator of g-protein signaling 4 HOPX - hop homeobox CALCRL - calcitonin receptor-like MICALCL - mical c-terminal like PAQR5 - progestin and adipoq receptor family member v ADAMTS4 - adam metallopeptidase with thrombospondin type 1 motif, 4 TPD52 - tumor protein d52 SPHK1 - sphingosine kinase 1 CA2 - carbonic anhydrase ii COL1A2 - collagen, type i, alpha 2 COL3A1 - collagen, type iii, alpha 1 POU3F4 - pou class 3 homeobox 4 EDIL3 - egf-like repeats and discoidin i-like domains 3 ADAM8 - adam metallopeptidase domain 8 EGF - epidermal growth factor CNTN1 - contactin 1 COL7A1 - collagen, type vii, alpha 1 COL6A3 - collagen, type vi, alpha 3 LAMC2 - laminin, gamma 2 COL9A3 - collagen, type ix, alpha 3

		COL8A2 - collagen, type viii, alpha 2 EBF1 - early b-cell factor 1 ADCYAP1 - adenylate cyclase activating polypeptide 1 (pituitary) OSGIN1 - oxidative stress induced growth inhibitor 1 SLC25A27 - solute carrier family 25, member 27 COL5A1 - collagen, type v, alpha 1 SNAI2 - snail family zinc finger 2 EDNRA - endothelin receptor type a IRX5 - iroquois homeobox 5 COL12A1 - collagen, type xii, alpha 1 COL27A1 - collagen, type xxvii, alpha 1 LAMA3 - laminin, alpha 3 COL10A1 - collagen, type x, alpha 1 COLEC11 - collectin sub-family member 11 COL15A1 - collagen, type xv, alpha 1 NR2E3 - nuclear receptor subfamily 2, group e, member 3 WDR72 - wd repeat domain 72 NKX2-5 - nk2 homeobox 5 CHST2 - carbohydrate (n-acetylglucosamine-6-o) sulfotransferase 2 ADRB2 - adrenoceptor beta 2, surface HILS1 - histone linker h1 domain, spermatid-specific 1, pseudogene HLA-DRB1 - major histocompatibility complex, class ii, dr beta 1 CLMP - cxadr-like membrane protein HLF - hepatic leukemia factor TRNP1 - tmf1-regulated nuclear protein 1 EMILIN1 - elastin microfibril interfacer 1 CALB1 - calbindin 1, 28kda VDR - vitamin d (1,25- dihydroxyvitamin d3) receptor VEGFC - vascular endothelial growth factor c

		FLRT2 - fibronectin leucine rich transmembrane protein 2 EXTL1 - exostosin-like glycosyltransferase 1 FMNL3 - formin-like 3 CREB3L1 - camp responsive element binding protein 3-like 1 NRG1 - neuregulin 1 CAMK4 - calcium/calmodulin-dependent protein kinase iv DDX39B - dead (asp-glu-ala-asp) box polypeptide 39b EYA4 - eyes absent homolog 4 (drosophila) HAPLN1 - hyaluronan and proteoglycan link protein 1 SLFN5 - schlafen family member 5 TTC39C - tetratricopeptide repeat domain 39c CHRDL1 - chordin-like 1 ERG - v-ets avian erythroblastosis virus e26 oncogene homolog JAK3 - janus kinase 3 SSTR3 - somatostatin receptor 3 AMBN - ameloblastin (enamel matrix protein) ALX1 - alx homeobox 1 HNMT - histamine n-methyltransferase SOHLH2 - spermatogenesis and oogenesis specific basic helix-loop-helix 2 EPHA7 - eph receptor a7 KLF4 - kruppel-like factor 4 (gut) BCAN - brevican EPHB6 - eph receptor b6 PLXDC1 - plexin domain containing 1 ERBB3 - v-erb-b2 avian erythroblastic leukemia viral oncogene homolog 3 CSPG4 - chondroitin sulfate proteoglycan 4 HMOX1 - heme oxygenase (decycling) 1 ERBB4 - v-erb-b2 avian erythroblastic leukemia

		viral oncogene homolog 4 VCAN - versican NCAN - neurocan HMX1 - h6 family homeobox 1 ANK3 - ankyrin 3, node of ranvier (ankyrin g) FN1 - fibronectin 1 MITF - microphthalmia-associated transcription factor PAX3 - paired box 3 POU6F2 - pou class 6 homeobox 2 ATP11C - atpase, class vi, type 11c INHBA - inhibin, beta a DCT - dopachrome tautomerase DCN - decorin RCN3 - reticulocalbin 3, ef-hand calcium binding domain RRP7A - ribosomal rna processing 7 homolog a (s. cerevisiae) CTTNBP2 - cortactin binding protein 2 MMP7 - matrix metallopeptidase 7 (matrilysin, uterine) MMP14 - matrix metallopeptidase 14 (membrane-inserted) TMEM132E - transmembrane protein 132e CYTL1 - cytokine-like 1 GDF6 - growth differentiation factor 6 IL7R - interleukin 7 receptor POSTN - periostin, osteoblast specific factor AQP2 - aquaporin 2 (collecting duct) PPARGC1B - peroxisome proliferator-activated receptor gamma, coactivator 1 beta PDGFA - platelet-derived growth factor alpha polypeptide NEBL - nebulette ERMN - ermin, erm-like protein FGF13 - fibroblast growth factor 13

		PAX8 - paired box 8 TSPEAR - thrombospondin-type laminin g domain and ear repeats DDR2 - discoidin domain receptor tyrosine kinase 2 FGF5 - fibroblast growth factor 5 FGF7 - fibroblast growth factor 7 NTRK2 - neurotrophic tyrosine kinase, receptor, type 2 CDSN - corneodesmosin MEF2C - myocyte enhancer factor 2c SCN5A - sodium channel, voltage-gated, type v, alpha subunit CYP1B1 - cytochrome p450, family 1, subfamily b, polypeptide 1 BARX1 - barx homeobox 1 AMIGO2 - adhesion molecule with ig-like domain 2 TBX15 - t-box 15 UNC5C - unc-5 homolog c (c. elegans) PCSK2 - proprotein convertase subtilisin/kexin type 2 HHIP - hedgehog interacting protein ASS1 - argininosuccinate synthase 1 TBX1 - t-box 1 SULF2 - sulfatase 2 DAB2 - dab, mitogen-responsive phosphoprotein, homolog 2 (drosophila) STC2 - stanniocalcin 2 UNC5B - unc-5 homolog b (c. elegans) ZIC4 - zic family member 4 FBN1 - fibrillin 1 NRCAM - neuronal cell adhesion molecule PCDHA11 - protocadherin alpha 11 PCDHA10 - protocadherin alpha 10 MAL - mal, t-cell differentiation protein TIMP2 - timp metallopeptidase inhibitor 2 CHRNA7 - cholinergic receptor, nicotinic, alpha 7

		(neuronal) PCDHA6 - protocadherin alpha 6 PGM5 - phosphoglucomutase 5 PCDHA5 - protocadherin alpha 5 PCDHA4 - protocadherin alpha 4 PCDHA3 - protocadherin alpha 3 TMEM119 - transmembrane protein 119 NOV - nephroblastoma overexpressed WNT10B - wingless-type mmtv integration site family, member 10b ARHGAP24 - rho gtpase activating protein 24 TLL2 - tolloid-like 2 INA - internexin neuronal intermediate filament protein, alpha CHL1 - cell adhesion molecule l1-like TLR4 - toll-like receptor 4 MOSPD1 - motile sperm domain containing 1 NR2E1 - nuclear receptor subfamily 2, group e, member 1 MXRA8 - matrix-remodelling associated 8 NGFR - nerve growth factor receptor RHCG - rh family, c glycoprotein NTNG1 - netrin g1 IRX2 - iroquois homeobox 2 PCDHB15 - protocadherin beta 15 DSP - desmoplakin NKX2-2 - nk2 homeobox 2 XYLT1 - xylosyltransferase i VAMP5 - vesicle-associated membrane protein 5 ATP8B1 - atpase, aminophospholipid transporter, class i, type 8b, member 1 TSHZ3 - teashirt zinc finger homeobox 3 TEK - tek tyrosine kinase, endothelial PAPSS2 - 3'-phosphoadenosine 5'-phosphosulfate synthase 2 OSR1 - odd-skipped related 1 (drosophila)

		TDRD6 - tudor domain containing 6 TFAP2B - transcription factor ap-2 beta (activating enhancer binding protein 2 beta) MICAL2 - microtubule associated monooxygenase, calponin and lim domain containing 2 NR2F2 - nuclear receptor subfamily 2, group f, member 2 LYN - v-yes-1 yamaguchi sarcoma viral related oncogene homolog ITGA11 - integrin, alpha 11 NR2F1 - nuclear receptor subfamily 2, group f, member 1 ST3GAL1 - st3 beta-galactoside alpha-2,3-sialyltransferase 1 DAAM2 - dishevelled associated activator of morphogenesis 2 NFATC2 - nuclear factor of activated t-cells, cytoplasmic, calcineurin-dependent 2 FOXD3 - forkhead box d3 TGFBI - transforming growth factor, beta-induced, 68kda RBM47 - rna binding motif protein 47 IGF1 - insulin-like growth factor 1 (somatomedin c) SEMA7A - semaphorin 7a, gpi membrane anchor (john milton hagen blood group) POTEE - pote ankyrin domain family, member e SGCA - sarcoglycan, alpha (50kda dystrophin-associated glycoprotein) SGCD - sarcoglycan, delta (35kda dystrophin-associated glycoprotein)
chondroitin sulfate biosynthetic process	8.02E-10	BCAN - brevican BGN - biglycan CHSY3 - chondroitin sulfate synthase 3 DCN - decorin CSPG4 - chondroitin sulfate proteoglycan 4 CHST9 - carbohydrate (n-acetylgalactosamine 4-0)

		sulfotransferase 9 XYLT1 - xylosyltransferase i VCAN - versican NCAN - neurocan DSE - dermatan sulfate epimerase
tissue development	4.11E-9	IFITM5 - interferon induced transmembrane protein 5 OSR1 - odd-skipped related 1 (drosophila) PGM5 - phosphoglucomutase 5 WDR72 - wd repeat domain 72 PAX8 - paired box 8 TSPEAR - thrombospondin-type laminin g domain and ear repeats NKX2-5 - nk2 homeobox 5 TMEM119 - transmembrane protein 119 DDR2 - discoidin domain receptor tyrosine kinase 2 TFAP2B - transcription factor ap-2 beta (activating enhancer binding protein 2 beta) SPP1 - secreted phosphoprotein 1 FGF7 - fibroblast growth factor 7 NOV - nephroblastoma overexpressed HLA-DRB1 - major histocompatibility complex, class ii, dr beta 1 NR2F2 - nuclear receptor subfamily 2, group f, member 2 DCT - dopachrome tautomerase COL1A2 - collagen, type i, alpha 2 CDSN - corneodesmosin MEF2C - myocyte enhancer factor 2c RCN3 - reticulocalbin 3, ef-hand calcium binding domain DCN - decorin AMBN - ameloblastin (enamel matrix protein) CYP1B1 - cytochrome p450, family 1, subfamily b, polypeptide 1 ENG - endoglin

		VDR - vitamin d (1,25- dihydroxyvitamin d3) receptor CALB1 - calbindin 1, 28kda COL7A1 - collagen, type vii, alpha 1 LAMC2 - laminin, gamma 2 IGF1 - insulin-like growth factor 1 (somatomedin c) UNC5C - unc-5 homolog c (c. elegans) NTNG1 - netrin g1 TBX1 - t-box 1 COL5A1 - collagen, type v, alpha 1 SNAI2 - snail family zinc finger 2 SGCA - sarcoglycan, alpha (50kda dystrophin-associated glycoprotein) STC2 - stanniocalcin 2 SGCD - sarcoglycan, delta (35kda dystrophin-associated glycoprotein) DSP - desmoplakin RGS4 - regulator of g-protein signaling 4 ERBB3 - v-erb-b2 avian erythroblastic leukemia viral oncogene homolog 3 ERBB4 - v-erb-b2 avian erythroblastic leukemia viral oncogene homolog 4 LAMA3 - laminin, alpha 3 VAMP5 - vesicle-associated membrane protein 5 POSTN - periostin, osteoblast specific factor
dermatan sulfate biosynthetic process	1.11E-8	BGN - biglycan BCAN - brevican DCN - decorin CSPG4 - chondroitin sulfate proteoglycan 4 VCAN - versican NCAN - neurocan DSE - dermatan sulfate epimerase

Table A1: Table displaying top ten GO pathways.

HipSci Only	RTT#27 Only
ZNF558	HLA-DQB1
MIR4458HG	HLA-DQA1
ZNF680	WT1
LINC02864	SULT1E1
nan	FAM218A
PAX7	AVPR1A
ZNF736	KIF25-AS1
DEFB115	nan
nan	nan
ALX1	nan
ERG	nan
nan	nan
MIR199A2	LY6K
HBB	GJB6
PTGS2	CSF3
nan	LINC00689
LINC02381	PROKR2
S100A9	IL6-AS1
MPEG1	NLRP11
nan	APOH
S100A8	TNMD
nan	nan
LILRB2	nan
nan	nan
FCGR3B	GAST
KCNC2	CYP4F30P
nan	POU4F2
CCR2	nan
nan	AMHR2
CLEC7A	LRCOL1
KRT79	HBZ
HOXB13	MT1M
PSG4	RFPL4A
PSORS1C2	STX19

ENTPD1-AS1	LINC00578
nan	MIR576
CCDC140	nan
IL2RG	LINC01845
CSF3R	PGC
nan	SPATS1
TUBA3E	LINC02532
SCML4	nan
GIMAP4	AL359313.1
nan	PON1
MIR9-1	KCNS2
CD48	nan
MILR1	nan
BPI	FAM223B
NCF4	nan
CCL28	OR2W3
CD52	nan
OR2L13	nan
TCERG1L	SFTPA1
nan	PRLHR
MS4A14	nan
CCR7	ELF5
PRAC2	CARD17
APBB1IP	HTR3A
JAML	FGF6
AC114689.3	nan
COL11A2	TAS2R43
MLN	nan
BLK	GSX1
DMRT2	COX8C
MIR214	SNORD18A
nan	nan
ASCL3	HSD17B2
CD5	SCIMP
CLEC4E	MIR142

HCAR2	ABCA9
RNASE1	nan
nan	NLRP12
C16orf54	RAB6C-AS1
CD300E	nan
CXCR2	AGXT
SAMSN1	COL6A4P1
SAMSN1	LINC00870
BHMT2	RHO
nan	NKX1-1
SLC25A48-AS1	nan
CDX1	nan
nan	nan
nan	H3C1
TAC1	PACRG-AS3
nan	nan
EZHIP	ZP3
nan	MIR2052HG
PKLR	MAGEC1
nan	FLG-AS1
PGA5	AQP10
nan	LY9
SNORD115-21	nan
nan	nan
LHX1	IL2RA
nan	LINC00840
nan	nan
nan	nan
LILRB1	F2
EGR4	MS4A12
MIR2355	TSPAN8
CCR5	IL31
SLC66A1L	nan

nan	nan
nan	nan
TRG-AS1	ACOT6
PIK3CG	nan
DEFA3	EXOC3L4
C8orf87	EXD1
MIR1302-9	nan
FAM205A	PRSS41
nan	HS3ST2
RNF186	MT1G
TAL1	nan
TMEM61	PRAC1
AMY1C	CA10
NHLH2	LPO
NPR1	GCGR
nan	LINC01539
LINC02817	THEG
ANKRD22	PRSS57
TLX1	IL12RB1
nan	VSTM1
nan	nan
KLRF1	CRYGA
SLC15A5	NMUR1
MIR148B	RAD21L1
SNORD115-26	WFDC12
nan	TFF3
TBC1D28	nan
MIR2909	GGTLC2
CFAP97D1	MIR3135A
FADS6	MIR564
CIDEA	MIR191
VAV1	IHO1
SIGLEC9	nan
nan	nan

APOL5	TMEM14EP
nan	ADIPOQ
PDCL2	nan
POU5F2	SLIT2-IT1
SLC6A7	LINC00575
LY86	MEPE
GSTA2	MIR578
FRMD1	UGT3A2
nan	ZNF366
GIMAP1	SNORA74A
nan	NMUR2
LINC00964	AC034199.1
nan	nan
nan	ZNRD1ASP
nan	PPP1R10
ACTL7B	IL17F
MIR32	SLC22A16
CSAG1	nan
FAM41C	TRGC1
TMCO2	nan
LDLRAD1	nan
LEXM	CPA1
nan	NKX6-3
CHIAP2	DKK4
nan	IFNB1
nan	RNF183
LCE1E	nan
S100A12	SCARNA9
FCRLA	SCARNA9
TDRD5	MAGEB6
OR2L2	DUSP21
nan	XPNPEP2
MRLN	GPR119
MUC15	MIR450A1
MS4A2	AC235097.1

MS4A6A	PASD1
ACTN3	HJV
SLCO2B1	FMO6P
nan	PIGR
MIR34B	nan
CD3E	nan
CLEC6A	AKR1C4
MIR1244-3	PTF1A
ADAMTS20	nan
TESPA1	IFIT1B
LINC02408	CYP2C18
HCAR3	GPR26
RNASE8	C11orf86
GPR65	GPR152
nan	MIR548K
nan	TRIM49
FAM30A	PGR
SNORD115-4	HTR3B
nan	APOA5
TNP2	CD3D
LINC01567	FOXR1
nan	nan
ITGAD	KCNJ1
DPEP2	NANOG
P2RX1	nan
CLEC10A	KRT6A
TBC1D29P	KRT1
nan	MIR548C
SLFN12L	SNORA70G
GPR142	DAO
CD300LB	CCDC63
nan	nan
MIR3189	LINC02347
VSTM2B	LINC00543
FFAR2	TNFSF11

NCCRP1	C13orf42
GPR4	LMO7DN
SIGLEC6	LINC00410
MIRLET7E	RNF113B
LILRA2	nan
FCAR	ADCY4
nan	GZMB
nan	LINC00520
NOTO	TMEM30B
MIR128-1	GPHB5
NEUROD1	nan
CRYGD	nan
nan	HIGD2B
nan	REC114
OR6B3	nan
FAM240C	nan
SIRPB2	nan
THBD	WASIR2
CD93	nan
MIR644A	TPSB2
SPINT4	TNFRSF17
PELATON	nan
TEKT4P2	CES5A
TEKT4P2	CDH16
nan	ADAD2
nan	MIR744
PIWIL3	nan
nan	SEBOX
LTF	MIR632
PLA1A	SLFN14
LRRIQ4	STH
GMNC	MIR548D2
TMPRSS11F	OTOP3
ENAM	CTAGE1
F11	nan

nan	ELOA2
H2BC14	MIR122
GLP1R	ARRDC5
nan	ACER1
nan	nan
nan	MIR199A1
RFX6	CYP4F12
nan	SLC5A5
NOX3	COX7A1
PLG	ZIM2
PAPOLB	LINC01185
nan	NAT8B
HECW1-IT1	MIR3127
RAMP3	nan
nan	nan
ZNF804B	LINC01854
LHFPL3-AS1	XIRP2
AKR1B15	nan
GIMAP8	MIR561
GIMAP7	FAM237A
DEFB109B	VWC2L
PRR23D1	PRKAG3
MIR1206	CRYBA2
nan	MOGAT1
nan	ALPP
nan	NCOR1P1
OR1L8	nan
nan	WFDC10B
TLR8	SNORA80A
nan	nan
LUZP4	nan
nan	nan
AVPR2	nan
MIR4252	GADL1
C1orf127	nan

nan	CCK
C1QA	CCR3
C1QC	CD200R1L
nan	H1-8
GJB4	AADACP1
GUCA2A	PTTG2
C8A	AC124017.1
C1orf141	EXOC1L
ADORA3	nan
nan	SULT1B1
nan	C4orf17
PPIAL4C	TNIP3
TDRD10	nan
CD244	APELA
SH2D1B	LINC01098
LRRC52	SLED1
nan	nan
IGFN1	nan
LAD1	nan
MIR194-1	nan
nan	nan
WNT3A	nan
nan	POU5F1
nan	SAPCD1
ST8SIA6-AS1	HSPA1A
LRIT1	HSPA1B
LIPF	PTCRA
CYP2C9	nan
ACSM6	nan
LINC00866	TAAR3P
NKX2-3	nan
nan	MIR3145
nan	TBXT
MUC2	LINC01558
KRTAP5-6	AGR3

nan	nan
OR52I1	RPL13AP17
OR51I2	WNT2
OR56B4	nan
OR10A3	AOC1
SAA4	HTR5A
SLC6A5	ADAM7
nan	SLURP1
SLC22A11	nan
nan	GLIS3-AS1
PATE2	IFNA14
SENCR	SNORD121A
nan	MIRLET7A1
TAS2R8	nan
TAS2R9	OR13C5
TAS2R13	ASMT
LINC00477	nan
OR10AD1	nan
KRT3	VSIG4
HOTAIR	FAM236A
OR6C3	AL450472.1
nan	ADGRG4
nan	SNORD61
ZAR1L	HSFX1
SLC10A2	MAGEA8
RNASE13	UTY
RNASE7	ONECUT3
nan	LINC01405
nan	ESRG
nan	FAM9C
nan	TPTEP1
LRRC74A	RAET1L
SNORA79	nan
MIR541	nan
LINC00605	HAND1

nan	GUCA1C
nan	AICDA
nan	nan
PWRN2	nan
SNORD115-20	GOLT1A
SNORD115-34	DUSP29
nan	ITPK1-AS1
DUOXA1	KCNG4
nan	POTEI
PPIAP46	DGKK
GOLGA6D	TSIX
nan	CTSE
FAM138E	SNORA49
nan	KRT13
nan	C19orf84
LINC00917	TMEM150B
AC134312.1	NT5DC4
SLC22A31	nan
nan	WFDC13
TEKT1	GPR15
nan	LINC01205
GUCY2D	SOX14
LINC00670	nan
nan	TRIM50
LGALS9C	MIR661
MIR365B	PNLIP
HEATR9	PLCZ1
nan	KRT4
nan	SLC5A8
C17orf64	nan
nan	BICDL2
DNAI2	MT1H
KIF19	SKOR2

nan	nan
nan	IGSF23
TTR	MIR99B
nan	nan
SLC14A1	CROCC2
SIGLEC15	RSPO4
TNFSF14	UPK3A
FCER2	nan
CD209	H4C1
PPAN-P2RY11	PKHD1
SNORD105	nan
MIR639	MIR182
MEF2B	MIR1205
MEF2B	IFNA1
ZNF257	nan
CLC	nan
CEACAM4	OR13H1
nan	AL591893.1
PSG11	POU5F1P4
MIR769	RGSL1
FGF21	IL19
CGB2	nan
nan	nan
SNORD88A	nan
VIT	C10orf99
LINC01121	CALHM3
MIR217	nan
MIR216A	nan
nan	nan
nan	nan
TEKT4	SIX6
SULT1C3	TPSAB1
SULT1C2P1	TRIM72
nan	nan

nan	TNFSF12-TNFSF13
IL36G	ARHGEF15
nan	SERPINB12
LINC01960	F2RL3
nan	nan
nan	PSG9
nan	MIR3190
CPS1-IT1	MIR4261
CXCR1	MYADML
MIR26B	SULT6B1
SNORD82	FOXI3
nan	MIR3133
SLC24A3-AS1	BANF2
MIR1302-5	EPPIN
RIPOR3-AS1	WFDC8
ZNF831	WFDC11
MIRLET7C	nan
nan	TMPRSS3
TMPRSS15	LINC00896
KRTAP26-1	SERPIND1
nan	MIR33A
KRTAP10-2	nan
nan	CIDEC
LINC00316	TMEM30CP
nan	MIR548I1
nan	KCNIP4-IT1
LL22NC01-81G9.3	LINC02232
SERHL	UGT2B17
TTLL8	RFPL4B
DAZL	TCF21
XIRP1	HOXA7
KRBOX1	SPDYE7P

CAMP	nan
MIR1324	FAM83A-AS1
GABRR3	GFI1B
ADGRG7	LCN8
CD86	GLOD5
C3orf22	CACNA1F
nan	SPTA1
KBTBD12	FASLG
LINC01210	LINC00272
GRK7	nan
TMEM212	RHEX
FAM90A26	nan
LINC01097	nan
MUC7	MIR604
PPBP	NPY4R
PDHA2	HPSE2
MIR367	DMBT1L1
LINC02432	VENTX
MIR3139	nan
LINC01095	ODF3
nan	MRGPRG
GZMK	nan
C5orf64-AS1	MIR3165
nan	TRIM29
FAM170A	MIR3167
CTXN3	GDF3
MZB1	TAS2R46
HTR4	MIR614
HAVCR1	PDE6H
C5orf52	HIGD1C
MIR218-2	KRT72
FAM153CP	KRT2
LY86-AS1	HOXC8
H4C6	MYF6
NKAPL	MIR1827

nan	nan
nan	nan
SNHG32	nan
EHMT2	nan
PSMB9	MIR3174
ZBTB22	nan
LINC00336	nan
CLPSL1	SPATA8
nan	MIR3178
nan	nan
TREM2	nan
nan	LINC00919
nan	SNORD111
CRISP3	nan
HCRTR2	ARL5C
TRAPPC3L	TNS4
PBOV1	MIR634
MYCT1	OTOP2
AL109910.1	ENPP7
MACC1	ANKRD30B
MIR1183	DSG1
HOXA1	nan
nan	CYP2F1
VWC2	CEACAM16
nan	C5AR2
ZAN	LIM2
DOCK4-AS1	DCDC2C
PPP1R3A	FAM138B
ANKRD7	nan
STRA8	nan
OR4F21	MIR3128
FAM87A	BOLL
nan	nan
EBF2	OVOL2
ESRP1	nan

GRHL2	MIR941-1
nan	TPTE
FAM138C	nan
nan	nan
nan	Z94160.1
FOXD4L6	WBP2NL
SPATA31D5P	CLRN1
nan	HTR3E
nan	QRFPR
LRRC37A5P	nan
ORM1	nan
OR1J4	nan
OR1B1	nan
OR1L6	BTNL8
MIR199B	nan
LCN1	H4C13
GLT6D1	C2
LHX3	HLA-DPB1
nan	SLC39A7
S100G	CLPSL2
DCAF8L2	PI16
DCAF8L1	PDE10A
PAGE2B	PDE10A
PAGE2	nan
CXorf65	NPVF
MIR545	MIR550A1
ESX1	MIR550A2
SNORD96B	MIR4284
PNMA5	ST7-AS2
CAPSL	AC000124.1
SERPINA11	TSGA13
BARHL2	OR9A2
TBX5	RNY1
CDH19	MIR4286

C6	FAM167A-AS1
nan	nan
LHX5	nan
HLA-DOB	SDR16C5
nan	LINC00968
C8orf89	nan
SERPINA9	nan
MIR133A1	MIR1299
nan	LINC01504
FAM217A	MUSK
PPP1R18	OR1K1
LLCFC1	LCN15
FGL1	SUPT20HL2
NUGGC	H2BW1
MIR1302-10	MIR363
PGBP	MIR19B2
nan	MAGEA4
KCNQ1DN	H2AB1
nan	PCDH11Y
nan	GSTT4
nan	MMP8
PTGDR	GNAT1
NGB	MINDY4B
RNU5A-1	XCL2
SCARNA14	GPHA2
nan	RNU5B-1
SCARNA20	nan
ASTL	nan
nan	CCL11
SEL1L2	nan
FAM230A	UBE2E2-AS1
PRSS50	C9
nan	CFTR
DTHD1	NR0B1

GYPA	GPR101
nan	OPN1LW
nan	C1orf105
MAGEA12	FAM177B
nan	nan
FNDC7	MIR607
LCE1D	FAM24A
RXFP4	FOLR2
FCRL6	C12orf77
FXYD4	HCAR1
RBP4	PITPNM2-AS1
MIR548E	ANHX
nan	nan
CASP12	EPB42
LINC01257	PTX4
MIR15A	MT4
nan	LINC00922
nan	MYH4
nan	YWHAEP7
PHGR1	KRTAP9-8
nan	G6PC
SPESP1	MIR4319
SSTR5-AS1	nan
DPEP3	MIR638
ASGR2	INSL3
nan	PSG7
nan	LILRA4
TBX4	nan
TMEM235	MARCO
C18orf63	HOXD11
MIR27A	nan
VN1R2	nan
nan	SEC14L3
nan	LINC00635

nan	RTP2
C22orf42	LINC00989
IL5RA	MIR1305
nan	nan
nan	SLC36A3
ERC2-IT1	SLC36A2
IBSP	TLX3
ADH1B	nan
FREM3	KAAG1
TRIML2	nan
nan	nan
H2AC7	TRHR
nan	SPINK4
ATP6V1G2	ETDB
MIR1273C	VHLL
nan	APOA2
SEPTIN14	SELP
nan	GPR25
RNF148	nan
CHRM2	nan
CREB3L2-AS1	CR2
MNX1-AS1	FAM71A
nan	MIR1537
nan	nan
ABRA	nan
HPYR1	MIR938
ZFAT-AS1	OPALIN
INSL6	SH3PXD2A-AS1
AL353753.1	PNLIPRP1
nan	PNLIPRP2
VCX3A	MIR4296
LINC01777	MIR4297
REG4	OR52B6

H3C14	AL035078.1
HORMAD1	MYRF-AS1
FCRL2	MIR192
PYHIN1	IL22
PBX1-AS1	RNU4-2
SHCBP1L	nan
GS1-279B7.1	nan
RGS21	SPACA7
RGS13	SNORD56B
MIR3122	PLA2G4D
nan	nan
LINC00845	nan
NPFFR1	LINC02167
AL133481.2	MIR138-2
DYDC1	nan
SCGB1C1	MYH8
OR2AG2	SLC13A2
RBMXL2	TMIGD1
LYVE1	KRT39
nan	AC003958.2
nan	EFCAB3
MIR3161	TCAM1P
AP001636.3	ANKRD62
MS4A8	MIR1539
FOLH1B	CREB3L3
NXPE1	OR1M1
OR8D4	CYP4F3
KRT6B	TPRX1
nan	nan
EPYC	KLK10
nan	ZSCAN4
CDX2	DNAJC5G
ARL11	TEX37
AL355390.1	HOXD10
ATP11AUN	C20orf141

nan	MIR663A
nan	MIR3193
nan	HNF4A
nan	nan
nan	RBBP8NL
nan	nan
ASPG	LL22NC03-63E9.3
SNORD115-13	ATP5MGL
SNORD115-14	PRR5-ARHGAP8
SNORD115-36	CCR4
SNORD115-41	nan
nan	IQCF6
KBTBD13	LINC01968
nan	ATOH1
nan	RBM46
MIR7-2	LINC02275
nan	TERT
MIR548G	MIR4278
nan	nan
AHSP	FGF10
AC009123.1	nan
nan	H1-6
FBXO39	TNXB
TMEM95	nan
nan	MEP1A
nan	ADGRF1
KRT222	DPPA5
KRT9	LINC02539
MAPT-IT1	OSTCP1
nan	SLC22A2

CD300C	UNC93A
CETN1	PRPS1L1
LINC00668	nan
nan	C7orf65
WBP11P1	nan
LINC00305	KPNA7
nan	MOGAT3
LINC00905	nan
HPN-AS1	MIR29A
ERICH4	AC009365.2
PSG8	AC100797.4
KASH5	AC091182.1
ERVV-2	ADRB3
LINC00299	nan
C1GALT1C1L	KCNV1
GTF2A1L	C9orf57
nan	MIR126
nan	FAM9A
HOXD1	SUPT20HL1
nan	ITIH6
ASB18	INGX
LINC01940	nan
OR6B2	MIR450A2
PDCD1	PNMA6A
CST9	nan
CST1	CTAG1A
LINC00314	XG
LINC00189	XG
nan	
GGT2	
nan	
nan	
nan	
MIR26A1	
SPINK8	

nan	
LRTM1	
CD80	
DNAJB8	
LINC01565	
nan	
nan	
GHSR	
CWH43	
GC	
SLC6A18	
HTR1A	
TMEM174	
MEIKIN	
nan	
GMCL2	
LINC01622	
H3C3	
C6orf136	
nan	
nan	
HLA-DPB2	
GGNBP1	
LINC01016	
nan	
RIPPLY2	
TMEM244	
HOXA4	
nan	
LINC01007	
SLC26A3	
MIR153-2	
nan	
nan	
LYPD2	

INSL4	
nan	
nan	
nan	
TEX48	
FAM163B	
FCN2	
CRLF2	
SCARNA23	
FAM236B	
CYSLTR1	
NXF2	
DCAF12L1	
GOLGA2P2Y	
GOLGA2P2Y	
FAM138A	
OR4F5	
OR4F29	
OR4F16	
MIR200B	
MIR200A	
MIR429	
TTLL10-AS1	
TTLL10	
nan	
nan	
ACTRT2	
MIR551A	
nan	
nan	
HES3	
nan	
nan	
SLC2A7	
MIR1285-1	

PIK3CD-AS1	
nan	
nan	
nan	
nan	
AADACL4	
AADACL3	
PRAMEF12	
PRAMEF1	
PRAMEF11	
PRAMEF2	
PRAMEF4	
PRAMEF10	
PRAMEF7	
PRAMEF6	
nan	
nan	
PRAMEF25	
HNRNPCL2	
PRAMEF26	
nan	
PRAMEF8	
PRAMEF9	
PRAMEF13	
PRAMEF18	
nan	
nan	
nan	
PRAMEF15	
PRAMEF14	
PRAMEF19	
PRAMEF17	
PRAMEF20	
LRRC38	
SRARP	

RNU1-1	
RNU1-3	
nan	
nan	
RNU1-4	
RNU1-2	
PADI6	
nan	
PLA2G2E	
PLA2G2C	
CELA3B	
C1QB	
LACTBL1	
MIR3115	
nan	
ZNF683	
MIR1976	
KDF1	
nan	
nan	
LDC1P	
nan	
nan	
HMGB4	
MIR552	
MIR4255	
nan	
NT5C1A	
MIR30E	
GUCA2B	
nan	
nan	
nan	
KNCN	
nan	

CYP4B1	
CYP4Z2P	
CYP4A11	
CYP4Z1	
CYP4A22	
nan	
C1orf185	
MIR761	
SLC25A3P1	
TTC22	
BSND	
nan	
MIR3116-1	
MIR3116-2	
UBE2U	
MIR101-1	
nan	
IL23R	
PIN1P1	
ASB17	
nan	
MGC27382	
CLCA1	
CLCA4	
nan	
LINC01761	
nan	
AMY2A	
AMY1A	
AC092506.1	
NBPF4	
nan	
nan	
NBPF6	
EPS8L3	

UBL4B	
nan	
KCNA10	
nan	
SYCP1	
TSHB	
nan	
HSD3B1	
nan	
HMGCS2	
NBPF7	
ADAM30	
nan	
nan	

Table A2: Lists of genes found exclusively in either the HipSci iPSC-derived astrocytes or RTT#27 iPSC-derived astrocytes.